THE EFFECTS OF THE PROTEOGLYCAN ANTAGONIST SURFEN ON ANIMAL MODELS OF DEMYELINATION WITH COMPARISON TO IN VITRO T CELL AND MACROPHAGE RESPONSES

by

Jordan Ryan Warford

Submitted in partial fulfilment of the requirements
for the degree of Doctor of Philosophy

at

Dalhousie University
Halifax, Nova Scotia
March 2017

Dedicated to the women who raised me and the woman who chose to stand beside me.

TABLE OF CONTENTS

LIST OF TABLES

LIST OF FIGURES

ABSTRACT

Multiple sclerosis (MS) is a debilitating neurodegenerative disorder that currently affects over 3000 Nova Scotians, and is characterized by the autoimmune-mediated destruction of myelin and axons in the central nervous system. Symptoms include loss of balance, impaired vision or speech, fatigue, and paralysis. Connective tissue components such as proteoglycans are known to be major inhibitors of remyelination and are found at the border of active demyelinating MS lesions. This thesis sought to characterize the immunomodulatory properties of the proteoglycan antagonist surfen (*bis*-2-methyl-4-amino-quinolyl-6-carbamide) using both *in vitro* and *in vivo* models relevant to the study of MS. Surfen decreased murine T cell proliferation whether activated *in vitro* by co-stimulation with anti-CD3/anti-CD28-coated T cell expander beads or *in vivo* by injecting mice with anti-CD3 antibody (Chapter 3). We extended these studies to two murine models that mimic aspects of MS. In the Experimental Autoimmune Encephalomyelitis (EAE) model, surfen treated mice displayed a reduction in clinical scores that were associated with decreased cellular infiltration of both $CD45^+CD3^+CD4^+$ T cells (spinal cord and cerebellum) and $F4/80^+CD11b^+$ myeloid cells (spinal cord; Chapter 4). Several potential mechanisms of action for surfen were identified including the selective regulation of T cell effector functions, decreased production of chemotactic cytokines that facilitate cellular infiltration, and a marked reduction in proteoglycan mRNA expression that positively correlated with clinical improvement. When these *in vivo* results were compared *in vitro* to murine bone-marrow derived macrophages (BMDMs), surfen produced a similar decrease in chemokine concentrations. Reductions in the pro-inflammatory mediators Interleukin (IL)-6, Tumor Necrosis Factor (TNF), and Nitric Oxide (NO) were also observed in BMDMs. Surfen produced a selective increase in the pro-inflammatory cytokine IL-12p40 in EAE, and IL-1β in BMDMs, suggesting that surfen has immunomodulatory capabilities that are likely mediated by macrophages. In contrast to EAE, surfen delayed remyelination when administered directly into a demyelinated lesion created by injecting lysolecithin into the corpus callosum of the murine brain, an effect associated with worsening disease (Chapter 5). The opposing effects of surfen observed in EAE and the lysolecithin model imply differing effects of proteoglycans on the inflammatory and repair-remyelination phases of MS.

LIST OF ABBREVIATIONS AND SYMBOLS USED

α	Alpha
Ab	Antibody
Abs	Antibodies
ANOVA	Analysis of Variance
APC	Antigen Presenting Cell
Arg-1	Arginase-1
ATCC	American Tissue Culture Collection
β	Beta
BBB	Blood Brain Barrier
BMDM	Bone Marrow-Derrived Macrophage
BSA	Bovine Serum Albumin
C	Celsius
c	Complete
Ca2+	Calcium
CaCl2	Calcium Chloride
CCL2	Chemokine (C-C Motif) Ligand 2
CCL3	Chemokine (C-C Motif) Ligand 3
CCL4	Chemokine (C-C Motif) Ligand 4
CCL5	Chemokine (C-C Motif) Ligand 5
CD	Cluster of Differentiation
CD11b	Cluster of Differentiation 11b
CD25	IL-2Rα Chain
CD4+	Cluster of Differentiation 4
CD8+	Cluster of Differentiation 8
cDNA	Complementary DNA
CFA	Complete Freund's Adjuvant
CFA-S	Complete Freund's Adjuvant + Pertussis Toxin – Surfen Treated
CFA-V	Complete Freund's Adjuvant + Pertussis Toxin – Vehicle Treated
CNS	Central Nervous System
CSF	Cerebrospinal Fluid
CSPG	Chondroitin Sulphate Proteoglycan
CTLL-2	Cytotoxic Lymphoid Line-2
d	Day
DC	Dendritic Cell
DMSO	Dimethyl Sulfoxide
DMT	Disease Modifying Therapy
DNA	Deoxyribonucleic Acid
EAE	Experimental Autoimmune Encephalomyelitis
EAE-S	Experimental Autoimmune Encephalomyelitis – Surfen Treated
EAE-V	Experimental Autoimmune Encephalomyelitis – VehicleTreated
ECM	Extracellular Matrix
EDTA	Ethylene Diamine Tetraacetic Acid
ELISA	Enzyme-Linked Immunosorbant Assay

FACS	Fluorescence-Activated Cell Sorting
FCS	Fetal Calf Serum
FGF	Fibroblast Growth Factor
FGF	Fibroblast Growth Factor
FGFR	FGF Receptor
FITC	Fluorescein Isothiocyanate
FoxP3	Forkhead box P3
γ	Gamma
g	Gravity
GAG	Glycosaminoglycan
h	Hour
HCl	Hydrogen Chloride
HEPES	4-(2-Hydroxyethyl)-1-Piperazineethanesulfonic Acid
HIV	Human Immunodeficiency Virus -1
HLA	Human Leukocyte Antigen
HSPG	Heparan Sulphate Proteoglycan
i.p.	Intraperitoneally
Iba-1	Ionized Calcium Binding Adaptor Molecule 1
ICAM	Intercellular Adhesion Molecule
IFN	Interferon
IFNγ	Interferon Gamma
Ig	Immunoglobulin
IGF	Insulin-Like Growth Factor
IL	Interleukin
IL-1	Interleukin-1
IL-10	Interleukin-10
IL-12p40	Interleukin-12 p40 subunit
IL-12p70	Interleukin-12 p70
IL-13	Interleukin-13
IL-17	Interleukin-17
IL-1β	Interleukin-1 Beta
IL-23	Interleukin-23
IL-4	Interleukin-4
IL-5	Interleukin-5
IL-6	Interleukin-6
iNOS	Inducible Nitric Oxide Synthase
IU	International Units
kDa	Kilodaltons
LPC	Lysophosphatidylcholine
LPS	Lipopolysaccharide
MBP	Myelin Basic Protein
MHC	Major Histocompatibility Complex
μM	Micromolar
μm	Micron
min	Minute
mM	Millimolar

MMPs	Matrix Metalloproteinases
MOG_{35-55}	Myelin Oligodendrocyte Glycoprotein Fragment 35-55
mRNA	Messenger RNA
MS	Multiple Sclerosis
MW	Molecular Weight
NaCl	Sodium Chloride
ND	Not Detected
NDST1	N-Deacetylase And N-Sulfotransferase 1
NF-κB	Nuclear Factor κ-Light-Chain-Enhancer of Activated B Cells
NO	Nitric Oxide
OPC	Oligodendrocyte Precursor Cell
%	Percent
PBS	Phosphate Buffered Saline
PDGF	Platelet-Derived Growth Factor
PE	Phycoerythrin
PG	Proteoglycan
PLP	Proteolipid Protein
PMA	Phorbol 12-Myristate 13-Acetate
PPMS	Primary-Progressive Multiple Sclerosis
PRMS	Progressive-Relapsing Multiple Sclerosis
PTX	Pertussis Toxin
q.o.d	Every Other Day
qRT-PCR	Quantitative Real-Time Polymerase Chain Reaction
RQI	RNA Quality Indicator
RoRγT	Retinoic Acid Receptor-Related Orphan Receptor Gamma T
ROS	Reactive Oxygen Species
RPMI	Roswell Park Memorial Institute
RRMS	Relapsing-Remitting Multiple Sclerosis
RT	Room Temperature
s.c.	Subcutaneously
sec	Second
SEM	Standard Error of the Mean
SPMS	Secondary-Progressive Multiple Sclerosis
TAE	Tris-Acetate-EDTA
TBST	Tris-Buffered Saline and Tween-20
[3H]TdR	Tritiated-Thymidine
TGFβ	Transforming Growth Factor Beta
T_H	T Helper Cell
T_H1	Type 1 T helper
T_H17	Type 17 T helper
T_H2	Type 2 T helper
TNF	Tumor Necrosis Factor
T_{REG}	T Regulatory Cells
UV	Ultraviolet
VEGF	Vascular Endothelial Growth Factor
VEH	Vehicle

ACKNOWLEDGEMENTS

Isaac Newton once said, "If I have seen further, it is by standing on the shoulders of giants." My journey to this point, both as an academic and an individual, has involved many larger than life individuals whom my success has been dependent upon. First, I would like to thank Dr. Alex Easton for his mentorship and steadfast support. Alex – together we have travelled the globe, solved world politics, identified the finest steaks coast-to-coast, and developed the uncanny ability to design the perfect experiments that inevitably get published by other groups shortly thereafter. I will be forever indebted to your kindness and friendship. Secondly, I would like to acknowledge Dr. David Hoskin as my co-supervisor. Dave – you have kept me on my toes, challenged me, and incorporated me into the fabric of your lab as one of your own. Thank you for always being fair, pragmatic, and pushing me to develop my scientific strengths… which clearly do not include molecular immunology.

A laboratory group quickly becomes a family. To Drs. Kathleen Attwood, Sara Lahsaee, and Linda Chen, thank you for always being there. To Anna-Claire Lamport, you are one of my greatest accomplishments as a scientist. I'm proud of who you are, the scientist you have become, and what you stand to accomplish. Don't lose yourself in the race to succeed and never stop laughing. To the Hoskin and Robertson labs, your conversations have lifted my spirits and made everyday life exceptionally fun. Shoutout to Javad (happy now?). A special thank you to the mentorship of Drs. Carolyn Doucette and Melanie Coombs whom I owe a great deal both scientifically and personally.

Finally, I would be remiss if I did not express my gratitude to God and my family. Sarah – I am grateful that we are in this adventure together. You are strong, devoted, stubborn, and a consistent source of inspiration. I love you. Mom – from the kid who couldn't read the Berenstain Bears to the arrival of Dr. Warford, you never doubted me. Words will never encapsulate how much you mean to me and you will always hold a special place in my heart. Nanny – From checking in just to see how I'm doing to praying me through the tough spots, thank you for being a constant presence in my life. Auntie Linda – You've loved me as your own and knowing you're in the background cheering me forward has always motivated me to keep my head held high. Maura and Jol – From Thanksgiving at Easter to the day-to-day, I couldn't ask for better in-laws. Love to all.

CHAPTER 1
INTRODUCTION

1.1 Overview of Multiple Sclerosis

Multiple sclerosis (MS) is a chronic neuroinflammatory disease of the central nervous system (CNS) affecting the lives of over 100 000 Canadians and an estimated 2.5 million people worldwide (Evans et al., 2013; Multiple Sclerosis International Federation, 2013). Acknowledged as the most common neurological disease in young adults, MS is characterized by autoimmune-mediated destruction of the myelin sheath that surrounds axons in the CNS which often leads to irreversible clinical disability. The pathological hallmarks of MS include demyelination, gliosis, perivascular infiltration by inflammatory cells, and ultimately axonal and neuronal loss (Frohman et al., 2006; Ludwin, 2006; Trapp et al., 1998). Focal areas of inflammatory-mediated demyelination called plaques produce the primary symptoms of MS, which include difficulty walking, poor coordination of voluntary muscle movement, fatigue, tremor, abnormal skin sensations, loss of sight, cognitive deficits, depression, and bladder dysfunction (Compston and Coles, 2008; Noseworthy et al., 2000). The lifetime economic burden associated with MS has been assessed at approximately $1.6 million per patient (The Canadian Burden of Illness Study Group, 1998).

While there is no cure for MS, Health Canada has approved 13 drug treatments collectively referred to as disease-modifying therapies (DMTs). The mechanisms of action for each DMT are diverse and include pleiotropic effects on multiple immune cell subsets, reflecting the complexities inherent in reprogramming the inflammatory response (Wingerchuk and Carter, 2014). Substantial neuroinflammation and axonal degradation has been shown to occur sub-clinically before the onset of detectable symptoms (Kappos et al., 1999; Kuhlmann et al., 2002). Early administration of DMTs delay disease progression by reducing the growth and manifestation of new plaques (Cocco et al., 2015; Kavaliunas et al., 2015). Nevertheless, many DMTs are associated with immunosuppressive side effects and fail to directly address progressive disease that corresponds structurally to gliosis, oligodendrocyte death, diffuse axonal injury, and a hostile extracellular microenvironment (Kuhlmann et al., 2017; Lassmann et al., 2012).

Components of the peripheral and CNS extracellular microenvironment in MS will serve as the focus of this thesis, with attention directed towards a class of complex extracellular matrix (ECM) macromolecules called proteoglycans (PGs). The diversity in

which PGs function is significant in the context of MS pathophysiology. PGs have been reported to inhibit remyelination, promote neuroinflammation, and are found at the border of MS plaques (Lau et al., 2012; Sobel and Ahmed, 2001). Moreover, PGs play integral roles in the regulation of inflammation by facilitating cellular infiltration, immune cell regulation, signaling, and the production of soluble factors (Sarrazin et al., 2011).

Whether PGs could serve as putative therapeutic targets in the context of MS has yet to be fully explored using a PG antagonist. The actions of PGs can be blocked pharmacologically by administering surfen, a compound 372 Daltons in molecular weight with the chemical structure of a bis (2-methyl, 4-amino, 6-quinolyl) amide (Hunter and Hill, 1961). The overarching objectives of this work are two-fold: 1) To characterize the effect of surfen on the function of T cells and macrophages, two primary effector cells in MS and 2) evaluate the efficacy of surfen in mouse models of chronic neuroinflammation and focal demyelination that mimic aspects of MS. Taken together, these studies aim to further our understanding of PG biology in MS.

1.2 Diagnosis and Natural History of MS

Clinical presentation of symptoms is heterogeneous between patients and often accompanied by a differential diagnosis that comprises other idiopathic demyelinating disorders such as transverse myelitis, neuromyelitis optica, and acute disseminated encephalomyelitis (Miller et al., 2008). No single test can definitively confirm a diagnosis of MS (Rovira et al., 2015). A neurological exam is taken into consideration alongside magnetic resonance imaging (MRI) with the contrast enhancing agent gadolinium (Polman et al., 2011). Plaques typical of MS appear as bright T1-weighted areas of inflammation, indicative of a compromised blood brain barrier (BBB; Rovira et al., 2015).

Diagnostic criteria call for evidence of plaque activity separated by time and location within the CNS (Otto et al., 2008; Polman et al., 2011). Given that initial disease presentation reflects only a small proportion of preexisting pathology, these criteria are often met with the first MRI. Occasionally a lumbar puncture is performed in more complex cases to test for the presence of immunoglobulin G (IgG) bands in cerebrospinal

fluid (CSF) as an additional verification of a MS diagnosis, although a small percentage of patients with clinically definite MS do not show evidence of oligoclonal bands in their CSF (Link and Huang, 2006).

1.2.1 Clinical Subtypes of MS

During diagnosis, the status of "clinically isolated syndrome" is conferred to describe neurologic symptoms that last for at least 24 hours and are associated with plaque activity on MRI (Polman et al., 2011). Administration of a DMT is often provided at this point since an estimated 80% of patients experiencing a clinically isolated syndrome move on to develop MS and early intervention limits future disease progression (Cocco et al., 2015; Kavaliunas et al., 2015; Tedeholm et al., 2015; Trojano et al., 2003). When clinically definite MS is established the patient is classified into one of four broad subtypes: relapsing-remitting MS (RRMS); secondary-progressive MS (SPMS); primary-progressive MS (PPMS); and progressive-relapsing MS (PRMS; Lublin et al., 2014).

Approximately 85% of patients initially present with RRMS, which involves periods of increased disease activity (relapse) followed by episodic recovery (remission). Eventually the mechanisms underlying endogenous repair fail and roughly 50% of patients transition into SPMS at the median age of 54 where symptom severity progressively worsens for the remainder of the individual's life (Koch et al., 2010; Scalfari et al., 2014). Progressive deterioration is also the central feature within 10% of the patient population living with PPMS; however, onset is aggressive, presents later in life (median age of 40), and remission is notably absent (Koch et al., 2010). PRMS represents the 5% of cases that feature acute relapses in addition to progressive disease, which may or may not recover (Koch et al., 2009; Lublin et al., 2014). A small proportion of the population who remain stable were previously designated as having benign MS; however, recent evidence points to significant cognitive deterioration and the classification is now only used retrospectively (Rovaris et al., 2008; Zivadinov et al., 2016).

1.2.2 Proposed Etiology and Environmental Risk Factors

The precise etiology of MS is unknown although several pieces of evidence point to the combined effect of genetic and environmental risk factors. Genome-wide association studies have identified over 110 loci associated with MS susceptibility, with HLA-DRB1*1501 and HLA-DRB5*0101 haplotypes displaying the strongest association amongst Caucasians, pointing to a strong immune component (Beecham et al., 2013; International Multiple Sclerosis Genetics Consortium et al., 2011). The observation that females develop MS in a 3:1 ratio to males has led to investigations on the influence of chromosome inactivation and differential gene dosage of regulatory transcription factors such as FoxP3 located on the X chromosome (Nie et al., 2015). However, similar X-linked inactivation patterns have also been reported in age-matched healthy female controls (Chitnis et al., 2000). Other factors could account for the higher incidence of MS in females such as changes in lifestyle, metabolism, occupation, birth control, etc. The concordance rate for MS is 25% in monozygotic twins and only 5% for dizygotic twins implying a large role for environmental risk factors in disease development (Willer et al., 2003).

Well established risk factors for MS include Vitamin D deficiency, cigarette smoking, increased body mass index, and exposure to Epstein-Barr virus (EBV; Amato et al., 2017). Evidence associating low levels of the Vitamin D precursor 25-hydroxyvitamin D3 with onset of MS has largely stemmed from epidemiological studies. Latitude appears to be a major factor in MS risk with northerly countries that are farthest from the equator displaying the highest prevalence and incidence rates in the world (Jelinek et al., 2015; Simpson et al., 2011). The Nurse's Health Study (n=200 000) and US military (n=7 million) cohorts have associated higher serum levels of Vitamin D (100 nM or higher) with a 40% reduced risk of developing MS (Munger et al., 2006, 2004). Perhaps the most convincing study linked several single nucleotide polymorphisms associated with decreased 25-hydroxyvitamin D3 production to an increased susceptibility of developing MS (Mokry et al., 2015).

Although clinical trials have been notoriously difficult to control given that Vitamin D is endogenously synthesized following exposure to ultraviolet light from the sun, data from phase III trials of the DMT interferon beta-1b associated higher 25-

hydroxyvitamin D3 levels with reduced disease severity over 5 years (Ascherio et al., 2014). Vitamin D supplementation is now standard clinical practice, with recommended doses of up to 4000 international units (IU) per day. New clinical trials are underway investigating the effect of high-dose Vitamin D (up to 10 000 IU/day) on disease activity (Smolders et al., 2010; Sotirchos et al., 2016).

Lifestyle factors such as smoking and increased body mass index are also linked to an increased risk of developing MS that range from 8 to 15%, respectively (Amato et al., 2017). Smoking has been associated with accelerated transitions from clinically isolated syndrome to clinically definite MS and progression from RRMS to SPMS (Di Pauli et al., 2008; Manouchehrinia et al., 2013; Ramanujam et al., 2015). Higher body mass index is also associated with disease progression as well as poor responsiveness to interferon Beta-1b treatment (Kvistad et al., 2015; Tettey et al., 2016).

Lastly, molecular mimicry by EBV is a candidate mechanism for autoimmunity that points to failed immune regulation in the periphery (Pender and Burrows, 2014; Wandinger et al., 2000; Woulfe et al., 2014). Virtually all individuals with clinically definite MS are positive for EBV; however, most of the general population is also infected. In the case of MS, it is hypothesized that cross-reactivity occurs when antigen presenting cells encounter EBV antigens that contain peptide sequences homologous with myelin basic protein (MBP), a major constituent of the myelin sheath, and present them to myelin-reactive naïve $CD4^+$ T cells in the context of human leukocyte antigen (HLA) class II molecules (Lang et al., 2002).

Taken together, these susceptibility factors point to the involvement of dysregulated immunomodulatory mechanisms. Unfortunately, epidemiological studies do not equate to causation and the varied methodologies and regional biases make widespread generalization difficult. Nevertheless, the sum benefit of smoking cessation, reducing body mass index, and vitamin D supplementation can statistically reduce risk of MS onset by up to 60% (Amato et al., 2017) and are worthwhile endeavors for improved quality of life.

1.3 Neuroinflammation in MS

Autoimmune-mediated demyelination is thought to be initiated in MS by the infiltration of myelin-specific T cells into the CNS following their activation in peripheral lymphoid tissues (Kuhlmann et al., 2017; Lassmann, 2011). The absence of adhesion molecules on resting endothelium of the BBB prevent the migration of primed T cells under normal conditions and fail to provide the necessary reactivation required for an inflammatory response. This raised the question of how a myelin-specific T cell might enter the CNS, which has been considered an immune privileged organ that mounts various mechanisms to limit immune cell infiltration. Today we understand that immune privilege does not confer absolute protection and lymphocytes are capable of crossing the BBB under healthy conditions, albeit in small numbers, performing a surveillance function in the CNS for potential pathogens (Anthony et al., 2003; Galea et al., 2007). Furthermore, mouse studies using a model of MS called experimental autoimmune encephalomyelitis (EAE) demonstrate that reactivation of primed myelin-specific T cells occurs principally in the subarachnoid space by antigen presenting cells (APCs) such as perivascular macrophages and dendritic cells (Greter et al., 2005; Kivisäkk et al., 2009). The combination of genetic and environmental factors in conjunction with a myelin-specific T cell conducting immune surveillance may represent the first step in the inflammatory cascade leading to demyelination in MS.

The reactivation of myelin-specific T cells produces a second wave of inflammation that activates endothelial cells to upregulate adhesion molecules, while T cells and glia produce chemotactic factors such as chemokine (C-C motif) ligand 2 (CCL2) capable of recruiting subsequent waves of T cells, B cells, and monocytes across the BBB and into the CNS parenchyma (Cannella and Raine, 1995; Simpson et al., 1998; Tanuma et al., 2006). These immune subsets produce soluble pro-inflammatory mediators such as interleukin-1beta (IL-1β), interleukin-6 (IL-6), and tumor necrosis factor (TNF) that compromise the integrity of the myelin sheath, producing demyelination and subsequent axonal damage (Brosnan et al., 1995; Trapp et al., 1998).

T cells can be subdivided into $CD4^+$ and $CD8^+$ subsets that are functionally responsible for delayed-type hypersensitivity responses and class-I restricted cellular lysis of antigen-specific targets, respectively (Chitnis, 2007). $CD4^+$ T cells also play an

important role in B cell differentiation, hence their subsets have been termed T "helper" cells. T cell signaling requires two signals, one from the T cell receptor which has bound to the cognate antigen, and the second from costimulatory molecules interacting with ligands expressed by antigen presenting cells (APCs) such as macrophages, microglia (brain macrophages), or dendritic cells (Bö et al., 1994; Bretscher and Cohn, 1970).

In the presence of the appropriate cytokine milieu, $CD4^+$ T cells can differentiate into T-helper 1 (T_H1), T_H2, T_H17, and T regulatory (T_{REG}) subsets that orchestrate the neuroinflammatory response in MS (Chitnis, 2007). During disease progression, encephalitogenic T_H1 subsets produce pro-inflammatory cytokines such as IL-2, interferon-gamma (IFN-γ), and TNF. Both IFN-γ and TNF are potent pro-inflammatory activators of macrophages, microglia, and astrocytes that then go on to contribute to inflammation and tissue damage (Brosnan et al., 1995; Chung and Benveniste, 1990; Tanuma et al., 2006). Similarly, T_H17 subsets are considered inflammatory and produce IL-17, IL-22, TNF, and the chemokine CCL20. Although the roles for each of these T_H17 cytokines and CCL20 in MS are still an active area of research, they have been associated with deleterious inflammation both in MS plaques and EAE mouse studies (Brucklacher-Waldert et al., 2009; Komiyama et al., 2006).

In contrast to T_H1 and T_H17 responses, T_H2 subsets produce IL-4, IL-5, IL-10, and IL-13 capable of dampening inflammation. The net benefit of the production of T_H2 cytokines has been demonstrated by DMTs such as glatiramer acetate that exert their effects in part by shifting from T_H1 to T_H2 subsets (Duda et al., 2000). Nevertheless, IL-4 and IL-5 also activate B cells which have been implicated in the pathogenesis of MS (Li et al., 2015). Whether these T_H2 subsets promote recovery or contribute to damage may be related to the type of MS and stage of disease. Progressive MS has been associated with B cell-mediated pathology, while on the other hand several DMTs that are efficacious early in RRMS promote T_H2 responses (Duda et al., 2000; Fraussen et al., 2016; Serafini et al., 2004). In addition to T_H2 subsets, T_{REG} cells have been shown to play an important role in the regulation of T_H1 and T_H17 responses; however, they often fail to overcome inflammation in the context of MS (Haas et al., 2005; Viglietta et al., 2004).

Aside from $CD4^+$ T cells, which are the dominant inflammatory T cell subtype, cytotoxic $CD8^+$ T cells are responsible for oligodendrocyte death and axonal transection, therefore contributing to both demyelination and irreversible clinical deficits (Babbe et al., 2000; Huseby et al., 2012). Moreover, $CD8^+$ T cells are present in greater numbers than $CD4^+$ T cells in actively demyelinating plaques. Neurons and oligodendrocytes are considered vulnerable to $CD8^+$ cytotoxicity in part due to increased expression of HLA-class I molecules on the cell surface during heightened inflammation (Höftberger et al., 2004). Taken together, both $CD4^+$ and $CD8^+$ T cells are important contributors to the pathogenesis of MS.

Infiltrated macrophages and resident microglia represent another important effector cell in MS that are also capable of eliciting both damage and repair. In the context of inflammation, macrophages are a primary source of the T_H1 inducing cytokine IL-12, as well as a variety of other cytokines such as TNF, IL-1β, and IL-6 (Fujiwara and Kobayashi, 2005). Moreover, macrophages also produce ECM proteins, including proteoglycans that create a myelin microenvironment that is inhibitory to repair by oligodendrocytes (Lau et al., 2012; Sobel and Ahmed, 2001; van Horssen et al., 2006). In addition to inflammation, phagocytic macrophages are responsible for the clearance of myelin debris from the demyelinating plaque (Bogie et al., 2011). This was initially considered pathogenic, but recent evidence in both MS and animal models has shown that the clearance of myelin promotes repair via the recruitment of oligodendrocyte precursor cells, which differentiate into mature oligodendrocytes capable of remyelinating denuded axons (Boven et al., 2006; Miron et al., 2013; Rawji et al., 2016). Moreover, myelin-laden macrophages are capable of inhibiting T_H1 responses in EAE, suggesting that macrophages have immunomodulatory capabilities in MS (Bogie et al., 2011).

1.4 Disease Modifying Therapies in MS

MS therapies target the early inflammatory phase of the disease of RRMS and are successful in prolonging remission and controlling relapse rate during the initial phases of the disease. The first DMTs were introduced in the 1990s and include IFNβ-1a, IFNβ-1b, and glatiramer acetate (Ransohoff et al., 2015). Both classes of interferon DMTs are thought to share similar mechanisms of action that include a T_H1-T_H2 shift, a reduction of

cellular infiltration, restoration of T_{REG} function, and the enhanced apoptosis of T-cells (Korporal et al., 2008; Noronha et al., 1993). The use of beta-interferons infers that modulation of multiple immune pathways is a promising path forward in the treatment of MS.

With a short half-life in the periphery, glatiramer acetate relies on blood-derived monocytes, lymphocytes, and dendritic cells to impart neuroprotective and immunomodulatory effects in the CNS by promoting an anti-inflammatory milieu (Aharoni, 2013; Liu et al., 2007). The effects of glatiramer acetate include increases in FoxP3 expression, and the generation of anti-inflammatory factors such as IL-10 and TGF-β by T_{REG} cells that confer neuroprotection (Aharoni et al., 2010; Haas et al., 2009; Miller et al., 1998). Although glatiramer acetate reduces plaque load, acts at peripheral and central sites, decreases pro-inflammatory gene expression, acts as a decoy for reactive lymphocytes, and polarizes cells towards an anti-inflammatory T_H2 phenotype, it does not improve chronic neuropathology; clinical trials show no benefit in progressive MS (Wolinsky et al., 2007). The next generation of DMTs that came soon after focused on limiting the transmigration of lymphocytes into the CNS.

Efforts to limit pro-inflammatory T cells from entering the CNS include a humanized monoclonal antibody against the adhesion molecule α4-integrin (natalizumab), preventing the transmigration of T cells across the BBB, and a sphingosine 1-phosphate receptor modulator (fingolimod) that prevents the egress of T cells from peripheral lymphoid tissues (Kappos et al., 2010; Polman et al., 2006). Clinically, both biologics reduce plaque burden in RRMS and the number of relapses by limiting lymphocyte infiltration into the CNS (Brinkmann et al., 2010; Niino et al., 2006).

Within the last decade treatment options for MS have increased over two-fold and include several different approaches to target inflammation. These include a monoclonal anti-CD52 antibody (alemtuzumab) that promotes cellular cytolysis of lymphocytes, monocytes, and dendritic cells (Cohen et al., 2012), teriflunomide which displays a cytostatic effect on proliferating lymphocytes by blocking pyrimidine synthesis (Confavreux et al., 2014), and dimethyl fumarate that demonstrates anti-inflammatory and cytoprotective effects (Gold et al., 2012). These next generation therapies have improved clinical outcomes relative to interferons or glatiramer acetate (Ransohoff et al.,

2015). The efficacy of the DMTs discussed here are, however, limited to RRMS patients. Furthermore, adverse events are commonly associated with MS therapeutics, which can include immunosuppression, depression, hepatic injury, cardiotoxicity, type I hypersensitivity reactions, infusion reactions, localized tissue damage, teratogencity, seizures, and progressive multifolcal leukoencephalopathy (Ransohoff et al., 2015; MS Coalition 2016). The ideal MS therapeutic of the future will aim to selectively modulate inflammation whilst minimizing side effects. There are currently multiple clinical trials underway to test the efficacy of a host of new compounds whose therapeutic potential in MS have yet to be proven.

1.5 Animal Models of MS

There are several animal models of demyelination which have been used in drug development as pre-clinical models for MS. These models include both immune mediated and chemically induced demyelination. Experimental autoimmune encephalomyelitis (EAE) features immune-mediated demyelination, while chemical models include administration of lysolecithin, cuprizone and ethidium bromide into CNS white matter tracts (Lassmann and Bradl, 2017). Chemical models result in complete remyelination with minimal immune responses, allowing investigation of the remyelination process, while immune mediated models produce partial remyelination but mimic the inflammatory milieu observed in MS.

1.5.1 Experimental Autoimmune Encephalomyelitis

EAE is a T cell mediated model of chronic neuroinflammation that is characterized by demyelination and ascending paralysis that recapitulate several neuropathological features seen in MS. Murine EAE studies have played an important role in the development of three Health Canada approved therapies for MS: natalizumab, glatiramer acetate, and mitoxantrone (Baxter, 2007). EAE has been successfully induced in many species including rodents, guinea pigs, and non-human primates, using a variety of antigens such as proteolipid protein, MBP, or myelin oligodendrocyte glycoprotein amino acids 35-55 (MOG_{35-55}). These antigens comprise various components of the

myelin sheath that envelop axons within the CNS; however, whole myelin has also been used to induced EAE (Baxter, 2007).

Mouse models of EAE can include relapsing-remitting and chronic clinical courses used to model aspects of relapsing-remitting disease in MS (McCarthy et al., 2012). A relapsing-remitting disease course is possible by immunizing SJL mice immunized with proteolipid protein, producing a spontaneous biphasic disease course featuring motor deficits followed by moderate periods of recovery (Miller et al., 2007). In contrast, C57BL/6 mice immunized with MOG_{35-55} produce a chronic disease course followed by minimal recovery and was used for this thesis (Berard et al., 2010). While each mouse strain/antigen combination produces a different time course and duration of maximal clinical severity, ascending hindlimb paralysis is common to all the models. Notwithstanding the chronic nature of the MOG_{35-55} model, to date there are no EAE models that reflect disease processes associated with SPMS or PPMS.

1.5.1.2 Induction of EAE

EAE can be induced by active or passive immunization which involves either immunization with an antigen, or the adoptive transfer of sensitized T cells from actively immunized animals into naïve recipient mice, respectively (Pender, 1995). In actively induced EAE, a myelin peptide is emulsified with complete Freund's adjuvant (CFA) containing mineral oil and heat-killed *Mycobacterium tuberculosis* to bolster a strong immune response (Lassmann and Bradl, 2017). Pertussis toxin (PTX) is also administered and is necessary to promote peripheral inflammation, prevent T cell anergy, and is thought to aid in increasing the permeability of the BBB (Chen et al., 2006; Kamradt et al., 1991). The ability of these adjuvants to produce immune activation independent of the antigen itself call for the use of CFA and PTX controls in EAE studies to monitor for non-specific side effects that could alter interpretation of immunological data.

1.5.1.3 EAE Disease Phases

The development of clinical signs in EAE occurs over three phases: 1) the induction phase, 2) the effector phase, and 3) the recovery phase. The induction phase of

the disease involves the priming of myelin-specific $CD4^+$ T cells following active immunization with myelin antigens along with CFA and PTX. By contrast, the effector phase involves the migration of myelin-specific $CD4^+$ T cells into the CNS via a disrupted BBB accompanied by an influx of peripheral immune cells into the CNS parenchyma. Demyelinated plaques in EAE are predominantly composed of $CD4^+$ T lymphocytes and macrophages with very few $CD8^+$ T cells and B cells, a marked difference between EAE and MS (Brown and Sawchenko, 2007). EAE neuropathology is primarily limited to the spinal cord and cerebellum, with little forebrain involvement, in contrast to the plaque patterns observed in MS (Brown and Sawchenko, 2007; Höftberger et al., 2015).

Lastly, the recovery phase varies between EAE subtypes but usually involves the presence of T_{REG} subsets that attempt to dampen CNS inflammation by reducing proliferation and cytokine production by encephalitogenic T_H1 and T_H17 subsets (Koutrolos et al., 2014). These phases permit a better understanding of the mechanisms underlying candidate MS therapeutics, as the distinct immunological profiles associated with each phase can inform the point in the MS disease course at which a drug may be most efficacious.

1.5.2 Chemical Models of Demyelination

1.5.2.1 Lysolecithin

Lysolecithin (lysophosphatidylcholine, generated by phospholipase A2) is a detergent capable of solubilizing lipid rich membranes, producing complete demyelination after injection of a 1% solution into various white matter tracts of rodents including the dorsal columns of spinal cord, caudal cerebellar peduncle, and corpus callosum (Lau et al., 2012; Miron et al., 2013; Woodruff and Franklin, 1999). In mice, remyelination commences by day 7 following lysolecithin injection into the spinal cord and total remyelination is completed by 1 month (Jeffery and Blakemore, 1995; Keough et al., 2015). Lysolecithin spares astrocytes and axons which can metabolize the agents but is toxic to oligodendrocytes, resulting in a relatively pure lesion (Jeffery and Blakemore, 1995).

1.5.2.2 Cuprizone

Cuprizone is a copper-chelator administered in the diet of rodents for 4-6 weeks, which produces widespread demyelination that is prominent in the corpus callosum. Complete remyelination occurs within 4 weeks of reverting to a normal diet (Ludwin, 1978). The curprizone model also selectively targets oligodendrocytes by the disruption of mitochondrial complex IV. This mechanism of demyelination is particularly relevant to MS, as mitochondrial dysfunction has been recognized as a contributor to both demyelination and axonal degeneration (Mahad et al., 2008; Schoenfeld et al., 2010; Ziabreva et al., 2010).

1.5.2.3 Ethidium bromide

Ethidium bromide can be injected into the spinal cord dorsal columns or the caudal cerebellar peduncle where it produces complete demyelination by 2 weeks following administration with remyelination not taking place until 3-4 months later (Woodruff and Franklin, 1999). Because ethidium bromide is a DNA damaging agent, it affects all cell types including astrocytes, and most remyelination is carried out through the migration of Schwann cells into the demyelinated region (Merrill, 2009; Woodruff and Franklin, 1999). However, in MS the principal cells responsible for remyelination are oligodendrocytes, calling into question the validity of this model.

1.6 The MS Plaque

The MS plaque is composed of a heterogeneous population of immune cells that produce distinct patterns of demyelination. Classic active plaques (pattern I), common in early RRMS, feature macrophage-mediated demyelination and marked inflammation produced by MHC class I/II restricted T_H cells along with activated microglia (Barnett and Prineas, 2004; Lassmann et al., 2001; Lucchinetti et al., 2000). In contrast to the inflammatory nature of active pattern I plaques, slowly expanding (pattern II) and inactive plaques (patterns III and IV) enlist neurodegenerative mechanisms also found in stroke, spinal cord injury, and Alzheimer's disease (Friese et al., 2014; Lucchinetti et al., 1996). Accounting for roughly 50% of the plaque load in progressive MS, slowly expanding pattern II lesions comprise antibody-mediated mechanisms. Lesions feature a

demyelinated core with immunoglobulin deposition, complement activation, astrocytic scar tissue, and patent axonal injury (Bramow et al., 2010; Kutzelnigg et al., 2005; Lucchinetti et al., 2000). Pattern III and IV plaques feature oligodendrocyte death and early stage axonal degeneration, with the primary difference between patterns being the extent of oligodendrocyte and axonal death.

When considered in the context of patterns III and IV, DMTs cannot accommodate the extent and duration of the inflammation in combination with degenerative pathology (Dutta and Trapp, 2014). Therefore, shifting focus from single targeted pharmacological approaches (i.e. monoclonal antibodies) in MS to therapeutics that target components of the CNS which regulate multiple aspects of inflammation and repair, such as extracellular matrix proteins, may produce a greater effect on reducing plaques that feature neurodegenerative processes.

1.7 The Extracellular Matrix

The ECM of the CNS is mainly composed of glycosaminoglycans (GAGs), either bound to proteins as PGs or as unbound hyaluronan (Lau et al., 2013). GAGs are linear polysaccharides made of repeating disaccharide units and an amino sugar that comprise heparin, heparan sulphate (HS), hyaluronic acid, chondroitin sulphate, dermatan sulphate and keratan sulphate (Bülow and Hobert, 2006). Proteoglycans are a large family of signaling molecules composed of a core protein covalently linked to GAG side chains associated both with cells (in storage granules or on the cell surface) and with the ECM (Esko et al., 2009). Two major classes of PGs include chondroitin sulphate PGs (CSPGs) and heparan sulphate PGs (HSPGs). The CSPG family is comprised of aggrecan, versican, neurocan, and brevican. HSPGs include perlecan, syndecan, serglycin, and agrin (Bülow and Hobert, 2006; Esko et al., 2009).

Proteoglycans are highly variable structures due to chemical modification of their GAG side chains. For example, the disaccharide backbone of HS is composed of galactosamine (either N-acetylated or N-sulphated) complexed with either of the uronic acids (Bishop et al., 2007). As many as 26 enzymes participate in the biosynthesis of HS side chains, which occurs in the endoplasmic reticulum, Golgi apparatus and trans-Golgi apparatus (Bishop et al., 2007; Esko et al., 2009). Key reactions include deacetylation of

the N terminus, O-sulphation, and addition of a negatively charged sulphate group (N-sulphation (Bishop et al., 2007).

There is great structural heterogeneity among HS side chains in terms of chain length and the extent of chemical modification. The HS side chains are attached to core proteins by enzymes in the Golgi apparatus to form HSPGs. Members of HSPGs found within the ECM are made up of agrin, collagen XVIII and perlecan. Cell surface HSPGs form syndecans (linked to a transmembrane core protein, syndecans 1-4) or glypicans (linked via glycosylphosphatidylinositol to a membrane protein, glypicans 1-6; Capila and Linhardt, 2002; Kolset and Tveit, 2008). Once expressed on or outside the cell, endosulphatases can remove sulphate groups, and enzymes can cleave the core protein or the HS side chains (heparatinase fulfilling this second role; Dhoot et al., 2001; Morimoto-Tomita et al., 2002).

HSPG family members bind to a range of proteins, known collectively as heparin-binding proteins (Capila and Linhardt, 2002). It was initially thought that binding between HSPGs and heparin-binding proteins was non-specific, based on the high negative charge of the GAG side chains. However, binding is now known to occur through specific binding motifs in heparin-binding proteins that contain the sequences XBBXBX or XBBBXXBX in which B refers to basic amino acids (arginine, lysine or histidine) and X is an aromatic or aliphatic amino acid (Hileman et al., 1998; Torrent et al., 2012).

There is a high degree of binding specificity based on binding sequences in GAGs, protein folding and three-dimensional configuration that depends on charge-charge interactions as well as hydrogen bonding (Cardin et al., 1989; Hileman et al., 1998). A bioinformatics screen for mouse immune system related proteins with heparin binding motifs identified 235 candidates, most of which (154 or 66%) were intracellular, with 18% on the cell surface and 10% extracellular (Simon Davis and Parish, 2013). Many of these intracellular candidates are key signaling molecules, implying a role for intracellular HS in signal transduction and cell function. There are also heparin binding motifs in several cytokines including IL-1α, IL-9 and TGFβ. Moreover, chemokines represent a large family with heparin binding motifs that include CCL17, CCL19, CCL25, CCL28, C-X-C Motif Chemokine Ligand 5 (CXCL5) and CXCL12, as well as

cytokine receptors (IL-2Rα, IL-7R) and C-C chemokine receptor type 3 (CCR3), CCR7 and CXCR5 chemokine receptors (Simon Davis and Parish, 2013).

Components of the innate immune system identified in this study include toll-like receptors (TLR-1, 2, 4, 6, 8 and 13) and several components of the complement system (including C4b, C5, C7, C8a, C8b and the complement receptor CD93; Simon Davis and Parish, 2013). Taken together, the broad base of studies reviewed here establish a key regulatory role for PGs in modulating the immune system. Functions include regulation of leukocyte adhesion, cytokine and chemokine function and sensing tissue injury. From a broader perspective, these interactions play key roles in embryonic development (Häcker et al., 2005), homeostasis (Bülow and Hobert, 2006) and disease progression (Simon Davis and Parish, 2013).

1.8 Proteoglycans in MS

The ECM of the CNS is mainly composed of GAGs, either bound to proteins as PGs or unbound in the form of hyaluronan (Lau et al., 2013). Interspersed among this network of PGs are additional glycoproteins like tenascins, thrombospondin and osteonectin. Transmembrane syndecans and glypicans are found in the cell membranes of neurons and glial cells. The HSPGs perlecan, agrin and collagen XVIII are mainly found in basement membranes around cerebral blood vessels in normal CNS tissues (Barros et al., 2011). In the developing brain, ECM proteins are readily detected, where they are used to guide the migration and targeting of neurons. However, after development control brain samples show minimal expression of PGs in the extracellular matrix by immunohistochemistry apart from the perivascular basement membranes (Barros et al., 2011; Reichardt and Tomaselli, 1991).

CSPG expression is increased following injury to the CNS by several resident cells, including macrophages/microglia, reactive astrocytes, and neurons. Members of the lectican family of CSPGs have been associated with MS plaques (Sobel and Ahmed, 2001; van Horssen et al., 2006). In the centre of active pattern I plaques their expression is decreased and found in macrophages, suggesting that they had been phagocytosed and may modulate macrophage function. By contrast, their expression is increased in association with reactive astrocytes in pattern II plaques. It has been suggested that this

expression might impede axonal outgrowth (Sobel and Ahmed, 2001; van Horssen et al., 2006). Hyaluronan also accumulates in MS plaques and inhibits myelin repair in EAE by preventing the differentiation of oligodendrocyte precursor cells (OPCs; Back et al., 2005). Lau and colleagues (2011) demonstrated that macrophages/microglia are a primary source of CSPGs in the spinal cord lesions of mice that received lysolecithin, although reactive astrocytes at the lesion edge are an additional source. This study also confirmed that CSPGs are profoundly inhibitory to OPCs in vitro. The administration of systemic xyloside, which inhibits CSPG by cleaving their GAG sidechains, accelerates remyelination and increases recruitment of OPCs in a murine lysolecithin model of demyelination (Lau et al 2011).

Several HSPGs normally associated with basement membranes (laminin, collagen type IV and fibronectin) are deposited in the parenchyma of pattern I and pattern II plaques, but not in chronic inactive pattern III plaques (van Horssen et al., 2006). However, unlike CSPGs, the roles of HSPGs during inflammation and repair in the CNS remain unexplored. Taken together, these studies suggest that PG expression in the ECM of the CNS impedes both axonal regeneration and impairs attempts at remyelination by oligodendrocytes.

1.9 Rationale and Objectives

PGs have been well characterized in the literature, including their expression in MS, yet few compounds have been tested to therapeutically target them in animal models of human disease. Recently, the small molecule CSPG antagonist fluorosamine was tested in both EAE and the lysolecithin model and improved both clinical outcomes and remyelination (Keough et al., 2016). However, a drug that binds both CSPGs and HSPGs has yet to be explored in animal models of MS.

Surfen (*bis*-2-methyl-4-amino-quinolyl-6-carbamide) was first described in 1938 as an excipient used in the production of depot insulin (Figure 1.1; Umber et al., 1938). Early work describes its modest ability to neutralize heparin in experimental rabbits (Hunter and Hill, 1961), to inhibit infection of experimental mice with trypanosomal microorganisms (Williamson and Rollo, 1959) and its ability to bind with growth factors (Schuksz et al., 2008). Surfen contains four quinoline rings with positively charged

amino or methyl groups that facilitate its binding to the negatively charged GAG side chains of PGs.

Given the recent evidence that multiple immune mediators bind HS, including chemokines, interleukins, growth factors, and complement, surfen was identified as a potential tool to further understand both HSPG and CSPG biology in the context of MS using the EAE and lysolecithin animal models.

Hypothesis:

Surfen will limit T cell function, ameliorate EAE severity, and reduce demyelination following administration in mouse models of MS.

The objectives of this thesis are:

1) To determine the effect of surfen on *in vitro* and *in vivo* T cell activation and function, including proliferation, activation marker expression, and cytokine production (Chapter 3).
2) To determine the effect of surfen on a MOG_{35-55} model of EAE, including T cell and macrophage profiles (Chapter 4).
3) To determine the effect of surfen on remyelination using a lysolecithin mouse model of demyelination (Chapter 5).

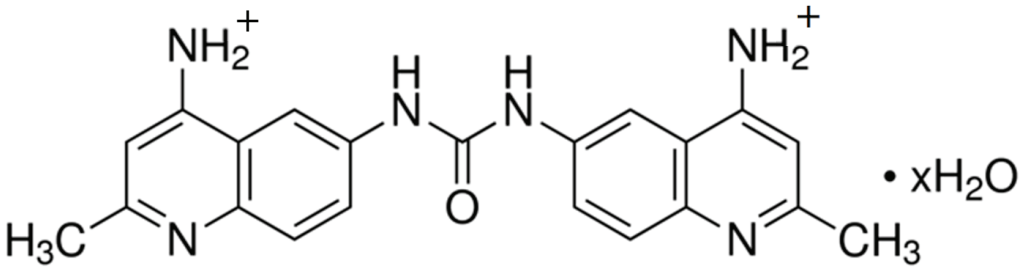

Exact Mass: 372.170
Molecular Weight: 372.432
Elemental Analysis: C, 67.73; H, 5.41; N, 22.57; O, 4.30
Boiling Point: 1258.04 [K]
Melting Point: 1047.76 [K]
Critical Temp: 1173.4 [K]
Critical Pres: 26.76 [Bar]
Critical Vol: 1058.5 [cm3/mol]
Gibbs Energy: 823.59 [kJ/mol]
Log P: 2.48
MR: 110.34 [cm3/mol]
Henry's Law: 25.11
Heat of Form: 384.03 [kJ/mol]
tPSA: 117.89

Figure 1.1: Structure of surfen (Bis-2-methyl-4-amino-quinolyl-6-carbamide).

CHAPTER 2
METHODS

2.1 Animal Care

Female C57BL/6 mice (6-8 weeks of age) were purchased from Charles River Canada (St. Constant, QC) and were used for all primary T cell, macrophage, EAE, and lysolecithin experiments. All mice were housed in the Carleton Animal Care Facility at Dalhousie University. The animal holding rooms were on a 12-hour light/dark cycle and fed a standard diet of rodent chow and water *ad libitum*. This work received approval from the Dalhousie University Committee on Laboratory Animals and was completed in accordance with guidelines from the Canadian Council on Animal Care.

2.2 General Reagents

Acetic acid, ammonium sulphamate ($H_6N_2O_3S$), bovine serum albumin (BSA), brefeldin A from *penicillium*, complete Freund's adjuvant (CFA), concanavalin A, dimethyl sulfoxide (DMSO), chondroitinase ABC, cysteine hydrochloric acid (HCL), 3-(4,5-dimethylthiazol-2-yl)-2,5-diphenyltetrazolium bromide (MTT), eriochrome cyanine, *Mycobacterium tuberculosis* H37RA, Dulbecco's Modified Eagle's Medium (DMEM), 10% buffered formalin, Griess reagent for nitrite, ketoprofen, L-α-Lysophosphatidylcholine from egg yolk, phosphate buffered saline (PBS; pH 7.4), pertussis toxin from *Bordetella pertussis,* Roswell Park Memorial Institute 1640 medium (RPMI), heparinase-III, ionomycin, lipopolysaccharide (LPS) from *E. coli* 0111:B4, papain from papaya latex, phorbol 12-myristate 13-acetate (PMA), sodium azide (NaN_3), sodium citrate, sodium nitrite ($NaNO_2$), sodium phosphate (NaH_2PO_4), SIGMA*FAST*® protease inhibitor cocktail tablets, surfen (bis-2-methyl-4-amino-quinolyl-6-carbamide hydrate), and Triton-X-100 were obtained from Sigma-Aldrich Canada (Oakville, ON). Fetal bovine serum (FBS), 10,000 U/ml penicillin/10,000 µg/mL streptomycin solution, 200 mM L-glutamine, 1M 4-(2-hydroyethyl)-1-piperazineethanesulfonic acid (HEPES) buffer solution, and 0.4% trypan blue dye solution were obtained from Invitrogen Canada (Oakville, ON). Ethylene diamine tetraacetic acid (EDTA) was purchased from EM 46 Industries Inc. (Hawthorne, NY). Anhydrous ethyl alcohol was obtained from Commercial Alcohols (Brampton, ON). Purified functional grade anti-mouse CD28 (clone 37.51), purified functional grade anti-mouse CD16/32 (clone 93), and 7-amino-actinomycin D (7-AAD) were purchased from eBioscience (San Diego, CA, USA).

Neutral red was obtained from Fisher Scientific (Nepean, ON). Bio-Rad Protein Assay Dye Reagent, complementaroy deoxyribonucleic acid (cDNA) iScript, and Arium Total ribonucleic acid (RNA) extraction kits were obtained from Bio-Rad Laboratories Inc. (Mississauga, ON). All cell culture plastics were obtained from Sarstedt Inc. (Montreal, QC) unless otherwise specified.

2.3 Antibodies

2.3.1 Used for Flow Cytometry

Phycoerythrin (PE)-conjugated anti-CD25 antibody (Ab), fluorescein isothiocyanate (FITC)-conjugated anti-CD69, PE-conjugated anti-mouse CD3e (clone eBio500A2), APC-conjugated anti-mouse IFN-γ (clone XMG1.2) were all purchased from eBioscience Inc. (San Diego, CA, USA). Alexa Fluor® 488-anti-mouse CD4 (RM4-5), PE-anti-mouse CD3e (145-2C11), PerCP/Cy5.5-anti-mouse CD8a (53-6.7), APC-anti-mouse CD45 (30-F11), and APC-F4/80 (BM8) were obtained from Biolegend (San Diego, CA, USA). FITC-anti-mouse CD11b (M1/70) was purchased from BD Bioscience (Mississauga, ON).

2.3.2 Used for Immunofluorescence

An unconjugated primary mouse anti-CSPG polyclonal Ab was obtained from Sigma-Aldrich Canada (Oakville, ON). An unconjugated rabbit anti-Iba-1 polyclonal Ab was obtained from Wako Chemicals (Wako, Tx, USA). Conjugated fluorescent secondary donkey anti-mouse IgG H&L (Alexa Fluor® 555) and donkey anti-rabbit IgG H&L (Alexa Fluor® 488, pre-adsorbed) Abs were obtained from Abcam (Cambridge, UK).

2.3.3 Used for Enzyme-Linked Immunosorbent Assay (ELISA)

Capture and biotin-conjugated detection antibodies against mouse IFNγ and IL-2 were obtained from eBioscience (San Diego, CA). Multiplexed-ELISA kits for eotaxin, G-CSF, GM-CSF, IFN-γ, IL-1α, IL-1β, IL-2, IL-3, IL-4, IL-5, IL-6, IL-9, IL-10, IL-12 (p40), IL-12 (p70), IL-13. IL-17A, KC, CCL2, CCL3, CCL4, CCL5, and TNF were obtained from Bio-Rad Laboratories Inc. (Mississauga, ON).

2.4 Preparation of Surfen

A stock solution of surfen was prepared in DMSO at a concentration of 60 mM and stored at -20^{o}C in the dark. Surfen binds avidly to cell culture plastics, therefore it was necessary to store it in opaque glass vessels or microcentrifuge tubes pre-saturated with serum-containing medium or a working solution of surfen (i.e. 20 μM in PBS). During experiments, all cell culture plastics were exposed to serum containing media before surfen administration into solution to prevent surfen binding. Pipettes and syringes were saturated with a surfen solution before use. Fresh working solutions of surfen were prepared for each experiment.

2.5 Cell Culture

Cells were maintained at 37^{o}C with 5% CO_2 in 95% humidity unless otherwise specified. Before use, cell suspensions were centrifuged for 5 min at 500 x gravity (g) unless otherwise specified. Cell viability for *in vitro* experimentation was determined using 0.1% trypan blue dye solution (v/v) in PBS. When multiple animals were harvested for *ex vivo* experimentation, cell counts were performed using a Countess® automated cell counter (Thermo Fisher Scientific, Waltham, MA, USA).

2.5.1 Primary Murine T Cell Isolation (Chapter 3)

Mice were euthanized by cervical dislocation and axillary, brachial, and inguinal lymph nodes were isolated under aseptic conditions in a laminar floor hood using sterile Dumont #10 curved forceps (Fine Science Tools, Foster City, USA). Isolated lymph nodes from 2 mice were placed in individual wells of a 6-well plate, containing 4 mL of ice cold PBS per well. The tissue was subsequently homogenized in each well using the grooved end of a plunger from a 10 mL syringe. The homogenate was separated from tissue debris with a pipette, washed with 10 mL of PBS, and centrifuged to collect cells. Erythrocytes were removed via osmotic shock with 20 sec exposure to 4 mL of hypotonic 0.2% NaCl solution followed by addition of 4 mL of hypertonic 1.6% NaCl solution and 2 mL of PBS to restore the solution to an isotonic state. Cells were centrifuged, resuspended in 1 mL of MACS® buffer (2% BSA [w/v], 2 mM EDTA in PBS, pH 7.4), and cell viability assessed with a hemocytometer based on exclusion of trypan blue.

Next, a pre-separation filter (Miltenyi Biotech, Auburn, CA) was placed on a 15 mL polypropylene tube and pre-activated with 1 mL of MACS® buffer to prevent loss of cells on the membrane. Contents of the homogenized lymph nodes were passed through the filter to produce a single-cell suspension. Cells were then centrifuged, resuspended in 450 µL of MACS® buffer, and incubated with 50 µL of a biotin-conjugated Ab cocktail for 10 min at 4°C. This cocktail contained Abs against CD11b (marker for monocytes, macrophages and neutrophils), CD11c (dendritic cells, monocytes, macrophages, neutrophils), CD19 (dendritic cells and B cells), CD45R (B cells, activated T subsets), CD49b (natural killer cells, platelets), CD105 (mesenchymal stem cells), MHC class II (dendritic cells, macrophages, B cells) and Ter-119 (mature erythrocytes and erythroid precursor cells) to enable the negative selection of $CD3^+$ T cells. Following incubation, 400 µL of MACS® buffer along with 100 µL of anti-biotin coated microbeads were added to the Ab cocktail and incubated for 15 min at 4°C. The cocktail was then washed with 10 mL of MACS® buffer and the cells were centrifuged.

Cells were resuspended in 500 µL of MACS® buffer and run through a preactivated MACS® magnetic bead isolation LS column attached to a MACS® separator magnet (Miltenyi Biotech, Auburn, CA). The column was washed with 12 mL of MACS® buffer to elute unbound T cells. Cells were centrifuged and washed with RPMI-1640 medium (Invitrogen, Burlington, ON) supplemented with 10% heat-inactivated FBS, 100 U/ml penicillin, 100 µg/ml streptomycin, 2 mM L-glutamine and 5 mM HEPES (pH 7.4), hereafter referred to as complete RPMI (cRPMI). Cell viability was assessed with trypan blue dye exclusion, and was typically over 95%.

2.5.2 CTLL-2 Cells (Chapter 3)

Cytotoxic lymphoid line-2 (CTLL-2) cells were obtained from the American Tissue Culture Collection (ATCC; Manassas, VA, USA) and maintained in T75 tissue culture flasks containing HEPES-free RPMI-1640 medium supplemented with 10% heat-inactivated FBS and 30 U/ml (6 ng/mL) of recombinant murine IL-2 (Pepro Tech Inc., Rocky Hill, NJ).

2.5.3 Murine L929 Fibroblasts (Chapter 4)

Mouse L929 fibroblasts were obtained from ATCC (Manassas, VA, USA). Cells were maintained in T75 tissue culture flasks at 37^{o}C and 10% CO_2 in DMEM supplemented with 10% FBS, 100 U/mL penicillin, 100 µg/mL streptomycin, 2 mM L-glutamine and 5 mM HEPES (pH 7.4) hereafter referred to as "complete DMEM." At 90% confluence, cells were passaged by detachment with trypsin-EDTA, followed by centrifugation and re-suspension in fresh DMEM media.

2.5.4 Isolation of Primary Murine Bone-Marrow Derived Macrophages (BMDMs) (Chapter 4)

Mice were euthanized by cervical dislocation and bone marrow flushed from both tibia and femurs under aseptic conditions with PBS using a 26_G3/8 PrecisionGlide® needle (Becton Dickinson & Co, Mississauga, ON). A single cell suspension was generated by pressing an 18_G1 PrecisionGlide® needle against the inside wall of a 15 mL polystyrene tube. Erythrocytes were removed by osmotic shock as previously described (section 2.4.1), centrifuged, and washed once in BMDM medium composed of 85% cRPMI and 15% L929-conditioned complete DMEM as a source of macrophage colony stimulating factor. Cells were counted and seeded in 6-well plates at a concentration of 1 x 10^6 cells per well. BMDMs were differentiated over the course of 7 days in BMDM medium. Cells were supplemented with fresh BMDM medium after 3 days of culture, and on day 6 culture medium and non-adherent cells were removed and replaced with fresh BMDM medium. Cells were harvested for experimental use on day 7. Prior to use in experiments on day 7, the BMDMs were detached with EDTA (10 mM in PBS), centrifuged, and re-suspended in fresh cRPMI. The purity of BMDMs was 90% based on surface expression of the macrophage markers F4/80 and CD11b, as measured by flow cytometry (FACSCalibur, BD Bioscience, Mississauga, ON, Canada).

2.6 Cell Seeding Conditions

2.6.1 T Cells

T cells for 7-AAD viability staining (section 2.9.1), Oregon green cell division (section 2.11.2), cell surface staining with fluorescent Ab (2.13), and ELISA (section

2.17) were cultured in 200 µL of cRPMI medium at 1.5 x 10^5 cells/well in 96-well round-bottom plates with at least 2 wells per treatment. In the case of tritiated-thymidine ([^{3}H]TdR) incorporation (section 2.11.1), T cells were cultured at 2.5 x 10^5 cells/well with a minimum of quadruplicate wells per treatment. For surfen binding assays, T cells were cultured at 5 x 10^6 cells/tube in 1.5 mL microcentrifuge tubes containing 1 mL of cRPMI medium.

CTLL-2 cells for [3H]TdR incorporation (section 2.11.1) were cultured at 1 x 10^4 cells/well in 96-well round-bottom plates containing 200 µL of cRPMI medium with at least 4 wells per treatment.

2.6.2 Macrophages

For BMDM nitric oxide assays (Section 2.12), flow cytometry (section 2.13), and multiplexed ELISAs (section 2.17.2.1) cells were seeded in 24-well plates at 2.5x10^5 cells/well in 1 mL of cRPMI medium. Cells were plated at 1 x 10^6 cells/well in a 6-well plate for quantitative real-time polymerase chain reaction (qRT-PCR; Section 2.15) in 3 mL of cRPMI medium. For 7-AAD viability staining (section 2.9.1), MTT assays (2.9.2), and surfen binding (section 2.10), cells were plated in 96-well plates at 1.5 x 10^4 cells/well in 100 µL cRPMI medium.

For all experiments described, BMDMs were detached into solution using 1 mL of 10 mM EDTA for 10 min at RT, transferred to a 15 mL polystyrene tube where the volume was adjusted to 10 mL with PBS, centrifuged, and subsequently washed once with cRPMI prior to use. For 6-well plates, a cell scraper was used to ensure maximal cell detachment and collection.

2.7 Cell Activation

2.7.1 T Cell Activation

For all *in vitro* primary T cell and CTLL-2 experiments, surfen and vehicle treatments were administered 15 min prior to cell activation. T cells were activated using either Dynabeads® Mouse T-Activator anti-CD3/anti-CD28 Ab-coated beads (Invitrogen) for cell surface receptor-mediated activation used at a ratio of 1 bead for every 2 T cells as per manufacturer recommendations. Treatment with PMA and

ionomycin was used to bypass cell surface activation mechanisms. PMA and ionomycin were used at concentrations of 10 ng/mL and 100 ng/mL, respectively.

2.7.2 Macrophage Activation

In all experiments, BMDMs were activated with 100 ng/mL of LPS, except for the Griess assay and iNOS gene expression studies (Section 2.12.3) which used 500 ng/mL. Treatment with surfen was administered 15 min following initial activation to avoid electrostatic interactions between the negatively charged LPS and positively charged surfen that could have altered binding kinetics.

2.8 Flow Cytometry

Fluorescence analysis of primary T cells, BMDMs, and *in vivo* anti-CD3 experiments was performed with a FACSCaliber flow cytometer using BD CellQuest™ software (version 3.3; BD Biosciences) and a minimum of 1 x 10^4 counts per sample. Counts were gated on the live cell population within each sample, except for 7-AAD viability staining in which all cells were included, and data analyzed using FCS Express software (version 3.0; De Novo Software, Thornhill, ON).

2.9 Cell Viability Assays

2.9.1 7-AAD (Chapters 3 & 4)

T cells were activated with anti-CD3/anti-CD28 expander beads, and treated with surfen (1, 2.5, 5, 10, or 20 μM) or vehicle (0.1 % DMSO) for 24 h. Following treatment, T cells were washed with PBS, resuspended in FACS buffer, and labeled with 7-AAD (0.25 μg in 5 μL) for 5 min. Samples were immediately analyzed by flow cytometry. Similarly, BMDMs were collected and treated with surfen (1, 2.5, 5, 10, 20 μM) or vehicle (0.1% DMSO) for 24 h. Labeling with 7-AAD was performed as described above.

2.9.2 MTT Cell Metabolism Assay (Chapter 4)

The metabolic activity of BMDMs treated with surfen (1, 2.5, 5, 10, 20 μM) or vehicle (0.1 % DMSO) was determined using an MTT assay, in which metabolically active cells reduce MTT from its yellow tetrazole form to purple formazan via the

activity of dehydrogenases (Berridge et al., 2005; Mosmann, 1983). Following 24 h of treatment with surfen, 10 µL of MTT solution (5 mg/ml in PBS) was added to each well and the BMDMs were incubated for 2 h at 37°C in a humidified 5% CO_2 incubator. Following incubation, the 96-well plates were centrifuged, supernatants discarded, and 100 µL of DMSO was added to each well to dissolve the formazan and produce the coloured product. Plates were then shaken for 5 min at 550 g on a Microplate Genie (Montreal Biotech Inc., Montreal, QC). The absorbance at 570 nm was read on an Expert 96 microplate reader (Biochrom ASYS, Cambridge, UK). Dehydrogenase activity is directly proportional to the absorbance reading that reflects the number of metabolically active cells in each well (Mosmann, 1983). Percent viability was determined by normalization to the untreated control (100% viable cells), and calculated using the formula ([T/C] x 100), where T is the absorbance value of the treatment well, and C is absorbance value of the untreated control.

2.10 Surfen Cell Surface Binding Assay

2.10.1 T Cells (Chapter 3)

Following the T cell isolation procedure described in section 2.4.1, 5 x 10^6 cells were added to 1.5 mL tubes, resuspended in cRPMI, and incubated with surfen (5, 10, 20 µM) or PBS as a negative control for 2 h at 37°C in a humidified 5% CO_2 incubator. Cells were then washed twice with PBS, and plated onto black Costar® 96-well flat-bottom polystyrene plates (Corning Inc., Corning, NY) at a concentration of 1 x 10^5 cells per well. Fluorescence was read at an emission wavelength of 488 nm in a SpectraMax® M3 luminescence spectrophotometer (VWR, Radnor, PA) using an excitation wavelength of 340 nm.

2.10.2 Macrophages (Chapter 4)

BMDMs were collected and treated with surfen (1, 2.5, 5 µM) or vehicle (0.1% DMSO) for 2 h. A separate group of BMDMs were pre-treated with heparinase-III (0.001 U/ml) or chondroitinase ABC (10 U/mL) for 2 h and washed once with PBS before surfen or vehicle was added at the stated doses for an additional 2 h. The cells were washed twice in PBS to remove excess surfen, and fluorescence read at an emission

wavelength of 488 nm in a SpectraMax® M3 luminescence spectrophotometer using an excitation wavelength of 340 nm.

2.11 T Cell Proliferation Assays

2.11.1 Tritiated-thymidine ([^{3}H]TdR) incorporation (Chapter 3)

To assess [^{3}H]TdR incorporation, cells were treated with either surfen (1, 2.5, 5, 10, or 20 μM) or vehicle (0.02% DMSO) and stimulated with anti-CD3/anti-CD28 expander beads or PMA/Ionomycin. Primary T cells were cultured for 24, 48 or 72 h while CTLL-2 cells were cultured for 48 h. For the last 6 h of incubation, cells were pulsed with 0.2 μCi of methyl [^{3}H]TdR (MP Biochemicals, Irvine, CA). Cells were harvested immediately onto fiberglass filter mats with a Titertek Cell Harvester (both from Skatron Instruments, Sterling, VA). [^{3}H]TdR incorporation into newly synthesized DNA was measured using a Beckman LS6000IC liquid scintillation counter (Beckman Coulter Inc., Mississauga, ON).

2.11.2 Oregon Green Proliferation Assay (Chapter 3)

Primary T cells were labeled with 2 μM Oregon Green 488 dye (Invitrogen) for 15 min at RT. FBS was warmed to 37 ^{o}C and subsequently added to saturate excess dye. The cells were centrifuged, resuspended in 10 mL of warm cRPMI, and incubated for 30 min at 37^{o}C to ensure proper conjugation of the dye within the cells. Next, cells were centrifuged, plated as previously described in section 2.6, treated with either surfen (1, 2.5, 5, 10, or 20 μM) or vehicle (0.2% DMSO) and stimulated for 72 h with anti-CD3/anti-CD28 expander beads (7.5×10^4/well). Cells were analyzed by flow cytometry to calculate the percentage of proliferating cells using ModFit LT software (Verity Software House, Topsham, ME, USA).

2.11.3 *In Vivo* Anti-CD3 Proliferation (Chapter 3)

T cell activation was induced *in vivo* by injecting each mouse intraperitoneally (i.p.) with a 5 μg dose of anti-CD3 Ab in a volume of 200 μL PBS (eBioscience). Mice were pretreated once daily for three days with either vehicle (0.2% DMSO) or surfen (20 mg/kg, i.p.), both dissolved in cRPMI. A single anti-CD3 Ab injection (i.p.) was given 6

h following the final injection of surfen on day 3. Mice were euthanized 24h following administration of anti-CD3 Ab to harvest lymph nodes and obtain $CD3^+$ T cells using methods described in section 2.4.1. Cells were counted and immediately pulsed with [^{3}H]TdR (section 2.11.1) to measure proliferation.

2.12 Macrophage Nitric Oxide (Griess) Assay (Chapter 4)

BMDMs were activated with LPS (500 ng/mL), and treated with surfen (5μM) or vehicle (0.1% DMSO) for 24 h. Supernatants were collected and 100 μL of supernatant was combined with 100 μL of Griess reagent in individual wells of a 96-well flat bottom plate and incubated for 5 min at RT in the dark. Nitric oxide levels for each condition were measured by reading the absorbance at 570 nm using a ELx800 UV universal microplate reader (BioTek Instruments, Winooski, VT) and comparing it with known concentrations of sodium nitrite (Sigma-Aldrich) in PBS using SOFTmax® PRO software (version 4.3; Molecular Devices Corp., Sunnyvale, CA).

2.13 Fluorescent Staining of Cell Surface Markers

Primary T cells were collected, washed once with PBS, and labeled on ice with fluorochrome-conjugated Abs or isotype matched fluorochrome-conjugated control Abs at a concentration of 0.5 μg in 100 μL FACS buffer (containing 0.2% NaN_3 and 1% BSA in PBS) for 45 min in the dark. Cells were then washed twice in FACS buffer, fixed in 300 μL of paraformaldehyde solution, and analyzed by flow cytometry.

In the case of BMDMs, cells were stained as described, washed twice with PBS containing 1% BSA (w/v), resuspended in a volume of 300 μL 1% BSA and immediately analyzed by flow cytometry.

2.14 In Vivo Animal Models of Multiple Sclerosis (Chapter 5)

2.14.1 Induction of EAE

Eighty-one female 6-8 week-old C57Bl/6 mice were immunized on day 0 of the study with myelin oligodendrocyte glycoprotein fragment 35-55 (MOG_{35-55}; Stanford Protein and Nucleic Acid Facility, CA) dissolved in PBS and emulsified in a 1:1 ratio with complete Freund's adjuvant (CFA; Sigma) containing 10 mg/mL of *Mycobacterium*

tuberculosis H37RA. Pertussis toxin (PTX; Sigma, St. Louis, MO, USA), an immune adjuvant, was diluted in sterile Type I water and administered i.p. (500 ng/mouse) on day 0, and again on day 2 after initial inoculation. Forty-eight age, sex, and weight matched C57Bl/6 mice served as antigen controls and received CFA plus PTX but not MOG_{35-55}. On day 0, mice were briefly anesthetized with isoflurane (3 L/min, O_2: 2 L/min) and injected subcutaneously (s.c.) bilaterally at the base of the tail with 100 µL of either the MOG_{35-55} emulsion (300 µg/mouse; EAE group) or CFA alone (200 µL/mouse; CFA group; Figure 1) under aseptic conditions in a biosafety level 2 cabinet. Care was taken to use a fresh needle for every injection to minimize skin irritation. A health check was carried out on day 3 and any animal with lower limb gait disturbances resulting from the immunization procedure was excluded from the study.

2.14.1.2 Group Assignment and Administration of Surfen

The initial presentation of clinical signs occurred between days 7-11, at which point EAE mice were assigned to one of two groups in which the average clinical scores (based on presenting score) for these groups were the same. The antigen control (CFA+PTX) mice were assigned to two groups matched for weight. The EAE and CFA+PTX groups received either vehicle (2.5% DMSO dissolved in PBS [v/v], i.p. every other day (q.a.d); CFA-V, EAE-V) or surfen (5 mg/kg, i.p.; q.a.d; CFA-S, EAE-S). The weight and clinical score of each mouse was recorded daily beginning at day 7. Animals were euthanized on day 21. CNS tissues were harvested from these animals for subsequent analysis as described in detail below (Figure 2).

2.14.1.3 Clinical Scores and Animal Maintenance

The following grading scheme was used to clinically score the animals (Fiander et al., 2017): 0, no clinical signs; 0.5, hooked tail; 1, hooked tail with splay; 1.5, flaccid tail with splay; 2, minor walking deficits, mild ataxia; 2.5, severe walking deficits, chronic ataxia; 3, dropped pelvis in addition to severe walking deficits; 3.5, unilateral hindlimb paralysis; 4, bilateral hindlimb paralysis; 4.5, forelimb paralysis; 5, moribund (Figure 3). The humane endpoint was defined as weight loss greater than 20% for three consecutive days or a clinical score of 5 for three consecutive days, or both. The designation of

"moribund" indicated that the animal displayed severe lateral recumbency deficits in addition to hind limb paralysis and was incapable of independent feeding or hydration.

Mice were supplied with DietGel® Recovery (ClearH20; Portland, ME, USA) and handfed Neutri-Cal® (Evsco Pharmaceuticals; Buena, NJ, USA) as a nutrient supplement when they were no longer able to reach food. Lactated Ringer's solution (50 U/Daily) was provided when a mouse reached a score ≥2.5 or when its weight fell 10% below baseline. A trained observer unaware of the treatment conditions recorded all clinical scores.

2.14.1.4 Flow Cytometry

Single-cell suspensions of immune cells were obtained from the spleen, spinal cord, and cerebellum. Fresh tissue was dissected, dissociated using a razor blade, and then filtered with 70 μm cell strainers to remove debris. Cells were washed in PBS containing 5 mM EDTA, and treated with ammonium chloride buffer for 30 min to lyse contaminating red blood cells. Cells were washed twice, blocked with anti-CD16/32 antibody, and incubated with primary conjugated antibodies as indicated in the results. Following incubation cells were washed twice and fixed with 4% paraformaldehyde prior to flow cytometry acquisition and analysis. Flow cytometry data were collected with a FACSCalibur flow cytometer and CellQuest Pro software (BD Bioscience) or collected with a BD LSRFortessa™ cell analyzer using BD FACSDiva™ software (BD Bioscience). Post-acquisition data analysis was conducted using FCS 6 Express software (DeNovo Software, Los Angeles, CA).

2.14.1.5 T Cell Restimulation Assay

Antigen-specific $CD4^+$ T cell responses to MOG_{35-55} peptide stimulation were analyzed by measuring interferon-gamma (IFN-γ) production. Splenocytes were harvested on day 21 from EAE and CFA control mice treated with either vehicle or surfen were cultured in complete RPMI medium in the presence of MOG_{35-55} peptide (20 μg/mL) and anti-CD28 antibodies (1 μg/mL). At 18 h following T cell stimulation, cells were treated with Brefeldin A (B7651; Sigma-Aldrich, St. Louis, MO) and incubated for an additional 6 h prior to extracellular and intracellular staining for T cell markers (CD3,

CD4, and CD8) and IFN-γ, respectively. The percentage of $CD4^+IFN\text{-}\gamma^+$ cells was analyzed via flow cytometry as described in section 2.14.1.4.

2.14.2 Lysolecithin Induced Demyelination

2.14.2.1 Administration of Lysolecithin into the Corpus Callosum

Female C57BL/6 mice aged 10-12 weeks were anesthetized with isoflurane (3 L/min, O_2: 2 L/min) and placed in a stereotactic frame (Model 900, Kopf). The skin overlying the head was shaved and isopropyl alcohol and 2% betadine applied as antiseptic agents. A vertical incision 1 cm in length was made, beginning above the bregma and extending anteriorly to the lambdoid suture. The skin was retracted and two holes were drilled in the skull, one 2.3 mm posterior and 1.0 mm left of bregma, the other 2.3 mm posterior and 1.0 mm right of bregma. Using a microinjection unit (Model 5000, Kopf), 1 μL of 1% lysolecithin [w/v] dissolved in PBS was injected on each side to a depth of 3.7 mm using a 2 μL Hamilton Neuros® 7001 syringe (Hamilton Company, NV, USA), to target the corpus callosum. To prevent backflow, the needle was kept in place and the lysolecithin permitted to diffuse into the parenchyma for 30 sec before the needle was retracted. The incision was then sutured with 5-0 prolene.

2.14.2.3 Experimental Timeline

Treatment was administered directly into the developing lesion either 2 or 7 days following lysolecithin injection (Figure 4). Mice were anesthetized with isoflurane and the incision was reopened. On the left side, 1 μL of vehicle (2% DMSO dissolved in PBS) was injected using a 2 μL Hamilton Neuros® 7001 syringe (Hamilton Company, NV, USA) through the existing hole at a depth of 3.7 mm. On the right side, 1 μL of 100 μM surfen (Sigma-Aldrich) was injected in a similar manner through the existing hole at a depth of 3.7 mm. The needle was kept in place for 30s, retracted and the incision sutured. Dedicated syringes were used for lysolecithin, vehicle, and surfen administration to prevent cross-contamination.

Sham control mice received an injection of either PBS or needle alone (needle was inserted but no injection was made) on the same days to control for the mechanical

damage of the procedure. Mice were euthanized 2, 7, 14, or 21 days after lysolecithin injection with a lethal dose of sodium pentobarbital (100 mg/kg, i.p.).

2.15 Histology

2.15.1 Preparation of Brain Tissue for Histology

After the administration of sodium pentobarbital on days 2, 7, 14, or 21, mice under deep anesthesia were transcardially perfused with PBS (10.0 mL) followed by 10% buffered formalin (10 mL). This was completed by exposing the thoracic cavity and inserting a $25_G1/4$ PrecisionGlide® needle into the left ventricle followed by an incision into the right atrium to create a continuous circuit. The skull was then carefully resected with blunt forceps and the brain removed and placed in 10% formalin to post-fix for a minimum of 4 days.

Following fixation, the brain was dehydrated overnight in a graded ethanol series of 70%, 95%, and 100%, followed by 100% xylene using a Leica ASP300 tissue processor (Leica Biosystems, Wetzlar, Germany). Tissue was subsequently embedded in Tissue Prep® embedding compound (paraffin; Fisher Scientific, Nepean, ON). Coronal sections 5 μm thick were cut at the level of the corpus callosum using a Leica RM2255 fully automated rotary microtome (Leica Biosystems, Wetzlar, Germany). Serial sections were placed in a 40°C water bath for several minutes and mounted three per slide onto numbered Superfrost® glass slides (Fisher Scientific, Nepean, ON). Tissue was dried in a 37°C oven for 2-3 days to ensure proper adherence to the slide before long-term storage at room temeperature.

2.15.2 Eriochrome Cyanine and Neutral Red Myelin Staining

Brain sections were deparaffinized in 100% xylene and rehydrated in a graded ethanol series of 100%, 95%, and 70%. Tissue sections were placed into Wheaton jars and submerged in tap water for ≈1 min. Next, sections were placed in eriochrome cyanine for 15 min, washed with tap water for ≈1 min, and differentiated in 0.5% ammonium hydroxide (NH_4OH) for 5 s followed by rinsing with tap water. The eriochrome solution consisted of 40 mL of 0.2% eriochrome [w/v] diluted in 0.5% aq. H_2SO_4 [v/v] brought to 50 mL with 2% $FeCl_3$ [v/v] dissolved in type I water. Tissue was counterstained with 1%

neutral red [w/v] for 2 min followed by the removal of excess stain with tap water for ≈1 min. The tissue was dehydrated with a graded ethanol series of 70%, 95%, and 100%, cleared in 100% xylene, and coverslipped using Cytoseal (Stephen's Scientific, Riverdale, NJ, USA).

2.15.3 Immunofluorescence Staining

Brain sections containing lysolecithin lesions as determined by eriochrome cyanine and neutral red staining were deparaffinized in 100% xylene and rehydrated in a graded ethanol series of 100%, 95%, and 70%. Antigen retrieval was performed by submerging sections into sodium citrate buffer (11 mM sodium citrate, 0.05% Tween 20, pH 6.0) and placing them in a decloaking chamber (Biocare Medical, CA, USA) that reached 125°C for 20 min. Sections were washed three times with tris-buffered saline and Tween 20 (TBST; 0.05 M Tris/HCl, 0.15 M NaCl, 0.05% Tween 20, pH 7.6; Agilent Technologies, CA, USA) and blocked for 1 h with donkey serum (Vector Laboratories Inc., CA, USA). Primary Abs were diluted in TBST and placed directly on each section and incubated for 18 h at RT in the dark using a Simport StainTray™ (Simport Scientific, Beloeil, QC). Next, sections were washed three times with buffer and fluorescent conjugated secondary Ab were diluted in TBST and placed directly on the sections for 2 h at RT in the dark. Lastly, sections were washed three times with TBST to remove excess secondary and immediately coverslipped using Vectashield® mounting medium for fluorescence with DAPI (Vector Laboratories Inc., CA, USA). Slides were sealed to prevent tissue desiccation using a generic nail polish.

Primary and secondary Ab concentrations were determined with titration experiments on lesioned tissue using the manufacturer recommended dilutations as a reference point. To ensure signal specificity, all immunohistochemistry was carried out in parallel with control sections incubated without primary antibody.

2.15.4 Electron Microscopy

Following sacrifice on day 7, brains were removed from mice administered lysolecithin on day 0 and treatment on day 2 without transcardial perfusion. Brains were gross dissected using the needle tracks as a guide and the corpus callosum was resected and placed in a solution of 3.5% glutaraldehyde and post-fixed for a minimum of 1 week. The fixative was

removed and washed with Sorensen's phosphate buffer (0.2M Na_2HPO_4, pH 7.4-7.6) for 2 min. The tissue was then treated with 1% osmium tetroxide (1 h, 4^oC), rinsed in buffer solution (2 min) and passed through a graded series of ethanols (70%, 100%, 100%, 15 min each) followed by treatment with propylene oxide (15 min on mixer, removed and repeated once). Embedding resin was then added to the tissue (1h on mixer, then added again for 1 more hour) and resin was also added to an embedding mold, prewarmed in a 70^oC oven. The tissue was transferred to the mold and kept at 70^oC overnight before cooling to RT. Ultrathin sections were cut with a diamond knife using an ultra microtome. The resulting grids were then stained with uranyl acetate (8 min), washed three times in 30% ethanol (10 s each wash) and then stained with lead citrate (8 min) and washed three times in distilled water (10 s each wash). The grids were dried, mounted and examined with a Hitachi TT7700 transmission electron microscope. Electron photomicrographs were obtained for different lesions, and stored in image files, coded to blind their identity during image analysis (section 2.16.3 below).

2.16 Image Analysis

2.16.1 Lysolecithin Lesion Quantification

Slides were imaged using an Aperio AT2 Digital Pathology scanner at 20X magnification (Leica Biosystems, Wetzlar, Germany). This scanner is capable of recording photomicrographs of each section of the mouse brain at multiple levels of magnification (5X, 10X, 20X). The size of the lesion was determined using Aperio ImageScope software (Leica Biosystems, Wetzlar, Germany), in which the region of demyelination within the corpus callosum was manually traced with a Wacom Intuos® touch tablet (Wacom Co. Ltd, Kazo, Japan) and the area was calculated in μm^2. The area of the lesion on each section was summed to represent the total lesioned area per hemisphere.

2.16.2 Immunohistochemistry Quantification

Representative photomicrographs of sections that displayed immunoreactivity in the lesioned area of the corpus callosum were captured at 100X amplification (10X objective and a 10X lens) using a Zeiss Axio Imager Z2 fluorescent microscope (Zeiss AG, Oberkochen, Germany). Image quantification was performed using ImageJ software

(NIH version). Briefly, preprocessing involved background substraction and application of a noise reduction filter. Next, a global threshold was set to define detection levels across all micrographs. Lastly, fluorescent intensities were quantified in terms of pixel counts translated to area by a scale bar.

2.16.3 Electron Microscopy G-Ratio Quantification

Myelination for individual nerve fibers in the corpus callosum (where all fibers are normally myelinated) was calculated using the ratio of the axon circumference to the full circumference (including myelin sheath, if present) of the fiber (G-ratio) using ImageTrak software (written by Dr. Peter Stys; http://www.ohri.ca/stys/imagetrak). Briefly, lesion electron photomicrographs were imported into the ImageTrak and each axon along with its respective myelin sheath was manually traced with a Wacom Intuos® touch tablet by an observer unaware of the treatment conditions. G-ratios were automatically calculated, and a minimum of 100 axons were counted per lesion. A ratio of 1 represents a completely denuded axon, whereas a ratio of 0.5 would be an average ratio of a large caliber axon.

2.17 ELISA Protein Quantification

2.17.1 *In Vitro* Plated Cytokine Assays (Chapter 3)

T cells were treated with either surfen (10 μM) or vehicle (0.1% DMSO) and activated with anti-CD3/anti-CD28 expander beads for 24 h. Supernatants were harvested and analyzed for the cytokines IL-2 and IFN-γ by sandwich-ELISA kits (BD Biosciences). In brief, Costar® 96-well flat-bottom high binding chemistry enzyme immunoassay plates (Corning Inc., Corning, NY) were coated overnight at 4°C with capture Ab diluted in coating buffer (0.1 M Na_2CO_3 [pH 9.5]). Plates were then washed 3 times with wash buffer (0.05% Tween-20 [v/v] in PBS) and blocked with assay diluent (10% FBS [v/v] in PBS) for 1 h at ambient temperature. Plates were then washed again (3X) and supernatants and recombinant cytokine standards were added and incubated overnight at 4°C. Plates were washed as described and incubated with biotinylated detection Ab and streptavidin-HRP together for 1 h. Plates underwent five 1 min washes

prior to the addition of the substrate solution (tetromethylbenzidine) to reduce background noise.

After sufficient color had developed (15-30 min), stop solution (0.3 M sulfuric acid) was added to the wells, and the absorbance of the plates was read at 450 nm on a ELx800 UV universal microplate reader using KCJunior software (version 1.17; BioTek Instruments, Inc.). Further analysis of the absorbance readings was performed using SOFTmax® PRO software (version 4.3; Molecular Devices Corp., Sunnyvale, CA) to quantify the cytokine concentrations in relation to the experimental standards.

2.17.2 Multi-plexed ELISA

Multiplexed ELISAs were conducted using the Bio-Plex® suspension array system that utilizes Luminex® xMAP® multiplexing technology to detect up to 100 cytokines in a single sample with a dynamic range capable of detecting 1-32 000 pg/mL of protein. The system works by using fluorescent monodisperse polystyrene beads conjugated with antibodies against a specific cytokine epitope. A flow cytometer equipped with a dual laser detector measures fluorescence emitted from the surface of monodisperse polystyrene beads and matches the spectra to a specific epitope while a high-speed digital signal processor quantifies the fluorescent signal (Houser, 2012).

2.17.2.1 BMDM Supernatants (Chapter 4)

BMDMs were collected, treated with either surfen (5 μM) or vehicle (0.1% DMSO), then activated with LPS, and incubated for 24 h. A separate cohort of BMDMs was identically treated with surfen or vehicle but not activated with LPS to serve as negative controls. Culture supernatants were then collected and stored at -80^{o}C prior to analysis. Cytokine levels in the supernatants were assessed using a Bio-Plex Pro™ premixed 8-plex mouse cytokine kit (Bio-Rad, Hercules, CA, USA) that measures the level of the cytokines IL-1β, IL-6, IL-10, TNF and the chemokines KC, CCL2, CCL4, CCL5. A standard curve was constructed using a 4-fold dilution series of beads with a known fluorescence spectrum unique to each cytokine. Standards were reconstituted in a standard diluent that closely matches the medium of the supernatant.

Magnetic anti-cytokine Ab conjugated beads (50 µL/well) were added to the wells of a 96-well plate and washed twice with 100 µL of assay buffer. Each sample was measured in duplicate wells, by adding 50 µL of undiluted supernatant to each well. The plate was covered and incubated in the dark at room temperature (RT) on a shaker set at 850 rpm for 30 min followed by 3 washes. Next, biotinylated detection Ab was added to each well and incubated in the dark at RT on a shaker set at 850 rpm for 30 min followed by 3 washes. Lastly, streptavidin-PE (50 µL) was added to the wells and incubated in the dark at RT on a shaker set at 850 rpm for 10 min. Lastly, beads were washed 3 times, resuspended in assay buffer and analyzed with the Bio-Plex® 200 Suspension Array System (Bio-Rad). Data was acquired using Bio-Plex Manager software version 6.1 with five-parameter logistic regression curve fitting (Bio-Rad).

2.17.2.2 EAE Spinal Cords (Chapter 5)

Protein extracts from EAE and CFA control spinal cord tissue were obtained by homogenization in 500 µL of PBS containing SIGMA*FAST*® protease inhibitor cocktail tablet (2 mM 4-[2-aminoethyl] benzenesulfonyl fluoride, 14 mM E-64, 130 µM bestatin, 1 µM leupeptin, 0.3 µM aprotinin, and 1 mM EDTA). Tissue was homogenized on ice for 1 min using a Pro 200 handheld homogenizer (Pro Scientific Inc., CT, USA). Homogenates were centrifuged at 10 000 x g for 10 min, supernatants collected, and protein concentrations determined using a Bradford protein assay. The supernatants were adjusted to a working concentration of 500 µg/mL in PBS containing protease inhibitor and stored at -80^{o}C prior to use.

A Bio-Plex Pro™ premixed 23-plex mouse cytokine kit was used to measure eotaxin, G-CSF, GM-CSF, IFN-γ, IL-1α, IL-1β, IL-2, IL-3, IL-4, IL-5, IL-6, IL-9, IL-10, IL-12 (p40), IL-12 (p70), IL-13. IL-17A, KC, CCL2, CCL3, CCL4, CCL5, and TNF. Standards were reconstituted with PBS buffer containing protease inhibitor and a 0.1% BSA [w/v] carrier. The remainder of the assay was performed as described in section 2.17.2.1.

2.18 Quantitative Reverse-Transcription Polymerase Chain Reaction (qRT-PCR)

All qRT-PCR experiments were conducted in accordance with the Minimum Information for Publication of Quantitative Real-Time PCR Experiments (MIQE) guidelines (Bustin, 2010; Taylor et al., 2010).

2.18.1 Tissue Preparation for RNA Extraction

2.18.1.2 BMDMs (Chapter 4)

BMDMs were collected, treated with either surfen (1, 2.5, 5 μM) or vehicle (0.1% DMSO), then activated with LPS for 4 h. A separate cohort of BMDMs was treated with surfen but not activated to serve as negative controls. Supernatants were removed, cells washed with PBS, and 345 μL of RLT cell lysis buffer (Qiagen, Toronto, ON) was administered to each well. Lysis buffer from each sample was collected into RNase free 1.5 mL microcentrifuge tubes and temporarily stored at -80°C until RNA extraction 2-3 days later.

2.18.1.3 EAE Spinal Cord (Chapter 5)

Following death, the spinal cord from each animal was collected, immediately submerged in RNAlater stabilization reagent (Qiagen, Toronto, ON), and stored at -20 °C until RNA extraction 1-2 months later.

2.18.2 RNA Extractions and Quality Control

2.18.2.1 BMDMs

RNA was harvested using an RNeasy Mini Kit purchased from Qiagen (Toronto, ON) following the procedures outlined by the manufacturer. The purity and concentration of each RNA sample was determined using a NanoDrop 2000 device (ThermoFisher Scientific, MA, USA). The purity of the sample was based on the ratio of absorbance at 280 nm over 260 nm (A_{280}/A_{260} ratio) with a value between 1.7-2.0 considered acceptable (Taylor et al., 2010). Samples were then stored at -80°C for future use.

2.18.2.2 EAE Spinal Cord

Spinal cord tissues from EAE and CFA control mice were removed from RNAlater stabilization reagent and placed in 2 mL tubes containing 1.5 mm triple-pure zirconium beads (Benchmark Scientific Inc., NJ, USA) and 1 mL of PureZol™ RNA isolation reagent (Bio-Rad Laboratories Inc., Mississauga, ON). Spinal cord tissues were thoroughly homogenized by placing the bead-filled tubes into a BeadBug microtube homogenizer (Benchmark Scientific Inc., NJ, USA) for 45 sec at 4000 rpm. Total RNA was extracted from the homogenized PureZol™ RNA reagent using an Aurum™ Total RNA Fatty and Fibrous Tissue kit (Bio-Rad) following the procedures outlined by the manufacturer.

To measure the concentration, quality and overall purity of isolated total RNA, an Experion RNA StdSens Analysis Kit (Bio-Rad, Hercules, CA, USA) was used in conjunction with an Experion bioanalyzer system. Total RNA (1 µL) from each spinal cord was run on an Experion RNA StdSens chip equipped with a dynamic range capable of detecting RNA concentrations from 5-5000 ng/µL. Briefly, a florescent dye interacts directly with the nucleic acids that are quantified by detection of laser-induced fluorescence using microfluidic electrophoresis technology to create a virtual gel for quantification to take place. Quality of the RNA samples was determined using an RNA quality indicator (RQI) that reports a number between 1 (very degraded RNA) to 10 (intact RNA). Any given sample must have obtained a RQI value ≥7 to be considered acceptable for downstream qRT-PCR experiments (Figure 4A; Taylor et al., 2010). RQI values are determined by comparing the ribosomal peaks of the 28S region, 18S region, and the pre-18S region from the electropherogram of the RNA sample relative to a series of standardized degraded RNA samples (Figure 4B). Conditional upon passing quality control, total RNA from each sample was aliquoted and stored at -80 °C.

2.19 cDNA Synthesis

Following total RNA isolation, approximately 500 ng of RNA from BMDM samples and 1000 ng of RNA from EAE and CFA control spinal cords were reverse transcribed using an iScript Advanced cDNA synthesis kit (Bio-Rad, Hercules, CA, USA). The iScript reaction mix (4 µL) and iScript reverse transcriptase (1 µL) were

added to 10 µL of nuclease-free water and 5 µL of input RNA. The reaction was incubated in a Bio-Rad T100^{TM} Thermocycler using the following reaction protocol: 20 min at 46°C, 1 min at 95°C, and 5 min at 25°C. Once synthesized, cDNA was stored at -20°C for future use. A no-RT control reaction was included in every run to control for genomic DNA carryover by replacing reverse transcriptase volume with nuclease-free water.

2.20 qRT-PCR Experimental Protocol

Transcript expression studies were conducted using SsoAdvanced Universal SYBR Green Supermix® (Bio-Rad, Hercules, CA, USA). Mouse KiCqStart® SYBR® Green Primers were purchased from Sigma-Aldrich Canada (Oakville, ON; Table 1). Each primer set contained a GC content of between 50-60%, no secondary structure, melting temperature between 60°C ± 5°C, and was between 18-24 base pairs long (Table 1). Before experimentation, the optimal annealing temperature for each primer set was determined with a temperature gradient that ranged from 53.0°C – 65°C in 2° increments using a CFX 96 Touch™ real-time PCR detection system with CFX manager 2.1 software (Bio-Rad, Hercules, CA, USA). The temperature which produced the lowest quantitation cycle value was chosen as the optimal annealing temperature for that specific primer pair. Next, the linear dynamic range of the samples was established for each primer set by pooling 2 µL of cDNA from each sample cDNA sample and making a two-fold serial dilution series that ranged from 1/5 to 1/640. Primer efficiency was calculated using the pooled cDNA standard curve and was kept within 90-105% with an R^2 value >0.980. Subsequent cDNA dilutions were specific to each primer set based on efficiency results.

Housekeeping genes were determined by calculating a geNorm "m-value". The m-value represents the maximum amount of heterogeneity across experimental groups that can be tolerated by any given housekeeping gene and must be a value ≤ 1 (Taylor et al., 2010). For BMDMs the optimal housekeeping gene was determined to be GAPDH whereas EAE and CFA control spinal cord tissues required GAPDH along with HPRT1 to determine relative expression. The gene B2M was also tested but produced an m-value >1 for spinal cord tissues.

PCR amplification and fluorescence detection were performed in triplicate using a CFX 96 Touch™ real-time PCR detection system with CFX manager 2.1 software. PCR cycling conditions were 95°C for 30 sec, followed by 40 cycles of 95°C for 30 sec and the experimentally determined annealing temperature (Table 1) for 20 sec. To confirm that the PCR reaction had produced the appropriate products, a melt curve analysis was conducted with temperatures ranging from 65-95°C in 0.5°C increments for 5 sec each. Results are expressed as relative changes from the housekeeping calibrators and calculated using the $2^{-\Delta\Delta Ct}$ method (Livak and Schmittgen, 2001).

2.21 Statistical Analyses

Where two groups were compared, Student's t-test and Mann Whitney U test were used to calculate differences between groups with normal and non-Gaussian distributions, respectively. Comparison between three or more groups was performed using a one-way ANOVA with Tukey's post-hoc analysis. EAE curves were analyzed using a two-way ANOVA followed by Bonferroni's post-hoc analysis. Correlations were computed between clinical scores and either protein concentrations or mRNA levels using a Spearman correlation. Area under the curve and the number of days with a clinical score greater than 2.5 were used as additional measures of EAE disease severity, as per the recommendations of Baker & Amor (2012). All statistics were computed using GraphPad Prism version 7.0 for Macintosh (GraphPad Software, San Diego, CA). Differences between groups for all tests were considered statistically significant at an alpha level of less than 0.05.

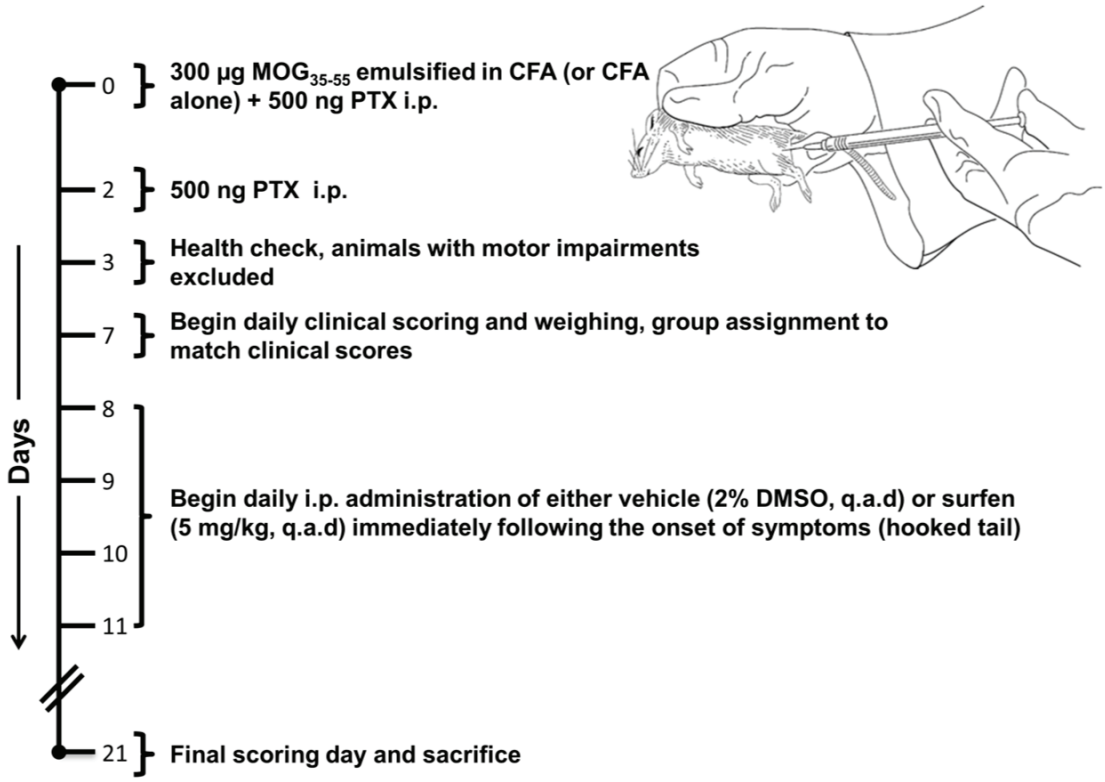

Figure 2.1: Timeline for CFA, MOG_{35-55} and PTX injections, determinations of bodyweight and clinical score, group assignments and sacrifice. Female adult C57BL/6 mice (6-8 weeks old) were immunized with MOG_{35-55} emulsified in a 1:1 ratio with CFA containing 0.5 mg/ml of *Mycobacterium tuberculosis* H37RA (EAE group). Age, sex, and weight matched C57BL/6 mice served as antigen controls and received CFA and pertussis toxin but not MOG_{35-55} (CFA group). On day 0, MOG_{35-55} (300 µg/mouse) or CFA alone (200 µL/mouse) was injected s.c. bilaterally at the base of the tail. PTX, an immune booster, was diluted in saline and administered i.p. (500 ng/mouse) on day 0, and again on day 2 to both groups. A health check was carried out on day 3 and scoring began on day 7. Initial presentation of clinical signs occurred between days 7-11, at which point mice in both the EAE and CFA groups were subdivided and randomly assigned to either a treatment group (5 mg/kg surfen, q.a.d) or a vehicle group (2% DMSO, q.a.d). The weights and clinical scores of each individual mouse were recorded daily over 21 days, at which point mice were euthanized and tissues were collected for downstream analyses.

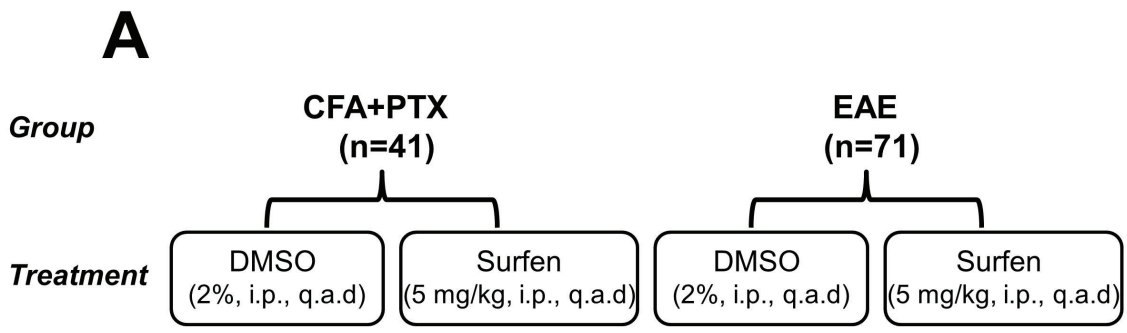

B

Technique	Sample Size	Tissue Type
qRT-PCR 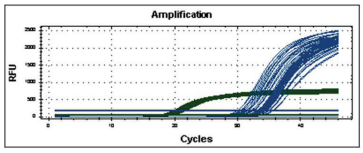	**CFA-V = 5** **CFA-S = 5** **EAE-V = 8** **EAE-S = 8**	**Spinal Cord**
Multi-Plex ELISA 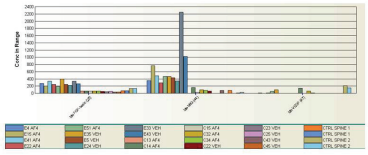	**CFA-V = 6** **CFA-S = 6** **EAE-V = 10** **EAE-S = 10**	**Spinal Cord**
Flow Cytometry 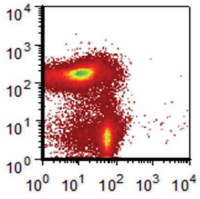	**CFA-V = 10** **CFA-S = 9** **EAE-V = 17** **EAE-S = 18**	**Spleen, Spinal Cord, and Cerebellum**

Figure 2.2: Experimental group assignment, techniques, and associated time points analyzed. **(A)** Female C57BL/6 mice were injected with CFA+PTX alone (n=47) or immunized with MOG_{35-55} and received either vehicle (2% DMSO) or surfen treatment (5 mg/kg/day, p.o). **(B)** Tissue was harvested at day 21 and processed for qRT-PCR, Bio-Plex multi-plexed ELISAs, and flow cytometry.

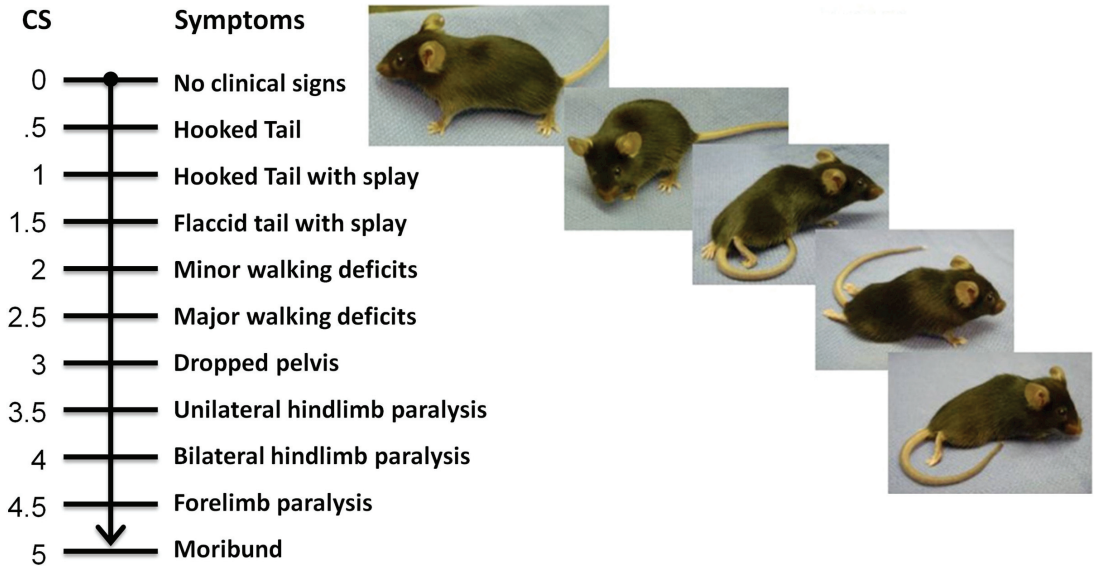

Figure 2.3: Grading scheme for clinical disease course in EAE. The following grading scheme was used to clinically score the animals (CS): 0, no clinical signs; 0.5, hooked tail; 1, hooked tail with splay; 1.5, flaccid tail with splay; 2, beginning of walking deficits with mild ataxia; 2.5, severe walking deficits with chronic ataxia; 3, dropped pelvis in addition to severe walking deficits; 3.5, unilateral hindlimb paralysis; 4, bilateral hindlimb paralysis; 4.5, forelimb paralysis 5, moribund. All clinical scores were recorded by an observer unaware of the treatment conditions. Mouse pictures from Peggy Ho (Stanford University).

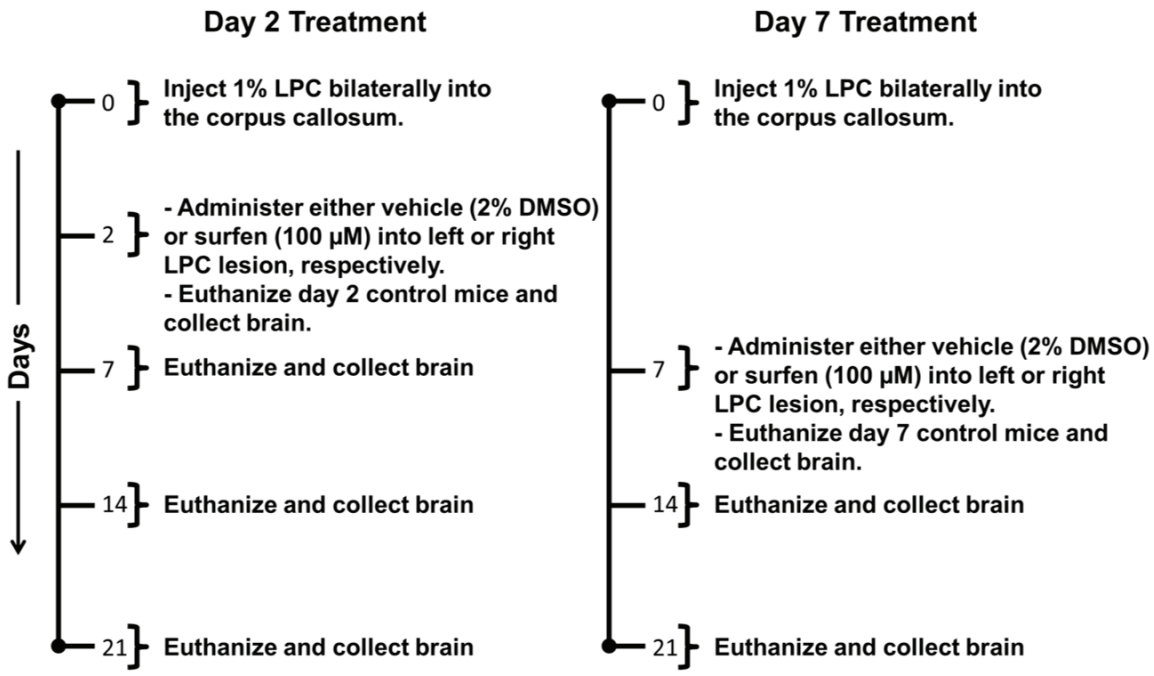

Figure 2.4: Experimental timeline of lysolecithin induced demyelination and treatment with surfen.

Lane	Sample Name	RNA Area	RNA Concentration (ng/µl)	Ratio [28S/18S]	RQI
L	Ladder	500.22	160		
1	**Spinal Cord** *Sample 1*	1047.26	553.32	1.26	9.6
2	**Spinal Cord** *Sample 2*	1052.81	556.24	1.30	9.7
3	**Spinal Cord** *Sample 3*	1050.89	555.21	1.32	9.7
4	**Spinal Cord** *Sample 4*	1108.92	585.89	1.33	9.7

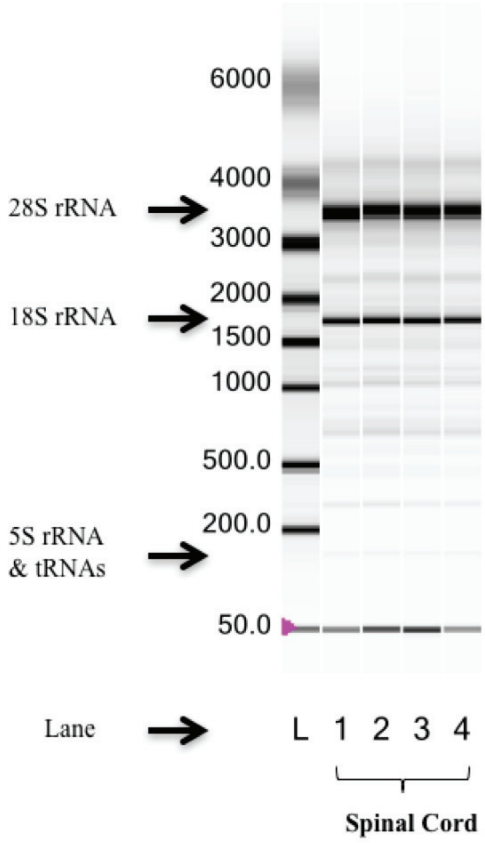

Figure 2.5: Experion automated electrophoresis RNA quality control system. (A) Results table detailing concentration, 28S/18S data, and RNA quality indicator (RQI) (B) Virtual gel of representative RNA samples from cerebellum, and spinal cord tissue.

Table 2.1: Primers used for qRT-PCR. For each respective sample, a total of 1000 ng of total RNA was reverse transcribed to generate first-strand cDNA and amplified using SsoAdvanced Universal SYBR Green Supermix® (Bio-Rad, Hercules, CA, USA). Mouse KiCqStart® SYBR® Green Primers were purchased from Sigma-Aldrich Canada (Oakville, ON).

Gene Name	*Annealing Temperature °C*	*Forward (5' - 3')*	*Reverse (5' - 3')*
Agrin	55	TGTGACTGAGAGTGAGAAAG	TAGGTCATAGCTCAGTTGTAG
Aggrecan	58	CTACCTTGGAGATCCAGAAC	TGGAACACAATACCTTTCAC
Perlecan	58	TATACCAAGGAGACAAGGTG	GCTTCCCAAAGCTTCTTATC
Serglycin	61.5	ATCTTCAGTGCAAGGTTATC	GAGATGAAATCTTTTGAGGGTC
Syndecan 1	58	CTTCTGTCATCAAAGAGGTTG	CAAAGGTGAAGTCTTGTTCTC
Syndecan 4	61.5	CAACCAAAGTATCCATGTCCAG	TTTGTAGATGGGTTTCTTGC
NDST1	60	GCTTCCCAAAGCTTCTTATC	AAGAACTCCATGTACCAGTC
Neurocan	58	CAACACAGGACTGCAATATG	ATAGGGTAGGTTGTAGTTGC
Versican	60	TGTTATCCTACCGAGACTTC	CATGTCTCAGTGTCTTGTTC
Tbet	60	GCCAGGGAACCGCTTATATGTC	CTGTGAGATCATATCCTTGGGCTG
RoRγT	60	TGCAAGACTCATCGACAAGG	AGGGGATTCAACATCAGTGC
GATA3	57.9	TATTAACAGACCCTGACTATG	CACCTTTTTGCACTTTTTCG
FoxP3	60	CCCATCCCCAGGAGTCTTG	ACCATGACTAGGGGCACTGTA
IL-12p40	58.4	AGGTCACACTGGACCAAAGG	TGGTTTGATGATGTCCCTGA
IL-1β	60	GAAATGCCACCTTTTGACAGTG	CTGGATGCTCTCATCAGGACA
IL-6	60	CTGCAAGAGACTTCCATCCAG	AGTGGTATAGACAGGTCTGTTGG
TNF	59	CAGGCGGTGCCTATGTCTC	CGATCACCCCGAAGTTCAGTAG
iNOS	60	CAGCTGGGCTGTACAAACCTT	TGAATGTGATGTTTGCTTCGG
Argenase-1	60	TTAGGCCAAGGTGCTTGCTGCC	TACCATGGCCCTGAGGAGGTTC
IL-10	60	ACAGCCGGGAAGACAATAACT	GCAGCTCTAGGAGCATGTGG
MMP2	55	TGGCAAGTACGGCTTCTGTC	TTCTTGTCGCGGTCGTAGTC
MMP9	58	GCACGACGTCTTCCAGTA	GCACTGCAGGATGTCATAGGT
CCL2	61.5	TCTGGGCCTGCTGTTCACA	GGCGTTAACTGCATCTGGCT
CCL3	61.5	TTCTCTGTACCATGACACTC	CTCTTAGTCAGGAAAATGACAC
CCL4	57.9	GGTATTCCTGACCAAAAGAG	TCCAAGTCACTCATGTACTC
CCL5	62.5	GCTGCTTTGCCTACCTCTCC	TCGAGTGACAAACACGACTGC
FGF2	61.5	CTGGCTTCTAAGTGTGTTAC	GAAGAAACAGTATGGCCTTC
VEGF	60	TCTCGCCATCTTTTATCTCCCAG	CAGAACCCAAATCCCGTTATT
TGFβ	60	AGCTGGTGAAACGGAAGCG	GCGAGCCTTAGTTTGGACAGG
GAPDH	60	AGGTCGGTGTGAACGGATTTG	GGGGTCGTTGATGGCAACA
HPRT1	60	TCAGTCAACGGGGGACATAAA	GGGGCTGTACTGCTTAACCAG

CHAPTER 3

MURINE T CELL ACTIVATION IS REGULATED BY SURFEN (BIS-2-METHYL-4-AMINO-QUINOLYL-6-CARBAMIDE)

Portions of this manuscript appeared in the following publication:
Warford, J., Doucette, C.D., Hoskin, D.W., Easton, A.S., 2014. Murine T cell activation is regulated by surfen (bis-2-methyl-4-amino-quinolyl-6-carbamide). Biochem. Biophys. Res. Commun. 443, 524–30. *Reprinted with copyright permission.*

Student Contributions to Manuscript: JRW performed all *in vivo* assays and the majority of the *in vitro* assays (75%). JRW contributed to the experimental design. Several replicate experiments included in Figures 3.1, 3.2, and 3.4 were performed with the assistance and intellectual contributions of CDD. Both DWH and EAS provided experimental guidance and assisted with reagents. JRW and ASE co-wrote the manuscript.

3.1 Introduction

There is considerable interest in characterizing the biological function of proteoglycans, given their ubiquitous expression and ability to bind hundreds of proteins including proteases, adhesion molecules, cytokines and chemokines. The interaction is often charge-based since proteoglycans and their GAG side chains have a high affinity for cationic (basic) proteins; however, this is not the only mechanism because proteoglycans can also bind to anionic (acidic) proteins (Xu and Esko, 2014). The major classes of GAG side chains in proteoglycans are heparan sulphate, heparin, chondroitin sulphate, dermatan sulphate, keratin sulphate and hyaluronic acid (Proudfoot, 2006).

Surfen (*bis*-2-methyl-4-amino-quinolyl-6-carbamide) was first described in 1938 as a component of depot insulin (Umber et al., 1938); however, subsequent studies have revealed its efficacy in binding to the GAG side chains of proteoglycans. Surfen contains four quinoline rings that contain positively charged amino or methyl groups. When characterized further, surfen was found to bind with greatest avidity to heparin, followed by dermatan sulphate, heparan sulphate and chondroitin sulphate (Schuksz et al., 2008). There are now a handful of studies on the biological effects of surfen, many of which relate to its ability to block the interaction between proteoglycan side chains and signaling proteins. These include effects on growth factors (fibroblast growth factor and vascular endothelial growth factor) and fibrils associated with the binding of human immunodeficiency virus (HIV)-1 to target cells (Roan et al., 2010; Schuksz et al., 2008; Xu et al., 2011).

The capacity of surfen to bind to many different targets raises the possibility that it may influence immune function. This opening chapter of my thesis details the effects of surfen on murine T cell activation, as an initial attempt to describe its immunomodulatory properties. The results informed our approach to the more complex animal models detailed in subsequent chapters. This chapter shows that surfen decreases T cell proliferation *in vitro* and *in vivo* and that these effects are related to cell surface binding. These results have implications for the function of proteoglycans in regulating T cell activation and they hold potential for downstream therapeutic development, based on detailed work in animal disease models, as we go on to describe. Although GAG synthesis, secretion and cell surface expression on T cells has been documented in several

studies (Christmas et al., 1988; Fadnes et al., 2012; Jones et al., 2005; Levitt and Ho, 1983; Shao et al., 2013; Steward et al., 1990; Teixé et al., 2008), the effects of a proteoglycan antagonist on T cells had not been reported prior to the publication of this work.

3.2 Results

3.2.1 Surfen reduces T cell proliferation *in vitro* and *in vivo*

$CD3^+$ murine T cells were stimulated with T cell expander beads, which resulted in an increase in proliferation as measured by [^{3}H]TdR incorporation that peaked at 48 h (Figure 3.1B). The presence of surfen during activation resulted in a dose-dependent reduction in [^{3}H]TdR incorporation. For wells stimulated for 24, 48, or 72 h, incorporation was significantly reduced at 10 and 20 μM compared to vehicle (Figure 3.1). Confirmation of the anti-proliferative effects of surfen was obtained by staining T cells with Oregon Green 488 dye, and analyzing the percentage of T cells undergoing proliferation for a period of 72 h (Figure 3.2A). Comparable dose-dependent reductions in proliferation were observed at 2.5, 5, 10 and 20 μM relative to vehicle. To assess whether the reduced T cell proliferation could be due to a toxic effect of surfen, T cells were stained with the viability marker 7-ADD (Figure 3.2B). At a dose of 20 μM surfen significantly reduced the percentage of viable cells by ≈ 33% relative to vehicle controls. By comparison, 20 μM surfen reduced proliferation via Oregon green dilution by ≈ 80% and [^{3}H]TdR incorporation by ≈ 88% compared to vehicle controls. The marked reduction in proliferation relative to cell death indicates that the effects of surfen are largely not due to toxicity.

To assess the *in vivo* efficacy of surfen, mice were treated with vehicle (2% DMSO, i.p.) or surfen (20 mg/kg, i.p.) for 3 days followed by anti-CD3 Ab injection (5 μg, i.p.) 6 h after the last treatment with surfen. T cells were isolated 24 h later and tested for [^{3}H]TdR incorporation in culture (Figure 3.3). Administration of anti-CD3 Ab induced significant uptake of [^{3}H]TdR in vehicle controls relative to naïve mice that received no treatment or anti-CD3 Ab. In contrast, [^{3}H]TdR incorporation in T cells from surfen treated mice remained similar to levels observed in naïve control mice and was significantly reduced relative to CD3 stimulated T cells from vehicle treated mice (Figure

3.3A). This effect is also present when the data is expressed as a proliferation index, dividing anti-CD3 proliferation results by those observed in naïve untreated mice (Figure 3.3B). As additional confirmation, there was a significant reduction in total cell counts for the lymph nodes removed from surfen treated mice relative to vehicle controls (Figure 3.3C). These data show that surfen reduces T cell proliferation following activation *in vitro* and *in vivo*.

3.2.2. Surfen reduces CD25 expression *in vivo* but not *in vitro*

T cells were labeled to detect the proportion of cells that express the cell-surface activation markers CD25 and CD69. T cells from mice treated with anti-CD3 Ab (5 μg, i.p.) and surfen (20 mg/kg, i.p.) exhibited reduced CD25 expression with no significant effect on CD69 compared to vehicle treated mice (Figure 3.4A). By contrast, there was no observed reduction in CD25 or CD69 in isolated T cells stimulated *in vitro* with T cell expander beads in the absence or presence of 10 μM surfen (Figure 3.4B). Additional information was obtained using CTLL-2 cells, whose growth is IL-2 dependent (Doucette et al., 2015). Surfen between 1-20 μM had no significant effect on [^{3}H]TdR incorporation in these cells (Figure 3.5A). Surfen treatment (10 μM) also had no significant effect on IL-2 (Figure 3.5B) or IFN-γ (Figure 3.5C) production following anti-CD3/anti-CD28 activation.

3.2.3 The inhibitory effect of surfen is receptor dependent and inhibited by heparin sulfate

Since surfen had effects on T cell receptor driven proliferation, the binding kinetics of surfen were assessed. Previous work by Schuksz et al. (2008) had demonstrated that surfen emits a fluorescent signal when excited at 340 nm, with an emission maximum of 488 nm. Following incubation of murine T cells with surfen for 2 h, a dose-dependent increase in fluorescence was observed (Figure 3.6A). As a positive control, surfen (20 μM) was incubated with its high affinity binding partner heparin at doses that ranged from 500 mg/mL to 62.5 mg/mL (Figure 3.6B). Again, a dose dependent increase in fluorescence was obtained.

Next, PMA/ionomycin was used to bypass surface receptor activation (Figure 3.7A). Co-treatment with surfen increased proliferation at 10 μM but had no effect at

other doses (2.5, 5, 20 μM). To explore the binding of surfen to GAGs and proteoglycans on T cells, it was combined with heparin sulfate at increasing doses which induced a dose-dependent reduction in the ability of 10 μM surfen to inhibit T cell proliferation after stimulation with T cell expander beads (Figure 3.7B) or its ability to stimulate T cell proliferation after PMA/ionomycin treatment (Figure 3.7C). Heparin sulfate alone had no effect on either response.

3.3 Discussion

3.3.1 Summary of results

When activated primary murine T cells were treated with surfen there was a dose-related inhibition of T cell proliferation (2.5-20 μM), as assessed from [^{3}H]TdR incorporation (Figure 3.1) and the fluorescence of cells stained with Oregon Green 488 dye (Figure 3.2A). The impact of surfen could not be attributed solely to cell toxicity given the marked decrease in proliferation relative to cell death, although some toxicity was detected (Figure 3.2B). Surfen treatment *in vivo* had an identical effect on T cells that were activated by treating mice with anti-CD3 Ab. Surfen co-treatment (20 mg/kg) reduced T cell proliferation (Figure 3 A, B) and total cell counts in isolated lymph nodes (Figure 3.3C).

The molecular mechanisms include downregulation of CD25 (the α-subunit of the IL-2 receptor), which would reduce the ability to utilize growth-promoting IL-2 when studied *in vivo* (Figure 3.4A) but not *in vitro* (Figure 3.4B). Surfen had no effect on T cell release of the cytokines IL-2 and IFN-γ and did not reduce proliferation of IL-2-dependent CTLL-2 cells (Figure 3.5). The effects of surfen on T cell receptor signaling appear to depend on binding to GAGs, since surfen increased its fluorescence following addition to T cells (Figure 3.6A). When receptor activation was bypassed by treating T cells with PMA/ionomycin, surfen induced a significant increase in proliferation (10 μM) or else had no effect (2.5, 5, 20 μM; Figure 3.7A). Moreover, the inhibitory effect of 10 μM surfen was blocked by co-treatment with the soluble GAG heparin sulfate in a dose-dependent manner (Figure 3.7 B, C). These data point to an inhibitory effect of surfen on T cell activation *in vitro* and *in vivo*, but point to possible stimulatory effects when surface receptor activation is bypassed.

3.3.2 Functional effects of surfen in other studies

Surfen antagonizes the effects of fibroblast growth factor (FGF) and vascular endothelial growth factor (VEGF), since both bind to heparan sulphate proteoglycans (HSPG) to potentiate interactions with receptor tyrosine kinases (Xu et al., 2011). Surfen reduced FGF binding to Chinese hamster ovary cells and downstream phosphorylation of ERK in vascular endothelial cells (with an IC_{50} of about 5 μM; Schuksz et al., 2008). Tubule formation by vascular endothelial cells treated with FGF and VEGF was prevented by surfen, suggesting an ability to inhibit the formation of vascular tubes during angiogenesis (Schuksz et al., 2008). Surfen inhibits the ability of VEGF to phosphorylate its receptor (VEGF-receptor 2) in primary mouse brain microvascular endothelial cells, and reduces the ability of VEGF to increase vascular permeability when injected into mouse skin (Xu et al., 2011).

Surfen also interferes with the ability of SEVI (semen-derived enhancer of viral infection) fibrils to bind to target cells, where they increase infectivity with HIV particles. In this example, surfen was shown to interact directly with the SEVI fibrils despite their net positive charge. This direct interaction bypassed the ability of surfen to prevent SEVI fibrils binding to cell surface HSPG (Roan et al., 2010).

3.3.3 The function of GAGs in T cells

GAGs have been implicated in several aspects of T cell function. T cells have been shown to synthesize both HSPGs and CSPGs (Shao et al., 2013). Some of this is cell associated and detected on the cell surface, while a component is released into the extracellular space. Although resting T cells synthesize proteoglycans, T cell activation results in a marked increase in mRNA expression, synthesis, release and surface expression (Christmas et al., 1988; Fadnes et al., 2012; Jones et al., 2005; Shao et al., 2013; Steward et al., 1990; Teixé et al., 2008). The main categories of HSPG are the syndecans and glypicans, while versican form the major category of CSPG (Esko et al., 2009). The function of T cell surface proteoglycans has been explored in several contexts. Syndecan-2 and 4 have been shown to act as co-receptors for the entry of HIV-1 (Bobardt et al., 2003; De Francesco et al., 2011; Gallay, 2004; Poiesi et al., 2008). Other studies show involvement of T cell surface HSPG with the entry of human T cell

leukemia virus (HTLV)-1 (Jones et al., 2005; Tanaka et al., 2012). Interestingly, the genetic deletion of the heparan sulphate biosynthetic enzymes N-deacetylase/N-sulphotransferase-1 and -2 (Ndst1 and Ndst2) produced hyper-responsivity following activation with as little as 25 ng/mL of anti-CD3 (Garner et al., 2008). The increased proliferation of NDST1 null T cells correlated with decreases in cell surface heparan sulfate using FGF Ab binding as a surrogate marker (Garner et al., 2008). This could partially explain the stimulatory effect of surfen when cell surface signaling is bypassed (Figure 3.7A).

Several exogenous proteins have been found to bind either to T cells or to T cell lines in a HSPG-dependent fashion. These include histones (Watson et al., 1999), cyclophilin B (Allain et al., 2002; Vanpouille et al., 2007) and the chemokine CCL5 (Oravecz et al., 1997). Binding of a dendritic cell ligand (dendritic cell-associated heparan sulphate proteoglycan-dependent integrin ligand) to syndecan-4 on T cells reduces T cell proliferation and IL-2 production (Akiyoshi et al., 2010; Chung et al., 2013, 2011, 2009, 2007). Binding of thrombospondin-1 to CD47 on Jurkat cells also has inhibitory effects on T cell function (Kaur et al., 2011). Binding of cyclophilin B to T cell HSPG induces integrin-mediated T cell adhesion to the extracellular matrix (Allain et al., 2002). The binding of human group IIA phospholipase A_2 to HSPG on T cells in the early stages of apoptosis results in the generation of arachidonic acid (Boilard et al., 2003). Binding of RANTES to T cell HSPG inhibits entry of HIV-1 (Oravecz et al., 1997). Cross-linking of syndecan-2 and -4 on human T cells inhibits T cell proliferation and TNF production (Jones et al., 2005).

The function of secreted proteoglycans in the context of T cell function is less well described. However, secreted proteoglycans are complexed to perforin (Masson et al., 1990), granzyme A (Spaeny-Dekking et al., 2000) and granzyme-B (Veugelers et al., 2006), all of which are involved in the function of cytotoxic T cells and natural killer cells. Exogenous CSPG has been found to enhance CNS inflammation during experimental autoimmune encephalomyelitis, while a disaccharide product of CSPG has the opposite effect (Zhou et al., 2010). In addition, T cell proliferation is inhibited when proteoglycan synthesis is inhibited by treatment with xyloside (Christmas et al., 1988).

3.3.4 Implications of this work

The implication of this work is that endogenous proteoglycans and their GAG side chains are involved in promoting T cell proliferation following activation. The apparent binding of GAGs by surfen results in reduced expression of CD25 *in vivo* and a net inhibitory effect on T cell proliferation *in vitro* and *in vivo* (Figures 3.1-3.3). However, surfen had the opposite effect on T cells activated with PMA/ionomycin, a treatment that induces receptor-independent increases in protein kinase C activity and intracellular calcium (Figure 3.7). In this circumstance, the postulated binding of GAGs by 10 μM surfen resulted in an increase in T cell proliferation, suggesting that GAGs also play a role in regulating endogenous inhibitory mechanisms such as checkpoint inhibitor CTLA-4 and/or PD-1 (Ceeraz et al., 2013).

The precise nature of the GAGs and proteoglycans involved are not known, although surfen has a preferential affinity for HSPG (Schuksz et al., 2008). Surfen can also interact directly with cationic peptides involved in signaling, as shown for the study with SEVI fibrils (Roan et al., 2010), raising the possibility that its effects on T cell activation are independent of proteoglycans or GAGs. However, the inhibitory effect of heparin sulfate shows that when GAG binding sites on surfen are occupied by a competing moiety, it no longer exerts effects on T cell proliferation, whether inhibitory or stimulatory (Figure 3.7 B, C). This suggests that GAG interactions are the primary mechanism for the actions of surfen on murine T cells. It is intriguing that in an earlier study (Christmas et al., 1988) the treatment of T cells with xyloside, which inhibits proteoglycan synthesis, also inhibited T cell proliferation, consistent with a stimulatory effect of proteoglycans and/or GAGs. Taken together, surfen demonstrated the ability to modulate T cell function that holds potential for the treatment of T cell-mediated diseases such as MS.

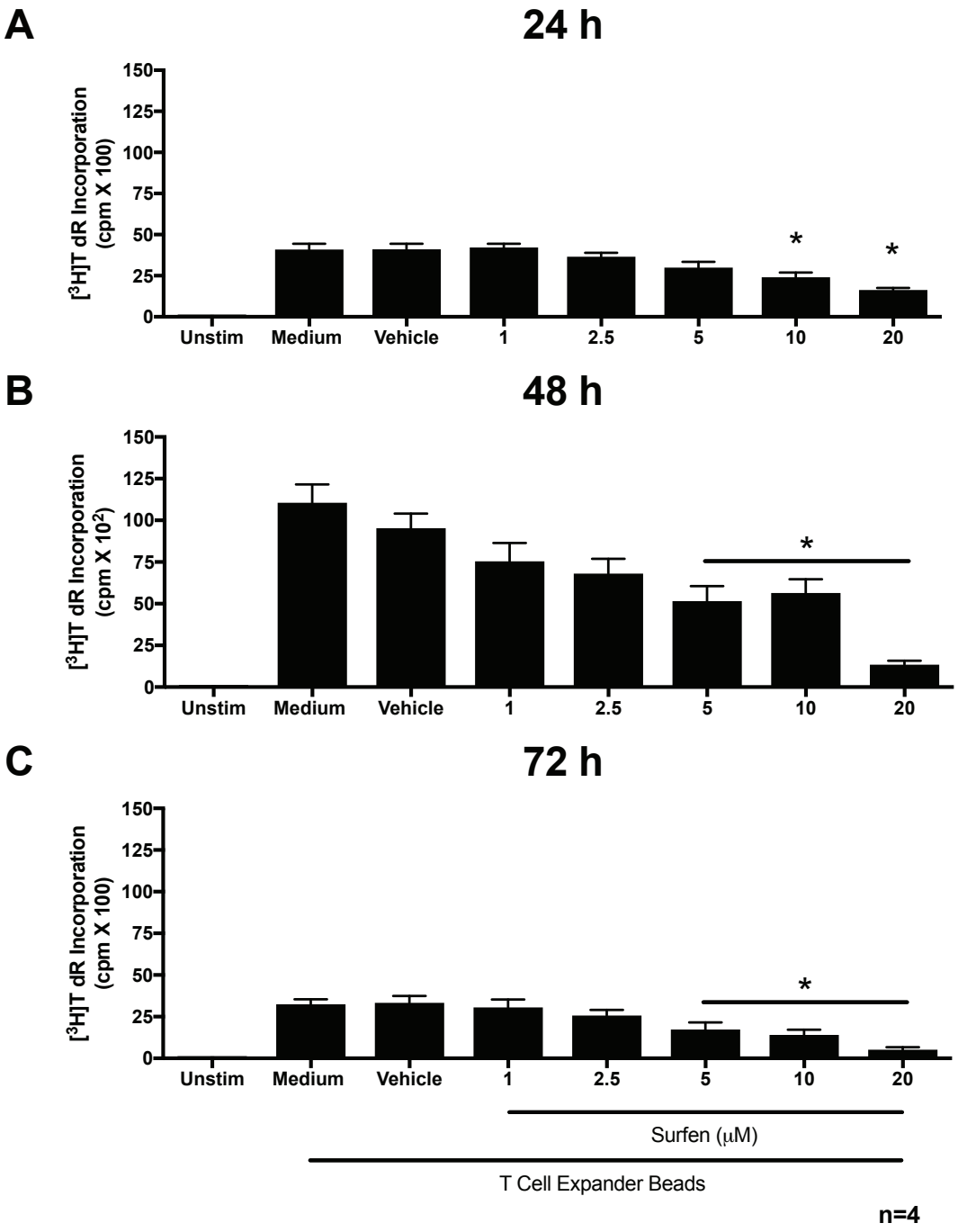

Figure 3.1: Surfen reduces proliferation of activated murine T cells *in vitro*. Tritiated thymidine ([^{3}H]TdR) incorporation was measured 24 **(A),** 48 **(B)** and 72 h **(C)** following treatment with 1, 2.5, 5, 10, and 20 μM surfen and stimulation with anti-CD3/anti-CD28 beads. Surfen (10 and 20 μM) reduced [^{3}H]TdR incorporation across all timepoints while 5 μM had effects at 48 and 72 h. Data shown as mean ± SEM, n=4 for all experiments. Significance is relative to vehicle control (*$p<0.05$).

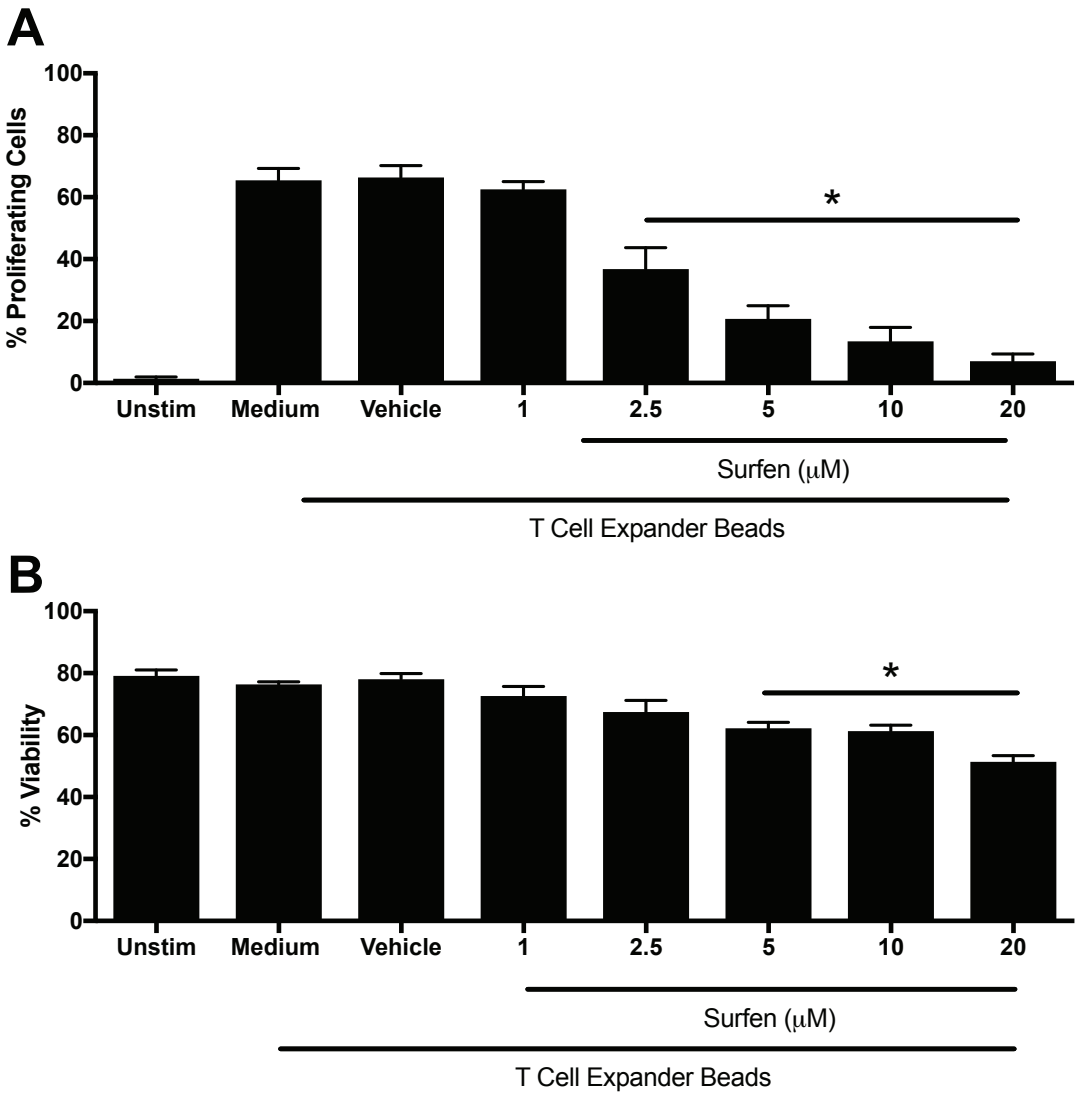

Figure 3.2: Effects of surfen on T cell proliferation and viability. **(A)** Surfen (2.5, 5, 10, and 20 μM) significantly reduced the % of proliferating T cells following stimulation with anti-CD3/anti-CD28 beads for 72 h as measured by Oregon Green incorporation. **(B)** Cell viability was measured with 7-AAD dye and found to be significantly reduced by surfen (5, 10, and 20 μM) 24 h following stimulation. Data shown as mean ± SEM, n=4 for all experiments. Significance is relative to vehicle control (*$p<0.05$).

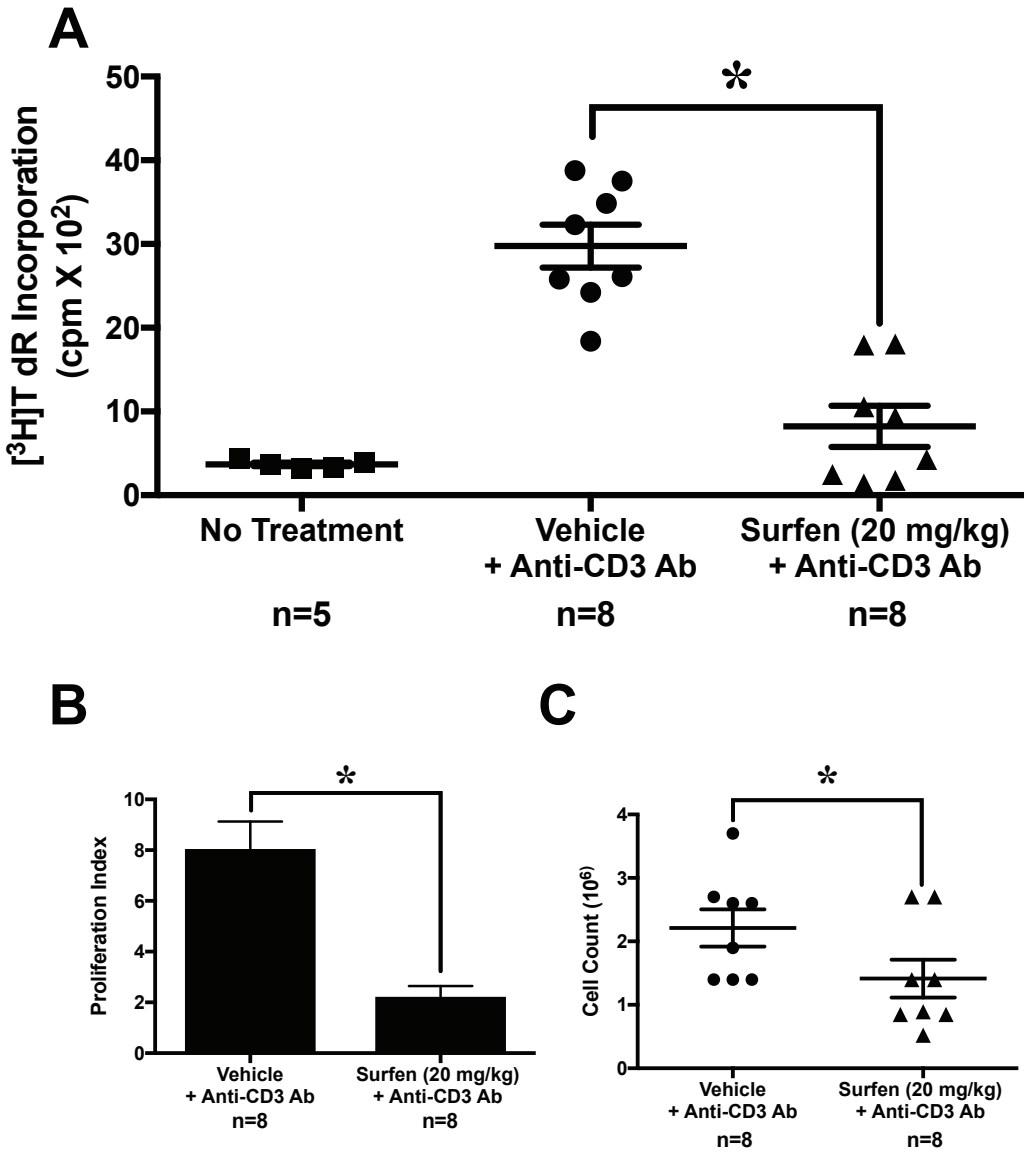

Figure 3.3: Prophylactic administration of surfen (25 mg/kg) reduces the *in vivo* proliferation of murine T cells stimulated with anti-CD3 Ab. To assess the *in vivo* efficacy of surfen, T cells were isolated from mice pre-treated with vehicle (2% DMSO, i.p.) or surfen (20 mg/kg, i.p.) for 3 days followed by an anti-CD3 Ab injection (5 µg, i.p.) 6 h after the last treatment with surfen and harvested 24 h later. **(A)** Surfen significantly reduced [^{3}H]TdR incorporation to the levels of naïve mice relative to anti-CD3 vehicle controls. **(B)** Surfen reduced the proliferation index (proliferation of treatment group/no treatment controls) relative to anti-CD3 vehicle controls. **(C)** Surfen reduced total lymphocyte cell count relative to anti-CD3 vehicle controls. Data shown as mean ± SEM, n=4 for all experiments. Significance is relative to vehicle control (*$p<0.05$).

Figure 3.4 Effects of surfen on murine T cell surface expression of CD25 and CD69 *in vivo* and *in vitro*. **(A)** Prophylactic administration of surfen (25 mg/kg, i.p.) followed by an injection of anti-CD3 (5 μg, i.p.) reduced CD25, but not CD69, on T cells *in vivo* relative to anti-CD3 vehicle controls. **(B)** Surfen (10 μM) has no effect on CD25 or CD69 surface expression on T cells stimulated with anti-CD3/anti-CD28 beads *in vitro* for 48 h. Data shown as mean ± SEM, n=≥6 or n=3 for *in vivo* and *in vitro* experiments, respectively. Significance is relative to vehicle control (*$p<0.05$).

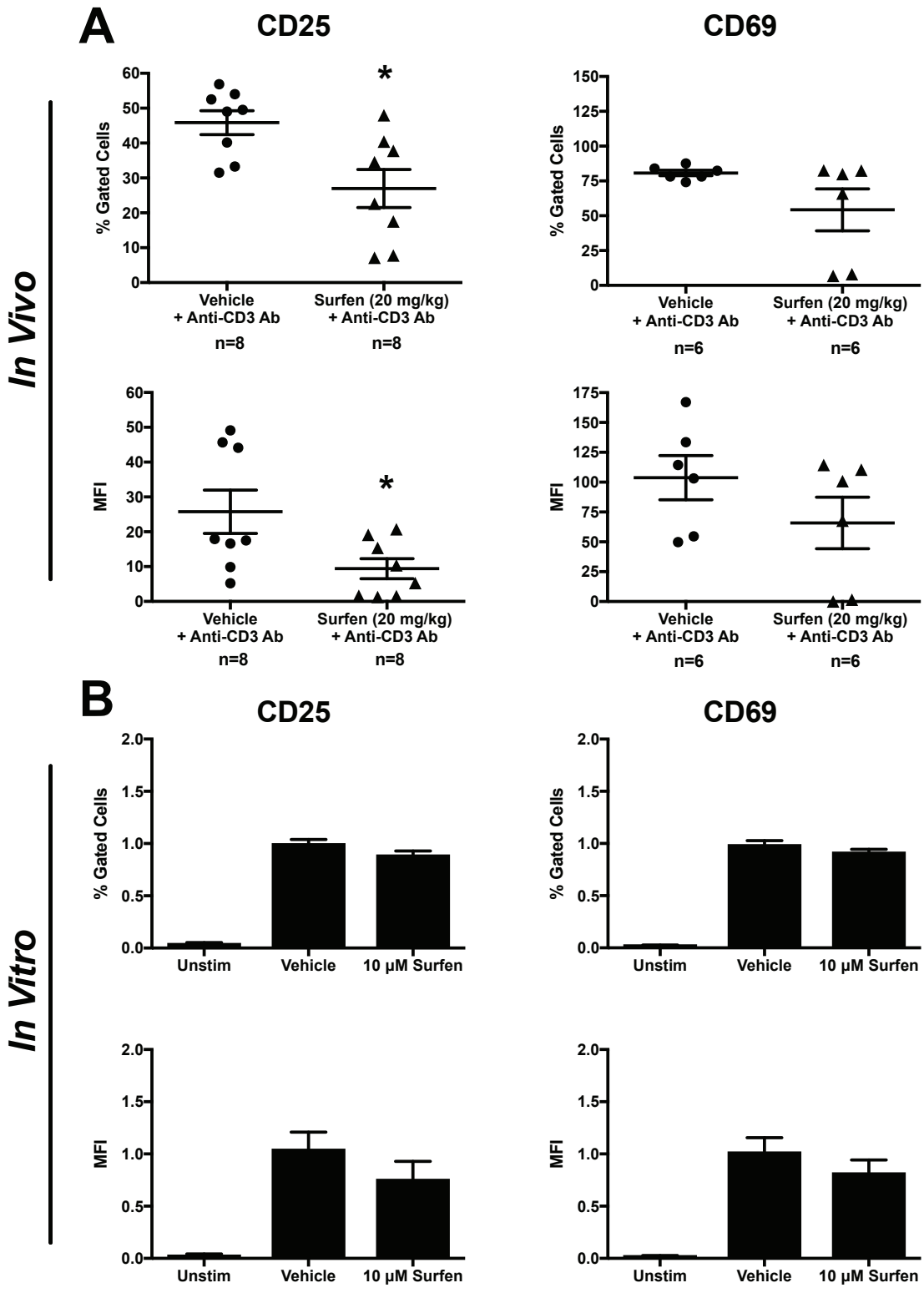
A
CD25
CD69
In Vivo
% Gated Cells
MFI
Vehicle
+ Anti-CD3 Ab
Surfen (20 mg/kg)
+ Anti-CD3 Ab
n=8
n=6
*
B
CD25
CD69
In Vitro
% Gated Cells
MFI
Unstim
Vehicle
10 μM Surfen

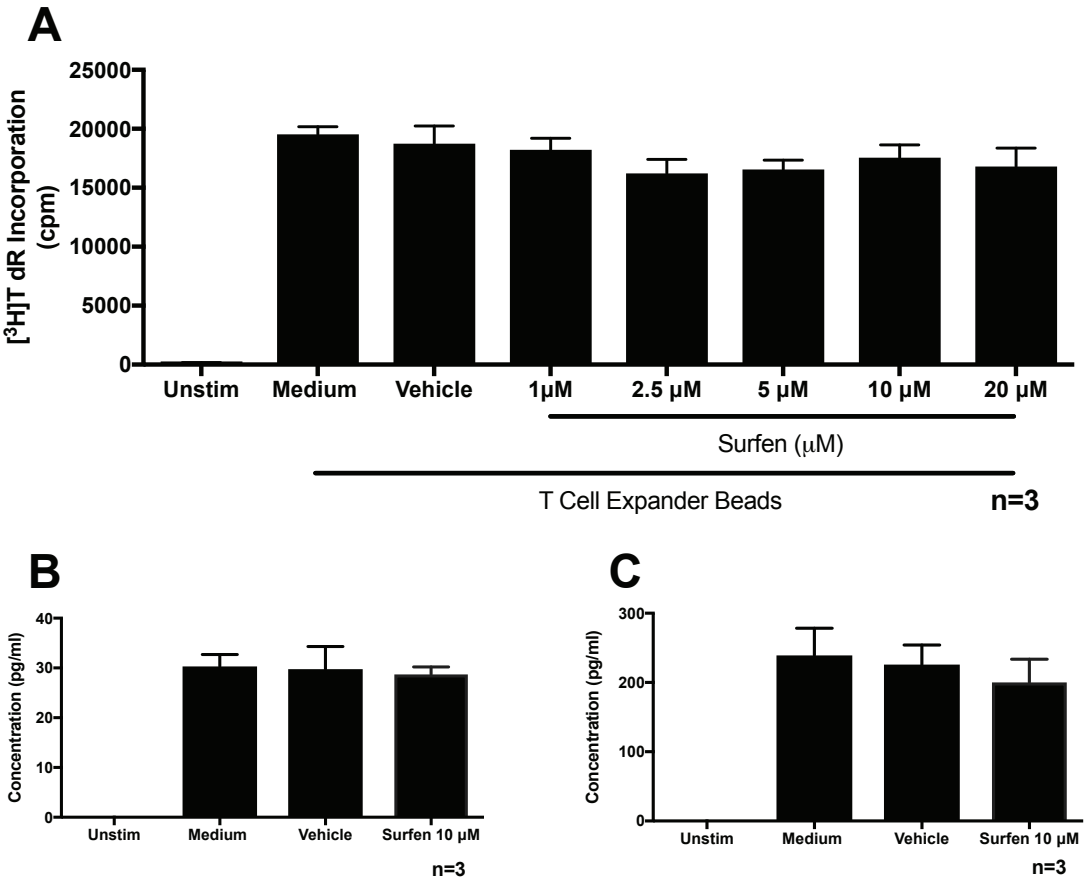

Figure 3.5 The anti-proliferative effects of surfen on murine T cell proliferation are independent of IL-2 and does not change IFN-γ production. **(A)** Surfen does not affect [^{3}H]TdR incorporation within the IL-2 dependent CTLL-2 cell line following stimulation with anti-CD3\anti-CD28 beads for 48 h. Cytokine production of IFN-γ **(B)** and IL-2 **(C)** from stimulated primary murine T cells remained unchanged following treatment with surfen (10 µM) for 48 h. Data shown as mean ± SEM, n=3 for all experiments. Significance is relative to vehicle control (*$p<0.05$).

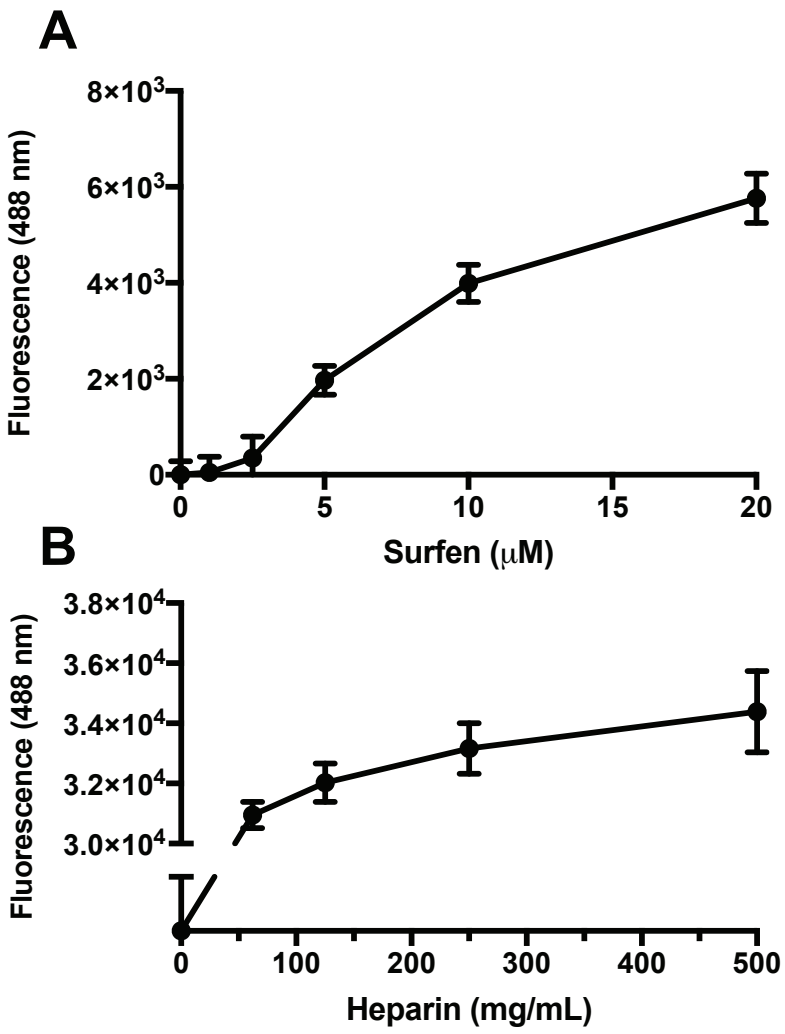

Figure 3.6 Surfen binding to the surface of murine T cells and heparin. **(A)** Murine T cells were incubated with increasing doses of surfen, washed thoroughly to remove unbound surfen, and then read in a with a plate reader (excitation 340nm, emission 488nm). There was minimal signal for untreated T cells (zero dose) but a dose-dependent increase in fluorescence following the addition of surfen. **(B)** As a positive control, surfen (20 μM) was added to increasing doses of heparin and produced dose-dependent increases in fluorescence. Data shown as mean ± SEM, n=3 for all experiments.

Figure 3.7 Effects of surfen on murine T cells treated with PMA/ionomycin or anti-CD3/anti-CD28 expander beads and the inhibitory effect of heparin sulfate on proliferation. **(A)** Surfen (10 μM) significantly increased [^{3}H]TdR incorporation in T cells treated with PMA/ionomycin. By contrast, surfen (10 μM) added in combination with heparin sulfate following stimulation with T cell expander beads **(B)** or co-treatment with PMA/ionomycin **(C)** reversed the anticipated proliferative responses**.** Data shown as mean ± SEM, **(A)** and **(C)** show means of replicate experiments (n=3-4) while **(B)** is representative of 3 independent experiments. Significance (*$p<0.05$) is relative to vehicle **(A)** or to 10 μM surfen treatment alone **(B, C**).

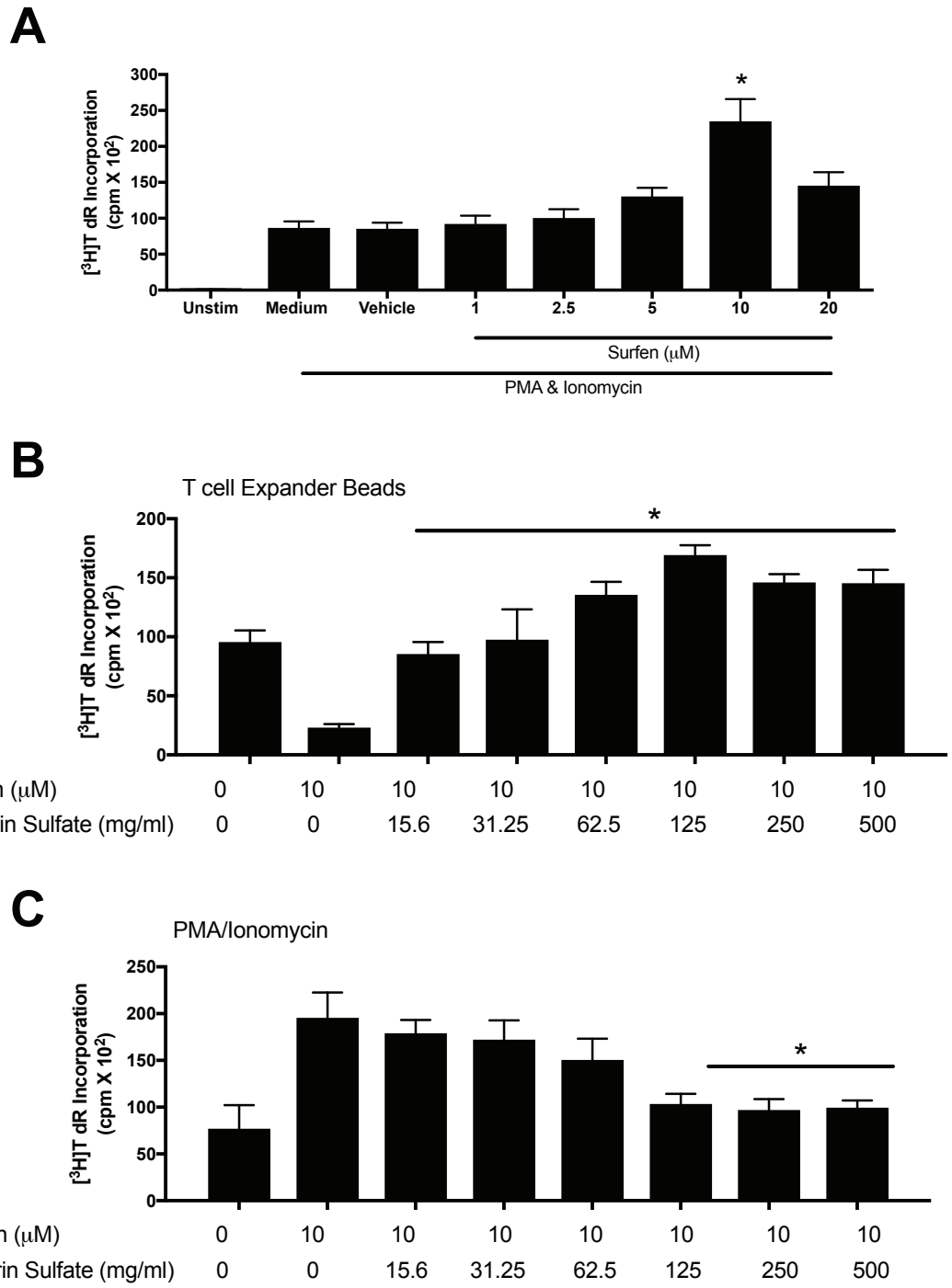
A
[3H]T dR Incorporation (cpm X 10²)
300
250
200
150
100
50
0
*
Unstim
Medium
Vehicle
1
2.5
5
10
20
Surfen (μM)
PMA & Ionomycin
B
T cell Expander Beads
[3H]T dR Incorporation (cpm X 10²)
200
150
100
50
0
*
Surfen (μM) 0 10 10 10 10 10 10 10
Heparin Sulfate (mg/ml) 0 0 15.6 31.25 62.5 125 250 500
C
PMA/Ionomycin
[3H]T dR Incorporation (cpm X 10²)
250
200
150
100
50
0
*
Surfen (μM) 0 10 10 10 10 10 10 10
Heparin Sulfate (mg/ml) 0 0 15.6 31.25 62.5 125 250 500

CHAPTER 4

ADMINISTRATION OF THE PROTEOGLYCAN ANTAGONIST SURFEN AMELIORATES EAE SEVERITY WITH ASSOCIATED EFFECTS ON MACROPHAGE FUNCTION

This manuscript is in preparation, with the following contributors:

Warford JR., Lamport AC, Clements, D, Malone, A, Kennedy, B, Kim, Y, Gujar, S, Lee, P., Hoskin, D.W., Easton A.S.

Student Contributions to Manuscript: JRW conducted and scored all EAE experiments (Figure 4.1), produced all multi-plexed ELISA data (Figures 4.3, 4.4, 4.5, 4.6, 4.8, 4.9, 4.11), performed the majority of EAE qRT-PCR (70%), contributed to the experimental design, conducted all experimental statistics, made all figures presented in this chapter. Figures 4.2, 4.3, 4.5D, and 4.7 were conducted in collaboration with ACL, DC, BK, and KB. This involved shared responsibilities for tissue harvest, flow cytometry, and data analysis. ACL also assisted JRW as a blind observer for EAE clincal evalulation. Several replicate experiments included in Figures 4.11A and 4.12 were performed with the technical assistance and intellectual contributions of AM. GY, DWH and ASE provided experimental guidance and assisted with reagents. JRW wrote the manuscript with editorial assistance from EAS.

4.1 Introduction

Having demonstrated the ability of the proteoglycan antagonist surfen to reduce T cell proliferation *in vitro* and *in vivo* (Chapter 3), we extended these studies into a mouse model of $CD4^+$ T cell-mediated chronic neuroinflammation called experimental autoimmune encephalomyelitis (EAE). This model recapitulates several pathological features reminiscent of MS such as multifocal areas of cellular infiltration, demyelination, clinical disability, and axonal degeneration (Lassmann and Bradl, 2017). Macrophages and $CD4^+$ T cells are the primary infiltrating cells found within the CNS parenchyma of EAE mice and their response to the administration of surfen will serve as the focus of this chapter.

The secretion of proteoglycans has been well established in cell culture studies using enzymatic digestion of GAG side chains to study their function in T cells, macrophages, and B cells (Laskin et al., 1991; Shao et al., 2013; Wrenshall et al., 1999). Approximately 70% of peritoneal macrophage cell surface proteoglycans are CSPGs sensitive to treatment with chondroitinase ABC, and the remaining 30% consist of HSPGs (Wegrowski et al., 2006). Despite the prominence of CSPGs on the cell surface, the secretion of HSPGs is higher in liver Kuppfer cells relative to CSPGs following stimulation with LPS (Laskin et al., 1991). Whether this ratio of HSPG to CSPG secretion is maintained in other resident tissue macrophages is unknown but peritoneal macrophages (Uhlin-Hansen et al., 1993) and Kuppfer cells (Laskin et al., 1991) appear to release similar amounts of CSPGs following LPS stimulation, implying the same for HSPGs. Increased secretion of HSPGs is consistent with the observation that most proteoglycan ligands bind to HSPGs and not CSPGs (Esko et al., 2009). Virtually all cells are capable of producing proteoglycans, including neurons, astrocytes, and microglia (Lander et al., 1998; McKeon et al., 1999; O'Callaghan et al., 2015).

Proteoglycans are potent immunomodulators capable of directly modifying the inflammatory response. The addition of heparan sulphate to murine peritoneal macrophages stimulates the release of the pro-inflammatory cytokines interleukin (IL)-1, IL-6, IL-12 and TNF (Wrenshall et al., 1999). By contrast, chondroitin sulphate has little effect on cytokine expression but is more effective than heparan sulphate in stimulating nitric oxide (NO) release (Wrenshall et al., 1999). Proteoglycans play pivotal roles in

axonal guidance during neurodevelopment. CSPGs direct axonal guidance by providing inhibitory signals whereas HSPGs bind with high affinity to growth factors to attract axons towards their location (Shen, 2014). These properties lead to the hypothesis that proteoglycans could be therapeutically targeted for axonal regeneration following CNS injury. CSPG degradation by chondroitinase in mouse models of spinal cord injury resulted in expedited recovery accompanied by axonal regeneration and restored post-synaptic activity below the lesion (Bradbury et al., 2002; Massey et al., 2008).

Comparable studies have not been completed with heparitinase treatment in spinal cord but HSPGs are involved in CNS injury. For example, accumulation of the HSPG perlecan following a mechanical stab injury in mouse brain delays recovery (De Yébenes et al., 2002). An *ex vivo* study using gliotic brain tissue as a substrate for neuronal cultures found a modest improvement in neurite outgrowth following heparitinase treatment although chondroitinase ABC was more efficacious, suggesting CSPGs are a less permissive substrate (Mckeon et al., 1995). Additionally, transgenic mice that overexpress heparitinase exhibit impaired inflammatory responses to systemic LPS challenge and intracortical injections of amyloid beta, signifying the importance of HSPGs in coordinating the neuroinflammatory response (Zhang et al., 2012).

Literature related to the involvement of proteoglycans in MS is limited. Accumulation of CSPGs and HSPGs have been described in both active MS lesions and EAE in the form of gliotic scars which are thought to prevent endogenous repair by oligodendrocytes (Haist et al., 2012; Sobel and Ahmed, 2001; van Horssen et al., 2006). Several studies point to a deleterious role for proteoglycans in EAE. The small molecule CSPG synthesis inhibitor fluorosamine ameliorates EAE when administered either prophylactically (before disease induction) or therapeutically (after onset of clinical signs) and is associated with decreased splenocyte proliferation and versican mRNA expression (Keough et al., 2016). Equivalent GAG antagonists selective for HSPGs have not been tested in EAE. However, one EAE study administered heparitinase systemically immediately following immunization, resulting in reduced clinical severity that was attributed to a T_H2 anti-inflammatory response (Bitan et al., 2010). In another study an amino acid co-polymer structurally similar to the disease modifying therapy glatiramer acetate bound HSPGs on antigen presenting cells with high affinity, reducing their

capacity to produce chemokines and providing a possible mechanism for this compound's ability to reduce EAE severity (Koenig et al., 2013).

Although the genetic deletion of select proteoglycan core protein genes in EAE remains largely unexplored, preliminary work points to a protective function for some CSPGs and HSPGs. Mice deficient in the CSPG enzyme chondroitin 6-*O*-sulfate transferase-1 display exacerbated EAE severity whereas its overexpression is protective. Recovery was attributed to reduced neuroinflammation and cellular infiltration; however, no direct evidence of inflammatory mediators was collected (Miyamoto et al., 2014). Similarly, upregulation of the CSPG neurocan has been correlated with increased neurogenesis in the subventricular zone during EAE (Sajad et al., 2011). Lastly, the HSPG syndecan-1 has been implicated in the recruitment of encephalitogenic T_H17 cells into the CNS via the choroid plexus (Zhang et al., 2013). Syndecan-1 null mice show increased EAE severity and augmented levels of IL-6, CCL20, and laminin on endothelium indicative of basement membrane disruption (Zhang et al., 2013). Given the ubiquitous nature of proteoglycans, a protective phenotype is not unexpected. However, none of these studies ruled out the possibility of compensatory responses by other proteoglycan family members. Taken together, further investigation is required before therapeutics targeting proteoglycans can be considered for MS.

In this chapter, we report for the first time the effects of the proteoglycan antagonist surfen in a chronic model of MOG_{35-55} induced EAE. In contrast to previous inhibitors described such as fluorosamine, surfen binds with greatest avidity to heparin, followed by dermatan sulphate, heparan sulphate and chondroitin sulphate (Schuksz et al., 2008). We show that administration of surfen following the onset of clinical symptoms ameliorates EAE severity by reducing chemokine-mediated cellular infiltration of $CD4^+$ T cells and myeloid cell populations while promoting an IL-4 mediated T_H2 response. We also demonstrate direct effects of surfen on the ability of bone-marrow derived macrophages (BMDMs) to produce chemokines and selected pro-inflammatory mediators. The reduced expression of a variety of HSPG transcripts was positively correlated with clinical improvement, whereas variable expression of different CSPGs was observed.

This study provides additional evidence that peripherally administered proteoglycan antagonists could represent a viable approach to preventing immune infiltration in MS.

4.2 Results

Eighty-four mice were separated into two groups and received either myelin oligodendrocyte glycoprotein amino acids 35-55 (MOG_{35-55}) + complete Freund's adjuvant (CFA) + pertussis toxin (EAE group) or CFA + pertussis toxin alone as an antigen control (CFA group). Following the onset of clinical signs, mice in each group were assigned to receive an intraperitoneal injection of either vehicle (2% DMSO, i.p.; CFA-V, EAE+V) or surfen (5 mg/kg, i.p.; CFA-S, EAE+S) every second day until the study concluded on day 21. All mice immunized with EAE developed clinical impairment from days 7-11 (Figure 4.1A). CFA mice remained asymptomatic for the duration of the study (data not shown).

4.2.1 Administration of surfen reduces clinical severity in EAE from days 13-21

Surfen significantly ameliorated EAE clinical severity from days 13-21, reducing the mean clinical score from 3 (significant gait impairment with partial hind limb paralysis) to a score of 2 (mild ataxia; Figure 4.1A). A limitation of the EAE 10-point ordinal scoring scale used for this study is that the degree of clinical severity is not equivalent between each interval (Fiander et al., 2017). For example, a mouse with a clinical score of 2 is not "half as sick" compared to bilateral paralysis observed in a mouse with a clinical score of 4. To address the limitation of using ordinal intervals, the median number of days any given mouse spent with a clinical score ≥ 2.5 was calculated. A score of 2.5 or higher represents substantial gait impairment associated with varying degrees of paralysis and is correlated to demyelination within the spinal cord (Fiander et al., 2017). Relative to EAE-V mice, administration of surfen reduced the median number of days that EAE-S mice displayed substantial clinical impairment (Figure 4.1B).

Clinical impairment in EAE-V mice was accompanied by significant weight loss between days 13-19, peaking at 17% loss on day 14 relative to baseline weights obtained

at the onset of clinical signs (Figure 4.1 C). Weights of EAE-S (Figure 4.1C) and CFA mice (Figure 4.1D) remained stable throughout their respective immunization periods.

4.2.2 Administration of surfen (5 mg/kg) reduces the precentage of $CD45^+CD3^+$ $CD4^+$ T cells in EAE spinal cord and cerebellum at day 21

Cellular infiltration by $CD4^+$ T cells is a significant pathological event in the EAE model that facilitates chronic neuroinflammation (Furtado et al., 2008; O'Connor et al., 2008). Flow cytometry was used to assess the percentage of $CD45^+CD3^+CD4^+$ T cells in spleen, spinal cord, and cerebellum of EAE and CFA control mice at day 21 (Figure 4.2, Panel A). No differences between groups were observed in the spleen. Administration of surfen significantly reduced the percentage of $CD45^+CD3^+CD4^+$ T cells in the spinal cord and cerebellum of EAE-S mice relative to EAE-V. Both EAE groups showed a marked increase in $CD45^+CD3^+CD4^+$ T cells in spinal cord and cerebellum relative to CFA control mice. A representative dot plot of our gating strategy is shown in Figure 4.2B.

Given the significant role of $CD8^+$ T cells in chronic active MS lesions (Babbe et al., 2000), and the recognition of their ability to induce EAE independent of $CD4^+$ T cell subsets (Huseby et al., 2001), flow cytometry was used to assess $CD45^+CD3^+CD8^+$ T cells in spleen, spinal cord, and cerebellum of EAE and CFA mice at day 21 (Figure 4.3). No differences between groups were observed in the spleen. The percentage of $CD45^+CD3^+CD8^+$ T cells was significantly increased in the spinal cord of both EAE groups relative to CFA controls. Nevertheless, EAE-V and EAE-S mice were not statistically different. No differences between groups were observed in cerebellum. A representative gating strategy for $CD8^+$ T cells is shown in Figure 4.2B.

4.2.3 Administration of surfen inhibits immune regulatory mechanisms associated with the EAE recovery phase

Following sustained chronic paralysis, EAE mice have been previously shown to enter a recovery phase whereby T_H2 and T_{REG} responses act to dampen pre-established T_H1-mediated inflammation (Issazadeh et al., 1995; Kennedy et al., 1992; Kohm et al., 2002). Expression of mRNA for the T cell transcription factors Tbet (T_H1 response), GATA3 (T_H2 response), RORγt (T_H17 response), and FoxP3 (T_{REG} response) were measured at day 21 post-immunization in CFA and EAE spinal cord using qRT-PCR

(Figure 4, Panel A). Relative to CFA controls, EAE-V mice showed a marked increase in Tbet, GATA3, and FoxP3 mRNA expression consistent with a recovery response. By contrast, expression of these transcripts in EAE-S mice was significantly reduced compared to EAE-V controls and remained at CFA control levels for all three transcription factors. No significant differences in RORγt mRNA expression between groups were observed.

Next, mRNA expression for the cytokines IL-12p40, IL-10, and TGFβ were measured as surrogate markers for T_H1, T_H2, and T_{REG} responses, respectively (Figure 4.4, Panel B). IL-12p40 acts as a co-receptor for both IL-23 and the biologically active IL-12p70 and is thought to negatively feedback onto IL-12p70 to reduce its availability (Cua et al., 2003; Mattner et al., 1993). Both IL-10 and TGFβ are immunomodulatory and capable of dampening T_H1-mediated inflammation (Johns and Sriram, 1993; Zhang et al., 2004). IL-12p40, IL-10, and TGFβ mRNA were all significantly elevated in EAE-V spinal cord, but levels in EAE-S mice were significantly reduced compared to the EAE-V group. EAE-S mice were not significantly different from CFA controls at day 21. The expression of these $T_H1/T_H2/T_{REG}$ mRNA aligns with the upregulation of Tbet, GATA3, and FoxP3, respectively, as well as the reductions seen in surfen treated EAE mice (Figure 4.4, Panels A and B).

Protein concentrations of T_H1/T_H17 associated cytokines were obtained from spinal cord on day 21 post-immunization and measured using multi-plexed ELISA (Figures 4 and 5). There were no significant differences between groups for concentrations of the T_H1 associated cytokine IFN-γ and T_H17 associated IL-17 (Figure 4.4, Panel C). Concentrations of the T_H1 cytokine IL-12p40 were significantly elevated in EAE-V mice relative to CFA controls, while levels in EAE-S mice reduced to those seen in the CFA controls (Figure 4.5, Panel A). By contrast, concentrations of IL-12p70 were significantly higher in EAE-S mice compared to the EAE-V group. Similarly, concentrations of IL-12p70 were elevated in the CFA-S treatment group (227.9 ± 36.2 pg/mL) relative to CFA-V (127.2 ± 15.1 pg/mL), but did not reach statistical significance (Figure 4.5, Panel A). The ratio of IL-12p40 to IL-12p70 was significantly higher in EAE-V mice relative to CFA controls, while levels in the EAE-S group were unaltered (Figure 4.5B). This indicates that EAE-V mice produced significantly more IL-12p40

relative to IL-12p70 compared to other groups. There were no significant differences between groups for IL-2 production (Figure 4.5C).

To address antigen-specific T cell responses, primary T cells were isolated from the spleens of mice with EAE or from CFA controls at day 21 post-immunization. These were, re-stimulated with MOG_{35-55} antigen for 24 h, and the percentage of $CD4^{+}IFN\gamma^{+}$ T cells was assessed with flow cytometry as a surrogate marker for immune activation (Figure 4.5, Panel D). There was a significant increase in the percentage of IFNγ $CD4^{+}$ antigen-responsive T cells in both EAE groups relative to CFA and healthy wildtype controls. No significant differences were observed between EAE-V and EAE-S groups. Concanavalin A (ConA) was added to naïve splenocytes as a positive control and produced an increase in the frequency of non-specific IFN-γ $CD4^{+}$ T cells.

Next, concentrations of the T_H2 cytokines IL-4, IL-5, IL-10, and IL-13 were examined in spinal cord at day 21 using multi-plexed ELISAs (Figure 4.6). Concentrations of IL-4 were significantly increased in EAE-S mice relative to EAE-V and CFA control groups (Figure 4.6, Panel A). Similarly, mean levels of IL-5 were elevated in EAE-S (43.1 ± 6.0 pg/mL) mice compared to EAE-V (27.4 ± 5.4 pg/mL) but this was not statistically significant (Figure 4.6, Panel A). By contrast, no significant differences in the concentrations of IL-10 or IL-13 were observed between EAE-V, EAE-S, or CFA control groups (Figure 4.6, Panel B).

4.2.4 Administration of surfen (5 mg/kg) reduces the percentage of $F4/80^{+}CD11b^{+}$ myeloid populations in EAE spinal cord at day 21

Circulating monocytes transmigrate into the CNS parenchyma to become tissue macrophages that work alongside resident microglia to navigate both inflammatory and restorative processes throughout the EAE disease course (Boven et al., 2006; Vainchtein et al., 2014; D. Y. S. Vogel et al., 2013). There are no reliable markers capable of distinguishing between infiltrated tissue macrophages and resident microglia within inflamed tissues (Yamasaki et al., 2014). Therefore, microglia and macrophages in the context of CNS tissues will be collectively referred to as myeloid cells. Myeloid cell populations were assessed in the spleen, spinal cord, and brain of EAE and CFA mice by flow cytometry using the surface markers F4/80 and CD11b (Figure 4.7A). No significant differences between groups were observed for spleen. The percentage of $F4/80^{+}CD11b^{+}$

myeloid cells was significantly decreased in the spinal cord, but not cerebellum, of EAE-S mice relative to EAE-V. Both EAE treatment groups displayed a higher percentage of myeloid cells in spinal cord and cerebellum relative to CFA control mice. A representative gating strategy for $F4/80^{+}CD11b^{+}$ myeloid cells is shown in Figure 4.7B.

4.2.5 Administration of surfen reduces chemokine mRNA expression and protein concentrations in EAE spinal cord

Myeloid cells constitute a major source of chemokines in EAE and these soluble factors play a central role in orchestrating cellular infiltration into the parenchyma (Fife et al., 2000). mRNA levels were determined for CCL2, CCL3, CCL4, and CCL5 in spinal cord at day 21 using qRT-PCR (Figure 4.8, Panel A). EAE-V mice showed nearly a two-fold increase in mRNA expression for all four cytokines relative to CFA controls. By contrast, levels in EAE-S mice did not increase and remained at control levels.

Multi-plexed ELISAs were used to determine protein concentrations of CCL2, CCL3, CCL4, and CCL5 in EAE spinal cord at day 21 (Figure 4.8, Panel B). As with mRNA expression, concentrations of CCL2 were significantly increased in EAE-V mice, but these increases were decreased in both EAE-S and CFA control groups. Concentrations of CCL3 were significantly increased in EAE-V mice relative to CFA controls while EAE-S mice had significantly lower levels compared to EAE-V, although significantly elevated relative to CFA controls. In contrast to other chemokines, concentrations of CCL4 were significantly increased in EAE-S and CFA-S mice compared to the EAE-V group (Figure 4.8, Panel A) Lastly, concentrations of CCL5 were significantly increased in EAE-V mice relative to EAE-S and CFA groups. EAE-S mice displayed elevated mean CCL5 concentrations (152.9 ± 36.6 pg/mL) relative to CFA controls (CFA-V = 48.39 ± 9.0 pg/mL, CFA-S = 91.75 ± 22.14 pg/mL) that were not statistically significant.

4.2.6 Surfen treatment reduces chemokine production in LPS stimulated bone-marrow derived macrophages

To determine whether surfen influences chemokine production specifically in macrophages, BMDMs were derived from healthy C57BL/6 female mice aged 8-12 weeks. To assess whether surfen has toxic effects on BMDMs, cell viability was assessed

using MTT assays and uptake of 7-AAD via flow cytometry (Figure 4.9). Maximum cell death was seen with 20 μM surfen (≈ 40% reduction in viability compared to untreated cells), with significant death with 10 μM surfen in both 7-AAD (Figure 4.9A) and MTT (Figure 4.9B) assays. The 10 and 20 μM doses of surfen were therefore excluded in all subsequent experiments.

When surfen binds to GAGs this causes a marked increase in fluorescence emission at 488 nm when cells are excited at 340 nm (Schuksz et al., 2008). Therefore, fluorescence was used to assess the ability of surfen to bind to GAGs on the surface of BMDMs (Figure 4.9C). Adding surfen at increasing concentrations (1, 2.5, 5 μM) to BMDMs produced an increase in fluorescence that reached significance at 5 μM. Although increases in fluorescence emission at 488 nm suggest binding to proteoglycans instead of non-specific binding, the assay was repeated using cells that had been treated with heparinase-III or chondroitinase ABC, enzymes which remove heparan sulphate and chondroitin sulphate moieties respectively. Both treatments induced a significant reduction in surfen binding at 5 μM (Figure 4.9C), providing evidence for specific binding to cell associated GAGs at this dose.

Having established the appropriate doses for surfen and its affinity for the cell surface of macrophages, BMDMs were stimulated with LPS and treated with 5 μM surfen for 24 h. Supernatants were analysed for chemokine production using a multi-plexed ELISA. An initial pre-screen of 23 cytokines with pooled supernatants from each group indicated changes in the chemokines CCL2, CCL4, and CCL5. When repeated with biological replicates, the concentrations for all three cytokines were markedly increased following stimulation of BMDMs with LPS (Figure 4.9, Panel D. Treatment with 5 μM surfen in the presence of LPS significantly reduced the concentrations of CCL2, CCL4, and CCL5 by 4-fold, 2-fold, and 3-fold, respectively (Figure 4.9, Panel D). There were no differences in chemokine concentrations when BMDMs were stimulated with LPS dissolved in medium or LPS combined with DMSO vehicle (0.02% DMSO).

4.2.7 Effects of surfen administration on pro-inflammatory cytokine production in EAE spinal cord

Pro-inflammatory mediators are produced by many cellular subsets in EAE, including T cells and myeloid cells. Collectively, chronic exposure to these mediators

contributes to disease progression (Furtado et al., 2008; Valentin-Torres et al., 2016). Levels of mRNA expression were determined for IL-1β, IL-6, and TNF in spinal cord at day 21 using qRT-PCR (Figure 4.10, Panel A). Expression of mRNA for IL-1β was significantly elevated in EAE-V mice relative to CFA groups and WT controls. IL-1β mRNA expression in EAE-S mice was not significantly different from any comparison group. Similarly, mRNA expression for IL-6 was significantly elevated in EAE-V mice relative to CFA mice and WT controls whereas EAE-S mice were not significantly different from any comparison group. Expression of mRNA for TNF was significantly elevated in EAE-V mice relative to EAE-S mice and CFA controls. EAE-S mice showed elevated mean TNF expression (0.4 ± 0.2) relative to CFA controls (CFA-V = 0.01 ± 0.003, CFA-S = 0.02 ± 0.004) that was not statistically significant (Figure 4.10, Panel A).

Aside from classic pro-inflammatory mediators, reactive oxygen species such as nitric oxide play an active role in producing tissue damage (Cross et al., 1994). Therefore, inducible nitric oxide synthase (iNOS) mRNA expression was evaluated in EAE spinal cord at day 21 post-immunization (Figure 4.10, Panel B). Several mice in the EAE-V and EAE-S groups showed elevated iNOS mRNA expression relative to CFA and WT controls; however, there were no significance differences between groups. Similarly, arginase-1 was also increased in EAE but the groups were not significantly different from each other (Figure 4.10, Panel B).

Multi-plexed ELISA was used to evaluate protein concentrations of IL-1β, IL-6, TNF and IL-1α in the spinal cords of EAE and CFA mice at 21 days post-immunization (Figure 4.8, Panels C and D). No significant differences were observed between treatment groups for concentrations of IL-1β, IL-6, or TNF (Figure 4.10, Panel C). However, concentrations of IL-1α were significantly higher in EAE-V mice relative to CFA controls while significant increases were not observed in the EAE-S mice (Figure 4.10D).

4.2.8 Divergent effects of pro-inflammatory cytokine production in BMDMs following treatment with surfen (5 µM)

A prominent source of pro-inflammatory mediators in the context of EAE are macrophages/myeloid cells. To complement findings from EAE spinal cord, BMDMs were stimulated with LPS (100 ng/mL) and treated with either vehicle (0.02% DMSO) or

surfen (5 μM) for 4 h. Levels of mRNA expression were determined for IL-1β, IL-6, and TNF by qRT-PCR (Figure 4.11, Panel A). Treatment with surfen (5 μM) profoundly reduced mRNA expression for all three pro-inflammatory mediators relative to vehicle treatment. No statistical differences in mRNA expression were found between LPS-stimulated vehicle and medium-treated cells, while mRNA expression for cells treated in the absence of LPS was not detected. Expression of mRNA for the T_H2 cytokine IL-4 was not detected 4 h post stimulation with LPS (data not shown).

A separate cohort of BMDMs were stimulated with LPS and treated with either vehicle (0.02% DMSO) or surfen (5 μM) for 24 h and protein concentrations in the overlying supernatants determined using multi-plexed ELISA (Figure 4.11, Panels B, C, and D). As with BMDM pro-inflammatory mRNA expression data (Figure 4.11, Panel A), concentrations of IL-6 and TNF were significantly reduced following treatment with surfen (5 μM) relative to LPS stimulated vehicle controls (Figure 4.11, Panel B). No statistical differences were found between LPS treated BMDMs exposed to medium alone and vehicle alone. Minimal changes were found in cells that did not receive LPS treatment.

By contrast, treatment with surfen produced a marked increase in the concentration of IL-1β relative to both LPS stimulated and unstimulated cells (Figure 4.11, Panel C. The remaining groups showed minimal changes in IL-1β concentrations, including the LPS stimulated cells not exposed to surfen. The selective increase in the concentration of IL-1β following treatment with surfen was associated with significantly decreased concentrations of IL-10 (Figure 4.11, Panel D). Relative to unstimulated controls, LPS-stimulated medium and vehicle treatments significantly increased IL-10 concentrations, which were reduced to background levels by surfen treatment (Figure 4.11, Panel D).

4.2.9 Nitric oxide production is reduced by surfen in BMDMs

BMDMs stimulated with LPS increase the production of iNOS, which catalyzes the production of NO from L-arginine (MacMicking et al., 1997). The production of NO represents a major defence against bacterial pathogens and combines with oxygen free radicals to generate peroxynitrite radicals that influence the surrounding

neuroinflammatory milieu (Fordham et al., 2007). To assess the impact of surfen on this aspect of macrophage activation, BMDMs were stimulated with a higher than normal dose of LPS (500 ng/mL) to induce detectable levels of iNOS transcripts. Cells were then treated with either vehicle (0.02% DMSO) or surfen (5 μM) for 4 h and iNOS mRNA expression was quantified with qRT-PCR (Figure 4.12A). Treatment with surfen decreased iNOS mRNA expression in BMDMs relative to vehicle and medium controls. Samples of cells that were not stimulated with LPS did not produce detectable levels of iNOS mRNA expression.

The Griess assay was used to quantify soluble nitrite production as a surrogate for NO (Figure 4.12B). BMDMs were stimulated with 500 ng/mL LPS and treated with either vehicle (0.02% DMSO) or surfen (1, 2.5, and 5 μM) for 24 h. Supernatants were collected, combined with Griess reagent, and measured at an absorbance of 570 nm. Treatment with surfen produced a significant dose-dependent decrease in nitrite production relative to vehicle controls (Figure 4.12B). No statistical differences in nitrite production were found when comparing LPS-stimulated cells treated with medium alone or vehicle alone. Nitrite production was not detected in cells that were not stimulated with LPS (data not shown).

4.2.10 Heparan sulphate proteoglycan mRNA expression is reduced following the administration of surfen (5 mg/kg) with differential effects on chondroitin sulphate proteoglycans in EAE spinal cord

Proteoglycans are well established immune mediators that have a variety of roles in chemotaxis and immune cell function. However, the relationship between HSPGs and EAE clinical severity is poorly understood. Expression of the HSPGs perlecan, agrin, serglycin, syndecan I, syndecan IV, and the HSPG enzyme NDST1 was assessed in spinal cord tissue using qRT-PCR (Figure 4.13, Panels A and B). Administration of surfen produced a striking reduction in HSPG mRNA expression in EAE-S mice relative to EAE-V mice. This relationship extended to CFA controls where CFA-S mice also showed reductions in HSPG expression relative to CFA-V mice, except for NDST1.

However, mRNA expression for the CSPGs neurocan, aggrecan, and versican were varied following administration of surfen (Figure 4.13, Panel C). Neurocan expression did not change in any of the groups tested whereas aggrecan was significantly

reduced in EAE-V mice relative to the CFA control mice. Conversely, versican was increased in EAE-V mice relative to CFA control mice. Surfen significantly reduced mRNA expression for aggrecan and versican relative to EAE-V mice and was not significantly different from the levels seen in CFA control mice.

To assess the impact of proteoglycan mRNA expression on EAE severity, each transcript was correlated with clinical scores (Table 4.1). Strong positive correlations (Spearman's rho (r_s) >0.8) were found between NDST1, perlecan, syndecan I, syndecan IV and clinical scores. Agrin showed a modest positive correlation ($r_s = 0.5$). Aggrecan showed a significant negative correlation with clinical score ($r_s = -0.76$). Similarly, neurocan was also negatively correlated with clinical score ($r_s = 0.53$). Lastly, versican was positively correlated with clinical score ($r_s = 0.7$).

4.3 Discussion

4.3.1 Summary of findings

This study demonstrates that surfen, a proteoglycan antagonist, successfully ameliorated EAE severity (Figure 4.1) and was associated with a marked reduction in cellular infiltration by $CD45^+CD3^+CD4^+$ T cells in spinal cord and cerebellum (Figure 4.2). Analysis of T cell effector function in the spinal cord showed that surfen reduced mRNA expression for T_H1, T_H2, and T_{REG} transcription factors and differentiation-associated cytokines relative to vehicle treated EAE mice (Figure 4.4). Nevertheless, only a subset of cytokines related to T cell function displayed elevated protein concentrations in EAE spinal cord compared to CFA controls (Figures 4.4 and 4.5). Surfen differentially regulated the subunits of IL-12 in EAE by decreasing concentrations of IL-12p40 and increasing IL-12p70 relative to vehicle (Figure 4.5, Panel A). However, surfen also produced a significant increase in the T_H2 associated cytokine IL-4 in EAE, suggesting that surfen has immunomodulatory properties (Figure 4.6, Panel A).

Surfen-mediated reductions in cellular infiltration in EAE spinal cord were not limited to $CD45^+CD3^+CD4^+$ T cells and extended to $F4/80^+CD11b^+$ myeloid populations (Figure 4.7A). To determine a potential mechanism for the observed decreases in cellular infiltration by T cells and myeloid cells, we evaluated mRNA expression and protein concentrations of chemokines in the spinal cord at day 21. Surfen significantly reduced

chemokine production in EAE mice relative to vehicle treatment, remaining at the levels of CFA controls (Figure 4.8). We extended this work *in vitro* using LPS-stimulated BMDMs to model the specific effects of surfen on chemokine production by myeloid cells and found similar reductions (Figure 4.9, Panel D). These findings suggest that surfen exerts its effects, at least in part, by directly modulating myeloid cell function.

Transcripts for the pro-inflammatory cytokines IL-1β, IL-6, and TNF was increased in EAE spinal cord, with a significant reduction in TNF mRNA expression in surfen treated EAE. However, this mRNA expression data did not translate into protein production as pro-inflammatory cytokine concentrations in EAE spinal cord were no different from levels in CFA spinal cord in day 21 mice, apart from an increase in IL-1α. Surfen treatment during EAE reduced the concentration of IL-1α to CFA control levels (Figure 4.10). By contrast, cytokine expression was broadly increased in LPS-stimulated BMDMs, and treatment with surfen reduced concentrations of IL-6 and TNF, as well as NO activity as measured by the Griess assay (Figures 4.11 and 4.12). Interestingly, surfen significantly increased IL-1β concentrations but decreased IL-10 relative to vehicle and medium controls, pointing again to the ability of surfen to selectively regulate myeloid function (Figure 4.12, Panels C and D). Lastly, we show that surfen potently decreased HSPG mRNA transcripts in both EAE and CFA controls (Figure 4.13, Panels A and B). Surfen had diverse effects on CSPG expression, reducing versican and preventing the inhibition of aggrecan that may serve a protective role (Figure 4.13, Panel C). Reductions in the mRNA expression of HSPGs and the CSPG versican produced by surfen were significantly correlated with clinical improvement (Table 1).

4.3.2 Surfen treated EAE mice do not show typical immune phenotypes associated with the EAE recovery phase

Protein concentrations of IFNγ, IL-2, and IL-17 in EAE spinal cord were reduced to the levels of CFA controls by day 21 (Figure 4.10). The decrease of these cytokines to control levels may be explained, at least in part, by the immunological phases that comprise the clinical disease course in actively-induced EAE. Three phases define EAE clinical progression: the induction phase (days 0-7), effector phase (days 8-16), and recovery phase (days 17-21; Barthelmes et al., 2016; Miller et al., 2007). The induction phase encompasses the priming of MOG_{35-55}-specific T cells and their subsequent

reactivation within the CNS. Upon initiation of an adaptive immune response, the effector phase fosters the production of inflammatory mediators that produce demyelination and axonal damage. Finally, the recovery phase features reduced concentrations of pro-inflammatory mediators and an increased T_H2/T_{REG} response that can promote repair. In our study, mice were sacrificed at the end of the recovery phase to enable the observation of the entire EAE clinical course.

The recovery phase of EAE features an upregulation of anti-inflammatory mediators capable of dampening the $CD4^+$ T_H1 and T_H17 responses. During this period, T_H2 and T_{REG} subsets simultaneously produce mediators that generate immune dysregulation in an effort to promote repair (Issazadeh et al., 1995; Kennedy et al., 1992; Kohm et al., 2002). The accumulation of IL-10 and TGFβ secreting $FoxP3^+$ T_{REG} cell subsets late in EAE progression is considered one of the definitive features of the recovery phase (McGeachy et al., 2005; O'Connor et al., 2007). In addition to IL-10, T_{REG} subsets also produce the potent immunomodulator transforming growth factor beta (TGFβ). TGFβ is thought to act by inducing anergy in T cell effector cells and reducing T cell proliferation (Johns and Sriram, 1993; Selvaraj and Geiger, 2008; Zhang et al., 2006). Blockade of TGFβ with neutralizing antibodies has been shown to prevent recovery in EAE (Johns and Sriram, 1993).

Analysis of T cell effector cell function in spinal cord showed significantly increased mRNA expression of the T cell transcription factors Tbet (T_H1 response), GATA3 (T_H2 response), and FoxP3 (T_{REG} response) in vehicle treated EAE mice (Figure 4.3, Panel A). Similar increases were noted for the T cell differentiation factors IL-12p40 (T_H1), IL-10 (T_H2/T_{REG}), and TGFβ (T_{REG}; Figure 4.3 Panel B). However, these increases were not seen in surfen treated EAE mice, with levels comparable to the CFA antigen controls for each of these transcripts. This raises two questions. First, why did vehicle EAE mice fail to recover clinically despite the indication of T_{REG} and T_H2 responses? Secondly, how did surfen reduce clinical severity without increasing T_{REG} and T_H2 transcripts?

Mice do not clinically recover in MOG_{35-55} induced EAE, the model used in this study, but do show evidence of T_{REG} and T_H2 responses during the recovery phase. Failed clinical recovery in this instance may reflect irreparable axonal injury caused by

heightened inflammation during the earlier effector phase. The sustained production of IL-12p40 concentrations in vehicle treated EAE spinal cords at day 21 compared to surfen provides evidence of ongoing inflammatory activity during the effector phase (Figure 4.4, Panel A).

As previously mentioned, IL-12p40 is a subunit of both the T_H1-differentiating cytokine IL-12p70 and the T_H17-differentiating cytokine IL-23. Biologically active IL-12p70 is a heterodimer comprised of both p40 and p35 subunits, whereas IL-23 includes p40 and p19 (Cua et al., 2003). Genetic deletion of IL-12p40 profoundly ameliorates EAE severity, whereas mice deficient in p35 display aggravated disease severity relative to wildtype EAE controls (Gran et al., 2002). Therefore, continuous production of IL-12p40 by EAE-V mice during the recovery phase could account for the clinical disability of vehicle EAE mice by promoting sustained damage, an effect that was significantly reduced in the surfen treated EAE mice.

In addition, administration of surfen significantly increased IL-4 production in EAE mice relative to the vehicle group, showing that there is induction by surfen treatment of some factors that mediate a T_H2 response (Figure 4.5, Panel A). This is consistent with a previous report describing *ex vivo* T_H2 responses following heparitinase treatment in EAE (Bitan et al., 2010). Peak gene expression for IL-4 occurs early in the effector phase and is capable of reducing T_H1 and T_H17 mediated inflammation if produced at sufficiently high levels (Kennedy et al., 1992). Therefore, it is likely that GATA3 mRNA expression occurs before day 21 in surfen treated EAE mice to account for this result. Mice null for IL-4 display enhanced EAE severity during the effector phase, but enter the recovery phase at the same time as their wildtype littermates (Falcone et al., 1998). Consequently, IL-4 serves a protective role in the effector phase that occurs before the recovery phase (Falcone et al., 1998). An early increase in IL-4 production during the effector phase following surfen treatment may have protected mice from inflammatory injury, reducing inflammation to levels that negated the need for T_{REG} gene expression typical of the recovery phase. The finding that concentrations of IL-4 remained elevated in surfen treated EAE mice at day 21 and concentrations of IL-12p40 are decreased is consistent with this hypothesis.

In addition to increasing concentrations of IL-4, administration of surfen during EAE produced a significant increase in concentrations of the biologically active IL-12p70 relative to the vehicle group (Figure 4.4, Panel B). Previous studies have demonstrated that human IL-4 drives the production of bioactive IL-12p70 by stimulated dendritic cells and macrophages while inhibiting generation of inactive IL-12p40 (Kaliński et al., 2000). This is thought to promote a T_H2 to T_H1 switch in situations where inflammation may be beneficial in host defence (Guenova et al., 2008), as subclinical inflammation is necessary for endogenous CNS repair (Arnett et al., 2001; Mason et al., 2001; Schönrock et al., 2000). For example, the removal of myelin debris by pro-inflammatory macrophages is a necessary step for oligodendrocyte precursor cell recruitment and subsequent remyelination (Huitinga et al., 1990; Rawji et al., 2016). This work raises the possibility that surfen promotes a selective switch from T_H2 to T_H1 via IL-4 induced IL-12p70 production to confer neuroprotection is tempting, but this could also represent an injurious response produced by surfen.

Taken together, these findings suggest that surfen treated mice bypass typical T_{REG}/T_H2 responses during the EAE recovery phase, possibly by generating protective T_H2 responses via IL-4 production during the effector phase. The ability of surfen to influence the induction phase of EAE remains unknown as administration began after the onset of symptoms during the effector phase, and would be addressed with prophylactic administration of surfen before EAE onset. Nevertheless, surfen does not impede antigen-specific T cell responses in EAE following MOG_{35-55} restimulation of $CD4^+$ T cells primed during the induction phase (Figure 4.5, Panel D). We previously reported that the prophylactic administration of surfen reduced T cell proliferation following an injection with mitogenic anti-CD3 Ab (Chapter 3). It stands to reason that earlier administration of surfen in EAE may have similar effects and have an even greater impact on T cell function through each clinical phase of the disease.

4.3.3 Surfen-mediated decreases in myeloid cell infiltration are related to impaired chemokine production in EAE spinal cord, reproduced in LPS-stimulated BMDMs

Reductions in mRNA expression and protein concentrations for the chemokines CCL2, CCL3, and CCL5 in EAE spinal cord following surfen administration point to decreased chemotactic signalling as one potential mechanism for the reduced cellular

infiltration of $CD45^+CD3^+CD4^+$ T cells and $F4/80^+CD11b^+$ myeloid populations observed in surfen treated EAE spinal cord (Figure 4.8, Panels A and B). In support of these *in vivo* observations, surfen also reduced the production of the chemokines CCL2, CCL4, and CCL5 in BMDMs *in vitro* (Figure 4.9, Panel C).

Aside from macrophages and other leukocytes, a multitude of cells are capable of producing chemokines in the context of MS and EAE, including endothelial cells and glia (Cheng and Chen, 2014; Miyagishi et al., 1997). However, myeloid cells and other leukocytes are the principle producers of chemokines within active MS lesions (Simpson et al., 1998). Proteoglycans, including HSPGs such as syndecan, show strong affinity for chemokines and provide the matrices required to form chemotactic gradients on luminal endothelial cells (Middleton et al., 2002; Wang et al., 2005). Many chemokines, including CCL2, have heparan sulfate binding motifs that mediate their function (Lortat-Jacob et al., 2002). Therefore, in addition to its effects on chemokine expression, surfen likely exerts some of its effects by binding to these motifs and preventing downstream chemokine signalling. Whether surfen has direct effects on chemokine receptors in EAE is unknown.

Intravital microscopy studies demonstrate that both CCL2 and CCL5 promote leukocyte and myeloid extravasation into the CNS during EAE by promoting adherence to the brain microvasculature (dos Santos et al., 2005). Furthermore, mice null for the CCL2 receptor CCR2 display virtually no signs of EAE or cellular infiltration critical for the development of clinical disease (Fife et al., 2000). CCL3 can push naïve effector T cells towards a T_H1 response and has been implicated in both EAE progression and relapse (Karpus and Kennedy, 1997; Manczak et al., 2002). The role of CCL4 is poorly understood, but expression is primarily restricted to myeloid cells within active MS lesions and is thought to promote myeloid cell infiltration (Simpson et al., 1998). We note that concentrations of CCL4 were elevated by surfen in EAE spinal cord (Figure 4.8, Panel B). However, both mRNA expression of CCL4 in EAE spinal cord and production of CCL4 by BMDMs were reduced following surfen treatment (Figure 4.9, Panels A and C). The extensive biological redundancy in chemokine signalling cascades may have produced a compensatory increase in CCL4.

These data suggest that surfen acted early to decrease cellular infiltration into the CNS parenchyma, possibly via direct actions on inflamed endothelium and activated macrophages and microglia. In the future, chemotaxis assays using brain endothelial cells and MOG_{35-55} stimulated T cells and macrophages from EAE mice could provide additional evidence to support this hypothesis.

4.3.4 The administration of surfen selectively regulates inflammation in EAE and BMDMs

Transcript expression and protein concentrations of the pro-inflammatory cytokines IL-1β, IL-6, and TNF were evaluated in EAE spinal cord (Figure 4.10). All three cytokine transcripts were significantly increased in vehicle treated EAE mice relative to CFA controls. By contrast, cytokines in surfen treated EAE mice remained at control levels; however, only TNF transcripts showed a significant reduction relative to EAE vehicle mice (Figure 4.10, Panel A). The significantly elevated mRNA expression of these pro-inflammatory cytokines in EAE vehicle mice may reflect elevated cytokine production in the earlier phases of EAE, since protein concentrations of IL-1β, IL-6, and TNF in EAE spinal cord were not increased above CFA control levels at day 21, consistent with other cytokine concentrations reported in this study. The reduction in TNF expression lends additional support to the notion that surfen reduces inflammation throughout the effector phase of EAE. We also measured mRNA associated with nitric oxide production. Although elevated in EAE, surfen treatment produced no differences in expression for the NO related iNOS and Arg1 mRNAs.

In contrast to IL-1β, IL-6, and TNF, the concentration of the cytokine IL-1α remained elevated in the spinal cord vehicle treated EAE mice. IL-1α mRNA expression occurs early in EAE and its protein concentrations remain stable throughout the disease, unlike many of the other pro-inflammatory cytokines we have discussed (Kennedy et al., 1992; Liu et al., 2016). Indeed, our study showed that IL-1α was increased in vehicle treated mice and was significantly suppressed by surfen (Figure 4.8, Panel B). IL-1α has been shown to drive expression of the HSPG perlecan following mechanical injury to murine brain (De Yébenes et al., 2002). Furthermore, the addition of IL-1α to hippocampal primary glial cultures produced an eight-fold increase in perlecan mRNA expression, suggesting an inflammatory role for this proteoglycan (De Yébenes et al.,

2002). The effects of surfen on proteoglycan mRNA expression are discussed in section 4.3.5. However, we suggest that its effects on this expression may, in part, be attributable to inhibition of IL-1α expression.

To address the direct effects of surfen on macrophage-mediated inflammation, BMDMs were stimulated with LPS, treated with either surfen or vehicle, and the cytokines IL-1β, IL-6, and TNF were assessed with qRT-PCR and multi-plexed ELISA (Figure 11). Surfen reduced both mRNA expression (Figure 11, Panel A) and protein concentrations (Figure 4.11, Panel B) of IL-6 and TNF in LPS stimulated BMDMs. However, IL-1β production was significantly increased following treatment with surfen (Figure 4.10C) whereas IL-10 was decreased (Figure 4.10D).

There are several possible explanations for the paradoxical ability of surfen to reduce BMDM release of IL-6 and TNF but to increase IL-1β despite reducing mRNA expression for all three cytokines. The first is that surfen could alter IL-1β secretion mechanisms. Synthesis begins with pro-IL-1β transcription, usually triggered by TLR2/4 signalling, followed by the conversion of pro-IL-1β protein to mature IL-1β by caspase-1 activated by either inflammasome dependent or independent mechanisms (Lopez-Castejon and Brough, 2011). Mature IL-1β does not have a signaling sequence and must rely on vesicular transport out of the cell (Auron et al., 1984). Therefore, message does not necessarily correlate with the amount of mature IL-1β accumulating in the cytosol.

LPS stimulated macrophages promote the recruitment of IL-1β into autophagosomes, a double membrane structure usually reserved for the proteolytic digestion of damaged organelles or proteins (Harris et al., 2011). When autophagy is prevented, IL-1β is released from the cell. Conversely, when autophagy is initiated the autophagosome fuses to a lysosome and the IL-1β is degraded. There is the possibility that surfen inhibits autophagy such that IL-1β stored in autophagosomes is released from the macrophage. Both TNF and IL-6 promote autophagy, possibly explaining the baseline concentrations of IL-1β observed in stimulated BMDMs (Keller et al., 2011; Li et al., 2013). The second possibility is that the structure of surfen ($C_{21}H_{20}N_6O$) mimics that of other secretion stimuli such as sodium urate ($C_5H_3N_4$) to a sufficient extent that IL-1β is released from the cell (Lopez-Castejon and Brough, 2011). Lastly, surfen could interact

directly with the inflammasome to influence cleavage of pro-IL-1β and downstream secretion.

Given the complexities of an *in vivo* model, it is difficult to ascertain whether the ability of surfen to selectively regulate inflammation by BMDMs can be directly compared to EAE. Nevertheless, there are some noteworthy parallels. Expression of mRNA for IL-10 was significantly increased in EAE-V mice (Figure 4.4, Panel B), as were concentrations of IL-10 in BMDM medium and vehicle treatments (Figure 4.11, Panel B) whereas concentrations in surfen treated EAE mice and BMDMs remained at control levels. Increased IL-10 production is likely a regulatory response triggered in part by high concentrations of proinflammatory mediators such as TNF (Foey et al., 1998; Wanidworanun and Strober, 1993). It is possible that surfen reduced the general inflammatory milieu below the threshold required to initiate IL-10 production.

Alternatively, both IL-4 (EAE; Figure 4.6) and IL-1β (BMDMs; Figure 4.11) were significantly increased by surfen, which can negatively regulate IL-10 production in dendritic cells and monocytes, respectively (Foey et al., 1998; Yao et al., 2005). IL-10 is considered protective in EAE and dampens pro-inflammatory and encephalitogenic T_H17 responses, in many cases via T_{REG} subsets (Bettelli et al., 1998; Huber et al., 2011). However, the reduction of IL-10 by surfen does not preclude alternative protective mechanisms. For example, IL-1β induces the production of insulin growth factor by macrophages capable of promoting oligodendrocyte precursor cell recruitment to lysolecithin-induced lesions (Hinks and Franklin, 1999; Mason et al., 2001; Merrill, 1991). Therefore, the indirect effects of surfen warrant further investigation.

Lastly, the effects of surfen on the expression of iNOS (Figure 4.12A) and NO production (Figure 4.12B) were assessed in LPS-stimulated BMDMs. Relative to controls, surfen significantly reduced both iNOS mRNA expression and soluble nitrite production in BMDMs. These results do not correspond to the lack of iNOS and Arg-1 expression observed in EAE spinal cord (Figure 4.10, Panel B) but suggest that surfen has the potential to reduce these factors in myeloid cells. It is also a possibility that peak NO production had passed by day 21 and therefore the effect of surfen on this inflammatory mediator in EAE has not been captured by this study.

4.3.5 Transcript expression of HSPGs is reduced by surfen and correlated with disease severity

We show marked increases in HSPG mRNA expression during EAE, much of which is suppressed by surfen treatment during the disease. Surfen reduced HSPG mRNA expression in the spinal cords of both EAE and some CFA control mice (Figure 4.11, Panels A and B). Many of these HSPGs, such as agrin and serglycin, have not been previously reported in EAE beyond immunohistochemical studies of basement membranes (Agrawal et al., 2006b). The expression of each HSPG correlated strongly with clinical scores when data from individual mice were evaluated (Table 4.1). However, the cells responsible for HSPG expression remain to be determined. It is possible that reduced expression in surfen treated EAE is simply related to reduced local numbers of T cell and myeloid cells, both of which are potent sources of proteoglycans. However, resident cells such as endothelial cells are an alternative source for proteoglycan expression. Astrocytes also harness proteoglycans to create gliotic scars and a reduction in proteoglycan expression by these cells may enable endogenous repair and reduced neuroinflammation (Jones et al., 2003; Properzi et al., 2008).

In contrast to the complete suppression of HSPGs mRNA expression by surfen, CSPG expression was differentially regulated. Neurocan expression remained unchanged between groups; however, neurocan showed a significant negative correlation with clinical score, consistent with the ability of neurocan to promote neurogenesis in EAE (Sajad et al., 2011). Aggrecan expression was decreased in vehicle treated EAE mice, while this reduction was prevented by surfen. Conversely, versican expression increased in vehicle treated EAE mice, while this increase was suppressed by surfen (Figure 4.11, Panel C). The expression of these CSPGs in EAE has been previously reported (Keough et al., 2016). Surfen acted similarly to the small molecule CSPG inhibitor fluorosamine in that both drugs decreased mRNA expression for versican and had no effect on the expression of neurocan. However, this study is the first report of a reduction in aggrecan expression during EAE by a proteoglycan antagonist, an effect that positively correlates with recovery (Table 1). Aggrecan is an integral component of the perineuronal nets responsible for synaptic transmission and aggrecan null mice develop severe cognitive

deficits (Giamanco et al., 2010). Therefore, its preservation by surfen may be favourable during EAE.

Taken together, these data indicate that the pivotal role of CSPGs as they relate to EAE immunopathology may be overstated as the disease is driven, at least in part, by upregulated HSPG mRNA expression. They also indicate that surfen may operate by reducing (or preserving) proteoglycan expression in the EAE lesion, whether by effects on resident cells, or by simply reducing the infiltration of proteoglycan producing inflammatory cells.

4.3.6 Conclusions

This chapter provides a broad overview of the immunomodulatory properties of the proteoglycan antagonist surfen in EAE. The ability of surfen to reduce cellular infiltration following the onset of clinical signs via reduced chemokine production, as well as its ability to increase IL-4 production while decreasing IL-12p40 and IL-1α, point to proteoglycans as a viable target in the treatment of MS. Not surprisingly, the major findings of this study link back to proteoglycan expression. Some chemokines have heparan sulfate binding motifs (Lortat-Jacob et al., 2002). IL-12p40 binds to heparan to stay close to its sites of secretion (Hasan et al., 1999), and IL-1α drives perlecan expression (De Yébenes et al., 2002). For the first time, this study shows that HSPG mRNA expression in individual mice is positively correlated to clinical scores in EAE. Few studies have fully explored this family of proteoglycans and their ability to regulate immune function. Moreover, this study also demonstrates for the first time a reduction in the expression of aggrecan in vehicle treated EAE mice that is prevented by surfen. CSPGs have been viewed as largely inhibitory to repair in EAE, therefore this represents a new avenue for investigation.

Nevertheless, caution must be taken to better understand whether the increases in IL-12p70 in EAE and IL-1β in BMDMs are beneficial or deleterious. Future work concentrated on earlier time points will enable a clearer picture of the ability of surfen to regulate inflammation during the effector phase of EAE. In conclusion, understanding the relationship between proteoglycans and neuroinflammation represents a fertile field of study that may yield novel therapeutic targets for future development.

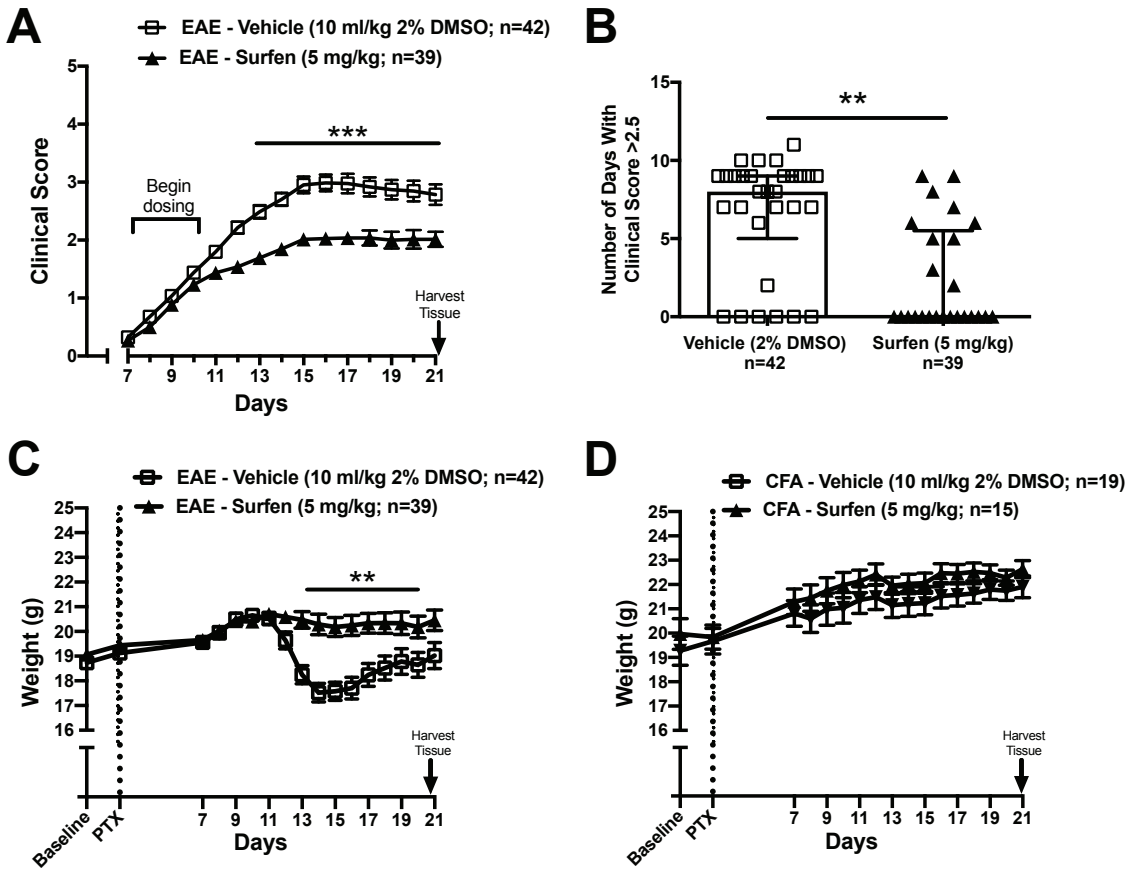

Figure 4.1: Administration of surfen reduces EAE clinical severity. Mice were immunized with CFA+PTX alone or in combination with MOG_{35-55} and received an intraperitoneal injection of either vehicle (2% DMSO; CFA-V; EAE-V) or surfen (5 mg/kg; CFA-S; EAE-S) every second day immediately following the onset of clinical symptoms. **(A)** EAE mice treated with surfen showed significantly reduced disease severity relative to vehicle treatment from days 13-21. **(B)** The median number of days each mouse spent with a severe clinical score was significantly reduced by administration of surfen relative to vehicle. **(C)** Weights were obtained from each EAE mouse from days 7-21. Relative to surfen treated EAE mice, EAE-V mice showed significantly reduced weights from days 13-19. **(D)** Weights were obtained from each CFA mouse from days 7-21. Weights of CFA mice did not significantly change throughout the duration of the study. Data shown as mean ± SEM and is representative of three independent experiments. ** = $p<0.01$, *** = $p<0.001$

Figure 4.2: Administration of surfen reduces the percentage of $CD45^+CD3^+CD4^+$ T cells in EAE spinal cord and cerebellum at day 21. Flow cytometry was used to assess the percentage of $CD45^+CD3^+CD4^+$ T cells in spleen, spinal cord, and cerebellum of EAE and CFA mice treated with either vehicle or surfen. **(A)** Frequencies are shown of $CD45^+CD3^+CD4^+$ T cells in EAE mice and CFA controls. No differences between groups were observed for the spleen. Administration of surfen significantly reduced the percentage of $CD45^+CD3^+CD4^+$ T cells in the spinal cord and cerebellum of EAE-S mice relative to EAE-V. Both EAE groups displayed an increased percentage of $CD45^+CD3^+CD4^+$ T cells in spinal cord and cerebellum relative to CFA control mice. **(B)** Representative gating strategy. Data shown as mean ± SEM and is representative of two independent experiments. # = $p<0.05$, * = $p<0.05$

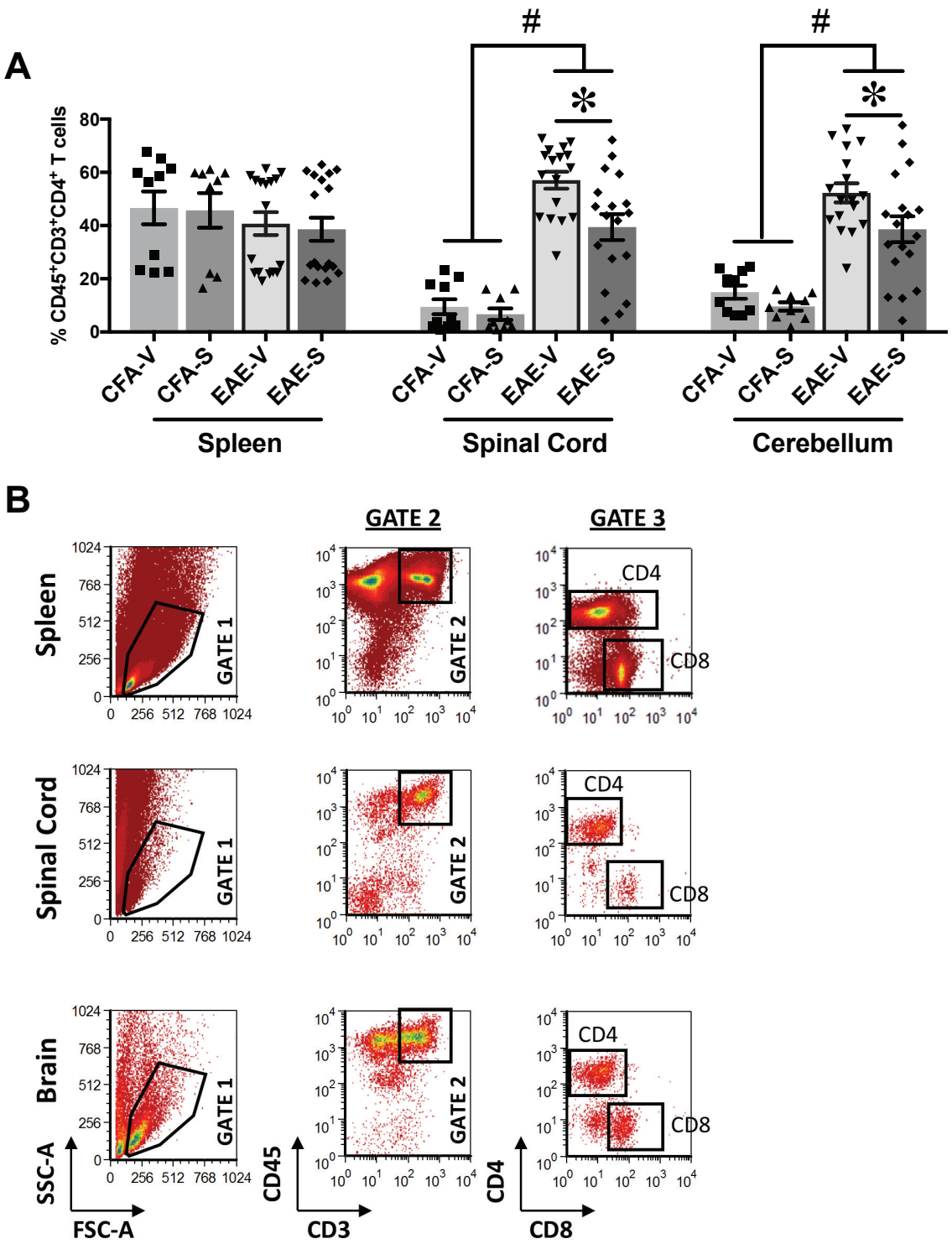
A
% CD45+CD3+CD4+ T cells
80
60
40
20
0
#
*
#
*
CFA-V
CFA-S
EAE-V
EAE-S
Spleen
Spinal Cord
Cerebellum
B
GATE 2
GATE 3
Spleen
Spinal Cord
Brain
GATE 1
GATE 2
CD4
CD8
SSC-A
FSC-A
CD45
CD3
CD4
CD8

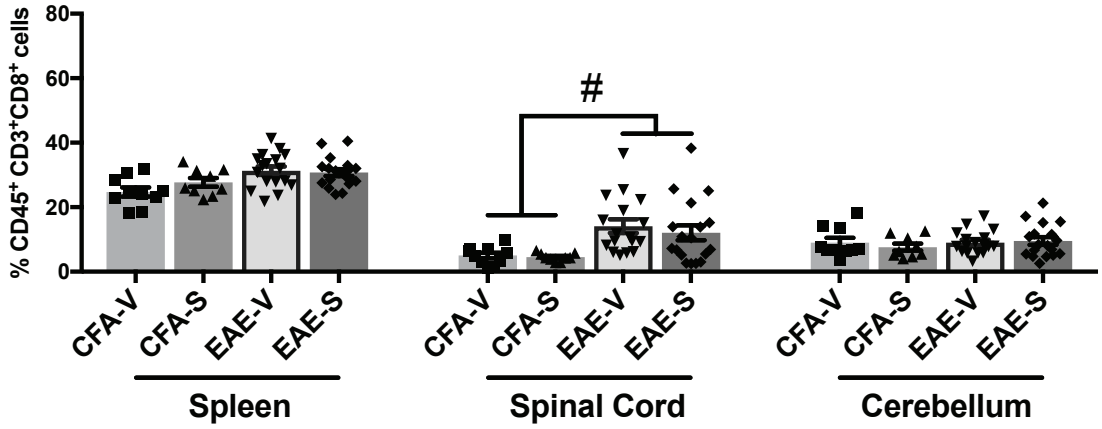

Figure 4.3: The percentage of $CD45^+CD3^+CD8^+$ T cells is increased in EAE spinal cord relative to CFA controls at day 21. Flow cytometry was used to assess cellular infiltration of $CD45^+CD3^+CD8^+$ T cells in spleen, spinal cord, and cerebellum of EAE and CFA mice treated with either vehicle or surfen. Frequencies are shown of $CD45^+CD3^+CD8^+$ T cells in EAE mice and CFA controls. No differences between groups were observed for the spleen or cerebellum. There was no effect of surfen on $CD45^+CD3^+CD8^+$ T cells, however, both EAE groups had significantly increased percentages of $CD45^+CD3^+CD8^+$ T cells in spinal cord relative to CFA controls. Data shown as mean ± SEM from two independent experiments. # = $p<0.05$

Figure 4.4: The effects of surfen on the transcriptional regulation of T effector cells and cytokine production in EAE spinal cord at day 21. **(A)** Transcript expression for the T cell transcription factors Tbet, Gata3, RORγT, and FoxP3 in spinal cord. Vehicle treated EAE mice displayed significantly increased expression for all four transcription factors relative to both surfen treated EAE mice and CFA controls. There were no significant differences in expression between groups for RoRγT **(B)** Transcript expression is shown for the cytokines IL-12p40 and IL-10 and the growth factor TGFβ. Vehicle treated EAE mice displayed significantly increased expression of all four transcription factors relative to both surfen treated EAE mice and CFA controls. **(C)** Protein concentrations are shown for the cytokines IL-17 and IFN-γ. There we no significant differences between groups for either cytokine. Data shown as mean ± SEM. * = $p<0.05$

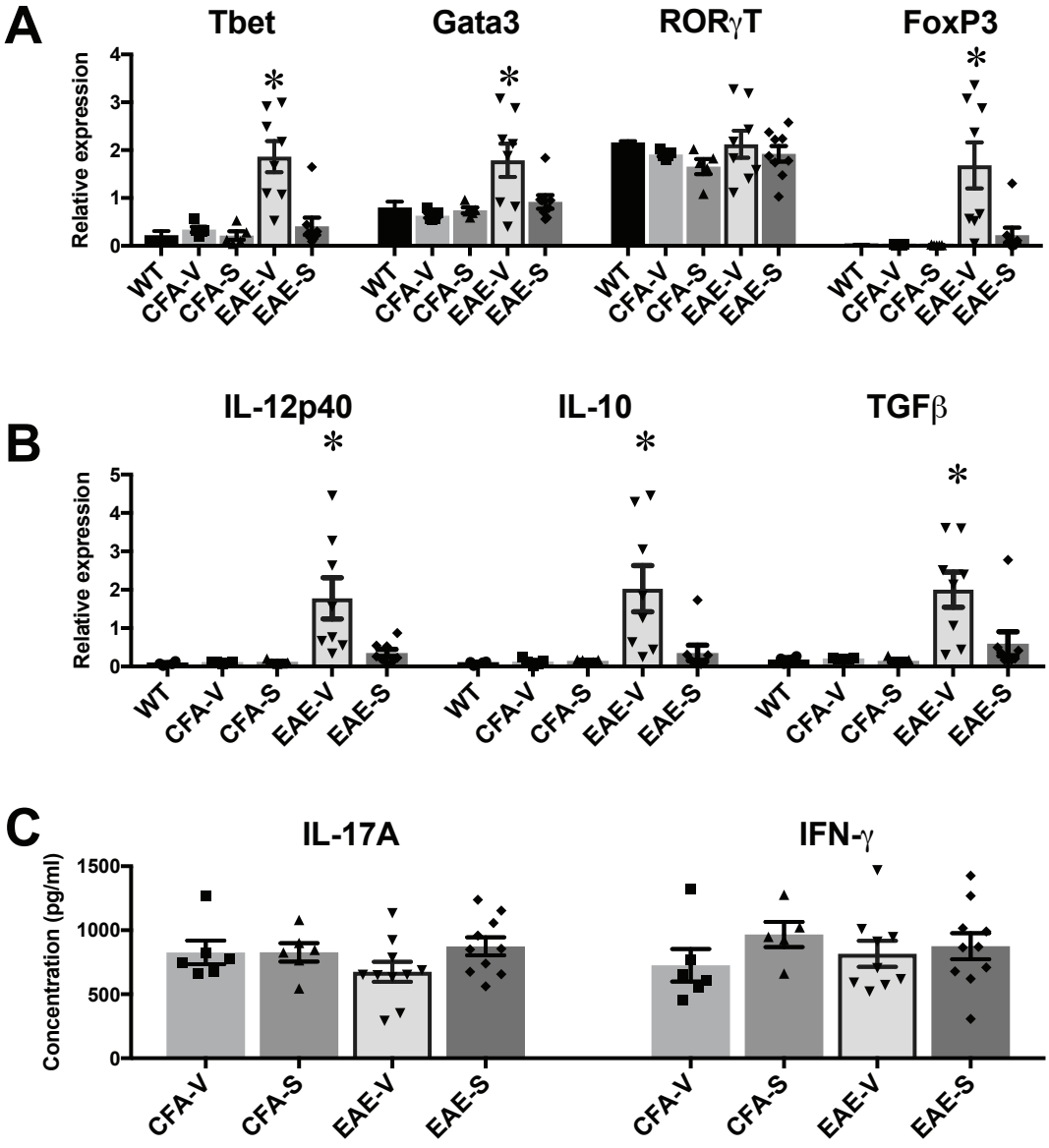
A
Tbet
Gata3
RORγT
FoxP3
Relative expression
WT
CFA-V
CFA-S
EAE-V
EAE-S
B
IL-12p40
IL-10
TGFβ
C
IL-17A
IFN-γ
Concentration (pg/ml)

Figure 4.5: The effects of surfen administration in EAE on factors related to $CD4^+$ T cell stimulation. **(A)** Protein concentrations are shown for IL-12p40 and IL-12p70 in spinal cord. Concentrations of IL-12p40 were significantly elevated in EAE-V mice relative to surfen treated EAE mice and CFA control groups. Conversely, concentrations of IL-12p70 were significantly higher in surfen treated EAE mice compared to EAE-V mice and CFA control groups. **(B)** The ratio is shown for IL-12p40/IL-12p70 protein concentrations in spinal cord. The ratio of IL-12p40 to IL-12p70 was significantly higher in EAE-V mice relative to both EAE-S and CFA controls. **(C)** Protein concentrations for the cytokine IL-2 in spinal cord are shown. No significant differences between groups were observed for IL-2 in the spinal cord. **(D)** Splenocytes were obtained from each EAE and CFA treatment group and restimulated *ex vivo* with MOG_{35-55} for 18 h. The frequencies of $CD4^+IFN\gamma^+$ T cells were determined using flow cytometry. Both EAE treatment groups showed a significant increase in the percentages of antigen-specific $CD4^+IFN\gamma^+$ T cells relative to CFA control groups. However, there was no significant effect of surfen on the percentage of $CD4^+IFN\gamma^+$ T cells following restimulation. Data shown as mean ± SEM. **(D)** is from two independent experiments. * = $p<0.05$, # = $p<0.05$

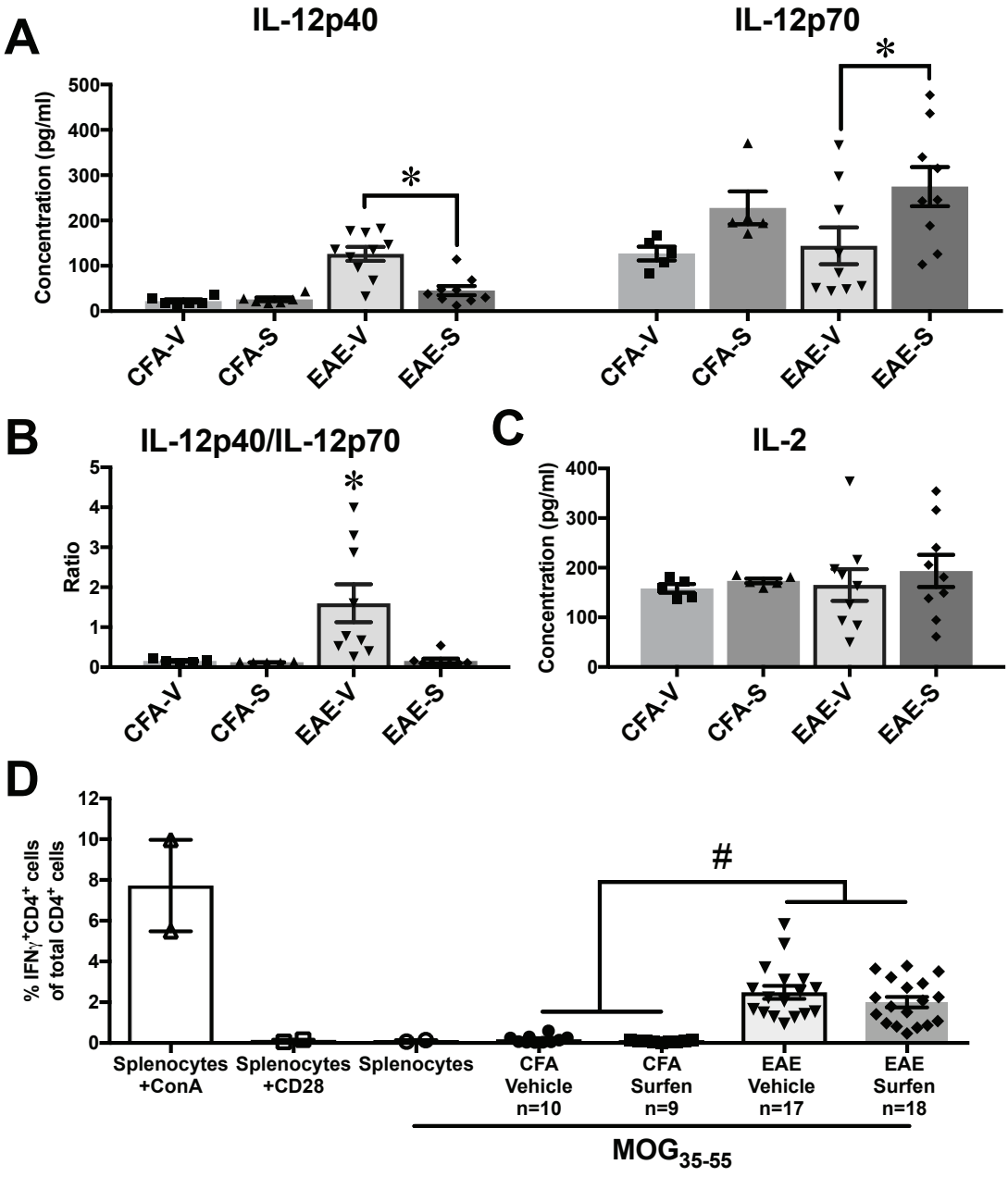
A
IL-12p40
IL-12p70
Concentration (pg/ml)
500
400
300
200
100
0
*
*
CFA-V
CFA-S
EAE-V
EAE-S
B
IL-12p40/IL-12p70
Ratio
5
4
3
2
1
0
*
C
IL-2
Concentration (pg/ml)
400
300
200
100
0
D
% IFNγ+CD4+ cells of total CD4+ cells
12
10
8
6
4
2
0
#
Splenocytes +ConA
Splenocytes +CD28
Splenocytes
CFA Vehicle n=10
CFA Surfen n=9
EAE Vehicle n=17
EAE Surfen n=18
MOG35-55

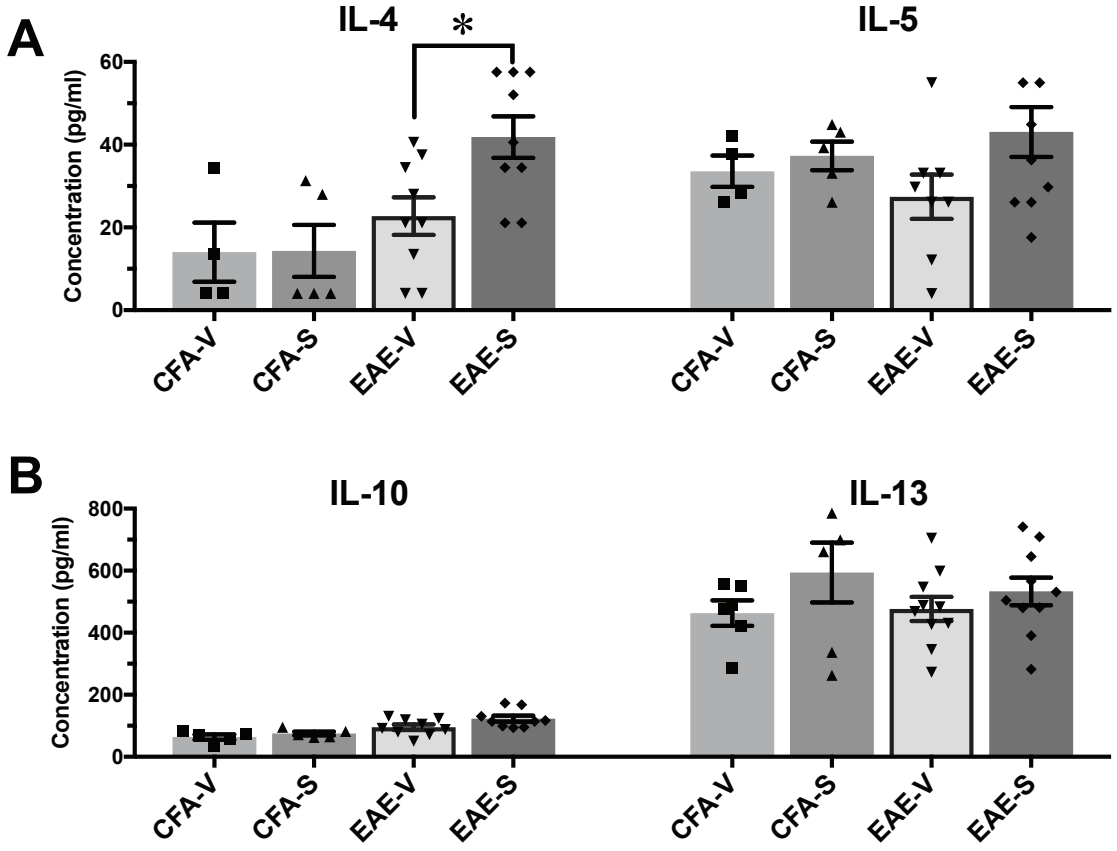

Figure 4.6: The effects of surfen on the production of the T_H2 cytokines IL-4, IL-5, IL-10, and IL-13 in EAE spinal cord at day 21. **(A)** Protein concentrations are shown for IL-4 and IL-5. Relative to EAE-V mice, surfen significantly increased the production of IL-4. Surfen produced a similar increase in the concentrations of IL-5 that did not reach significance. **(B)** Protein concentrations are shown for IL-10 and IL-13. There were no significant differences in concentrations between groups for either cytokine. Data shown as mean ± SEM. * = $p<0.05$

Figure 4.7: Administration of surfen (5 mg/kg) reduces the percentage of F4/80^{+}CD11b^{+} myeloid cells in EAE spinal cord at day 21. Flow cytometry was used to assess percentage of F4/80^{+}CD11b^{+} in spleen, spinal cord, and cerebellum of EAE and CFA mice treated with either vehicle or surfen **(A)** Frequencies are shown of F4/80^{+}CD11b^{+} myeloid cells in EAE mice and CFA controls. No significant differences between groups were observed for the spleen. Administration of surfen significantly reduced the percentage of F4/80^{+}CD11b^{+} myeloid cells in the spinal cord of EAE-S mice relative to EAE-V. Both EAE groups displayed an increased percentage of F4/80^{+}CD11b^{+} myeloid cells in spinal cord and cerebellum relative to CFA control mice. **(B)** Representative gating strategy. Data shown as mean ± SEM from two independent experiments. # = $p<0.05$, * = $p<0.05$

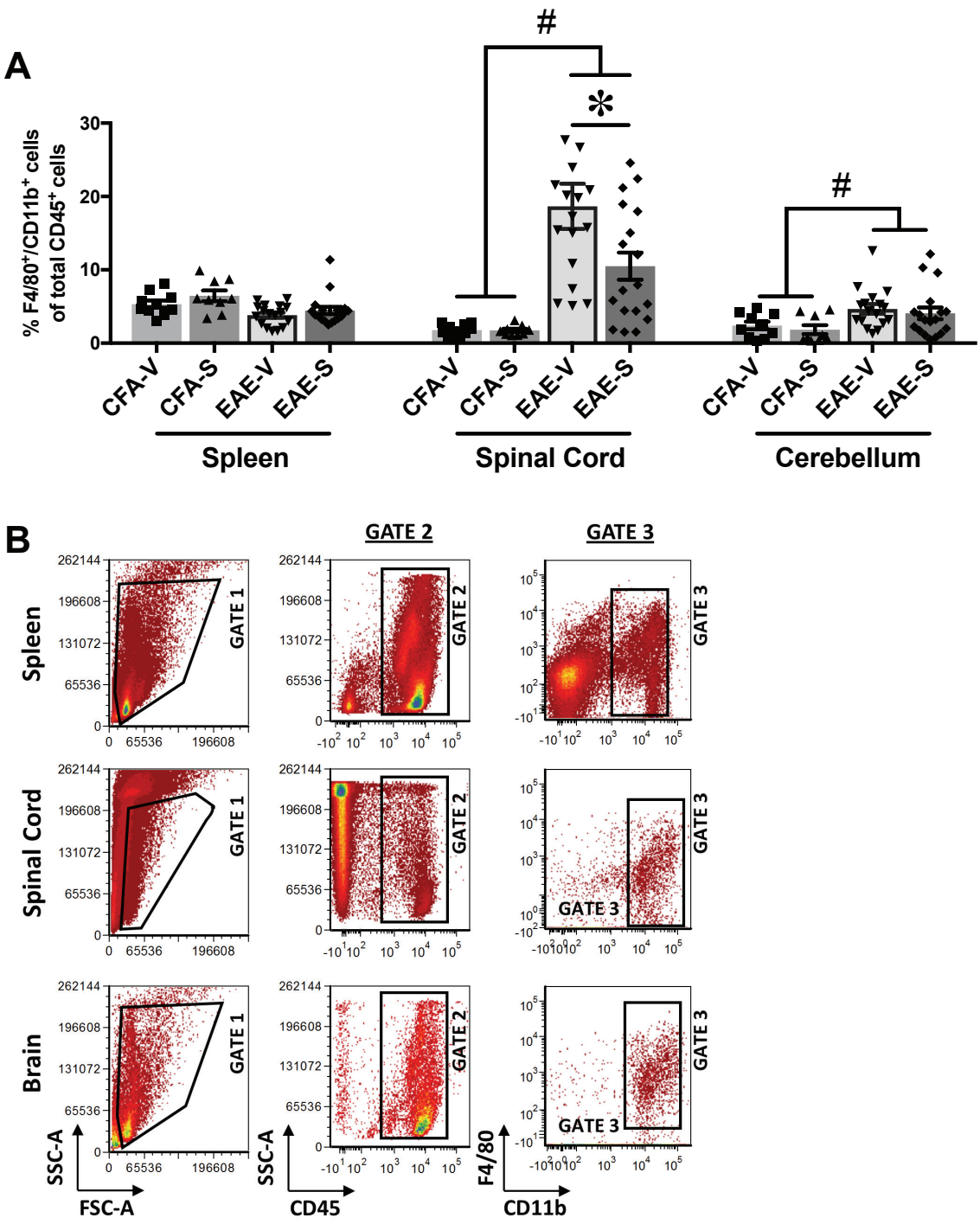
A
% F4/80+/CD11b+ cells of total CD45+ cells
30
20
10
0
#
*
#
CFA-V
CFA-S
EAE-V
EAE-S
Spleen
Spinal Cord
Cerebellum
B
GATE 2
GATE 3
Spleen
Spinal Cord
Brain
GATE 1
GATE 2
GATE 3
262144
196608
131072
65536
0
65536
196608
SSC-A
FSC-A
CD45
F4/80
CD11b

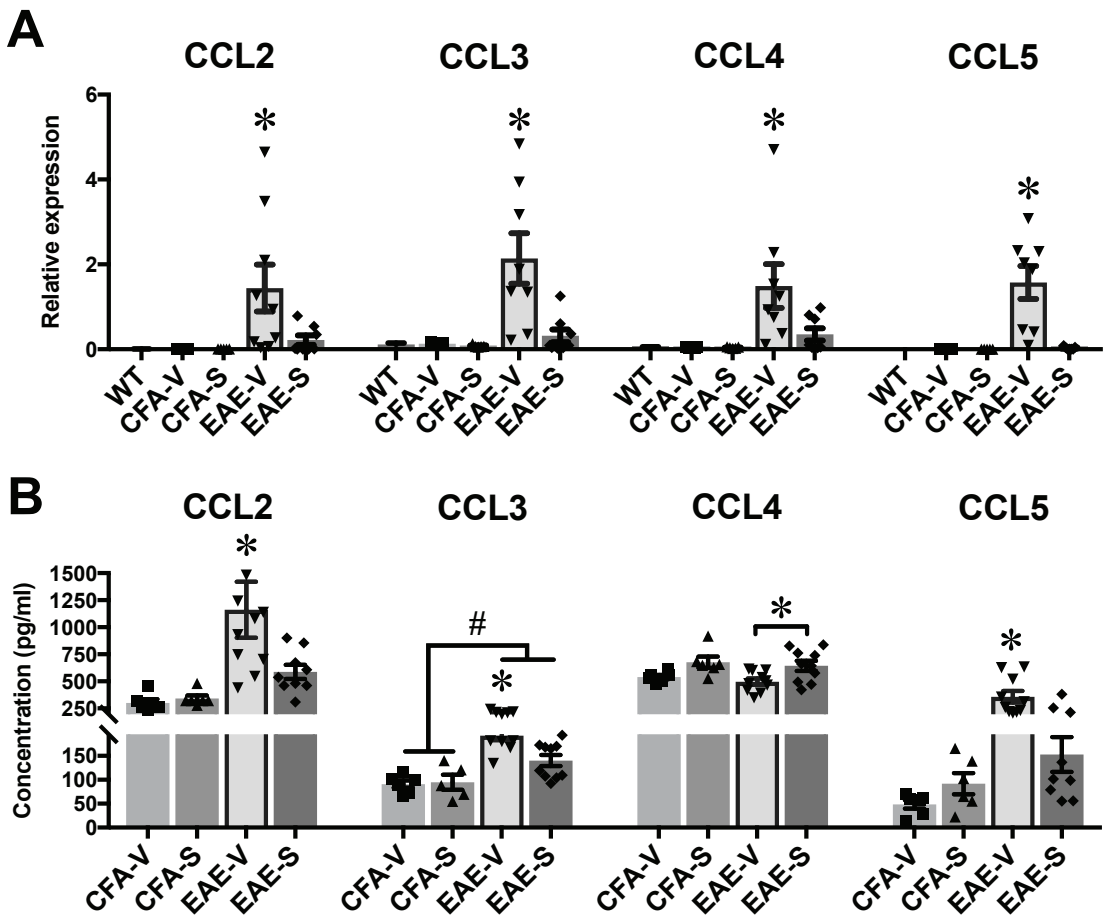

Figure 4.8: Administration of surfen reduces chemokine mRNA expression and protein concentrations in EAE spinal cord. **(A)** Transcript expression results are shown for the chemokines CCL2, CCL3, CCL4, and CCL5 in spinal cord. Vehicle treated EAE mice displayed significantly increased expression for all four chemokine mRNAs relative to both surfen treated EAE mice and CFA controls. **(B)** Protein concentrations are shown for the chemokines CCL2, CCL3, CCL4, and CCL5 in spinal cord. Concentrations of CCL2, CCL3, and CCL5 were significantly elevated in EAE-V mice relative to surfen treated EAE mice and CFA controls. Except for CCL3, EAE-S mice were not significantly different from CFA control groups. In contrast, surfen treatment increased concentrations of CCL4 in EAE mice relative to vehicle. No other significant differences were observed between groups for CCL4. Data shown as mean ± SEM. # =p<0.05, * = p<0.05

Figure 4.9: Treatment of BMDMs with surfen: viability, cell surface binding, and associated effects on chemokine production. **(A, B)** BMDMs were isolated from the tibias of healthy C57BL/6 female mice aged 8-12 weeks and unstimulated cells were treated with surfen for 24 h. Cell viability was assessed either with the marker 7-AAD with flow cytometry **(A)** or an MTT assay **(B)**. Both 10 μM and 20 μM surfen significantly reduced the percentage of viable cells relative to vehicle in both assays. **(C)** Fluorescence binding assay for surfen. Unstimulated murine BMDMs were collected and treated with surfen (5, 10, 20 μM) or vehicle (0.1% DMSO) for 2 h. A separate group of BMDMs were pre-treated with heparitinase-III (0.001 U/ml) or chondroitinase ABC (10 U/ml) for 2 h and washed once with PBS before surfen or vehicle was added at the stated doses for an additional 2 h. The cells were washed to remove excess surfen, and fluorescence read at an emission wavelength of 488 nm in a spectrophotometer. Surfen significantly bound to the surface of BMDMs at a concentration of 5 μM. Binding of 5 μM surfen was significantly inhibited by heparitinase and chondroitinase treatment. **(D)** BMDMs were collected, stimulated with LPS (100 ng/mL), and treated with either surfen (5 μM) or vehicle (0.1% DMSO). Protein concentrations are shown for the chemokines CCL2, CCL4, and CCL5. Relative to vehicle treatment, surfen significantly reduced the production of CCL2, CCL4, and CCL5 in LPS stimulated BMDMs. Data shown as mean ± SEM from four independent experiments. * = $p<0.05$ # = $p<0.05$

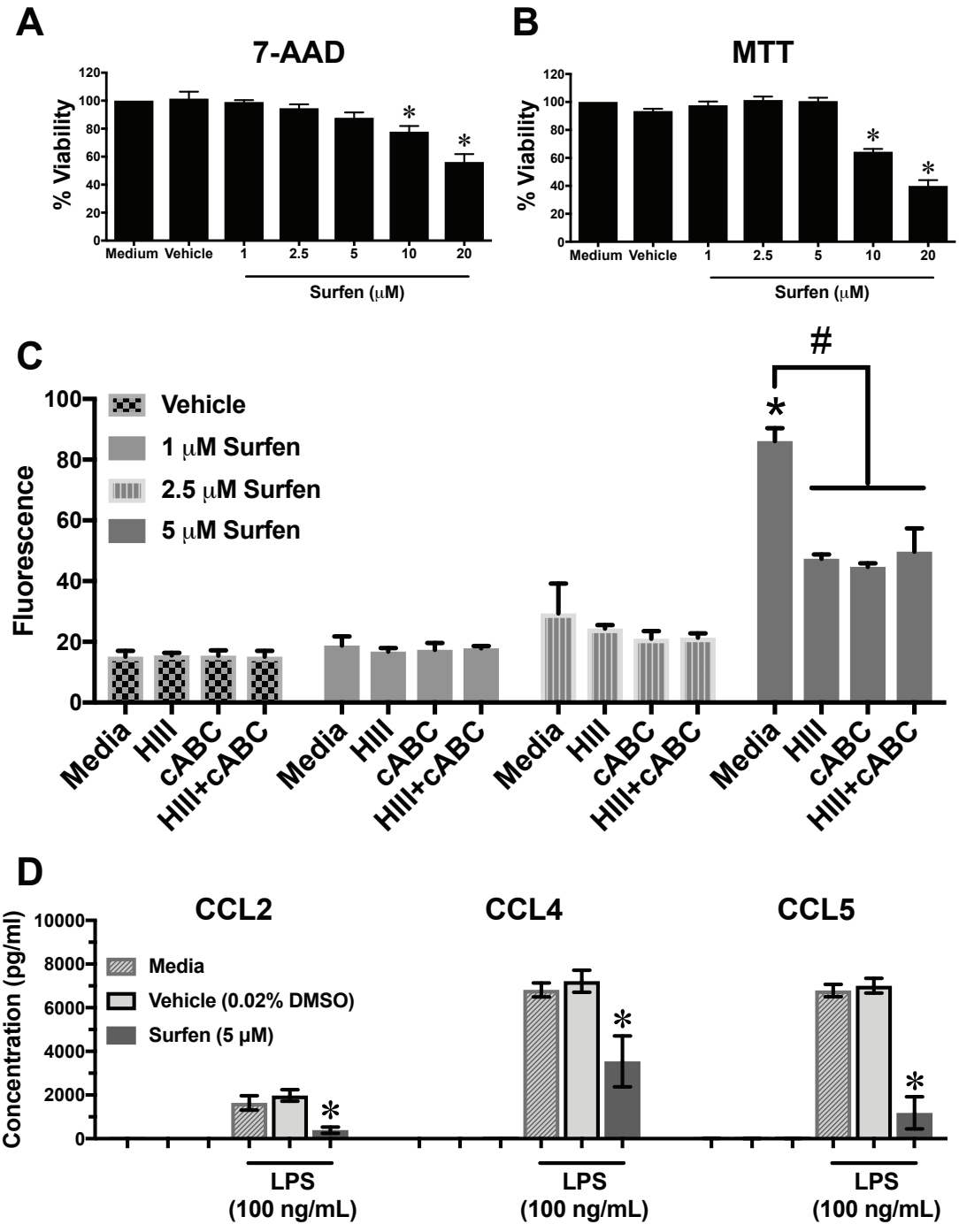
A
7-AAD
% Viability
120
100
80
60
40
20
0
Medium
Vehicle
1
2.5
5
10
20
Surfen (μM)
B
MTT
% Viability
Medium
Vehicle
1
2.5
5
10
20
Surfen (μM)
C
Fluorescence
100
80
60
40
20
0
Vehicle
1 μM Surfen
2.5 μM Surfen
5 μM Surfen
#
Media
HIII
cABC
HIII+cABC
D
CCL2
CCL4
CCL5
Concentration (pg/ml)
10000
8000
6000
4000
2000
0
Media
Vehicle (0.02% DMSO)
Surfen (5 μM)
LPS
(100 ng/mL)

Figure 4.10: Effects of surfen administration on pro-inflammatory cytokine production in EAE spinal cord at day 21. **(A)** Results are shown for IL-1β, IL-6, and TNF. There were no significant differences between groups for the mRNA expression of IL-1β or IL-6. Surfen treatment significantly reduced the expression of TNF in EAE mice relative to vehicle. EAE-S mice were elevated relative to CFA controls but did not reach significance. **(B)** Results are shown for iNOS and Arg-1. There were no significant differences between groups in mRNA expression for either iNOS or Arg-1. **(C)** Protein concentrations are shown for IL-1β, IL-6, and TNF. There were no significant differences between groups for concentrations of IL-1β, IL-6, or TNF. **(D)** Protein concentrations are shown for IL-1α. Relative to vehicle, surfen treatment significantly reduced concentrations of IL-1α in EAE mice. In contrast to EAE-V, EAE-S were not significantly different from CFA controls. Data shown as mean ± SEM. * = $p<0.05$

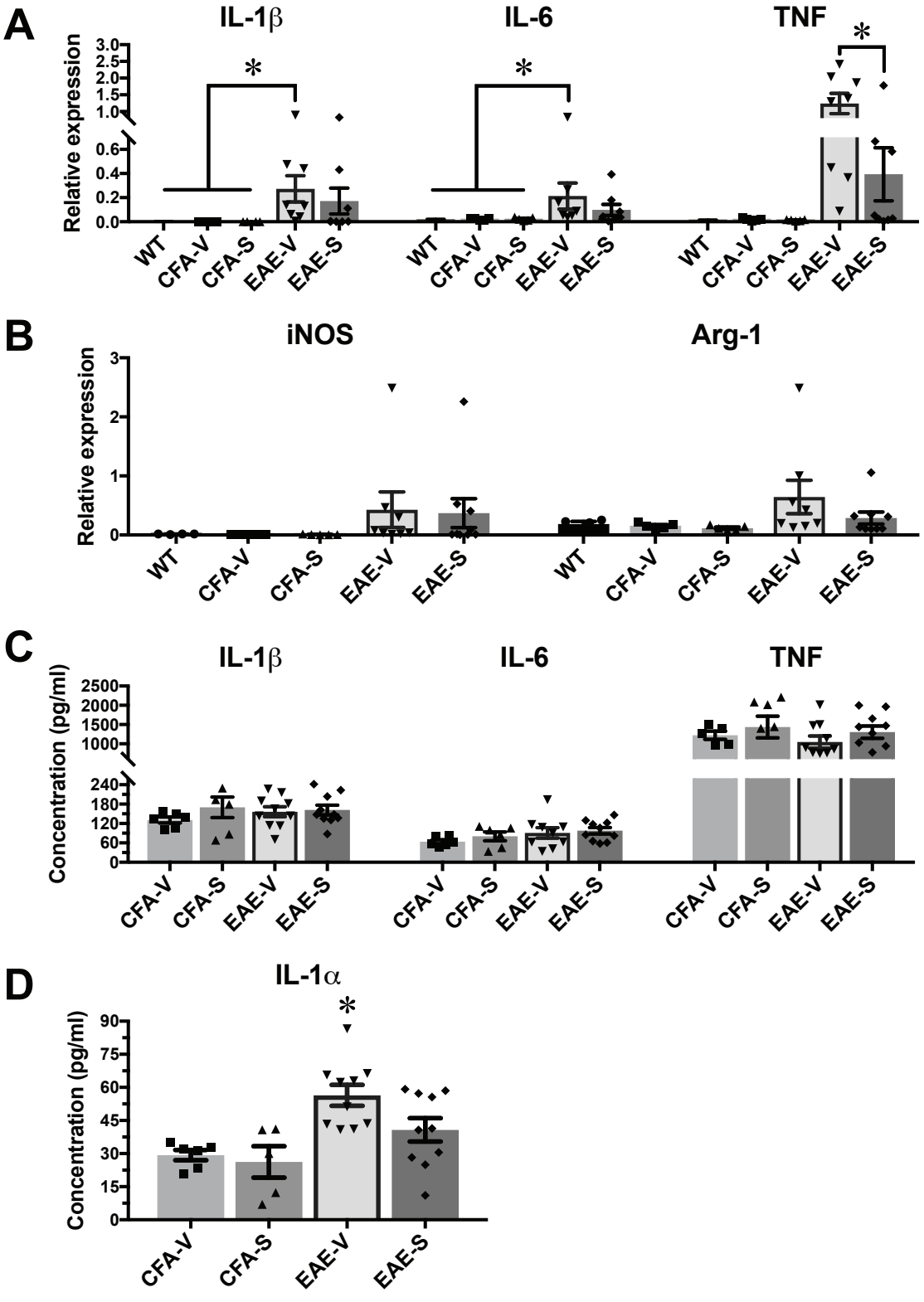
A
IL-1β
IL-6
TNF
Relative expression
3.0
2.5
2.0
1.5
1.0
0.6
0.4
0.2
0.0
*
*
*
WT
CFA-V
CFA-S
EAE-V
EAE-S
B
iNOS
Arg-1
Relative expression
3
2
1
0
WT
CFA-V
CFA-S
EAE-V
EAE-S
C
IL-1β
IL-6
TNF
Concentration (pg/ml)
2500
2000
1500
1000
240
180
120
60
0
CFA-V
CFA-S
EAE-V
EAE-S
D
IL-1α
Concentration (pg/ml)
90
75
60
45
30
15
0
*
CFA-V
CFA-S
EAE-V
EAE-S

Figure 4.11: Effects of surfen treatment (5 μM**)** on pro-inflammatory cytokine production in LPS-stimulated BMDMs. Following isolation, BMDMs were stimulated with LPS (100 ng/mL) and treated with either vehicle (0.02% DMSO) or surfen (5 μM) for 24 h. **(A)** Transcript expression is shown for the cytokines IL-1β, IL-6, and TNF. Surfen treatment significantly reduced the expression of all three cytokines in LPS-stimulated BMDMs relative to vehicle treatment. **(B)** Protein concentrations are shown for the cytokines IL-6 and TNF. Surfen significantly reduced the concentrations of both cytokines in LPS-stimulated BMDMs relative to vehicle treatment. **(C)** Protein concentrations are shown for IL-1β. Surfen significantly increased the concentrations of IL-1β in LPS-stimulated BMDMs relative to vehicle treatment. LPS stimulated media and vehicle controls were not significantly different from their unstimulated counterparts. **(D)** Protein concentrations are shown for IL-10. LPS-stimulated media and vehicle treatments significantly increased IL-10 concentrations whereas surfen treatment reduced IL-10 to the levels of unstimulated controls. Data shown as mean ± SEM from four independent experiments. ND denotes not detected. * = $p<0.05$

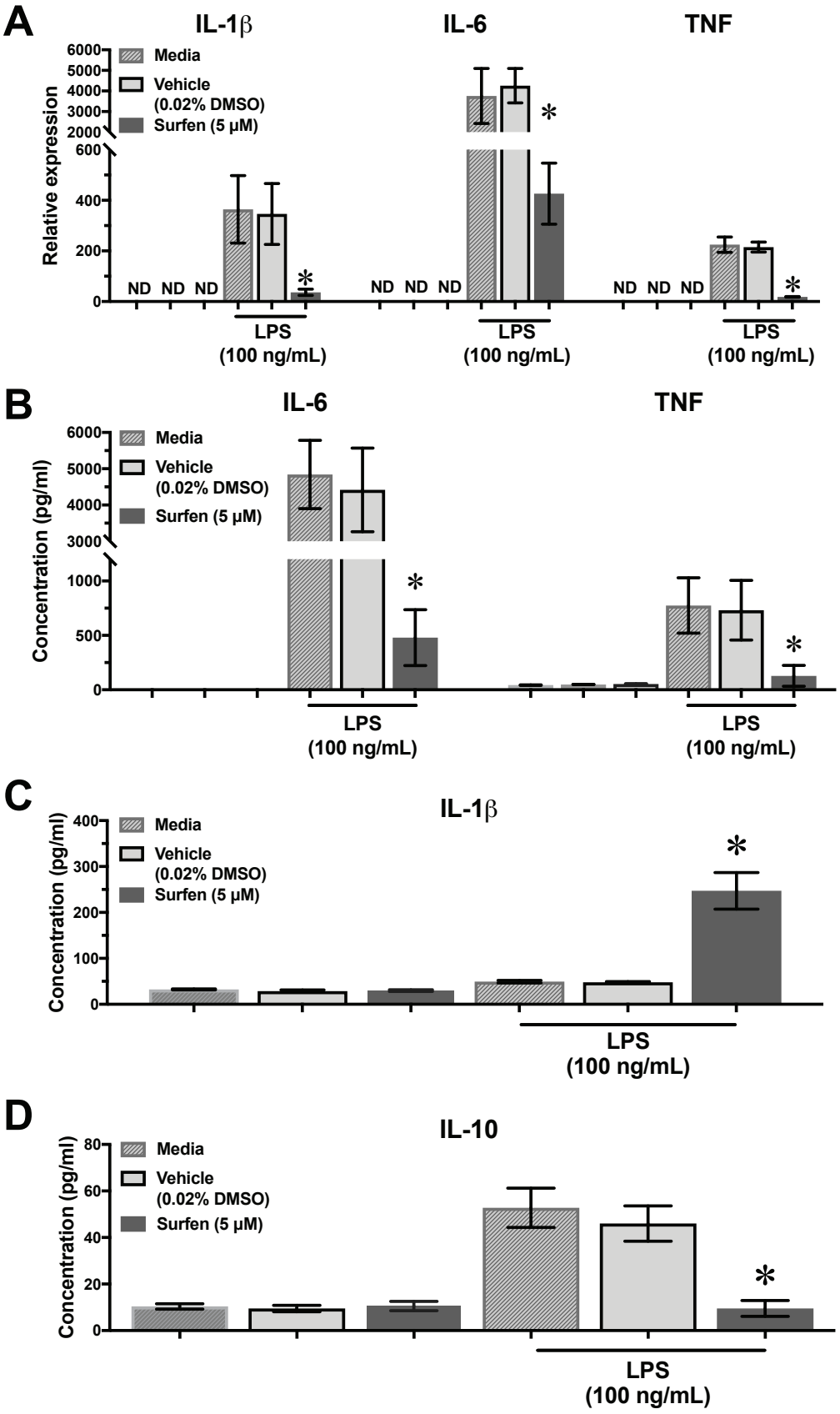
A
IL-1β
IL-6
TNF
Media
Vehicle
(0.02% DMSO)
Surfen (5 μM)
Relative expression
6000
5000
4000
3000
2000
600
400
200
0
ND ND ND
*
LPS
(100 ng/mL)
B
IL-6
TNF
Concentration (pg/ml)
1000
500
C
IL-1β
100
D
IL-10
80
60
40
20

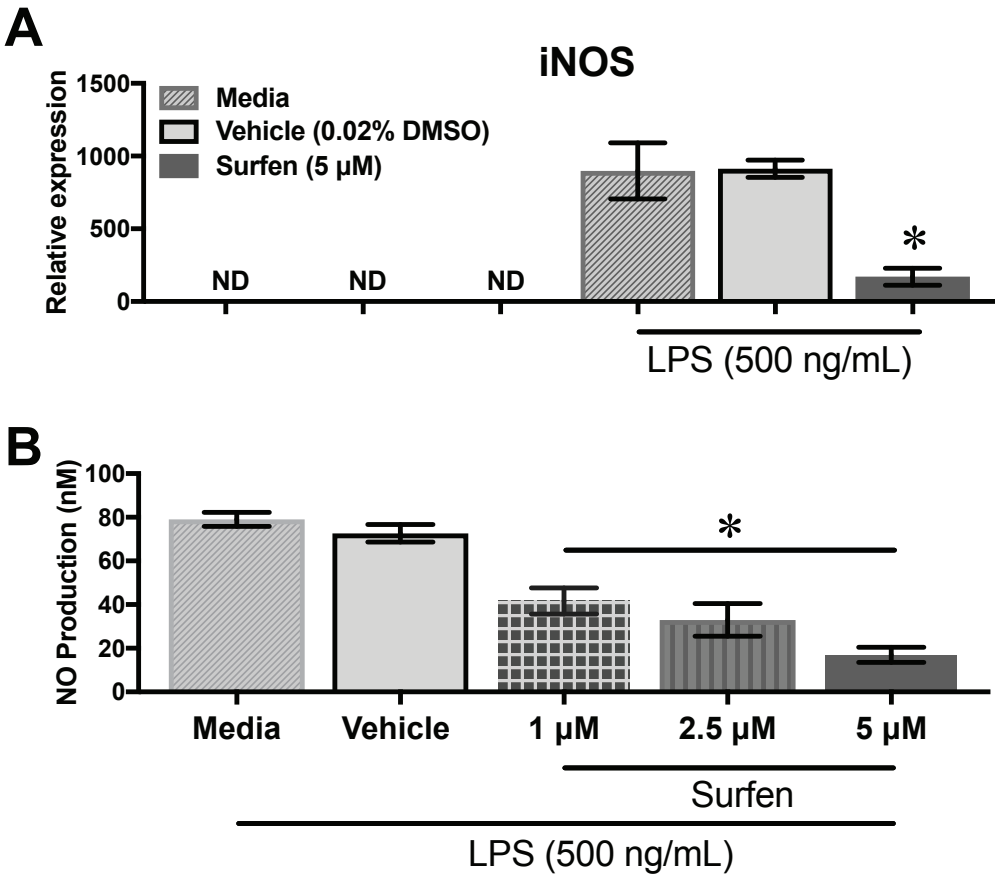

Figure 4.12: Nitric oxide production is reduced by surfen treatment in LPS-stimulated BMDMs. Following isolation, BMDMs were stimulated with LPS (500 ng/mL) and treated with either vehicle (0.02% DMSO) or surfen for 24 h. **(A)** Transcript expression is shown for iNOS. Surfen (5 µM) significantly reduced the expression of iNOS relative to vehicle treated LPS-stimulated BMDMs. **(B)** Concentrations of nitric oxide (NO) production from the supernatants of LPS-stmualted BMDMs are shown. Surfen (1-5 µM) significantly reduced NO production relative to vehicle treated LPS-stimulated BMDMs. Data shown as mean ± SEM and are representative of four independent experiments. ND denotes not detected. * = $p<0.05$

Figure 4.13: Heparan sulphate proteoglycan mRNA expression is reduced following the administration of surfen (5 mg/kg) with differential effects on chondroitin sulphate proteoglycans in EAE spinal cord at day 21. **(A)** Transcript expression is shown for the heparan sulphate proteoglycans NDST1, agrin, and syndecan IV in spinal cord. Administration of surfen reduced HSPG expression in EAE-S mice relative to EAE-V for all three mRNAs. This relationship extended to CFA controls where CFA-S mice also showed mRNA reductions in agrin and syndecan IV expression relative to CFA-V mice. Expression for NDST1 in CFA mice was not significantly different. **(B)** Transcript expression is shown for the heperan sulphate proteoglycans perlecan, serglycin, and syndecan I in spinal cord. EAE-V mice showed significantly elevated expression of all three mRNAs relative to surfen treated EAE mice and CFA controls. EAE-S mice were not significantly different from CFA controls; however, surfen did reduce expression for these mRNAs in CFA mice. **(C)** Transcript expression is shown for the chondroitin sulphate proteoglycans neurocan, aggrecan, and versican in spinal cord. No differences between groups were observed for the expression of neurocan. Vehicle treated EAE mice displayed significantly reduced expression for aggrecan relative to both surfen treated EAE mice and CFA controls. In contrast, versican expression was significantly increased relative to both surfen treated EAE mice and CFA controls. Data shown as mean ± SEM. * = $p<0.05$

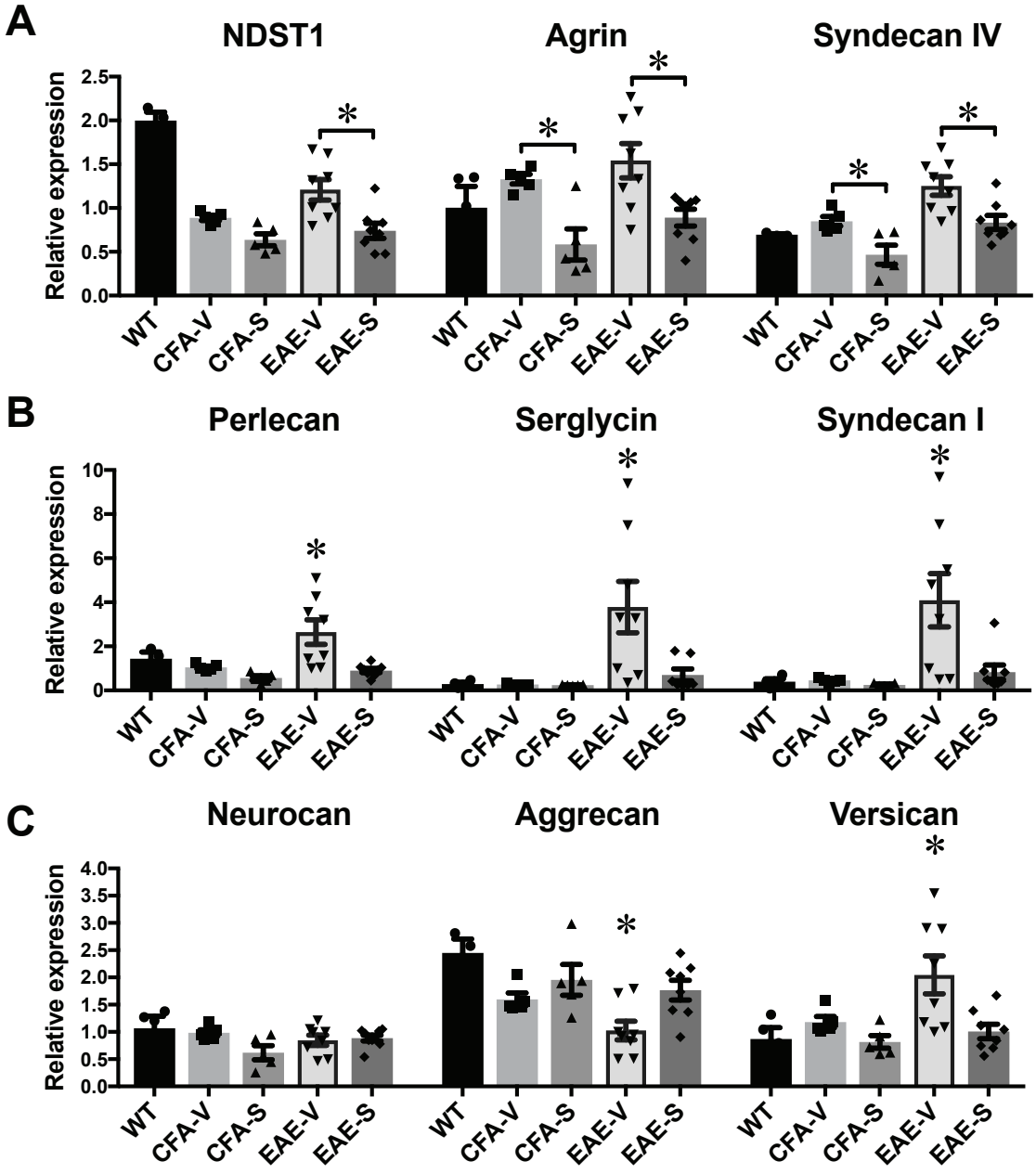
A
NDST1
Agrin
Syndecan IV
Relative expression
2.5
2.0
1.5
1.0
0.5
0.0
WT
CFA-V
CFA-S
EAE-V
EAE-S
B
Perlecan
Serglycin
Syndecan I
10
8
6
4
2
0
C
Neurocan
Aggrecan
Versican
4.0
3.5
3.0
2.5
2.0
1.5
1.0
0.5
0.0

Table 4.1: Correlation between proteoglycan mRNA expression and EAE clinical scores.

Gene Name	*Spearman r (r_s)*	*Significance*
NDST1	0.77	p=0.0005
Agrin	0.51	p=0.03
Syndecan IV	0.80	p=0.0003
Perlecan	0.73	p=0.001
Serglycin	0.80	p=0.0002
Syndecan I	0.86	p=0.0001
Neurocan	-0.54	p=0.03
Aggrecan	-0.76	p=0.0006
Versican	0.70	p=0.002

CHAPTER 5

ADMINISTRATION OF THE PROTEOGLYCAN ANTAGONIST SURFEN DELAYS REMYELINATION IN A LYSOLECITHIN MODEL OF DEMYELINATION

This manuscript is in preparation, with the following contributors:

Warford JR., Lamport AC, Hoskin, D.W., Easton A.S.

Student Contributions to Manuscript: JRW conducted the majority of lysolecithin surgeries, processed tissue, assisted with quantitative analysis of lesion area, performed histology, designed the experiments, conducted statistical analysis, and made all of the figures for this chapter. ACL provided technical assistance for surgeries, contributed intellectually, assisted with histology, assisted with quantitative analysis of lesion area, and sectioned all tissues for this manuscript. DWH and ASE provided experimental guidance and assisted with reagents. JRW wrote this manuscript with editorial assistance from EAS.

5.1 Introduction

Demyelinated axons are the hallmark pathological feature of MS yet the capacity of disease modifying therapies (DMTs) to promote their repair remains limited. Proteoglycans, particularly CSPGs, have been implicated in the disease mechanisms underlying failed remyelination (Keough et al., 2016; Lau et al., 2012). We have now established that the proteoglycan antagonist surfen reduces clinical severity in EAE, a murine disease used to model aspects of MS (Chapter 4). However, the capacity of surfen to promote remyelination is unknown. Demyelination during EAE is highly variable, making it difficult to determine repair mechanisms (Keough et al., 2015). Experimental models of demyelination, such as the lysolecithin model, use either detergents or toxins to produce demyelinated lesions making it possible to characterize the direct effects of experimental compounds on endogenous repair.

In the case of the lysolecithin model, a focal lesion is created by injecting the detergent lysolecithin, whose full chemical name is lysophosphatidylcholine (LPC) into a white matter tract, producing demyelination (Jeffery and Blakemore, 1995). Demyelination occurs because LPC is toxic to oligodendrocytes, the myelinating cells of the CNS. Nearby cells are unaffected through their ability to acylate lysolecithin into lecithin which limits overall cell death while maintaining axonal integrity (Webster & Alpern, 1964). Myelin is formed by compressed sheets of oligodendrocyte cytoplasmic processes that wrap around individual axons; multiple oligodendrocytes contribute to the myelination of one axon in the CNS. The LPC model of demyelination is an ideal alternative to EAE in assessing the ability of candidate compounds to promote remyelination. Therefore, the effects of surfen on remyelination following LPC induced demyelination will serve as the focus of this chapter.

Remyelination within the CNS occurs in two phases: (1) *the recruitment phase* whereby oligodendrocyte progenitors called oligodendrocyte precursor cells (OPCs) proliferate and migrate to the region of demyelination and (2) *the differentiation phase* that differentiates OPCs into fully functional mature oligodendrocytes, which then wrap their cytoplasmic processes around CNS axons to produce the myelin sheath (Chari, 2007). Mature oligodendrocytes are frequently found on the periphery of MS lesions; however, they are only able to remyelinate a small proportion of the denuded axons in the

plaque (Prayoonwiwat and Rodriguez, 1993). The presence of a partially remyelinated edge to some MS plaques has been termed a 'shadow plaque', but only a fraction of MS lesions (≈ 20%) develop this characteristic, and other plaques remain completely devoid of remyelinated axons (Frischer et al., 2015). Moreover, post-mortem examination suggests that the extent of remyelination in MS varies significantly between individuals (Patrikios et al., 2006). Failed remyelination in most MS plaques has been attributed to genetic variability between individuals, reduced OPC recruitment, and inefficient OPC differentiation (Chari, 2007; Franklin, 2002).

Inflammation is required for OPC recruitment and differentiation, but this represents a delicate balance between damage and repair (Madsen et al., 2016; Patel and Klein, 2011). MS therapies target the early inflammatory phase of the disease, and are successful in prolonging remission and controlling relapse rate during initial disease onset (Comi et al., 2013; Kappos et al., 2006; Miller et al., 2014). Nevertheless, few therapies have shown great promise with respect to promoting remyelination (Franklin, 2002; Keough and Yong, 2013). This may be due in part to the peripheral benefits of immunosuppression in MS (preventing peripheral T cell activation that leads to CNS infiltration and disease) versus the more finely tuned role of inflammation within the MS lesion, where immune suppression may have deleterious as well as beneficial effects. For example, ablation of macrophages following administration of clodronate-liposomes within 7 days of LPC injection in rat spinal cord delayed remyelination by oligodendrocytes (Kotter et al., 2001). In the same study, delaying macrophage depletion until 8 days after LPC administration produced no differences in patterns of remyelination (Kotter et al., 2001), pointing to time-dependent effects of inflammatory cell subsets on remyelination in animal models.

The delayed remyelination observed by Kotter and colleagues following macrophage depletion early in the LPC model was later attributed to impaired OPC differentiation rather than recruitment (Kotter et al., 2005, 2006). Mechanisms that prevent OPC differentiation include the reduced expression of growth factors by macrophages such as insulin growth factor (IGF; Kotter et al., 2005) and reduced phagocytosis of myelin debris by macrophages, which must be cleared before OPCs can engage in remyelination and repair (Kotter et al., 2006). More recent work using

CX3CR1 knockout mice to impair myeloid cell function in a cuprizone model of demyelination showed similarly delayed remyelination in association with the accumulation of myelin debris from decreased phagocytosis by myeloid cells (Lampron et al., 2015). Interestingly, astrocytes also phagocytose myelin in human MS lesions (Ponath et al., 2017). Cell culture assays suggest that astrocytes respond to myelin ingestion by upregulating pro-inflammatory mediators and chemokines (Ponath et al., 2017). These astrocyte derived mediators may represent a failed attempt at promoting remyelination, much as macrophages appear to promote remyelination through myelin phagocytosis and the production of growth factors in experimental models.

The detrimental effect of macrophage depletion in LPC models conflicts with autoimmune inflammatory models such as EAE, where macrophage depletion with clodronate-liposomes resulted in reduced clinical severity and inflammation (Huitinga et al., 1990; Miron et al., 2013). However, these studies also demonstrate that macrophages can transition from one phenotype to another based on environmental cues. Analogous to the T_H1/T_H2 axis, transcriptional changes within macrophages are thought to promote either a pro-inflammatory classic "M1" phenotype or an alternatively activated "M2" phenotype involved in immunomodulation and tissue repair (Martinez and Gordon, 2014).

Macrophages pushed towards an M2 phenotype *in vitro* with anti-inflammatory IL-13 promote OPC differentiation (Miron et al., 2013). These findings were extended *in vivo* and the selective deletion of M2 monocytes using mannose-receptor specific clodronate-liposomes decreased OPC differentiation markers in an LPC model of demyelination within the corpus callosum (Miron et al., 2013). Although the "M1/M2" paradigm is controversial, with evidence that approximately 70% of macrophages in MS lesions display both M1 and M2 markers (D. Y. Vogel et al., 2013), altered transcriptional regulation of myeloid cells in response to inflammation does appear to play a significant role in remyelination.

Experimental models of demyelination have identified several other factors that interfere with both the recruitment and differentiation of OPCs in addition to myelin debris. LINGO1 (leucine-rich repeat and Ig domain-containing, Nogo receptor interacting protein) was identified as an inhibitor of oligodendrocyte differentiation (Mi et al., 2009).

Anti-LINGO monoclonal antibodies showed promise in EAE and co-culture studies, but failed to improve clinical outcomes in a phase II clinical trial (Mi et al., 2009, 2007; ClincalTrials.gov identifier NCT01864148). The failure of LINGO to improve clinical outcomes despite promise in experimental models suggests the need to therapeutically target an inhibitor of remyelination that displays a broader role in both immune function and delayed repair. Proteoglycans are one potential candidate for therapeutic development that are involved in both scenarios.

Proteoglycans such as CSPGs are potent inhibitors of OPC recruitment, process outgrowth, and differentiation *in vitro* (Keough et al., 2016; Lau et al., 2012; Siebert and Osterhout, 2011). Moreover, CSPGs have been shown to accumulate in both MS and LPC lesions (Lau et al., 2012; Sobel and Ahmed, 2001). Treatment of LPC lesions with the CSPG side chain inhibitor xyloside promoted remyelination by increasing OPC recruitment (Lau et al., 2012). Endogenous clearance of CSPGs does occur in LPC lesions via matrix metalloproteinases-9 (MMP-9), enabling OPC process outgrowth and permitting remyelination to proceed (Larsen et al., 2003; Uhm et al., 1998). Mice null for MMP9 display impaired remyelination, and are deficient in OPCs, suggesting a protective role for this MMP (Larsen et al., 2003). However, the cost of augmenting MMP expression therapeutically in MS may be greater than the reward, as MMPs are partly responsible for breaching the BBB and promoting disease severity in EAE (Yong et al., 2001). Alternatively, selective antagonism of CSPGs with the small molecule fluorosamine promoted remyelination in an LPC mouse model (Keough et al., 2016), providing proof of concept that proteoglycan antagonists hold clinical potential for the treatment of MS.

A proteoglycan antagonist capable of binding both HSPGs and CSPGs has yet to be tested in an LPC model. As with CSPGs, HSPGs also accumulate within MS lesions yet their role in poorly understood (van Horssen et al., 2006). The HSPGs syndecan-3, glypan-1, and perlecan have been linked to OPC proliferation and differentiation *in vitro* (Winkler et al., 2002). Syndecan-3 and glypan-1 promote OPC proliferation by binding growth factors such as FGF, while perlecan is increased two-fold during the transition from OPC to mature oligodendrocyte, implicating these HSPGs in both the recruitment and differentiation phases of remyelination (Winkler et al., 2002).

In this chapter, we demonstrate that direct injection of surfen into the corpus callosum of mice at the peak of LPC-induced demyelination delayed remyelination. Peak demyelination occurs approximately 2 days after the injection of LPC, followed by rapid recruitment of OPCs and remyelination which reduces lesion size by day 7 (Keough et al., 2015; Kotter et al., 2005). Surfen treated lesions also showed increased myeloid activity as measured by Iba-1 and increased CSPG production. By contrast, administration of surfen at day 7 following LPC-induced demyelination had no significant effect on lesion size, indicating that surfen may interfere with the early phase of remyelination associated with OPC recruitment. This provocative finding implies a potentially protective role of proteoglycans early in the remyelination process.

5.2 Results

5.2.1 Co-injection of either surfen or vehicle with lysolecithin into the corpus callosum does not affect lesion area at day 7

To assess whether surfen had any direct effects on the ability of LPC to induce demyelination, either vehicle (2% DMSO) or surfen (100 μM) were co-injected with 1% LPC into the corpus callosum on day 0. Each mouse received one individual lesion containing either LPC + vehicle or LPC + surfen. A separate group of mice were injected with LPC alone as a control group. Mice were sacrificed at day 7 and brain tissue sections stained for myelin using eriochrome cyanine and neutral red (Figure 5.1). The mean area of surfen treated lesions was not significantly different from vehicle treated lesions at day 7. The mean area of both lesions was not significantly different from that of control mice injected with LPC alone.

5.2.2 Administration of surfen into the corpus callosum 2 days following lysolecithin increases lesion area at days 7 and 14, but not at day 21

Having established that surfen had no effect on lesion size when administered at day 0, it was asked whether surfen could promote recovery when administered during peak demyelination before the recruitment phase of remyelination had started. Two days following LPC administration was selected as the appropriate time at which the lesion had reached, or was near, its maximal size before OPCs are recruited (Figure 5.2A). Foamy phagocytic cells were present at the border of day 2 lesions and contained

eriochrome cyanine stained myelin debris indicative of active myelin phagocytosis (see panel labeled 'LPC border', Figure 5.2A).

We injected LPC bilaterally into each side of the corpus callosum to create a set of paired lesions in each mouse. Either surfen (100 μM) or vehicle (2% DMSO) were injected directly into each lesion 2 days following injection of LPC at day 0. A separate cohort of mice received a bilateral injection of LPC into the corpus callosum on day 0 and a sham procedure involving the mechanical insertion of the needle 2 days later. Mice were carried out to day 7, 14, or 21, at which point they were killed and brain tissue sections stained for myelin with eriochrome cyanine and neutral red. The administration of surfen 2 days after LPC significantly increased the mean lesion area relative to LPC + vehicle at days 7 and 14, but not 21. The mean lesion area was not significantly different between LPC + vehicle and LPC + sham injection. The time course of lesion development is shown in Figure 5.2B.

Histologically, LPC + surfen treatment produced large lesions at day 7 displaying cellularity and demyelination that extended into the striatum (Figure 5.2A). By contrast, LPC + vehicle treatment produced smaller lesions that generally remained within the confines of the corpus callosum. Patchy remyelination along the lesion border was evident by day 14 in LPC + vehicle lesions whereas LPC + surfen treatment did not produce clear signs of remyelination at day 14 and maintained a sharply demarcated lesion border comparable to lesions at day 7 (see LPC border, Figure 5.3A). By day 21, both LPC + surfen and LPC + vehicle lesions showed similar evidence of remyelination and were not significantly different. Neither surfen, vehicle, or sham LPC groups showed complete remyelination at day 21.

5.2.3 Administration of surfen on day 2 delays endogenous remyelination at day 7

Surfen administered into an LPC lesion on day 2 increased the mean lesion area by day 7 (Figure 5.2A). Next, the mechanism by which this occurs was investigated. The hypothesis raised was that surfen delays remyelination of axons in the corpus callosum following LPC injection. To test this, mice were injected with LPC bilaterally into the corpus callosum on day 0 and the resulting lesions were injected with either vehicle or surfen on day 2. A separate group of mice received no surgery and served as healthy

controls to evaluate the normal corpus callosum. Mice were sacrificed at day 7 and ultrathin 1 μm thick sections of lesions in the corpus callosum were examined by electron microscopy. The extent of axonal myelination was calculated using the ratio of axon circumference to the outer circumference of myelinated fibers (G-ratio) within the lesion. As myelin thickness decreases, the G-ratio increases until a ratio of 1 is reached, indicating a completely denuded axon (Mei et al., 2016).

Surfen treated lesions showed profound demyelination relative to vehicle treated lesions, as signified by sparse axonal remyelination and increased frequency of denuded axons (Figure 5.3A). Both surfen and vehicle treated LPC lesions showed histological signs of demyelination relative to healthy controls. LPC + surfen treated lesions had a significantly higher G-ratio relative to LPC + vehicle lesions (Figure 5.3B). Both surfen and vehicle treated LPC lesions displayed significantly higher G-ratios relative to healthy controls. G-ratio frequencies were used to quantify the number of axons undergoing remyelination within the lesion. Remyelination produces myelin sheaths that are thinner than normal, therefore the G ratio is higher than normal. A G-ratio between 0.80 and less than 1 is an indication of an axon that has undergone remyelination (Mei et al., 2016). Using this range, the frequency of remyelinated axons in LPC + vehicle treated lesions was 24% compared to just 7.3% in LPC + surfen treated lesions. Moreover, LPC + surfen treated lesions contained 34% more denuded axons (G ratio of 1) relative to vehicle treated lesions (Figure 5.3C). By contrast, 92% of the axons in healthy controls had a G-ratio under 0.80 compared to 37% of LPC + vehicle lesions and only 19% within LPC + surfen lesions. This high proportion of axons with a lower G ratio reflects normally myelinated axons.

5.2.4 Administration of surfen on day 2 increases Iba-1 and CSPG production at day 7

Thus far, it has been established that surfen produces larger lesions by day 7 when administered during peak disease, and electron microscopy confirmed that this was associated with reduced remyelination. Given the role of surfen as a proteoglycan antagonist, and our previous work describing its effects on macrophage function (Chapter 4), we evaluated Iba-1, a marker for myeloid cells, and CSPG expression using immunofluorescence in LPC lesions at day 7 following treatment on day 2 (Figure 5.4A).

LPC + surfen treated lesions displayed significantly increased fluorescence intensity of both Iba-1 and CSPGs relative to LPC + vehicle treated lesions. There was no overlap between the two signals, suggesting that CSPGs are located outside the myeloid cells, in the extracellular space. No significant differences were observed between LPC + vehicle lesions and LPC + sham controls (Appendix Figure 1).

5.2.5 Surfen treatment on day 7 does not cause a significant difference in lesion size on days 14 and 21

To assess the effects of surfen on lesion area when endogenous repair mechanisms were active, we injected LPC bilaterally into the corpus callosum and treated the resulting lesions with either vehicle or surfen at day 7, when lesion size is normally already reduced (Figure 5.2B). Mice were carried out until either day 14 or day 21, at which point they were sacrificed and brain tissue sections processed and stained for myelin with eriochrome cyanine and neutral red. The mean lesion area was elevated in the LPC + surfen group ($2.9 \times 10^6 \pm 9 \times 10^5$) compared to LPC + vehicle ($1.6 \times 10^6 \pm 4.7 \times 10^5$) at day 14 but this was not statistically significant (Figure 5.5B). There were no significant differences in mean lesion area between LPC + vehicle and LPC + sham groups. By day 21, the mean lesion area was similar for LPC + surfen, LPC + vehicle and LPC + sham groups, with no significant differences between groups.

Histologically, LPC + vehicle lesions at both day 14 and 21 showed signs of repair that included patchy remyelination on the lesion border. Sham controls showed a similar pattern. The lesion following LPC + surfen treatment still had sharply demarcated edges at day 14 relative to vehicle treatment, which may indicate a relative lack of remyelination. However, surfen produced an apparent increase in cellularity at the border of the corpus callosum at day 14 not observed in vehicle or sham controls. By day 21, vehicle and sham treatments exhibited blurred lesion edges, usually associated with partial remyelination while surfen treated lesions maintained a sharp border, which may indicate more efficient repair in vehicle lesions. Taken together, administration of surfen at day 7 did not significantly increase mean lesion area but produced unique neuropathological changes.

5.3 Discussion

5.3.1 Summary

Remyelination following LPC-induced demyelination occurs in several distinct phases that mimic those observed in MS lesions. First, demyelination occurs rapidly between days 0-3 (Keough et al., 2015; Kotter et al., 2001). During this time, chemokines and pro-inflammatory mediators are upregulated as early as 6 h post LPC injection and promote monocyte recruitment into the developing lesion (Ousman and David, 2001). Recruited monocytes are activated by T cells within the first 12 h after LPC injection (Ghasemlou et al., 2007) and begin producing a host of chemokine and inflammatory mediators. Next, the recruitment of OPCs into the lesion occurs from approximately 2-8 days after peak demyelination. Upon arrival, endogenous remyelination is only possible following the differentiation of OPCs into mature myelin producing oligodendrocytes, occurring approximately from days 8-21 (Keough et al., 2015; Kotter et al., 2005). Studies that have characterized these OPC recruitment and differentiation phases using LPC have been conducted in rodent spinal cord. The current study examines remyelination within the corpus callosum, which may alter this timeline. Nevertheless, work by Miron et al. (2013) is one of the few studies that have used LPC in the corpus callosum, and their analysis of OPCs suggests the rate of remyelination is similar in the two structures.

In this study, we took advantage of these phases to probe the effects of surfen on endogenous remyelination using three time points for injection: (1) At the time of LPC administration before lesion development, (2) at day 2 during peak demyelination before the recruitment of OPCs was likely to have become established, and (3) at day 7 when OPC differentiation and remyelination were underway, producing a reduced lesion volume. Unlike MS, where some lesions may persist indefinitely, recovery is relative rapid following LPC injection.

We show that surfen does not impede lesion development when co-injected with LPC at day 0, but delays remyelination when administered at day 2. Increased lesion size at day 7 was associated with augmented myeloid cell numbers (as indicated by Iba-1 staining) and CSPG production in the lesion. By contrast, surfen lesions were no different from vehicle lesions at day 14 or 21 when treatment was administered on day 7. These

findings suggest surfen disrupts the OPC recruitment phase, but has relatively little effect on lesion size when administered during the later differentiation phase.

5.3.2 Surfen does not prevent demyelination following co-injection with LPC

To exclude the possibility that surfen interfered with the ability of LPC to demyelinate axons through toxic effects on oligodendrocytes, we co-injected surfen with LPC on day 0 and quantified mean lesion area during recovery at day 7 (Figure 5.1). No significant differences between LPC + vehicle, LPC + surfen or LPC only groups were observed. This suggests that surfen does not interfere with the ability of LPC to induce demyelination. Indeed, our data for surfen co-injection at day 2 would suggest the opposite effect, that surfen might enhance the toxic effects of LPC to create larger lesions, however significant increases in the LPC + surfen lesion size were not observed.

Furthermore, the failure of co-injection of surfen with LPC to affect lesion area by day 7 implies that surfen does not impede events associated with early demyelination (i.e. within the first 1-2 days). This is unexpected for two reasons. First, T cells and monocytes have been observed in murine spinal cord LPC lesions as early as 6 h following injection (Ghasemlou et al., 2007; Ousman and David, 2001). Second, CCL2, CCL3, TNF, and GM CSF expression peaks within the first 24 h of LPC injection (Ousman and David, 2001). We have previously demonstrated that surfen reduces T cell proliferation (Chapter 3) in addition to decreasing mRNA expression and protein concentrations for several chemokines (CCL2, CCL3, and CCL5), both in EAE and LPS-stimulated BMDMs, in addition to reducing TNF mRNA expression (Chapter 4). If surfen had similar effects here, then the absence of an effect seems surprising. It is possible that surfen may have already bound to other substrates such as cells and the extracellular matrix before the subsequent arrival of T cells and monocytes into the lesion. Alternatively, surfen may have been more efficacious when administered peripherally by interfering with peripheral T cell priming or cellular infiltration into the CNS.

5.3.3 Surfen disrupts early events associated with remyelination resulting in delayed lesion recovery

Stereotactic administration of surfen 2 days following administration of LPC significantly increased the mean lesion area at day 7 relative to the LPC + vehicle group (Figure 5.2A). LPC + surfen treated lesions remained significantly larger relative to LPC + vehicle at day 14, before showing signs of remyelination at day 21 when the mean lesion area was comparable between groups (Figure 5.2B). Electron microscopy indicates that the increased lesion size following LPC + day 2 surfen treatment at was the result of delayed remyelination, with LPC + surfen treated mice displaying axons with a significantly higher G-ratio (thin or absent myelin sheaths) and a decreased frequency of remyelinated fibres (with a G ratio > 0.8) (Figure 5.3). Lastly, the expression of Iba-1 and CSPG was significantly increased at day 7 in LPC + surfen lesions treated on day 2 relative to LPC + vehicle (Figure 5.4).

The effect of surfen during the recruitment phase may be the result of direct effects on myeloid cells. Surfen treated lesions showed a per area increase in Iba-1 fluorescence intensity, a marker expressed by microglia and macrophages. The data also shows the presence of myelin-laden cells at the border of LPC lesions on day 2 before the injection of surfen or vehicle. This raises the possibility that surfen has direct effects on these myeloid cells that prevents adequate clearance of myelin debris and/or production of growth factors such as IGF-1 which impact OPC recruitment and remyelination as described by Kotter et al. (2006).

Chapter 4, it was shown that surfen modulates pro-inflammatory cytokine and chemokine production by macrophages *in vitro* (Figures 4.9 and 4.12). While TNF and IL-6 were decreased, IL-1β was markedly increased. In the LPC model, IL-1β mRNA expression has been shown to be biphasic, peaking shortly after LPC injection and again 48 h later (Ousman and David, 2001). Mice null for IL-1β exhibited delayed remyelination in a cuprizone model of demyelination, pointing towards a protective role for the cytokine (Mason et al., 2001). However, increased IL-1β production from both the LPC lesion and surfen treatment may have deleterious consequences that impair macrophage function, and OPC recruitment/differentiation. Alternatively, surfen also reduced the *in vitro* production of the pro-inflammatory mediators IL-6, TNF, and NO in

LPS-stimulated BMDMs. These reductions may have occurred following the administration of surfen into the lesion and altered the phagocytic function of myeloid cells.

Lastly, there remains the distinct possibility that surfen reduces OPC proliferation by blocking OPC growth factor binding during proliferation. Perlecan is increased two-fold during the differentiation of OPCs into mature olgiodendrocytes (Winkler et al., 2002). In Chapter 4, we demonstrate the capacity of surfen to reduce perlecan mRNA expression, therefore it is possible that surfen is producing a similar effect in the lysolecithin model. Taken together, HSPGs such as perlecan may have important roles during remyelination via the regulation of OPC function. Whether the delayed remyelination observed following surfen treatment at day 2 is a result of reduced OPC recruitment, or impaired OPC differentiation resulting from a hostile inflammatory milieu, accumulated myelin debris, or a combination of all three requires further investigation.

5.3.4 Treatment with surfen on day 7 following the initiation of remyelination produces unique histological changes that do not correlate with lesion size.

To assess the effect of surfen during the differentiation phase, lesions were treated 7 days post LPC injection when the OPC recruitment phase would be nearly complete, based on previous studies (Figure 5.5). Surfen treated LPC lesions did not significantly differ from vehicle or sham controls; however, they did have a unique neuropathological signature that included increased cellularity at the border of the corpus callosum. While the identity of these cells remains unknown, their appearance and number suggest they are myeloid cells. It is of interest to consider whether surfen is recruiting these cells to the lesion, or preventing them from efficiently leaving.

Whether these cells are immunosuppressed, pro-inflammatory, or phagocytic is unknown. The similar lesion sizes between surfen and vehicle treatments, while a non-trivial metric, do not fully encapsulate our histological findings during the differentiation phase. For example, the lesion border of surfen treated lesions remains sharply demarcated relative to vehicle, which show signs of patchy remyelination. Taken together, these observations suggest that surfen may still have adverse effects on the later differentiation of OPCs, in addition to early recruitment, that can impact later patterns of

remyelination.

5.3.5 Conclusions

This is the first report of a proteoglycan antagonist producing deleterious effects in an experimental model of demyelination. Previous reports using either enzymatic digestion of CSPGs (Siebert and Osterhout, 2011) or selective antagonists for CSPGs (Keough et al., 2016) demonstrate enhanced remyelination. However, these previous studies did not use compounds with selective binding to HSPGs. Chapter 4 of this thesis reports the direct effects of surfen on macrophage function *in vitro* (Chapter 4). The ability of surfen to reduce chemokine, IL-6, TNF, and NO production in LPS-stimulated macrophages *in vitro*, while augmenting IL-1β could lead to a multitude of possible mechanisms that explain the delayed remyelination observed on days 7 and 14 following early (day 2) treatment with surfen.

A limitation of this study is that the characteristics of OPCs have not been directly assessed, thus the question of whether surfen delays OPC recruitment, diminishes OPC differentiation, or both, remains to be fully explored. Moreover, this work raises the possibility that HSPGs may play an early role in OPC recruitment, an effect that is antagonized by surfen. Indeed, increased HSPG production is linked to OPC proliferation and differentiation *in vitro*, but these roles have not been explored in a model of demyelination (Winkler et al., 2002). Surfen lesions showed increased CSPG expression, so this may also explain the results, since CSPGs have been shown to inhibit OPC recruitment in other studies (Keough et al., 2016; Lau et al., 2012). However, because surfen preferentially binds to heparan sulfate, this leaves open the possibility that HSPGs play unique roles in remyelination from their CSPG counterparts.

Nevertheless, it is likely the observations reported here are also related to the effects of surfen on myeloid cells, indicating a complex interplay of potential mechanisms for delayed remyelination. In conclusion, caution must be taken to properly characterize the broader role of proteoglycans in remyelination, including HSPGs, before moving forward with therapeutic development.

Figure 5.1: Co-injection of either surfen or vehicle with lysolecithin into the corpus callosum does not affect lesion size at day 7. (A) On day 0, female C57BL/6 mice received a 1 μL bilateral injection containing 1% lysolecithin (lysophosphatidylcholine; LPC) and either vehicle (2% DMSO) or surfen (100 μM) into one side of the corpus callosum. Mice were sacrificed at day 7 and tissue sections stained for myelin with eriochrome cyanine and neutral red. The mean lesion area was quantified for each mouse. There was no significant difference in lesion size between vehicle and surfen treated mice. Data are expressed as the mean ± SEM pooled from two independent experiments. Significance evaluated with a Student's t-test. Lesions in photomicrographs denoted by * in the lesion epicenter. Scale bar = 200 μm.

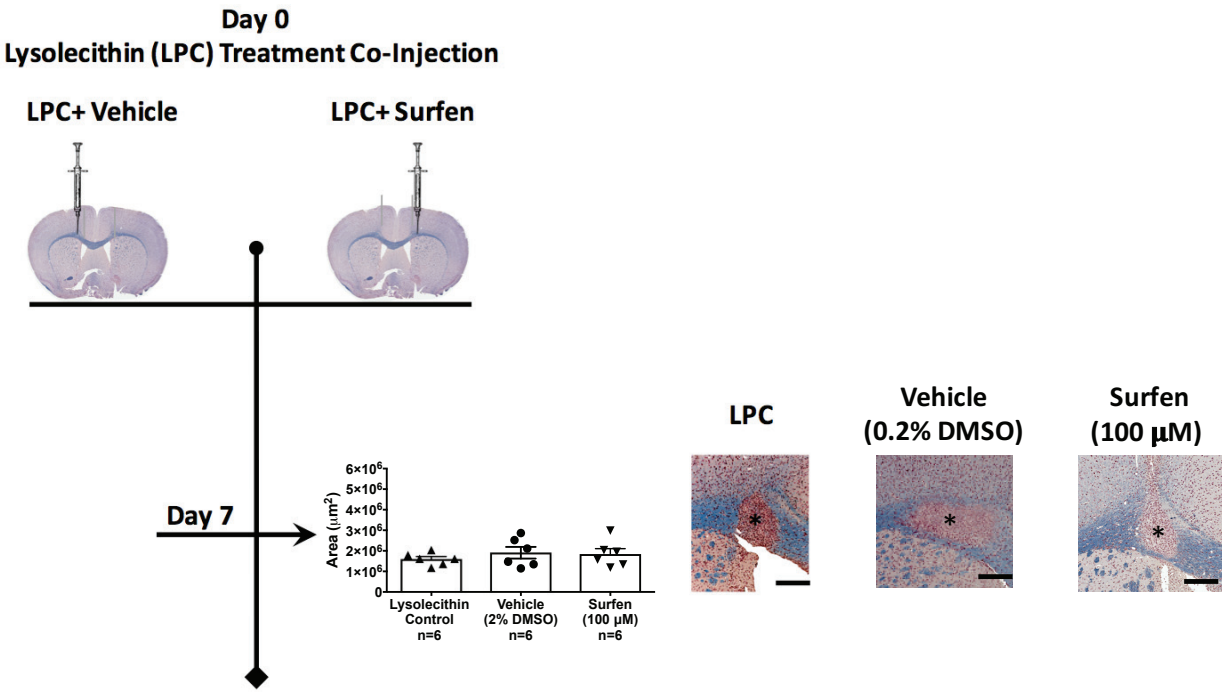
Day 0
Lysolecithin (LPC) Treatment Co-Injection
LPC+ Vehicle
LPC+ Surfen
Day 7
Area (μm²)
6×10⁶
5×10⁶
4×10⁶
3×10⁶
2×10⁶
1×10⁶
0
Lysolecithin Control n=6
Vehicle (2% DMSO) n=6
Surfen (100 μM) n=6
LPC
Vehicle (0.2% DMSO)
Surfen (100 μM)

Figure 5.2: Administration of surfen into the corpus callosum two days following lysolecithin produced significantly larger lesions on days 7 and 14. **(A)** On day 0, female C57BL/6 mice received a 1 μL bilateral injection of 1% lysolecithin (lysophosphatidylcholine; LPC) into each side of the corpus callosum. Treatment of either vehicle (2% DMSO) or surfen (100 μM) was administered into each of the lesions 48 h later. In a separate set of mice, lysolecithin was administered on day 0 and a sham procedure involving the mechanical insertion of the needle was performed 48 h later. Mice were sacrificed on days 2 (to assess the lesion before treatment), 7, 14, and 21. Tissues were processed for histology and sections stained for myelin with eriochrome cyanine and neutral red and lesion area quantified for each mouse. Surfen significantly increased lesion size relative to vehicle and lysolecithin controls on days 7 and 14. Lesion size was no different between surfen, vehicle, and lysolecithin controls at day 21. **(B)** Representative time course of mean lesion area for days 2, 7, 14, and 21 following administration of lysolecithin. Data are expressed as the mean ± SEM pooled from two independent experiments. *$p<0.05$, one-way ANOVA with Tukey post-hoc analysis. Lesions in photomicrographs denoted by * in the lesion epicenter. Scale bar sizes for photo micrographs are as follows: LPC and LPC + Sham = 300 μm, LPC Boarder = 100 μm, Vehicle and Surfen = 500 μm.

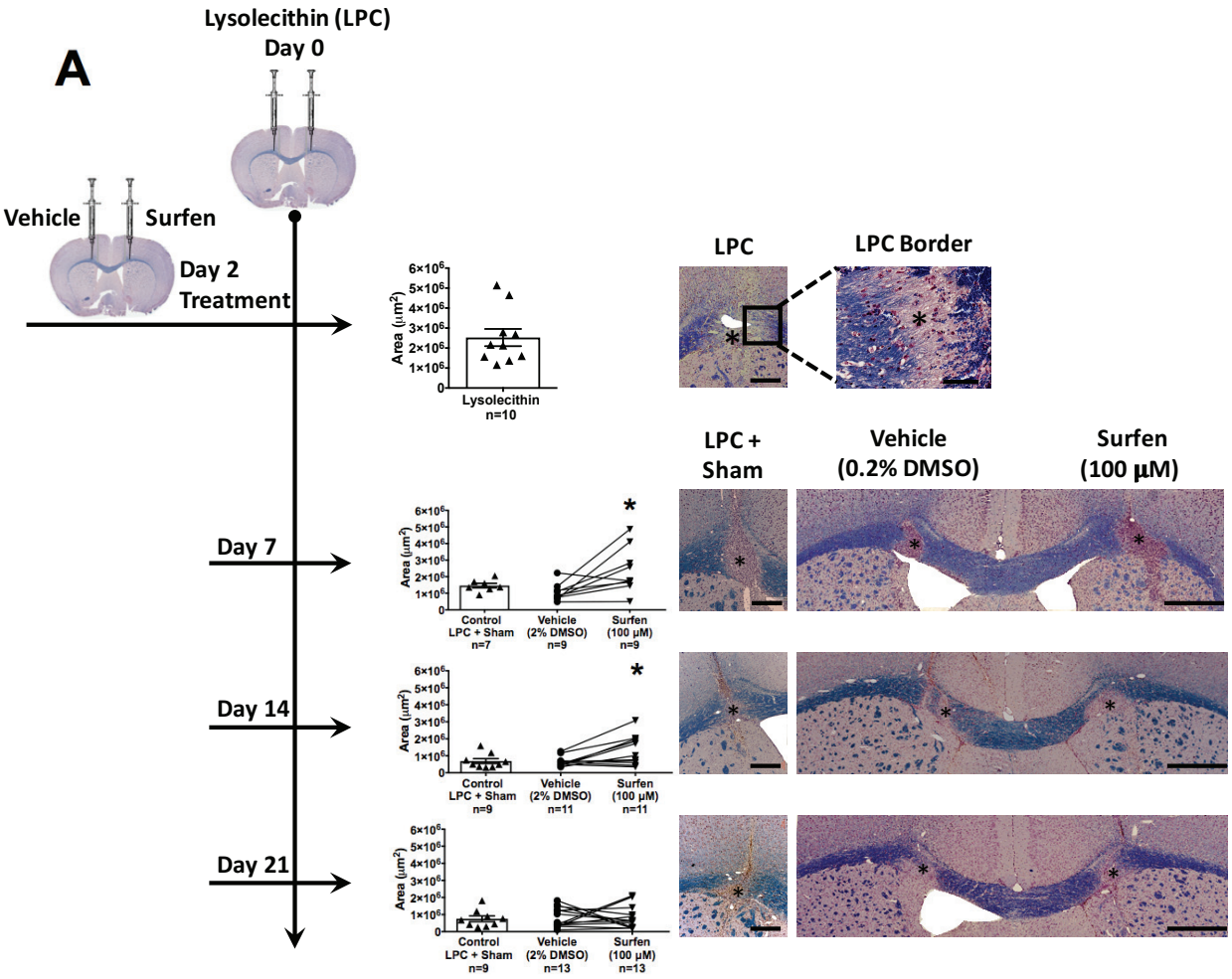
A
Lysolecithin (LPC)
Day 0
Vehicle
Surfen
Day 2
Treatment
Day 7
Day 14
Day 21
Area (µm²)
Lysolecithin
n=10
LPC
LPC Border
LPC +
Sham
Vehicle
(0.2% DMSO)
Surfen
(100 µM)
Control
LPC + Sham
n=7
Vehicle
(2% DMSO)
n=9
Surfen
(100 µM)
n=9
Control
LPC + Sham
n=9
Vehicle
(2% DMSO)
n=11
Surfen
(100 µM)
n=11
Control
LPC + Sham
n=9
Vehicle
(2% DMSO)
n=13
Surfen
(100 µM)
n=13

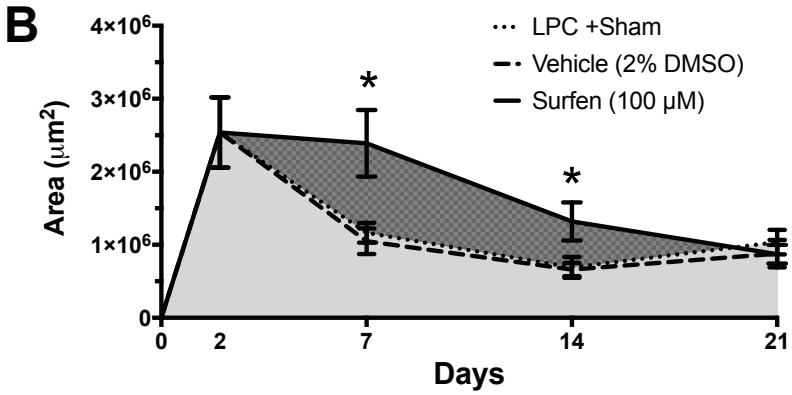
B
LPC +Sham
Vehicle (2% DMSO)
Surfen (100 µM)
Area (µm²)
Days

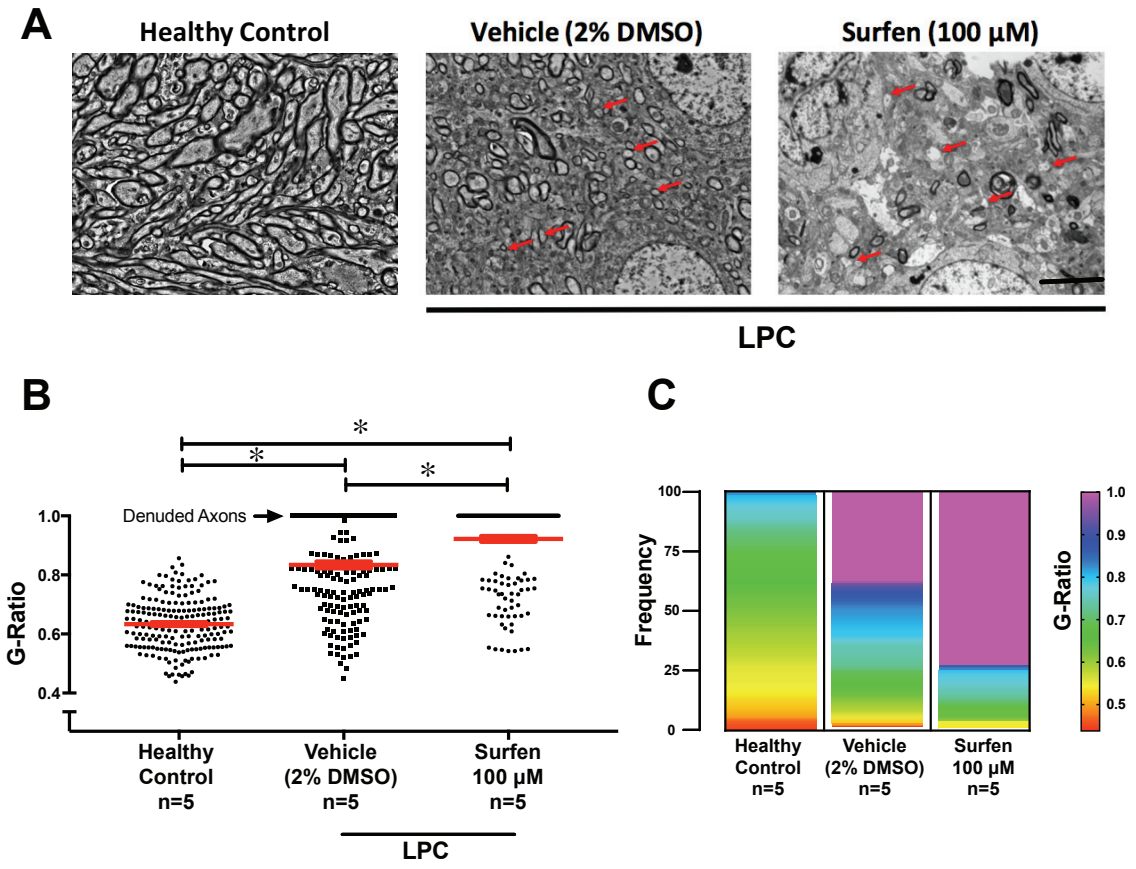

Figure 5.3: Administration of surfen into the corpus callosum two days following lysolecithin delays remyelination by day 7. On day 0, female C57BL/6 mice received a 1 µL bilateral injection of 1% lysolecithin (lysophosphatidylcholine; LPC) into each side of the corpus callosum. Treatment of either vehicle (2% DMSO) or surfen (100 µM) was administered into the lesion 48 h later. Mice were sacrificed on day 7 and tissues processed for electron microscopy. Healthy age-matched C57BL/6 mice were used as controls. **(A)** Representative photomicropgrahs from healthy controls, vehicle, and surfen mice. Red arrows indicate areas of remyelination (vehicle) and denuded axons (surfen). **(B)** Myelin thickness was calculated using the ratio of the axon perimeter to the outer perimeter of myelinated fibers (G-ratio) and 100 axons were counted per mouse (n=5/group). Shown here is a representative sample of G-Ratios from each group. **(C)** The frequency of G-Ratios indicates that surfen mice displayed a two-fold increase in completely denuded axons (shown in pink) relative to vehicle mice signifying delayed remyelination. Data are expressed as the mean ± SEM pooled from two independent experiments. *$p<0.05$, one-way ANOVA with Tukey post-hoc analysis. Scale bar = 50 µm.

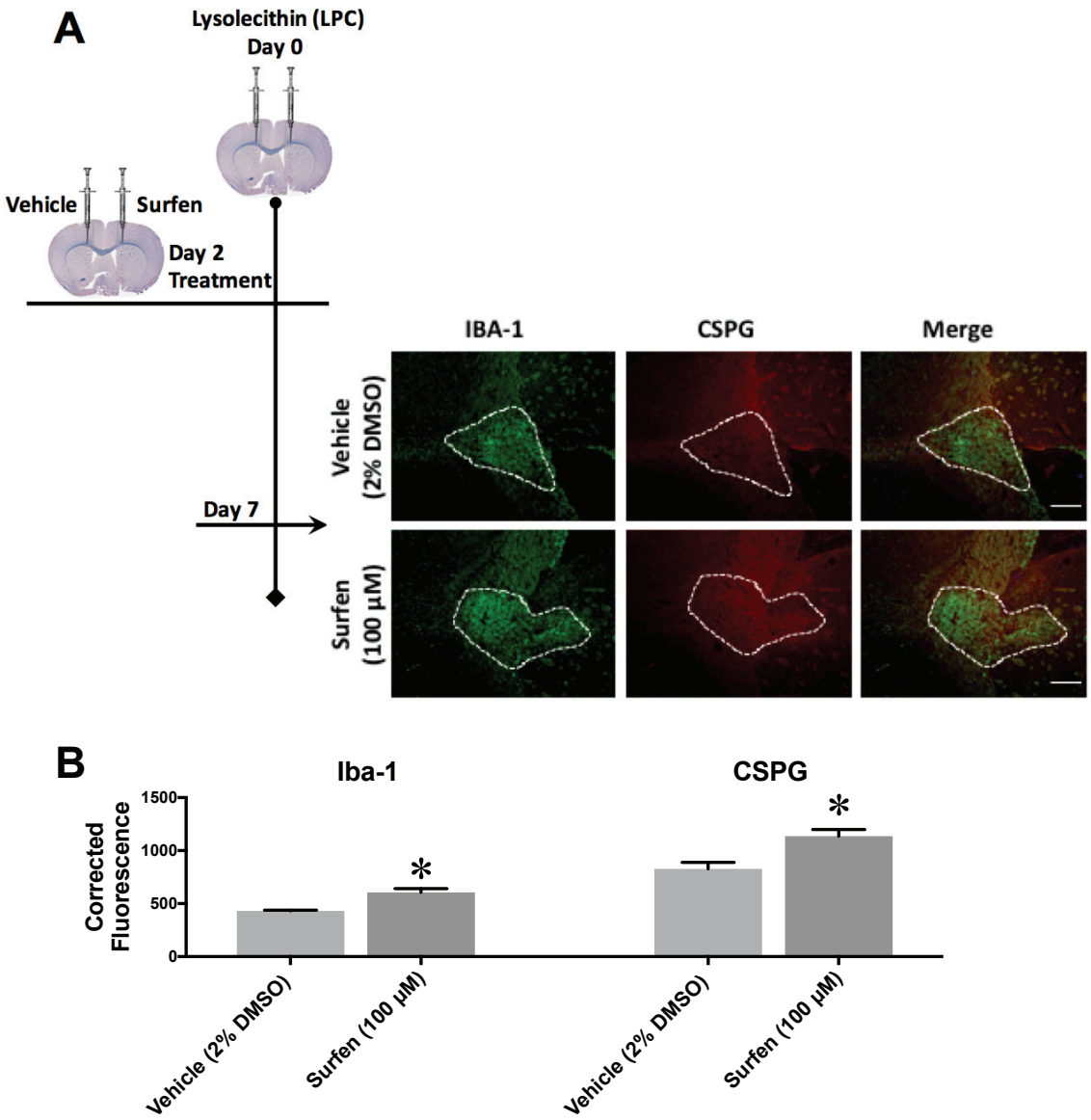

Figure 5.4: Administration of surfen into the corpus callosum two days following lysolecithin increases Iba-1 and CSPG expression by day 7. On day 0, female C57BL/6 mice received a 1 µL bilateral injection of 1% lysolecithin (lysophosphatidylcholine; LPC) into each side of the corpus callosum. Treatment of either vehicle (2% DMSO) or surfen (100 µM) was administered into the lesion 48 h later. Mice were sacrificed on day 7 and tissues processed for immunohistochemistry. **(A)** Representative photomicropgrahs from vehicle and surfen mice. Lesions are traced in white for each fluorescent channel. **(B)** Fluorescent intensity was quantified per lesion area and both Iba-1 and CSPG fluorescence intensities were significantly increased, indicating increased myeloid activity and CSPG production. Data are expressed as the mean ± SEM, n=3 per group. *$p<0.05$, Student's paired t-test.

Figure 5.5: Administration of surfen into the corpus callosum seven days following lysolecithin did not significantly alter lesion size on days 14 and 21. **(A)** On day 0, female C57BL/6 mice received a 1 μL bilateral injection of 1% lysolecithin (lysophosphatidylcholine; LPC) into each side of the corpus callosum. Treatment of either vehicle (2% DMSO) or surfen (100 μM) was administered into each of the lesions 7 days later. In a separate set of mice, lysolecithin was administered on day 0 and a sham procedure involving the mechanical insertion of the needle was performed 7 days later. Mice were sacrificed on days 7 (to assess the lesion before treatment), 14, and 21. Tissues were processed for histology and sections stained for myelin with eriochrome cyanine and neutral red and lesion area quantified for each mouse. Surfen did not significantly alter lesion size relative to vehicle and lysolecithin controls on days 14 and 21. **(B)** Representative time course of mean lesion area for days 7, 14, and 21 following administration of lysolecithin. Data are expressed as the mean ± SEM pooled from two independent experiments. *$p<0.05$, one-way ANOVA with Tukey post-hoc analysis. Lesions in photomicrographs denoted by * in the lesion epicenter. Scale bar sizes for photo micrographs are as follows: LPC and LPC + Sham = 300 μm, LPC Boarder = 100 μm, Vehicle and Surfen = 500 μm.

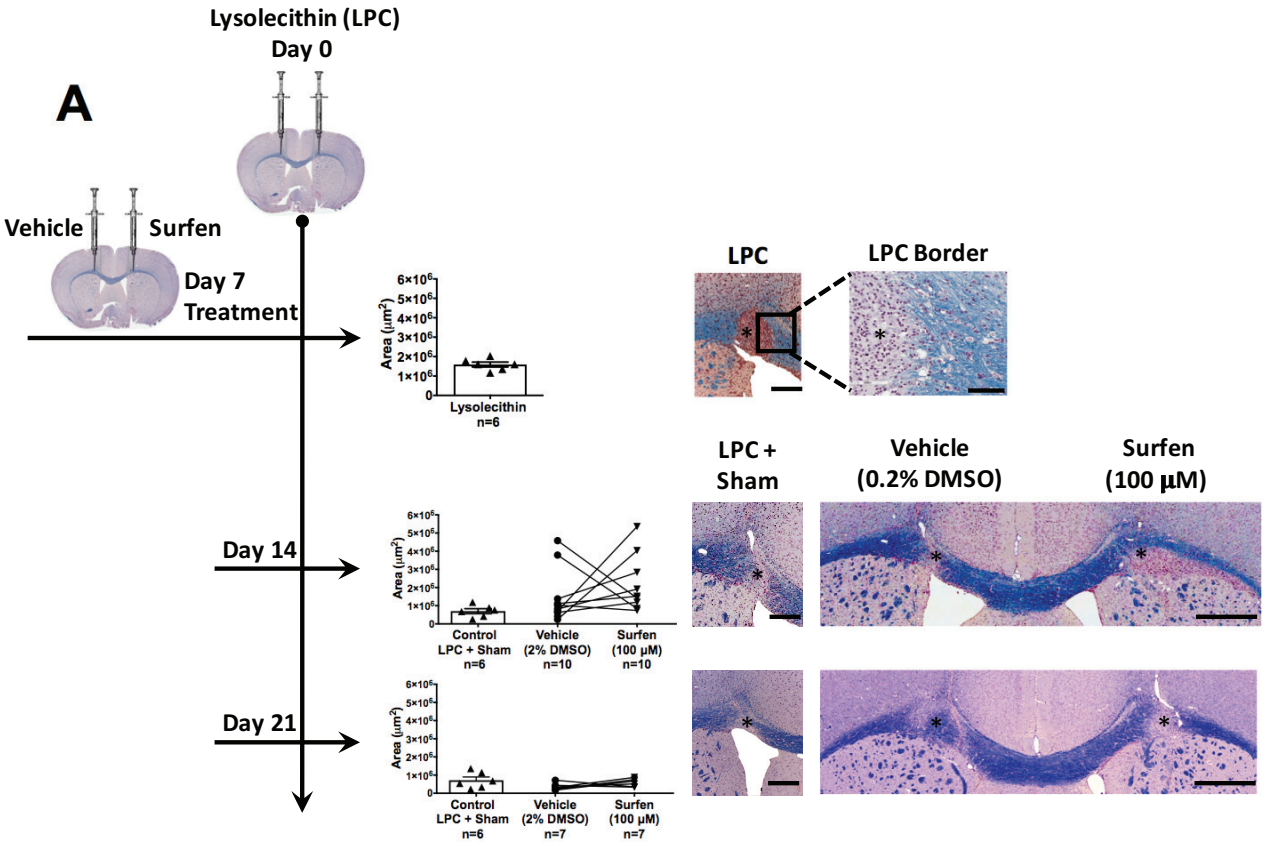
A
Lysolecithin (LPC)
Day 0
Vehicle
Surfen
Day 7
Treatment
Day 14
Day 21
Area (µm²)
Lysolecithin
n=6
Control
LPC + Sham
n=6
Vehicle
(2% DMSO)
n=10
Surfen
(100 µM)
n=10
n=7
LPC
LPC Border
LPC +
Sham
Vehicle
(0.2% DMSO)
Surfen
(100 µM)

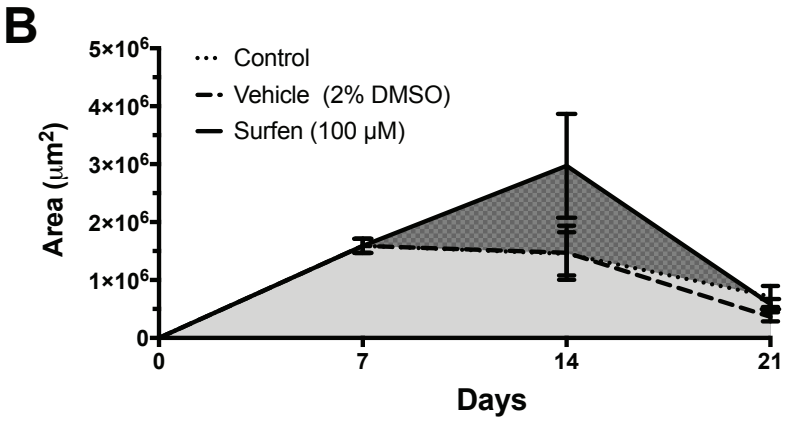
B
Control
Vehicle (2% DMSO)
Surfen (100 µM)
Area (µm²)
Days
0
7
14
21

CHAPTER 6
DISCUSSION

6.1 Summary of Central Findings

This thesis sought to characterize the proteoglycan antagonist surfen using both *in vitro* and *in vivo* models relevant to the study of MS. In Chapter 3, surfen decreased murine T cell proliferation whether activated *in vitro* by co-stimulation with anti-CD3/anti-CD28-coated T cell expander beads or *in vivo* by injecting mice with anti-CD3 Ab. The effect of surfen on T cell proliferation *in vitro* was inhibited in a dose dependent manner by adding heparan sulphate, which suggests that when GAG binding sites on surfen are occupied, it is no longer effective. Having demonstrated the capacity of surfen to influence T cell function, and its utility as an *in vivo* agent, we investigated the effects of surfen in EAE, a mouse model with features akin to several aspects of MS, in Chapter 4.

Surfen reduced EAE clinical severity and was associated with decreased cellular infiltration of both $CD45^+CD3^+CD4^+$ T cells (spinal cord and cerebellum) and $F4/80^+CD11b^+$ myeloid cells (spinal cord). Several potential mechanisms of action for surfen were identified including regulation of T cell effector functions, decreased production of chemotactic cytokines that facilitate cellular infiltration, and finally a marked reduction in proteoglycan transcript expression that positively correlated with clinical improvement. Nevertheless, surfen significantly increased concentrations of the pro-inflammatory cytokine IL-12p70. When these studies were extended *in vitro* to BMDMs, surfen produced a similar decrease in chemokine production. Reductions in the pro-inflammatory mediators IL-6, TNF, and NO were also observed; however, surfen increased the production of the pro-inflammatory cytokine IL-1β. These results suggest that the immunomodulatory properties of surfen could be related to direct effects on myeloid cell function.

Lastly, in Chapter 5 we asked whether surfen could enhance endogenous remyelination using a LPC mouse model of focal demyelination. Three time points were chosen to administer treatment that coincided with initial demyelination (day 0), early demyelination before peak OPC recruitment (day 2), or the phase of remyelination involving both OPC recruitment and differentiation (day 7; Keough et al., 2015; Kotter et al., 2001). Surfen had no effect on demyelination if administered at the same time as LPC (day 0), but treatment with surfen at day 2 increased the mean lesion area on days 7 and

14, pointing towards an unexpected inhibition of remyelination. Indeed, surfen treated lesions had significantly fewer remyelinated fibres when examined with electron microscopy which coincided with augmented myeloid cell activity and increased CSPG production. By contrast, administration of surfen at day 7 had no effect on lesion size, although neuropathological abnormalities were observed that may be related to further inefficiencies in remyelination, even when surfen was introduced after peak recruitment of OPCs.

6.2 Surfen: A Double-edged Sword?

The opposing effects of surfen in the EAE (clinical improvement) and the LPC (delayed remyelination) models demonstrate that surfen acts as a double-edged sword, related to its effect on pro-inflammatory and anti-inflammatory processes (Figure 6.1). These results reinforce the role of proteoglycans in regulating immune function, although surfen may also have functions independent of proteoglycan binding. The question remains as to whether surfen-mediated increases in the pro-inflammatory cytokines IL-12p70 (EAE) and IL-1β (BMDMs) represent harmful or protective responses in the context of these models and whether they explain the delayed remyelination observed in the LPC model. It is important to note that one of the principal sources of IL-12p70 in the context of inflammation is macrophages (Kaliński et al., 2000). Moreover, macrophages play a central role in facilitating remyelination in the LPC model (Kotter et al., 2005). Taken together, it is possible that the ability of surfen to ameliorate EAE on the one hand and delay remyelination on the other are attributable to the effect of surfen on macrophage function.

6.3 Limitations and Future Directions of This Study

6.3.1 Clarifying the role of individual proteoglycans in experimental models of MS

A limitation of the present body of work is that we cannot discern which specific proteoglycans are responsible for the effects of surfen. Conditional knockout mice engineered to silence specific proteoglycans at various time points in EAE and after LPC injection would enable a better understanding of their roles in disease pathogenesis. For example, the ability to silence perlecan or syndecan IV gene expression at day 2 in the

LPC model could clarify the role of HSPGs in remyelination. To date, no study has used transgenic mice deficient in specific proteoglycans to study endogenous remyelination.

With respect to EAE, mice null for syndecan I have increased clinical severity characterized by early leukocyte recruitment into the CNS (Zhang et al., 2013). Another study focused on the deletion of syndecan IV and implicated this HSPG in the regulation of autoreactive T cells, showing increased EAE severity following the adoptive transfer of syndecan IV null T cells into recipient mice (Chung et al., 2014). By contrast, mice lacking the CSPG NG2 were no different from wildtype controls with respect to EAE induction, effector, or recovery phases (Moransard et al., 2011). These select studies are among the handful that examine proteoglycans in the context of EAE using transgenic models. We show that proteoglycan transcript expression positively correlates with EAE clinical scores, with emphasis on the potentially deleterious roles of HSPGs including syndecans I and IV (Chapter 4).

6.3.2 Limitations of Using *In Vitro* Cell Cultures

6.3.2.1 Murine T cells

The use of anti-CD3/anti-CD28 expander beads as surrogate antigen presenting cells is useful for providing a robust T cell proliferation *in vitro*. Notwithstanding CD28 as a major co-stimulatory molecule in T cell biology, there are other co-stimulatory molecules capable of eliciting T cell proliferation, such as inducible co-stimulator (ICOS; Yoshinaga et al., 1999). Moreover, T cell proliferation in the context of MS is antigen-specific and occurs in the presence of activated macrophages, microglia, and dendritic cells, all of which produce cytokines capable of modulating proliferative responses. Therefore, T cell expander beads do not fully encompass the T cell responses observed in EAE or MS.

Several differences exist between murine and human T cells. First, virtually all murine $CD3^+$ T cells express the co-stimulatory molecule CD28 on their surface compared to 80% of $CD4^+$ and 50% of $CD8^+$ T cells observed in humans (J. Mestas and Hughes, 2004). Secondly, the co-existence of both T_H1 and T_H2 cells in human disease makes it difficult to discern whether “anti-inflammatory” cytokines are promoting repair or contributing to disease processes (Del Prete et al., 1993).

6.3.2.2 Murine BMDMs

In the present study, BMDMs were stimulated with LPS, promoting the production of a pro-inflammatory response principally through the TLR4 pathway (Chow et al., 1999). Had we used IL-13 or IL-4 in BMDM cultures, an entirely different set of cytokines more conducive to repair could have been studied (Mia et al., 2014). In contrast to culture studies, macrophages *in vivo* are exposed to a plethora of cytokines and chemokines that feedback and alter their transcriptional phenotype and function during disease processes.

Murine macrophages display several important differences from their human counterparts with respect to their pro-inflammatory responses. For example, NO production is well established in murine macrophages but its production by human macrophages is debated (Schneemann and Schoeden, 2007). LPS responses also differ, with mouse macrophage cells lines requiring much higher doses to elicit pro-inflammatory responses relative to human, suggesting rodents display a more LPS-tolerant innate immune system (Javier Mestas and Hughes, 2004). This is supported by the differential gene expression downstream of various TLR pathways between mouse and human following LPS stimulation (Jann et al., 2009). Another study showed that production of pro-inflammatory cytokines in response to LPS-stimulation *in vitro* is inversely correlated to the presence of serum, reinforcing the need to verify findings using *in vivo* models (Warren et al., 2010).

6.3.3 Limitations of Modelling MS

There are no available animal models that fully recapitulate the immunological and neuropathological changes associated with the initiation and progression of MS (Lassmann and Bradl, 2017). In recognition of this limitation, the present study used EAE as a model of chronic autoimmune-mediated neuroinflammation and a separate model of LPC-mediated demyelination to study components of MS-like disease in rodents.

The MOG_{35-55} induced EAE model is limited by a biased $CD4^+$ T cell response resulting from the use of adjuvants and a known CNS antigen. As discussed in Chapter 1, the etiology of MS is unknown, spontaneous, and likely results from a combination of epigenetic factors. A recent histological study compared results from prior MOG_{35-55}

induced EAE studies with plaques from human MS, a rare case of human autoimmune encephalomyelitis, and a marmoset EAE model (Höftberger et al., 2015). Although myeloid cells were prominently featured in lesions from each group, the ratio of $CD3^+CD4^+$ to $CD3^+CD8^+$ T cell infiltrates was disproportionately higher in murine EAE by comparison. Previous studies implicate a role for $CD8^+$ T cells in promoting demyelination and tissue damage within the MS plaque to a much larger extent than $CD4^+$ T cells (Booss et al., 1983; Hayashi et al., 1988; Neumann et al., 2002). Furthermore, lesions in murine EAE did not show the typical variety of inflammatory plaque patterns observed in MS, human autoimmune encephalomyelitis and even marmoset EAE (Höftberger et al., 2015).

These findings may partly explain the failure of several candidate MS therapeutics to achieve their experimental end points in clinical trials. Prominent examples of therapeutics that showed promise in EAE but failed in clinical trials include monoclonal anti-IL-12p40 (Segal et al., 2008) and a recombinant fusion protein targeting TNF (The Lenercept Multiple Sclerosis Study Group, 1999), which in the latter case exacerbated disease severity. Consequently, caution must be taken before interpreting EAE findings as mechanisms of disease pathogenesis in MS.

In comparison to EAE, inflammation in the LPC model occurs in the absence of persistent autoimmune mediated inflammation. Although inflammation is present early following LPC injection as a component of the OPC recruitment phase (Ousman and David, 2001), a limitation of this model is that complete endogenous remyelination occurs in a microenvironment conducive to repair. This contrasts with MS, where plaques rarely remyelinate to a significant degree, due in part to the presence of inflammation, proteoglycans, and ultimately axonal death (Kuhlmann et al., 2017). Additionally, the genetic variability that underlies variable remyelination efficiency in MS patients (Patrikios et al., 2006) is most certainly absent in our inbred C57BL/6 mice.

Models of autoimmune-mediated demyelination have been described that generate a focal lesion in murine brain using autoreactive T cells by priming the peripheral immune system with MOG_{35-55} and using VEGF to permeabilize the BBB (Sasaki et al., 2010). More recent efforts include the combination of lysolecithin with EAE (personal correspondence, endMS 2016 winter conference). These improved models

of focal demyelination may serve as a more appropriate vehicle to study proteoglycan antagonists in the context of autoimmune-mediated demyelination.

6.4 Future Experimental Considerations

6.4.1 Investigating Peripheral Immune Responses in EAE

Surfen reduces T cell proliferation both *in vitro* and *in vivo* following stimulation (Chapter 3). Nevertheless, the peripheral effects of surfen on T cell function in EAE remain unexplored. We conducted a pilot study to assess whether the ability of surfen to reduce T cell proliferation also occurred in EAE. Inguinal, axial and brachial lymph nodes were collected at day 21 from EAE mice treated with either vehicle or surfen. Lymphocytes were isolated, pooled, stained with Oregon green, and stimulated with anti-CD3/anti-CD28 expander beads for 24 h. Proliferation was assessed for $CD4^+$ T cell subsets using flow cytometry. Relative to vehicle EAE mice, administration of surfen significantly reduced the percentage of $CD4^+$ T cells that proliferated (Figure 6.2A). This surfen-mediated reduction in T cell proliferation is consistent with the results described in Chapter 3. A similar study using the small molecule CSPG inhibitor fluorosamine inhibited the proliferation of anti-CD3/anti-CD28 stimulated splenocytes obtained from EAE mice (Keough et al., 2016). Nevertheless, the mechanisms by which surfen and fluorosamine reduce proliferation of T cells and splenocytes are unknown. Studies that focus on downstream signaling mechanisms in a head-to-head study using both surfen and fluorosamine would enable a better understanding of proteoglycan-mediated regulation of T cell proliferation.

Interestingly, total lymphocyte cell counts from the lymph nodes of surfen treated EAE mice were significantly higher than those in the EAE vehicle-treated group (Figure 6.2B). While the mechanism underlying this observation is unknown, one explanation is that surfen is trapping lymphocytes within the lymphoid tissue. This may partly account for the surfen-mediated reduction in T cell infiltration in EAE spinal cord and cerebellum. The DMT fingolimod (FTY720) also reduces cellular infiltration, in large part by trapping T cells within the lymph node. Fingolimod targets the sphingosine-1-phosphate receptor expressed on lymphocytes and upon ligation the receptor is internalized, preventing the egress of lymphocytes from lymphoid tissues (Chun and

Hartung, 2010). Studies focused on determining whether surfen binds sphingosine-1-phosphate, or other factors that contribute to lymphocyte homing and egress such as CCR7, could identify an additional mechanism by which surfen reduces EAE clinical severity.

6.4.2 Investigating the role of MMPs in EAE

The expression of some MMPs in EAE and MS plaques have been associated with increased disease severity (Yong et al., 2007, 2001). On the other hand, MMPs have been shown to clear CSPGs and promote remyelination (Larsen et al., 2003). Upwards of 30 MMP family members have been identified (Rempe et al., 2016). Further characterization of MMP mRNA expression during peak EAE suggests both protective and deleterious roles for MMPs (Weaver et al., 2005). For example, both MMP2 and MMP9 are elevated during peak EAE and involved in promoting T cell migration during the induction and effector phases of EAE, respectively (Song et al., 2015; Weaver et al., 2005). However, MMP9 is also implicated in CSPG clearance during remyelination and plays a protective role in this context (Larsen et al., 2003).

Considering these studies, mRNA expression for MMP2 and MMP9 was measured in EAE spinal cords treated with either vehicle or surfen to explore the relevance of these proteases to the study. Relative to vehicle-treated EAE mice, surfen significantly reduced the expression of MMP2 mRNA (Figure 6.3A) to levels comparable to CFA controls but no statistical differences were found between groups for MMP9 (Figure 6.3B). The observation that MMP2 mRNA expression, which is implicated in cellular infiltration during the effector phase, was reduced by surfen supports our hypothesis that surfen has early effects in EAE (Song et al., 2015). Nevertheless, MMP2 is not essential for EAE induction (Agrawal et al., 2006a) hence other MMPs are likely involved and the diversity of their functions in the context of proteoglycan function and inflammation warrant further study.

6.4.3 Investigating Surfen and Growth Factor Responses in EAE and Lysolecithin

Growth factors are potent modulators of inflammation and repair in the context of EAE and LPC. Surfen has been previously shown to bind with high affinity to the growth

factors FGF and VEGF (Schuksz et al., 2008; Xu et al., 2011). Cell surface expression of HSPGs on the surface of OPC and oligodendrocytes are critical for binding growth factors, including FGF (Winkler et al., 2002). EAE mice null for FGF show similar cellular infiltration relative to wildtype littermates but display delayed remyelination suggestive of poor OPC differentiation (Rottlaender et al., 2011). We hypothesize that the binding of HPSGs by surfen in the LPC model blocked growth factor signalling in OPCs, preventing their subsequent maturation leading to delayed remyelination.

In the EAE study, surfen reduced TGFβ mRNA expression in EAE spinal cord at day 21 (Chapter 4). We extended this work to include FGF and VEGF. Relative to vehicle-treated EAE mice, surfen significantly reduced FGF mRNA expression in EAE spinal cord (Figure 6.4). By contrast, no significant differences were observed for VEGF mRNA expression (Figure 6.4). Included in Figure 6.4 is TGFβ expression from Chapter 4 for comparison. Interpretation of these results is difficult as we have established that vehicle treated mice are in the recovery phase at day 21 and FGF may be elevated in vehicle EAE mice as a component of this disease stage. In contrast to growth factors such as FGF2, expression of VEGF has been associated with EAE severity, which can be reduced following treatment with the VEGF antagonists bevacizumab (MacMillan et al., 2012) or B20-4.1.1 (MacMillan et al., 2014). By day 21, VEGF expression in EAE spinal cord decreases substantially from early disease (MacMillan et al., 2012) and this may partly explain why no changes were observed.

The effect of surfen on growth factors earlier, during the EAE effector phase or in the LPC model is unknown. It is possible surfen may have inhibitory effects on growth factor binding to OPCs that account for the delayed remyelination reported in the LPC model in Chapter 5. Moving forward these questions could be answered with immunohistochemistry or *in situ* hybridization techniques to assess growth factor production directly within the LPC lesion.

6.4.4 Early Effects of Surfen in EAE and Route of Administration

The present assessment of the immunological effects of surfen in EAE is limited to the recovery phase. We have hypothesized that the ability of surfen to reduce clinical severity is linked to the reduction of cellular infiltration and the promotion of an early

T_H2 response during the effector phase (Chapter 4). Ideal time points to investigate the effects of surfen in EAE moving forward include day 11 (early effector phase before peak disease) and day 14 (peak disease) to further clarify the mechanisms by which surfen acts to reduce EAE severity.

The timing of surfen administration and route of administration would also be interesting variables to explore. In Chapter 3 we show that prophylactic dosing with surfen reduced T cell proliferation following administration of anti-CD3 Ab. Whether prophylactic dosing with surfen would produce similar reductions in proliferation and disease severity during EAE remains to be determined. A more clinically relevant dosing schedule would involve the administration of surfen at the peak of disease. Would surfen reduce EAE severity in this context, or exacerbate symptoms via increased pro-inflammatory cytokine production? Similarly, what effect would direct administration of surfen into the cerebrospinal fluid have on symptomatic EAE mice? The answers to these questions may inform the future development of improved proteoglycan antagonists that have clinical utility for the treatment of MS.

6.4.5 OPC and Myeloid Functions in LPC Demyelination

A limitation in the interpretation of our LPC studies is the lack of data related to OPCs within surfen and vehicle treated LPC lesions. Although our time course suggests that surfen interferes with the recruitment phase of remyelination, we cannot exclude the possibility that surfen also has effects on OPC differentiation or effects independent of OPCs. As previously discussed, expression of HSPGs such as perlecan increase almost two-fold during the maturation of an OPC into a mature oligodendrocyte (Winkler et al., 2002), suggesting a positive role for this proteoglycan in remyelination that could be blocked by surfen.

Alternatively, surfen may have direct effects on myeloid cells involved in the clearance of myelin debris. Too much or too little inflammation could impact the clearance of myelin debris by macrophages, or create an environment that inhibits OPC differentiation (Kotter et al., 2006, 2005). Future work involving laser-capture microdissection of OPCs and macrophages from surfen treated lesions could provide more detailed information regarding the effects of surfen on these cells.

6.5 Concluding Remarks

Taken together, these studies implicate surfen as an immunomodulatory drug capable of reducing T cell proliferation and EAE disease progression through a variety of potential mechanisms. However, we report for the first time that this proteoglycan antagonist is capable of delaying remyelination in the LPC model of demyelination. These studies show the promise of proteoglycan antagonists as future therapeutics for the treatment of MS, but also identify the need to further study HSPGs in addition to their well characterized CSPG counterparts.

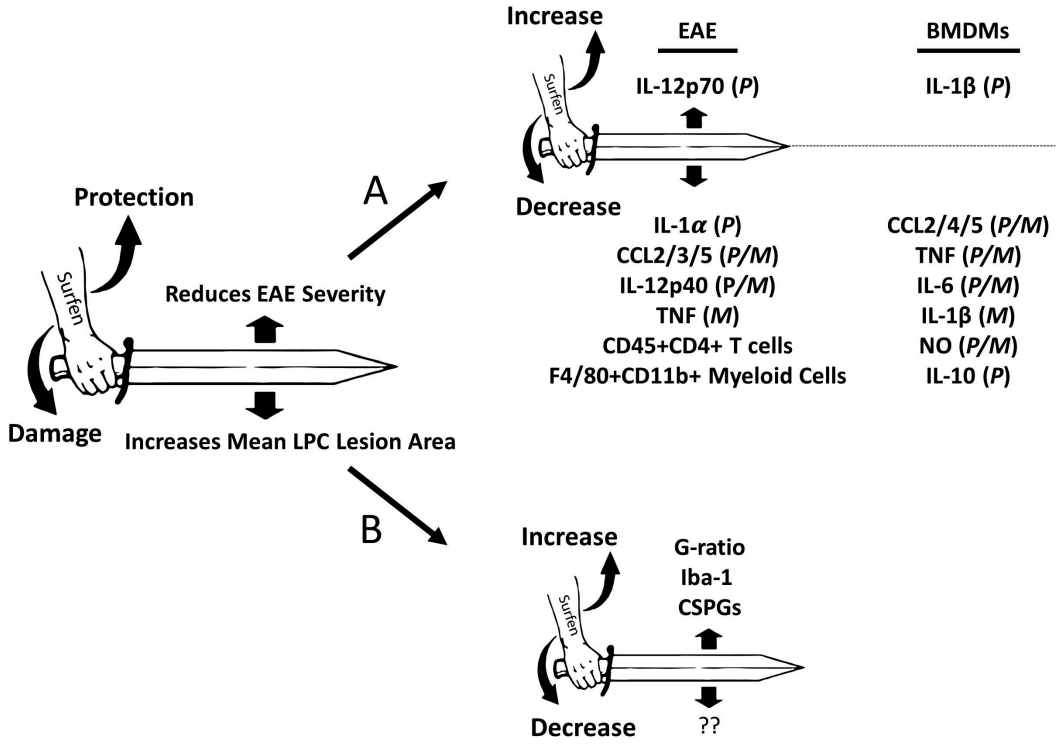

Figure 6.1: Surfen as a double-edged sword in inflammation and repair. **(A)** A summary of cytokine and chemokine results following the administration of surfen in EAE and in vitro LPS-stimulated BMDM studies. **(B)** A summary of day 7 results in the lysolecithin model following the administration of surfen into the lesion two days following LPC injection. (*M)=mRNA, (P)=protein concentrations*

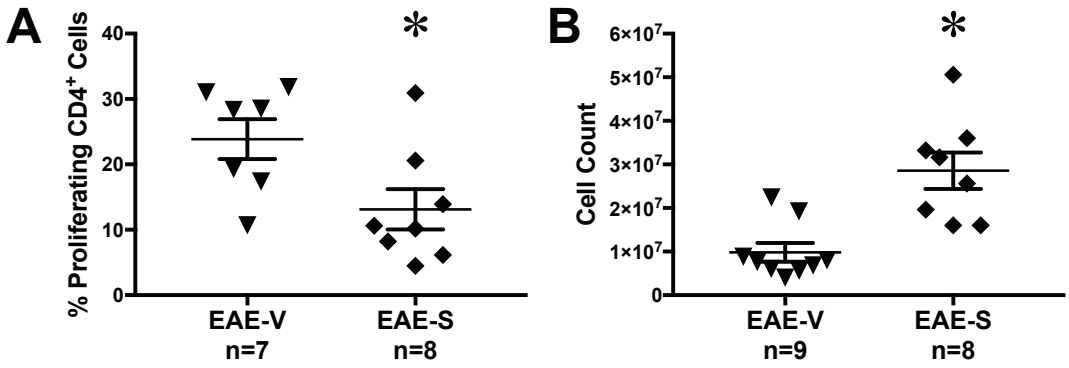

Figure 6.2: Surfen reduces the proliferation of $CD4^+$ T cells in EAE lymphocytes at day 21 but increases the number of cells in lymphoid tissue. Inguinal, axial and brachial lymph nodes from EAE mice were collected at day 21 from mice treated with either vehicle or surfen. Lymphocytes were collected, pooled, counted, stained with Oregon green, and stimulated with anti-CD3/anti-CD28 T cell expander beads for 24 h. Proliferation of CD4+ T cells was assessed with flow cytometry. **(A)** Surfen significantly reduced the percentage of proliferating CD4+ T cells relative to vehicle mice. **(B)** Surfen significantly increased the number of lymphocytes in collected lymphoid tissue in EAE mice relative to vehicle mice. Data shown as mean ± SEM. * = $p<0.05$

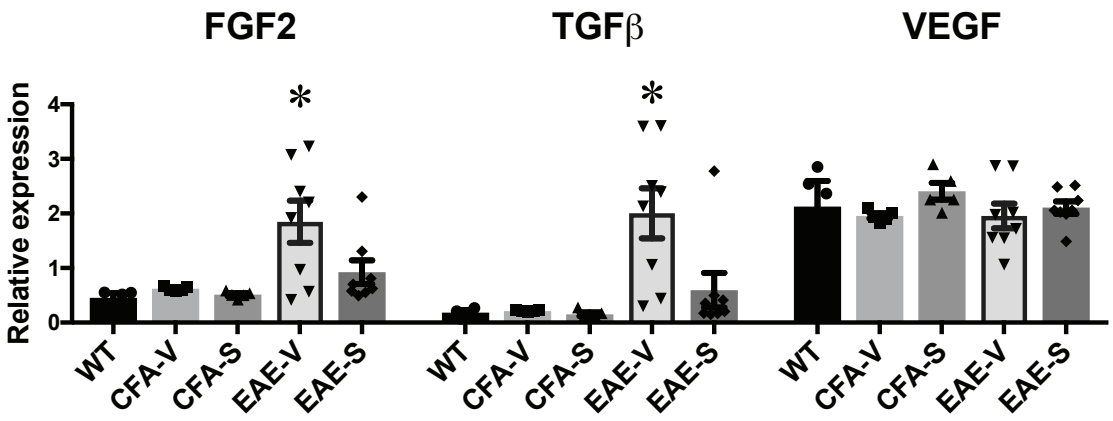

Figure 6.3: Surfen decreases the expression of the growth factors FGF2 and TGFβ in EAE spinal cord at day 21. Transcript expression results are shown for the growth factors FGF2, TGFβ, and VEGF in spinal cord. Vehicle treated EAE mice displayed significantly increased expression for FGF2 and TGFβ mRNA relative to both surfen treated EAE mice and CFA controls. No significant differences between groups were observed for VEGF. Data shown as mean ± SEM. * = $p<0.05$

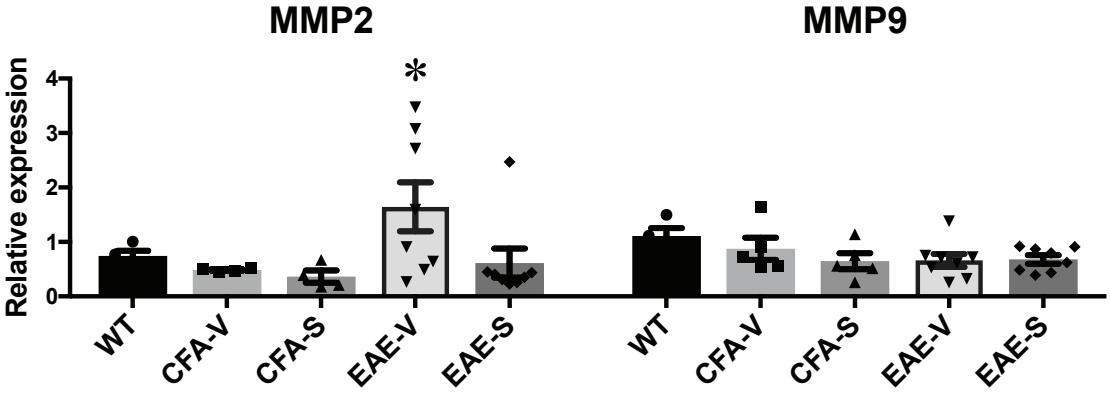

Figure 6.4: Surfen decreases the expression of MMP2 in EAE spinal cord at day 21. Transcript expression results are shown for the growth factors FGF2, TGFβ, and VEGF in spinal cord. Vehicle treated EAE mice displayed significantly increased expression for FGF2 and TGFβ mRNA relative to both surfen treated EAE mice and CFA controls. No significant differences between groups were observed for VEGF. Data shown as mean ± SEM. # =p<0.05, * = p<0.05

REFERENCES

Agrawal, S., Anderson, P., Durbeej, M., van Rooijen, N., Ivars, F., Opdenakker, G., Sorokin, L.M., 2006a. Dystroglycan is selectively cleaved at the parenchymal basement membrane at sites of leukocyte extravasation in experimental autoimmune encephalomyelitis. J. Exp. Med. 203, 1007–19.

Agrawal, S., Anderson, P., Durbeej, M., Van Rooijen, N., Ivars, F., Opdenakker, G., Sorokin, L.M., 2006b. Dystroglycan is selectively cleaved at the parenchymal basement membrane at sites of leukocyte extravasation in experimental autoimmune encephalomyelitis. J. Cell Biol. 173, 1007–1019.

Aharoni, R., 2013. The mechanism of action of glatiramer acetate in multiple sclerosis and beyond. Autoimmun. Rev. 12, 543–53.

Aharoni, R., Eilam, R., Stock, A., Vainshtein, A., Shezen, E., Gal, H., Friedman, N., Arnon, R., 2010. Glatiramer acetate reduces Th-17 inflammation and induces regulatory T-cells in the CNS of mice with relapsing-remitting or chronic EAE. J. Neuroimmunol. 225, 100–11.

Akiyoshi, H., Chung, J.-S., Tomihari, M., Cruz, P.D., Ariizumi, K., 2010. Depleting syndecan-4+ T lymphocytes using toxin-bearing dendritic cell-associated heparan sulfate proteoglycan-dependent integrin ligand: a new opportunity for treating activated T cell-driven disease. J. Immunol. 184, 3554–61.

Allain, F., Vanpouille, C., Carpentier, M., Slomianny, M.-C., Durieux, S., Spik, G., 2002. Interaction with glycosaminoglycans is required for cyclophilin B to trigger integrin-mediated adhesion of peripheral blood T lymphocytes to extracellular matrix. Proc. Natl. Acad. Sci. U. S. A. 99, 2714–9.

Amato, M.P., Derfuss, T., Hemmer, B., Liblau, R., Montalban, X., Soelberg Sørensen, P., Miller, D.H., Alfredsson, L., Aloisi, F., Amato, M.P., Ascherio, A., Baldin, E., Bjørnevik, K., Comabella, M., Correale, J., Cortese, M., Derfuss, T., D'Hooghe, M., Ghezzi, A., Gold, J., Hellwig, K., Hemmer, B., Koch-Henricksen, N., Langer Gould, A., Liblau, R., Linker, R., Lolli, F., Lucas, R., Lünemann, J., Magyari, M., Massacesi, L., Miller, A., Miller, D.H., Montalban, X., Monteyne, P., Mowry, E., Münz, C., Nielsen, N.M., Olsson, T., Oreja-Guevara, C., Otero, S., Pugliatti, M., Reingold, S., Riise, T., Robertson, N., Salvetti, M., Sidhom, Y., Smolders, J., Soelberg Sørensen, P., Sollid, L., Steiner, I., Stenager, E., Sundstrom, P., Taylor, B. V, Tremlett, H., Trojano, M., Uccelli, A., Waubant, E., Wekerle, H., 2017. Environmental modifiable risk factors for multiple sclerosis: Report from the 2016 ECTRIMS focused workshop. Mult. Scler. J. 135245851668684.

Anthony, I.C., Crawford, D.H., Bell, J.E., 2003. B lymphocytes in the normal brain: contrasts with HIV-associated lymphoid infiltrates and lymphomas. Brain 126, 1058–1067.

Arnett, H.A., Mason, J., Marino, M., Suzuki, K., Matsushima, G.K., Ting, J.P., 2001. TNF alpha promotes proliferation of oligodendrocyte progenitors and remyelination. Nat. Neurosci. 4, 1116–22.

Ascherio, A., Munger, K.L., White, R., Köchert, K., Simon, K.C., Polman, C.H., Freedman, M.S., Hartung, H.-P., Miller, D.H., Montalbán, X., Edan, G., Barkhof, F., Pleimes, D., Radü, E.-W., Sandbrink, R., Kappos, L., Pohl, C., 2014. Vitamin D as an early predictor of multiple sclerosis activity and progression. JAMA Neurol. 71, 306–14.

Auron, P.E., Webb, A.C., Rosenwasser, L.J., Mucci, S.F., Rich, A., Wolff, S.M., Dinarello, C.A., 1984. Nucleotide sequence of human monocyte interleukin 1 precursor cDNA. PNAS 81, 7907–11.

Babbe, H., Roers, A., Waisman, A., Lassmann, H., Goebels, N., Hohlfeld, R., Friese, M., Schröder, R., Deckert, M., Schmidt, S., Ravid, R., Rajewsky, K., 2000. Clonal expansions of CD8(+) T cells dominate the T cell infiltrate in active multiple sclerosis lesions as shown by micromanipulation and single cell polymerase chain reaction. J. Exp. Med. 192, 393–404.

Back, S.A., Tuohy, T.M.F., Chen, H., Wallingford, N., Craig, A., Struve, J., Luo, N.L., Banine, F., Liu, Y., Chang, A., Trapp, B.D., Bebo, B.F., Rao, M.S., Sherman, L.S., 2005. Hyaluronan accumulates in demyelinated lesions and inhibits oligodendrocyte progenitor maturation. Nat. Med. 11, 966–972.

Baker, D., Amor, S., 2012. Publication guidelines for refereeing and reporting on animal use in experimental autoimmune encephalomyelitis. J. Neuroimmunol. 242, 78–83.

Barnett, M.H., Prineas, J.W., 2004. Relapsing and remitting multiple sclerosis: pathology of the newly forming lesion. Ann. Neurol. 55, 458–68.

Barros, C.S., Franco, S.J., Müller, U., 2011. Extracellular matrix: functions in the nervous system. Cold Spring Harb. Perspect. Biol. 3, a005108.

Barthelmes, J., Tafferner, N., Kurz, J., de Bruin, N., Parnham, M.J., Geisslinger, G., Schiffmann, S., 2016. Induction of Experimental Autoimmune Encephalomyelitis in Mice and Evaluation of the Disease-dependent Distribution of Immune Cells in Various Tissues. J. Vis. Exp.

Baxter, A.G., 2007. The origin and application of experimental autoimmune encephalomyelitis. Nat. Rev. Immunol. 7, 904–12.

Beecham, A.H., Patsopoulos, N.A., Xifara, D.K., Davis, M.F., Kemppinen, A., Cotsapas, C., Shah, T.S., Spencer, C., Booth, D., Goris, A., Oturai, A., Saarela, J., Fontaine, B., Hemmer, B., Martin, C., Zipp, F., D'Alfonso, S., Martinelli-Boneschi, F., Taylor, B., Harbo, H.F., Kockum, I., Hillert, J., Olsson, T., Ban, M., Oksenberg, J.R., Hintzen, R., Barcellos, L.F., Agliardi, C., Alfredsson, L., Alizadeh, M., Anderson, C., Andrews, R., Søndergaard, H.B., Baker, A., Band, G., Baranzini, S.E., Barizzone, N., Barrett, J., Bellenguez, C., Bergamaschi, L., Bernardinelli, L., Berthele, A., Biberacher, V., Binder, T.M.C., Blackburn, H., Bomfim, I.L., Brambilla, P., Broadley, S., Brochet, B., Brundin, L., Buck, D., Butzkueven, H., Caillier, S.J., Camu, W., Carpentier, W., Cavalla, P., Celius, E.G., Coman, I., Comi, G., Corrado, L., Cosemans, L., Cournu-Rebeix, I., Cree, B.A.C., Cusi, D., Damotte, V., Defer, G., Delgado, S.R., Deloukas, P., di Sapio, A., Dilthey, A.T., Donnelly, P., Dubois, B., Duddy, M., Edkins, S., Elovaara, I., Esposito, F., Evangelou, N., Fiddes, B., Field, J., Franke, A., Freeman, C., Frohlich, I.Y., Galimberti, D., Gieger, C., Gourraud, P.-A., Graetz, C., Graham, A., Grummel, V., Guaschino, C., Hadjixenofontos, A., Hakonarson, H., Halfpenny, C., Hall, G., Hall, P., Hamsten, A., Harley, J., Harrower, T., Hawkins, C., Hellenthal, G., Hillier, C., Hobart, J., Hoshi, M., Hunt, S.E., Jagodic, M., Jelčić, I., Jochim, A., Kendall, B., Kermode, A., Kilpatrick, T., Koivisto, K., Konidari, I., Korn, T., Kronsbein, H., Langford, C., Larsson, M., Lathrop, M., Lebrun-Frenay, C., Lechner-Scott, J., Lee, M.H., Leone, M.A., Leppä, V., Liberatore, G., Lie, B.A., Lill, C.M., Lindén, M., Link, J., Luessi, F., Lycke, J., Macciardi, F., Männistö, S., Manrique, C.P., Martin, R., Martinelli, V., Mason, D., Mazibrada, G., McCabe, C., Mero, I.-L., Mescheriakova, J., Moutsianas, L., Myhr, K.-M., Nagels, G., Nicholas, R., Nilsson, P., Piehl, F., Pirinen, M., Price, S.E., Quach, H., Reunanen, M., Robberecht, W., Robertson, N.P., Rodegher, M., Rog, D., Salvetti, M., Schnetz-Boutaud, N.C., Sellebjerg, F., Selter, R.C., Schaefer, C., Shaunak, S., Shen, L., Shields, S., Siffrin, V., Slee, M., Sorensen, P.S., Sorosina, M., Sospedra, M., Spurkland, A., Strange, A., Sundqvist, E., Thijs, V., Thorpe, J., Ticca, A., Tienari, P., van Duijn, C., Visser, E.M., Vucic, S., Westerlind, H., Wiley, J.S., Wilkins, A., Wilson, J.F., Winkelmann, J., Zajicek, J., Zindler, E., Haines, J.L., Pericak-Vance, M.A., Ivinson, A.J., Stewart, G., Hafler, D., Hauser, S.L., Compston, A., McVean, G., De Jager, P., Sawcer, S.J., McCauley, J.L., De Jager, P., Sawcer, S.J., McCauley, J.L., 2013. Analysis of immune-related loci identifies 48 new susceptibility variants for multiple sclerosis. Nat. Genet. 45, 1353–1360.

Berard, J.L., Wolak, K., Fournier, S., David, S., 2010. Characterization of relapsing-remitting and chronic forms of experimental autoimmune encephalomyelitis in C57BL/6 mice. Glia 58, 434–45.

Berridge, M. V, Herst, P.M., Tan, A.S., 2005. Tetrazolium dyes as tools in cell biology: new insights into their cellular reduction. Biotechnol. Annu. Rev. 11, 127–52.

Bettelli, E., Das, M.P., Howard, E.D., Weiner, H.L., Sobel, R.A., Kuchroo, V.K., 1998. IL-10 is critical in the regulation of autoimmune encephalomyelitis as demonstrated by studies of IL-10- and IL-4-deficient and transgenic mice. J. Immunol. 161, 3299–306.

Bishop, J.R., Schuksz, M., Esko, J.D., 2007. Heparan sulphate proteoglycans fine-tune mammalian physiology. Nature 446, 1030–1037.

Bitan, M., Weiss, L., Reibstein, I., Zeira, M., Fellig, Y., Slavin, S., Zcharia, E., Nagler, A., Vlodavsky, I., 2010. Heparanase upregulates Th2 cytokines, ameliorating experimental autoimmune encephalitis. Mol. Immunol. 47, 1890–1898.

Bö, L., Mörk, S., Kong, P.A., Nyland, H., Pardo, C.A., Trapp, B.D., 1994. Detection of MHC class II-antigens on macrophages and microglia, but not on astrocytes and endothelia in active multiple sclerosis lesions. J. Neuroimmunol. 51, 135–146.

Bobardt, M.D., Saphire, A.C.S., Hung, H.-C., Yu, X., Van der Schueren, B., Zhang, Z., David, G., Gallay, P.A., 2003. Syndecan captures, protects, and transmits HIV to T lymphocytes. Immunity 18, 27–39.

Bogie, J.F.J., Stinissen, P., Hellings, N., Hendriks, J.J. a, 2011. Myelin-phagocytosing macrophages modulate autoreactive T cell proliferation. J. Neuroinflammation 8, 85.

Boilard, E., Bourgoin, S.G., Bernatchez, C., Poubelle, P.E., Surette, M.E., 2003. Interaction of low molecular weight group IIA phospholipase A2 with apoptotic human T cells: role of heparan sulfate proteoglycans. FASEB J. 17, 1068–80.

Booss, J., Esiri, M.M., Tourtellotte, W.W., Mason, D.Y., 1983. Immunohistological analysis of T lymphocyte subsets in the central nervous system in chronic progressive multiple sclerosis. J. Neurol. Sci. 62, 219–32.

Boven, L.A., Van Meurs, M., Van Zwam, M., Wierenga-Wolf, A., Hintzen, R.Q., Boot, R.G., Aerts, J.M., Amor, S., Nieuwenhuis, E.E., Laman, J.D., 2006. Myelin-laden macrophages are anti-inflammatory, consistent with foam cells in multiple sclerosis. Brain 129, 517–26.

Bradbury, E.J., Moon, L.D.F., Popat, R.J., King, V.R., Bennett, G.S., Patel, P.N., Fawcett, J.W., McMahon, S.B., 2002. Chondroitinase ABC promotes functional recovery after spinal cord injury. Nature 416, 636–640.

Bramow, S., Frischer, J.M., Lassmann, H., Koch-Henriksen, N., Lucchinetti, C.F., Sørensen, P.S., Laursen, H., 2010. Demyelination versus remyelination in progressive multiple sclerosis. Brain 133, 2983–98.

Bretscher, P., Cohn, M., 1970. A theory of self-nonself discrimination. Sci. 169, 1042–9.

Brinkmann, V., Billich, A., Baumruker, T., Heining, P., Schmouder, R., Francis, G., Aradhye, S., Burtin, P., 2010. Fingolimod (FTY720): discovery and development of an oral drug to treat multiple sclerosis. Nat. Rev. Drug Discov. 9, 883–97.

Brosnan, C.F., Cannella, B., Battistini, L., Raine, C.S., 1995. Cytokine localization in multiple sclerosis lesions: correlation with adhesion molecule expression and reactive nitrogen species. Neurology 45, S16-21.

Brown, D.A., Sawchenko, P.E., 2007. Time course and distribution of inflammatory and neurodegenerative events suggest structural bases for the pathogenesis of experimental autoimmune encephalomyelitis. J. Comp. Neurol. 502, 236–60.

Brucklacher-Waldert, V., Stuerner, K., Kolster, M., Wolthausen, J., Tolosa, E., 2009. Phenotypical and functional characterization of T helper 17 cells in multiple sclerosis. Brain 132, 3329–3341.

Bülow, H.E., Hobert, O., 2006. The Molecular Diversity of Glycosaminoglycans Shapes Animal Development. Annu. Rev. Cell Dev. Biol. 22, 375–407.

Bustin, S. a, 2010. Why the need for qPCR publication guidelines?--The case for MIQE. Methods 50, 217–26.

Cannella, B., Raine, C.S., 1995. The adhesion molecule and cytokine profile of multiple sclerosis lesions. Ann. Neurol. 37, 424–435.

Capila, I., Linhardt, R.J., 2002. Heparin-Protein Interactions. Angew. Chemie Int. Ed. 41, 390–412.

Cardin, A.D., Jackson, R.L., Sparrow, D.A., Sparrow, J.T., 1989. Interaction of glycosaminoglycans with lipoproteins. Ann. N. Y. Acad. Sci. 556, 186–93.

Ceeraz, S., Nowak, E.C., Noelle, R.J., 2013. B7 family checkpoint regulators in immune regulation and disease. Trends Immunol. 34, 556–63.

Chari, D.M., 2007. Remyelination in multiple sclerosis. Int. Rev. Neurobiol. 79, 589–620.

Chen, X., Winkler-Pickett, R.T., Carbonetti, N.H., Ortaldo, J.R., Oppenheim, J.J., Howard, O.M.Z., 2006. Pertussis toxin as an adjuvant suppresses the number and function of CD4+CD25+ T regulatory cells. Eur. J. Immunol. 36, 671–680.

Cheng, W., Chen, G., 2014. Chemokines and chemokine receptors in multiple sclerosis. Mediators Inflamm. 2014, 659206.

Chitnis, S., Monteiro, J., Glass, D., Apatoff, B., Salmon, J., Concannon, P., Gregersen, P.K., 2000. The role of X-chromosome inactivation in female predisposition to autoimmunity. Arthritis Res. 2, 399–406.

Chitnis, T., 2007. The Role of CD4 T Cells in the Pathogenesis of Multiple Sclerosis. Int. Rev. Neurobiol. 79, 43–72.

Chow, J.C., Young, D.W., Golenbock, D.T., Christ, W.J., Gusovsky, F., 1999. Toll-like receptor-4 mediates lipopolysaccharide-induced signal transduction. J. Biol. Chem. 274, 10689–92.

Christmas, S.E., Steward, W.P., Lyon, M., Gallagher, J.T., Moore, M., 1988. Chondroitin sulphate proteoglycan production by NK cells and T cells: effects of xylosides on proliferation and cytotoxic function. Immunology 63, 225–31.

Chun, J., Hartung, H.-P., 2010. Mechanism of Action of Oral Fingolimod (FTY720) in Multiple Sclerosis. Clin. Neuropharmacol. 33, 91–101.

Chung, I.Y., Benveniste, E.N., 1990. Tumor necrosis factor-alpha production by astrocytes. Induction by lipopolysaccharide, IFN-gamma, and IL-1 beta. J. Immunol. 144, 2999–3007.

Chung, J.-S., Bonkobara, M., Tomihari, M., Cruz, P.D., Ariizumi, K., 2009. The DC-HIL/syndecan-4 pathway inhibits human allogeneic T-cell responses. Eur. J. Immunol. 39, 965–74.

Chung, J.-S., Cruz, P.D., Ariizumi, K., 2011. Inhibition of T-cell activation by syndecan-4 is mediated by CD148 through protein tyrosine phosphatase activity. Eur. J. Immunol. 41, 1794–9.

Chung, J.-S., Dougherty, I., Cruz, P.D., Ariizumi, K., 2007. Syndecan-4 mediates the coinhibitory function of DC-HIL on T cell activation. J. Immunol. 179, 5778–84.

Chung, J.-S., Tamura, K., Akiyoshi, H., Cruz, P.D., Ariizumi, K., Ariizumi, K., 2014. The DC-HIL/syndecan-4 pathway regulates autoimmune responses through myeloid-derived suppressor cells. J. Immunol. 192, 2576–84.

Chung, J.-S., Tomihari, M., Tamura, K., Kojima, T., Cruz, P.D., Ariizumi, K., 2013. The DC-HIL ligand syndecan-4 is a negative regulator of T-cell allo-reactivity responsible for graft-versus-host disease. Immunology. 138, 173–182.

Cocco, E., Sardu, C., Spinicci, G., Musu, L., Massa, R., Frau, J., Lorefice, L., Fenu, G., Coghe, G., Massole, S., Maioli, M.A., Piras, R., Melis, M., Porcu, G., Mamusa, E., Carboni, N., Contu, P., Marrosu, M.G., 2015. Influence of treatments in multiple sclerosis disability: A cohort study. Mult. Scler. J. 21, 433–441.

Cohen, J.A., Coles, A.J., Arnold, D.L., Confavreux, C., Fox, E.J., Hartung, H.-P., Havrdova, E., Selmaj, K.W., Weiner, H.L., Fisher, E., Brinar, V. V, Giovannoni, G., Stojanovic, M., Ertik, B.I., Lake, S.L., Margolin, D.H., Panzara, M.A., Compston, D.A.S., CARE-MS I investigators, 2012. Alemtuzumab versus interferon beta 1a as first-line treatment for patients with relapsing-remitting multiple sclerosis: a randomised controlled phase 3 trial. Lancet 380, 1819–1828.

Comi, G., Martinelli, V., Rodegher, M., Moiola, L., Leocani, L., Bajenaru, O., Carra, A., Elovaara, I., Fazekas, F., Hartung, H.-P., Hillert, J., King, J., Komoly, S., Lubetzki, C., Montalban, X., Myhr, K.-M., Preziosa, P., Ravnborg, M., Rieckmann, P., Rocca, M.A., Wynn, D., Young, C., Filippi, M., 2013. Effects of early treatment with glatiramer acetate in patients with clinically isolated syndrome. Mult. Scler. J. 19, 1074–1083.

Compston, A., Coles, A., 2008. Multiple sclerosis. Lancet 372, 1502–17.

Confavreux, C., O'Connor, P., Comi, G., Freedman, M.S., Miller, A.E., Olsson, T.P., Wolinsky, J.S., Bagulho, T., Delhay, J.-L., Dukovic, D., Truffinet, P., Kappos, L., 2014. Oral teriflunomide for patients with relapsing multiple sclerosis (TOWER): a randomised, double-blind, placebo-controlled, phase 3 trial. Lancet Neurol. 13, 247–256.

Cross, A.H., Misko, T.P., Lin, R.F., Hickey, W.F., Trotter, J.L., Tilton, R.G., 1994. Aminoguanidine, an inhibitor of inducible nitric oxide synthase, ameliorates experimental autoimmune encephalomyelitis in SJL mice. J. Clin. Invest. 93, 2684–90.

Cua, D.J., Sherlock, J., Chen, Y., Murphy, C.A., Joyce, B., Seymour, B., Lucian, L., To, W., Kwan, S., Churakova, T., Zurawski, S., Wiekowski, M., Lira, S.A., Gorman, D., Kastelein, R.A., Sedgwick, J.D., 2003. Interleukin-23 rather than interleukin-12 is the critical cytokine for autoimmune inflammation of the brain. Nature 421, 744–748.

De Francesco, M.A., Baronio, M., Poiesi, C., 2011. HIV-1 p17 matrix protein interacts with heparan sulfate side chain of CD44v3, syndecan-2, and syndecan-4 proteoglycans expressed on human activated CD4+ T cells affecting tumor necrosis factor alpha and interleukin 2 production. J. Biol. Chem. 286, 19541–8.

De Yébenes, E.G., Ho, A., Damani, T., Fillit, H., Blum, M., 2002. Regulation of the Heparan Sulfate Proteoglycan, Perlecan, by Injury and Interleukin-1α. J. Neurochem. 73, 812–820.

Del Prete, G., De Carli, M., Almerigogna, F., Giudizi, M.G., Biagiotti, R., Romagnani, S., 1993. Human IL-10 is produced by both type 1 helper (Th1) and type 2 helper (Th2) T cell clones and inhibits their antigen-specific proliferation and cytokine production. J. Immunol. 150, 353–60.

Dhoot, G.K., Gustafsson, M.K., Ai, X., Sun, W., Standiford, D.M., Emerson, C.P., 2001. Regulation of Wnt Signaling and Embryo Patterning by an Extracellular Sulfatase. Science (80-.). 293, 1663–1666.

Di Pauli, F., Reindl, M., Ehling, R., Schautzer, F., Gneiss, C., Lutterotti, A., O'Reilly, E., Munger, K., Deisenhammer, F., Ascherio, A., Berger, T., 2008. Smoking is a risk factor for early conversion to clinically definite multiple sclerosis. Mult. Scler. 14, 1026–30.

dos Santos, A.C., Barsante, M.M., Esteves Arantes, R.M., Bernard, C.C.A., Teixeira, M.M., Carvalho-Tavares, J., 2005. CCL2 and CCL5 mediate leukocyte adhesion in experimental autoimmune encephalomyelitis—an intravital microscopy study. J. Neuroimmunol. 162, 122–129.

Doucette, C.D., Greenshields, A.L., Liwski, R.S., Hoskin, D.W., 2015. Piperine blocks interleukin-2-driven cell cycle progression in CTLL-2 T lymphocytes by inhibiting multiple signal transduction pathways. Toxicol. Lett. 234, 1–12.

Duda, P.W., Schmied, M.C., Cook, S.L., Krieger, J.I., Hafler, D.A., 2000. Glatiramer acetate (Copaxone) induces degenerate, Th2-polarized immune responses in patients with multiple sclerosis. J. Clin. Invest. 105, 967–76.

Dutta, R., Trapp, B.D., 2014. Relapsing and progressive forms of multiple sclerosis: insights from pathology. Curr. Opin. Neurol. 27, 271–8.

Esko, J.D., Kimata, K., Lindahl, U., 2009. Proteoglycans and Sulfated Glycosaminoglycans, Essentials of Glycobiology. Cold Spring Harbor Laboratory Press.

Evans, C., Beland, S.-G., Kulaga, S., Wolfson, C., Kingwell, E., Marriott, J., Koch, M., Makhani, N., Morrow, S., Fisk, J., Dykeman, J., Jetté, N., Pringsheim, T., Marrie, R.A., 2013. Incidence and prevalence of multiple sclerosis in the Americas: a systematic review. Neuroepidemiology 40, 195–210.

Fadnes, B., Husebekk, A., Svineng, G., Rekdal, Ø., Yanagishita, M., Kolset, S.O., Uhlin-Hansen, L., 2012. The proteoglycan repertoire of lymphoid cells. Glycoconj. J. 29, 513–23.

Falcone, M., Rajan, A.J., Bloom, B.R., Brosnan, C.F., 1998. A critical role for IL-4 in regulating disease severity in experimental allergic encephalomyelitis as demonstrated in IL-4-deficient C57BL/6 mice and BALB/c mice. J. Immunol. 160, 4822–30.

Fiander, M.D.J., Stifani, N., Nichols, M., Akay, T., Robertson, G.S., 2017. Kinematic gait parameters are highly sensitive measures of motor deficits and spinal cord injury in mice subjected to experimental autoimmune encephalomyelitis. Behav. Brain Res. 317, 95–108.

Fife, B.T., Huffnagle, G.B., Kuziel, W.A., Karpus, W.J., 2000. CC chemokine receptor 2 is critical for induction of experimental autoimmune encephalomyelitis. J. Exp. Med. 192, 899–905.

Foey, A.D., Parry, S.L., Williams, L.M., Feldmann, M., Foxwell, B.M.J., Brennan, F.M., 1998. Regulation of Monocyte IL-10 Synthesis by Endogenous IL-1 and TNF-α: Role of the p38 and p42/44 Mitogen-Activated Protein Kinases. J. Immunol. 160, 920–928.

Fordham, S., O'Brien, N., Linares, D., 2007. The contribution of nitric oxide and interferon gamma to the regulation of the neuro-inflammation in experimental autoimmune encephalomyelitis. J. Neuroimmunol. 191, 16–25.

Franklin, R.J.M., 2002. Why does remyelination fail in multiple sclerosis? Nat. Rev. Neurosci. 3, 705–714.

Fraussen, J., de Bock, L., Somers, V., 2016. B cells and antibodies in progressive multiple sclerosis: Contribution to neurodegeneration and progression. Autoimmun. Rev. 15, 896–899.

Friese, M.A., Schattling, B., Fugger, L., 2014. Mechanisms of neurodegeneration and axonal dysfunction in multiple sclerosis. Nat. Rev. Neurol. 10, 225–38.

Frischer, J.M., Weigand, S.D., Guo, Y., Kale, N., Parisi, J.E., Pirko, I., Mandrekar, J., Bramow, S., Metz, I., Brück, W., Lassmann, H., Lucchinetti, C.F., 2015. Clinical and pathological insights into the dynamic nature of the white matter multiple sclerosis plaque. Ann. Neurol. 78, 710–721.

Frohman, E.M., Racke, M.K., Raine, C.S., 2006. Multiple sclerosis--the plaque and its pathogenesis. N. Engl. J. Med. 354, 942–55.

Fujiwara, N., Kobayashi, K., 2005. Macrophages in Inflammation. Curr. Drug Targets - Inflamm. Allergy 4, 281–286.

Furtado, G.C., Marcondes, M.C.G., Latkowski, J.-A., Tsai, J., Wensky, A., Lafaille, J.J., 2008. Swift entry of myelin-specific T lymphocytes into the central nervous system in spontaneous autoimmune encephalomyelitis. J. Immunol. 181, 4648–55.

Galea, I., Bechmann, I., Perry, V.H., 2007. What is immune privilege (not)? Trends Immunol. 28, 12–8.

Gallay, P., 2004. Syndecans and HIV-1 pathogenesis. Microbes Infect. 6, 617–22.

Garner, O.B., Yamaguchi, Y., Esko, J.D., Videm, V., 2008. Small changes in lymphocyte development and activation in mice through tissue-specific alteration of heparan sulphate. Immunology 125, 420–9.

Ghasemlou, N., Jeong, S.Y., Lacroix, S., David, S., 2007. T cells contribute to lysophosphatidylcholine-induced macrophage activation and demyelination in the CNS. Glia 55, 294–302.

Giamanco, K.A., Morawski, M., Matthews, R.T., 2010. Perineuronal net formation and structure in aggrecan knockout mice. Neuroscience 170, 1314–1327.

Gold, R., Kappos, L., Arnold, D.L., Bar-Or, A., Giovannoni, G., Selmaj, K., Tornatore, C., Sweetser, M.T., Yang, M., Sheikh, S.I., Dawson, K.T., 2012. Placebo-Controlled Phase 3 Study of Oral BG-12 for Relapsing Multiple Sclerosis. N. Engl. J. Med. 367, 1098–1107.

Gran, B., Zhang, G.-X., Yu, S., Li, J., Chen, X.-H., Ventura, E.S., Kamoun, M., Rostami, A., 2002. IL-12p35-Deficient Mice Are Susceptible to Experimental Autoimmune Encephalomyelitis: Evidence for Redundancy in the IL-12 System in the Induction of Central Nervous System Autoimmune Demyelination. J. Immunol. 169, 7104–7110.

Greter, M., Heppner, F.L., Lemos, M.P., Odermatt, B.M., Goebels, N., Laufer, T., Noelle, R.J., Becher, B., 2005. Dendritic cells permit immune invasion of the CNS in an animal model of multiple sclerosis. Nat. Med. 11, 328–334.

Group, T.L.M.S.S., 1999. TNF neutralization in MS: results of a randomized, placebo-controlled multicenter study. The Lenercept Multiple Sclerosis Study Group and The University of British Columbia MS/MRI Analysis Group. Neurology 53, 457–65.

Guenova, E., Volz, T., Sauer, K., Kaesler, S., Müller, M.R., Wölbing, F., Chen, K., Schwärzler, C., Brossart, P., Röcken, M., Biedermann, T., 2008. IL-4-mediated fine tuning of IL-12p70 production by human DC. Eur. J. Immunol. 38, 3138–3149.

Haas, J., Hug, A., Viehöver, A., Fritzsching, B., Falk, C.S., Filser, A., Vetter, T., Milkova, L., Korporal, M., Fritz, B., Storch-Hagenlocher, B., Krammer, P.H., Suri-Payer, E., Wildemann, B., 2005. Reduced suppressive effect of CD4+CD25high regulatory T cells on the T cell immune response against myelin oligodendrocyte glycoprotein in patients with multiple sclerosis. Eur. J. Immunol. 35, 3343–3352.

Haas, J., Korporal, M., Balint, B., Fritzsching, B., Schwarz, A., Wildemann, B., 2009. Glatiramer acetate improves regulatory T-cell function by expansion of naive CD4(+)CD25(+)FOXP3(+)CD31(+) T-cells in patients with multiple sclerosis. J. Neuroimmunol. 216, 113–7.

Häcker, U., Nybakken, K., Perrimon, N., 2005. Heparan sulphate proteoglycans: the sweet side of development. Nat. Rev. Mol. Cell Biol. 6, 530–41.

Haist, V., Ulrich, R., Kalkuhl, A., Deschl, U., Baumgärtner, W., 2012. Distinct Spatio-Temporal Extracellular Matrix Accumulation within Demyelinated Spinal Cord Lesions in Theiler's Murine Encephalomyelitis. Brain Pathol. 22, 188–204.

Harris, J., Hartman, M., Roche, C., Zeng, S.G., O'Shea, A., Sharp, F.A., Lambe, E.M., Creagh, E.M., Golenbock, D.T., Tschopp, J., Kornfeld, H., Fitzgerald, K.A., Lavelle, E.C., 2011. Autophagy Controls IL-1 Secretion by Targeting Pro-IL-1 for Degradation. J. Biol. Chem. 286, 9587–9597.

Hasan, M., Najjam, S., Gordon, M.Y., Gibbs, R. V., Rider, C.C., 1999. IL-12 is a heparin-binding cytokine. J. Immunol. 162, 1064–1070.

Hayashi, T., Morimoto, C., Burks, J.S., Kerr, C., Hauser, S.L., 1988. Dual-label immunocytochemistry of the active multiple sclerosis lesion: major histocompatibility complex and activation antigens. Ann. Neurol. 24, 523–31.

Hileman, R.E., Fromm, J.R., Weiler, J.M., Linhardt, R.J., 1998. Glycosaminoglycan-protein interactions: definition of consensus sites in glycosaminoglycan binding proteins. BioEssays 20, 156–167.

Hinks, G.L., Franklin, R.J.M., 1999. Distinctive Patterns of PDGF-A, FGF-2, IGF-I, and TGF-β1 Gene Expression during Remyelination of Experimentally-Induced Spinal Cord Demyelination. Mol. Cell. Neurosci. 14, 153–168.

Höftberger, R., Aboul-Enein, F., Brueck, W., Lucchinetti, C., Rodriguez, M., Schmidbauer, M., Jellinger, K., Lassmann, H., 2004. Expression of Major Histocompatibility Complex class l Molecules on the Different Cell Types in Multiple Sclerosis Lesions. Brain Pathol. 14, 43–50.

Höftberger, R., Leisser, M., Bauer, J., Lassmann, H., 2015. Autoimmune encephalitis in humans: how closely does it reflect multiple sclerosis ? Acta Neuropathol. Commun. 3, 80.

Houser, B., 2012. Bio-Rad's Bio-Plex® suspension array system, xMAP technology overview. Arch. Physiol. Biochem. 118, 192–196.

Huber, S., Gagliani, N., Esplugues, E., O'Connor, W., Huber, F.J., Chaudhry, A., Kamanaka, M., Kobayashi, Y., Booth, C.J., Rudensky, A.Y., Roncarolo, M.G., Battaglia, M., Flavell, R.A., 2011. Th17 Cells Express Interleukin-10 Receptor and Are Controlled by Foxp3− and Foxp3+ Regulatory CD4+ T Cells in an Interleukin-10-Dependent Manner. Immunity 34, 554–565.

Huitinga, I., van Rooijen, N., de Groot, C.J., Uitdehaag, B.M., Dijkstra, C.D., 1990. Suppression of experimental allergic encephalomyelitis in Lewis rats after elimination of macrophages. J. Exp. Med. 172, 1025–33.

Hunter, D.T., Hill, J.M., 1961. Surfen: a quinoline with oncogenic and heparin-neutralizing properties. Nature 191, 1378–9.

Huseby, E.S., Huseby, P.G., Shah, S., Smith, R., Stadinski, B.D., 2012. Pathogenic CD8 T cells in multiple sclerosis and its experimental models. Front. Immunol. 3, 64.

Huseby, E.S., Liggitt, D., Brabb, T., Schnabel, B., Ohlén, C., Goverman, J., 2001. A pathogenic role for myelin-specific CD8(+) T cells in a model for multiple sclerosis. J. Exp. Med. 194, 669–76.

International Multiple Sclerosis Genetics Consortium, S., Wellcome Trust Case Control Consortium 2, G., Sawcer, S., Hellenthal, G., Pirinen, M., Spencer, C.C.A., Patsopoulos, N.A., Moutsianas, L., Dilthey, A., Su, Z., Freeman, C., Hunt, S.E., Edkins, S., Gray, E., Booth, D.R., Potter, S.C., Goris, A., Band, G., Oturai, A.B., Strange, A., Saarela, J., Bellenguez, C., Fontaine, B., Gillman, M., Hemmer, B., Gwilliam, R., Zipp, F., Jayakumar, A., Martin, R., Leslie, S., Hawkins, S., Giannoulatou, E., D'alfonso, S., Blackburn, H., Martinelli Boneschi, F., Liddle, J., Harbo, H.F., Perez, M.L., Spurkland, A., Waller, M.J., Mycko, M.P., Ricketts, M.,

Comabella, M., Hammond, N., Kockum, I., McCann, O.T., Ban, M., Whittaker, P., Kemppinen, A., Weston, P., Hawkins, C., Widaa, S., Zajicek, J., Dronov, S., Robertson, N., Bumpstead, S.J., Barcellos, L.F., Ravindrarajah, R., Abraham, R., Alfredsson, L., Ardlie, K., Aubin, C., Baker, A., Baker, K., Baranzini, S.E., Bergamaschi, L., Bergamaschi, R., Bernstein, A., Berthele, A., Boggild, M., Bradfield, J.P., Brassat, D., Broadley, S.A., Buck, D., Butzkueven, H., Capra, R., Carroll, W.M., Cavalla, P., Celius, E.G., Cepok, S., Chiavacci, R., Clerget-Darpoux, F., Clysters, K., Comi, G., Cossburn, M., Cournu-Rebeix, I., Cox, M.B., Cozen, W., Cree, B.A.C., Cross, A.H., Cusi, D., Daly, M.J., Davis, E., de Bakker, P.I.W., Debouverie, M., D'hooghe, M.B., Dixon, K., Dobosi, R., Dubois, B., Ellinghaus, D., Elovaara, I., Esposito, F., Fontenille, C., Foote, S., Franke, A., Galimberti, D., Ghezzi, A., Glessner, J., Gomez, R., Gout, O., Graham, C., Grant, S.F.A., Guerini, F.R., Hakonarson, H., Hall, P., Hamsten, A., Hartung, H.-P., Heard, R.N., Heath, S., Hobart, J., Hoshi, M., Infante-Duarte, C., Ingram, G., Ingram, W., Islam, T., Jagodic, M., Kabesch, M., Kermode, A.G., Kilpatrick, T.J., Kim, C., Klopp, N., Koivisto, K., Larsson, M., Lathrop, M., Lechner-Scott, J.S., Leone, M.A., Leppä, V., Liljedahl, U., Bomfim, I.L., Lincoln, R.R., Link, J., Liu, J., Lorentzen, A.R., Lupoli, S., Macciardi, F., Mack, T., Marriott, M., Martinelli, V., Mason, D., McCauley, J.L., Mentch, F., Mero, I.-L., Mihalova, T., Montalban, X., Mottershead, J., Myhr, K.-M., Naldi, P., Ollier, W., Page, A., Palotie, A., Pelletier, J., Piccio, L., Pickersgill, T., Piehl, F., Pobywajlo, S., Quach, H.L., Ramsay, P.P., Reunanen, M., Reynolds, R., Rioux, J.D., Rodegher, M., Roesner, S., Rubio, J.P., Rückert, I.-M., Salvetti, M., Salvi, E., Santaniello, A., Schaefer, C.A., Schreiber, S., Schulze, C., Scott, R.J., Sellebjerg, F., Selmaj, K.W., Sexton, D., Shen, L., Simms-Acuna, B., Skidmore, S., Sleiman, P.M.A., Smestad, C., Sørensen, P.S., Søndergaard, H.B., Stankovich, J., Strange, R.C., Sulonen, A.-M., Sundqvist, E., Syvänen, A.-C., Taddeo, F., Taylor, B., Blackwell, J.M., Tienari, P., Bramon, E., Tourbah, A., Brown, M.A., Tronczynska, E., Casas, J.P., Tubridy, N., Corvin, A., Vickery, J., Jankowski, J., Villoslada, P., Markus, H.S., Wang, K., Mathew, C.G., Wason, J., Palmer, C.N.A., Wichmann, H.-E., Plomin, R., Willoughby, E., Rautanen, A., Winkelmann, J., Wittig, M., Trembath, R.C., Yaouanq, J., Viswanathan, A.C., Zhang, H., Wood, N.W., Zuvich, R., Deloukas, P., Langford, C., Duncanson, A., Oksenberg, J.R., Pericak-Vance, M.A., Haines, J.L., Olsson, T., Hillert, J., Ivinson, A.J., De Jager, P.L., Peltonen, L., Stewart, G.J., Hafler, D.A., Hauser, S.L., McVean, G., Donnelly, P., Compston, A., 2011. Genetic risk and a primary role for cell-mediated immune mechanisms in multiple sclerosis. Nature 476, 214–9.

Issazadeh, S., Mustafa, M., Ljungdahl, A., Höjeberg, B., Dagerlind, A., Elde, R., Olsson, T., 1995. Interferon gamma, interleukin 4 and transforming growth factor beta in experimental autoimmune encephalomyelitis in Lewis rats: dynamics of cellular mRNA expression in the central nervous system and lymphoid cells. J. Neurosci. Res. 40, 579–90.

Jann, O.C., King, A., Corrales, N., Anderson, S.I., Jensen, K., Ait-ali, T., Tang, H., Wu, C., Cockett, N.E., Archibald, A.L., Glass, E.J., 2009. Comparative genomics of Toll-like receptor signalling in five species. BMC Genomics 10, 216-222.

Jeffery, N.D., Blakemore, W.F., 1995. Remyelination of mouse spinal cord axons demyelinated by local injection of lysolecithin. J. Neurocytol. 24, 775–81.

Jelinek, G.A., Marck, C.H., Weiland, T.J., Pereira, N., van der Meer, D.M., Hadgkiss, E.J., 2015. Latitude, sun exposure and vitamin D supplementation: associations with quality of life and disease outcomes in a large international cohort of people with multiple sclerosis. BMC Neurol. 15, 132-144.

Johns, L.D., Sriram, S., 1993. Experimental allergic encephalomyelitis: neutralizing antibody to TGF beta 1 enhances the clinical severity of the disease. J. Neuroimmunol. 47, 1–7.

Jones, K.S., Petrow-Sadowski, C., Bertolette, D.C., Huang, Y., Ruscetti, F.W., 2005. Heparan sulfate proteoglycans mediate attachment and entry of human T-cell leukemia virus type 1 virions into CD4+ T cells. J. Virol. 79, 12692–702.

Jones, L.L., Margolis, R.U., Tuszynski, M.H., 2003. The chondroitin sulfate proteoglycans neurocan, brevican, phosphacan, and versican are differentially regulated following spinal cord injury. Exp. Neurol. 182, 399–411.

Kaliński, P., Smits, H.H., Schuitemaker, J.H., Vieira, P.L., van Eijk, M., de Jong, E.C., Wierenga, E.A., Kapsenberg, M.L., 2000. IL-4 is a mediator of IL-12p70 induction by human Th2 cells: reversal of polarized Th2 phenotype by dendritic cells. J. Immunol. 165, 1877–81.

Kamradt, T., Soloway, P.D., Perkins, D.L., Gefter, M.L., 1991. Pertussis toxin prevents the induction of peripheral T cell anergy and enhances the T cell response to an encephalitogenic peptide of myelin basic protein. J. Immunol. 147, 3296–3302.

Kappos, L., Moeri, D., Radue, E.W., Schoetzau, A., Schweikert, K., Barkhof, F., Miller, D., Guttmann, C.R., Weiner, H.L., Gasperini, C., Filippi, M., 1999. Predictive value of gadolinium-enhanced magnetic resonance imaging for relapse rate and changes in disability or impairment in multiple sclerosis: a meta-analysis. Gadolinium MRI Meta-analysis Group. Lancet 353, 964–9.

Kappos, L., Polman, C.H., Freedman, M.S., Edan, G., Hartung, H.P., Miller, D.H., Montalban, X., Barkhof, F., Bauer, L., Jakobs, P., Pohl, C., Sandbrink, R., 2006. Treatment with interferon beta-1b delays conversion to clinically definite and McDonald MS in patients with clinically isolated syndromes. Neurology 67, 1242–1249.

Kappos, L., Radue, E.-W., O'Connor, P., Polman, C., Hohlfeld, R., Calabresi, P., Selmaj, K., Agoropoulou, C., Leyk, M., Zhang-Auberson, L., Burtin, P., 2010. A placebo-controlled trial of oral fingolimod in relapsing multiple sclerosis. N. Engl. J. Med. 362, 387–401.

Karpus, W.J., Kennedy, K.J., 1997. MIP-1alpha and MCP-1 differentially regulate acute and relapsing autoimmune encephalomyelitis as well as Th1/Th2 lymphocyte differentiation. J. Leukoc. Biol. 62, 681–7.

Kaur, S., Kuznetsova, S.A., Pendrak, M.L., Sipes, J.M., Romeo, M.J., Li, Z., Zhang, L., Roberts, D.D., 2011. Heparan sulfate modification of the transmembrane receptor CD47 is necessary for inhibition of T cell receptor signaling by thrombospondin-1. J. Biol. Chem. 286, 14991–5002.

Kavaliunas, A., Stawiarz, L., Hedbom, J., Glaser, A., Hillert, J., 2015. The Influence of Immunomodulatory Treatment on the Clinical Course of Multiple Sclerosis, in: Advances in Experimental Medicine and Biology. pp. 19–24.

Keller, C.W., Fokken, C., Turville, S.G., Lunemann, A., Schmidt, J., Munz, C., Lunemann, J.D., 2011. TNF- Induces Macroautophagy and Regulates MHC Class II Expression in Human Skeletal Muscle Cells. J. Biol. Chem. 286, 3970–3980.

Kennedy, M.K., Torrance, D.S., Picha, K.S., Mohler, K.M., 1992. Analysis of cytokine mRNA expression in the central nervous system of mice with experimental autoimmune encephalomyelitis reveals that IL-10 mRNA expression correlates with recovery. J. Immunol. 149, 2496–505.

Keough, M.B., Jensen, S.K., Wee Yong, V., 2015. Experimental Demyelination and Remyelination of Murine Spinal Cord by Focal Injection of Lysolecithin Video Link. J. Vis. Exp. 97, 526793791–52679.

Keough, M.B., Rogers, J.A., Zhang, P., Jensen, S.K., Stephenson, E.L., Chen, T., Hurlbert, M.G., Lau, L.W., Rawji, K.S., Plemel, J.R., Koch, M., Ling, C.-C., Yong, V.W., 2016. An inhibitor of chondroitin sulfate proteoglycan synthesis promotes central nervous system remyelination. Nat. Commun. 7, 11312.

Keough, M.B., Yong, V.W., 2013. Remyelination Therapy for Multiple Sclerosis. Neurotherapeutics 10, 44–54.

Kivisäkk, P., Imitola, J., Rasmussen, S., Elyaman, W., Zhu, B., Ransohoff, R.M., Khoury, S.J., 2009. Localizing central nervous system immune surveillance: meningeal antigen-presenting cells activate T cells during experimental autoimmune encephalomyelitis. Ann. Neurol. 65, 457–69.

Koch, M., Kingwell, E., Rieckmann, P., Tremlett, H., 2009. The natural history of primary progressive multiple sclerosis. Neurology 73, 1996–2002.

Koch, M., Kingwell, E., Rieckmann, P., Tremlett, H., UBC MS Clinic Neurologists, 2010. The natural history of secondary progressive multiple sclerosis. J. Neurol. Neurosurg. Psychiatry 81, 1039–1043.

Koenig, P.-A., Spooner, E., Kawamoto, N., Strominger, J.L., Ploegh, H.L., 2013. Amino acid copolymers that alleviate experimental autoimmune encephalomyelitis in vivo interact with heparan sulfates and glycoprotein 96 in APCs. J. Immunol. 191, 208–16.

Kohm, A.P., Carpentier, P.A., Anger, H.A., Miller, S.D., 2002. Cutting edge: CD4+CD25+ regulatory T cells suppress antigen-specific autoreactive immune responses and central nervous system inflammation during active experimental autoimmune encephalomyelitis. J. Immunol. 169, 4712–6.

Kolset, S.O., Tveit, H., 2008. Serglycin – Structure and biology. Cell. Mol. Life Sci. 65, 1073–1085.

Komiyama, Y., Nakae, S., Matsuki, T., Nambu, A., Ishigame, H., Kakuta, S., Sudo, K., Iwakura, Y., 2006. IL-17 plays an important role in the development of experimental autoimmune encephalomyelitis. J. Immunol. 177, 566–573.

Korporal, M., Haas, J., Balint, B., Fritzsching, B., Schwarz, A., Moeller, S., Fritz, B., Suri-Payer, E., Wildemann, B., 2008. Interferon beta-induced restoration of regulatory T-cell function in multiple sclerosis is prompted by an increase in newly generated naive regulatory T cells. Arch. Neurol. 65, 1434–9.

Kotter, M.R., Li, W.-W., Zhao, C., Franklin, R.J.M., 2006. Myelin Impairs CNS Remyelination by Inhibiting Oligodendrocyte Precursor Cell Differentiation. J. Neurosci. 26, 328–332.

Kotter, M.R., Setzu, A., Sim, F.J., Van Rooijen, N., Franklin, R.J., 2001. Macrophage depletion impairs oligodendrocyte remyelination following lysolecithin-induced demyelination. Glia 35, 204–12.

Kotter, M.R., Zhao, C., Van Rooijen, N., Franklin, R.J.M., 2005. Macrophage-depletion induced impairment of experimental CNS remyelination is associated with a reduced oligodendrocyte progenitor cell response and altered growth factor expression. Neurobiol. Dis. 18, 166–175.

Koutrolos, M., Berer, K., Kawakami, N., Wekerle, H., Krishnamoorthy, G., 2014. Treg cells mediate recovery from EAE by controlling effector T cell proliferation and motility in the CNS. Acta Neuropathol. Commun. 2, 163.

Kuhlmann, T., Lingfeld, G., Bitsch, A., Schuchardt, J., Brück, W., 2002. Acute axonal damage in multiple sclerosis is most extensive in early disease stages and decreases over time. Brain 125, 2202–2212.

Kuhlmann, T., Ludwin, S., Prat, A., Antel, J., Brück, W., Lassmann, H., 2017. An updated histological classification system for multiple sclerosis lesions. Acta Neuropathol. 133, 13–24.

Kutzelnigg, A., Lucchinetti, C.F., Stadelmann, C., Brück, W., Rauschka, H., Bergmann, M., Schmidbauer, M., Parisi, J.E., Lassmann, H., 2005. Cortical demyelination and diffuse white matter injury in multiple sclerosis. Brain 128, 2705–12.

Kvistad, S.S., Myhr, K.-M., Holmøy, T., Šaltytė Benth, J., Wergeland, S., Beiske, A.G., Bjerve, K.S., Hovdal, H., Lilleås, F., Midgard, R., Pedersen, T., Bakke, S.J., Michelsen, A.E., Aukrust, P., Ueland, T., Sagen, J. V, Torkildsen, Ø., 2015. Body mass index influence interferon-beta treatment response in multiple sclerosis. J. Neuroimmunol. 288, 92–7.

Lampron, A., Larochelle, A., Laflamme, N., Préfontaine, P., Plante, M.-M., Sánchez, M.G., Yong, V.W., Stys, P.K., Tremblay, M.-È., Rivest, S., 2015. Inefficient clearance of myelin debris by microglia impairs remyelinating processes. J. Exp. Med. 212, 481–95.

Lander, C., Zhang, H., Hockfield, S., 1998. Neurons produce a neuronal cell surface-associated chondroitin sulfate proteoglycan. J. Neurosci. 18, 174–83.

Lang, H.L.E., Jacobsen, H., Ikemizu, S., Andersson, C., Harlos, K., Madsen, L., Hjorth, P., Sondergaard, L., Svejgaard, A., Wucherpfennig, K., Stuart, D.I., Bell, J.I., Jones, E.Y., Fugger, L., 2002. A functional and structural basis for TCR cross-reactivity in multiple sclerosis. Nat. Immunol. 3, 940–3.

Larsen, P.H., Wells, J.E., Stallcup, W.B., Opdenakker, G., Yong, V.W., 2003. Matrix metalloproteinase-9 facilitates remyelination in part by processing the inhibitory NG2 proteoglycan. J. Neurosci. 23, 11127–35.

Laskin, J.D., Dokidis, A., Gardner, C.R., Laskin, D.L., 1991. Changes in sulfated proteoglycan production after activation of rat liver macrophages. Hepatology 14, 306–12.

Lassmann, H., 2011. Review: The architecture of inflammatory demyelinating lesions: Implications for studies on pathogenesis. Neuropathol. Appl. Neurobiol. 37, 698–710.

Lassmann, H., Bradl, M., 2017. Multiple sclerosis: experimental models and reality. Acta Neuropathol. 133, 223–244.

Lassmann, H., Brück, W., Lucchinetti, C., Parisi, J., Scheithauer, B., Rodriguez, M., 2001. Heterogeneity of multiple sclerosis pathogenesis: implications for diagnosis and therapy. Trends Mol. Med. 7, 115–21.

Lassmann, H., van Horssen, J., Mahad, D., 2012. Progressive multiple sclerosis: pathology and pathogenesis. Nat. Rev. Neurol. 8, 647–656.

Lau, L.W., Cua, R., Keough, M.B., Haylock-Jacobs, S., Yong, V.W., 2013. Pathophysiology of the brain extracellular matrix: a new target for remyelination. Nat. Rev. Neurosci. 14, 722–9.

Lau, L.W., Keough, M.B., Haylock-Jacobs, S., Cua, R., Döring, A., Sloka, S., Stirling, D.P., Rivest, S., Yong, V.W., 2012. Chondroitin sulfate proteoglycans in demyelinated lesions impair remyelination. Ann. Neurol. 72, 419–32.

Levitt, D., Ho, P.L., 1983. Induction of chondroitin sulfate proteoglycan synthesis and secretion in lymphocytes and monocytes. J. Cell Biol. 97, 351–8.

Li, R., Rezk, A., Miyazaki, Y., Hilgenberg, E., Touil, H., Shen, P., Moore, C.S., Michel, L., Althekair, F., Rajasekharan, S., Gommerman, J.L., Prat, A., Fillatreau, S., Bar-Or, A., Canadian B cells in MS Team, 2015. Proinflammatory GM-CSF-producing B cells in multiple sclerosis and B cell depletion therapy. Sci. Transl. Med. 7, 310ra166.

Li, X., Sui, C., Chen, Q., Chen, X., Zhang, H., Zhou, X., 2013. Promotion of autophagy at the maturation step by IL-6 is associated with the sustained mitogen-activated protein kinase/extracellular signal-regulated kinase activity. Mol. Cell. Biochem. 380, 219–227.

Link, H., Huang, Y.-M., 2006. Oligoclonal bands in multiple sclerosis cerebrospinal fluid: An update on methodology and clinical usefulness. J. Neuroimmunol. 180, 17–28.

Liu, J., Johnson, T. V, Lin, J., Ramirez, S.H., Bronich, T.K., Caplan, S., Persidsky, Y., Gendelman, H.E., Kipnis, J., 2007. T cell independent mechanism for copolymer-1-induced neuroprotection. Eur. J. Immunol. 37, 3143–54.

Liu, Q., Sanai, N., Jin, W.-N., La Cava, A., Van Kaer, L., Shi, F.-D., 2016. Neural stem cells sustain natural killer cells that dictate recovery from brain inflammation. Nat. Neurosci. 19, 243–252.

Livak, K.J., Schmittgen, T.D., 2001. Analysis of relative gene expression data using real-time quantitative PCR and the 2(-Delta Delta C(T)) Method. Methods 25, 402–8.

Lopez-Castejon, G., Brough, D., 2011. Understanding the mechanism of IL-1β secretion. Cytokine Growth Factor Rev. 22, 189–95.

Lortat-Jacob, H., Grosdidier, A., Imberty, A., 2002. Structural diversity of heparan sulfate binding domains in chemokines. PNAS 99, 1229–34.

Lublin, F.D., Reingold, S.C., Cohen, J.A., Cutter, G.R., Sørensen, P.S., Thompson, A.J., Wolinsky, J.S., Balcer, L.J., Banwell, B., Barkhof, F., Bebo, B., Calabresi, P.A., Clanet, M., Comi, G., Fox, R.J., Freedman, M.S., Goodman, A.D., Inglese, M., Kappos, L., Kieseier, B.C., Lincoln, J.A., Lubetzki, C., Miller, A.E., Montalban, X., O'Connor, P.W., Petkau, J., Pozzilli, C., Rudick, R.A., Sormani, M.P., Stüve, O., Waubant, E., Polman, C.H., Polman, C.H., 2014. Defining the clinical course of multiple sclerosis: the 2013 revisions. Neurology 83, 278–86.

Lucchinetti, C., Brück, W., Parisi, J., Scheithauer, B., Rodriguez, M., Lassmann, H., 2000. Heterogeneity of multiple sclerosis lesions: implications for the pathogenesis of demyelination. Ann. Neurol. 47, 707–17.

Lucchinetti, C.F., Brück, W., Rodriguez, M., Lassmann, H., 1996. Distinct patterns of multiple sclerosis pathology indicates heterogeneity on pathogenesis. Brain Pathol. 6, 259–74.

Ludwin, S.K., 2006. The pathogenesis of multiple sclerosis: relating human pathology to experimental studies. J. Neuropathol. Exp. Neurol. 65, 305–18.

Ludwin, S.K., 1978. Central nervous system demyelination and remyelination in the mouse: an ultrastructural study of cuprizone toxicity. Lab. Investig. 39, 597–612.

MacMicking, J., Xie, Q., Nathan, C., 1997. Nitric Oxide and Macrophage Function. Annu. Rev. Immunol. 15, 323–350.

MacMillan, C.J., Doucette, C.D., Warford, J., Furlong, S.J., Hoskin, D.W., Easton, A.S., 2014. Murine Experimental Autoimmune Encephalomyelitis Is Diminished by Treatment with the Angiogenesis Inhibitors B20-4.1.1 and Angiostatin (K1-3). PLoS One 9, e89770.

MacMillan, C.J., Furlong, S.J., Doucette, C.D., Chen, P.-L., Hoskin, D.W., Easton, A.S., 2012. Bevacizumab Diminishes Experimental Autoimmune Encephalomyelitis by Inhibiting Spinal Cord Angiogenesis and Reducing Peripheral T-Cell Responses. J. Neuropathol. Exp. Neurol. 71, 983–999.

Madsen, P.M., Motti, D., Karmally, S., Szymkowski, D.E., Lambertsen, K.L., Bethea, J.R., Brambilla, R., 2016. Oligodendroglial TNFR2 Mediates Membrane TNF-Dependent Repair in Experimental Autoimmune Encephalomyelitis by Promoting Oligodendrocyte Differentiation and Remyelination. J. Neurosci. 36, 5128–5143.

Mahad, D., Ziabreva, I., Lassmann, H., Turnbull, D., 2008. Mitochondrial defects in acute multiple sclerosis lesions. Brain 131, 1722–35.

Manczak, M., Jiang, S., Orzechowska, B., Adamus, G., 2002. Crucial role of CCL3/MIP-1alpha in the recurrence of autoimmune anterior uveitis induced with myelin basic protein in Lewis rats. J. Autoimmun. 18, 259–70.

Manouchehrinia, A., Tench, C.R., Maxted, J., Bibani, R.H., Britton, J., Constantinescu, C.S., 2013. Tobacco smoking and disability progression in multiple sclerosis: United Kingdom cohort study. Brain 136, 2298–2304.

Martinez, F.O., Gordon, S., 2014. The M1 and M2 paradigm of macrophage activation: time for reassessment. F1000Prime Rep. 6, 13.

Mason, J.L., Suzuki, K., Chaplin, D.D., Matsushima, G.K., 2001. Interleukin-1beta promotes repair of the CNS. J. Neurosci. 21, 7046–52.

Massey, J.M., Amps, J., Viapiano, M.S., Matthews, R.T., Wagoner, M.R., Whitaker, C.M., Alilain, W., Yonkof, A.L., Khalyfa, A., Cooper, N.G.F., Silver, J., Onifer, S.M., 2008. Increased chondroitin sulfate proteoglycan expression in denervated brainstem targets following spinal cord injury creates a barrier to axonal regeneration overcome by chondroitinase ABC and neurotrophin-3. Exp. Neurol. 209, 426–445.

Masson, D., Peters, P.J., Geuze, H.J., Borst, J., Tschopp, J., 1990. Interaction of chondroitin sulfate with perforin and granzymes of cytolytic T-cells is dependent on pH. Biochemistry 29, 11229–35.

Mattner, F., Fischer, S., Guckes, S., Jin, S., Kaulen, H., Schmitt, E., Rüde, E., Germann, T., 1993. The interleukin-12 subunit p40 specifically inhibits effects of the interleukin-12 heterodimer. Eur. J. Immunol. 23, 2202–8.

McCarthy, D.P., Richards, M.H., Miller, S.D., 2012. Mouse models of multiple sclerosis: experimental autoimmune encephalomyelitis and Theiler's virus-induced demyelinating disease. Methods Mol. Biol. 900, 381–401.

McGeachy, M.J., Stephens, L.A., Anderton, S.M., 2005. Natural recovery and protection from autoimmune encephalomyelitis: contribution of CD4+CD25+ regulatory cells within the central nervous system. J. Immunol. 175, 3025–3032.

Mckeon, R.J., Höke, A., Silver, J., 1995. Injury-Induced Proteoglycans Inhibit the Potential for Laminin-Mediated Axon Growth on Astrocytic Scars. Exp. Neurol. 136, 32–43.

McKeon, R.J., Jurynec, M.J., Buck, C.R., 1999. The chondroitin sulfate proteoglycans neurocan and phosphacan are expressed by reactive astrocytes in the chronic CNS glial scar. J. Neurosci. 19, 10778–88.

Mei, F., Lehmann-Horn, K., Shen, Y.-A.A., Rankin, K.A., Stebbins, K.J., Lorrain, D.S., Pekarek, K., A Sagan, S., Xiao, L., Teuscher, C., von Büdingen, H.-C., Wess, J., Lawrence, J.J., Green, A.J., Fancy, S.P., Zamvil, S.S., Chan, J.R., 2016. Accelerated remyelination during inflammatory demyelination prevents axonal loss and improves functional recovery. Elife 5.

Merrill, J.E., 2009. In vitro and in vivo pharmacological models to assess demyelination and remyelination. Neuropsychopharmacology 34, 55–73.

Merrill, J.E., 1991. Effects of interleukin-1 and tumor necrosis factor-alpha on astrocytes, microglia, oligodendrocytes, and glial precursors in vitro. Dev. Neurosci. 13, 130–7.

Mestas, J., Hughes, C.C.W., 2004. Of Mice and Not Men: Differences between Mouse and Human Immunology. J. Immunol. 172, 2731–2738.

Mestas, J., Hughes, C.C.W., 2004. Of mice and not men: differences between mouse and human immunology. J. Immunol. 172, 2731–8.

Mi, S., Hu, B., Hahm, K., Luo, Y., Kam Hui, E.S., Yuan, Q., Wong, W.M., Wang, L., Su, H., Chu, T.-H., Guo, J., Zhang, W., So, K.-F., Pepinsky, B., Shao, Z., Graff, C., Garber, E., Jung, V., Wu, E.X., Wu, W., 2007. LINGO-1 antagonist promotes spinal cord remyelination and axonal integrity in MOG-induced experimental autoimmune encephalomyelitis. Nat. Med. 13, 1228–1233.

Mi, S., Miller, R.H., Tang, W., Lee, X., Hu, B., Wu, W., Zhang, Y., Shields, C.B., Zhang, Y., Miklasz, S., Shea, D., Mason, J., Franklin, R.J.M., Ji, B., Shao, Z., Chédotal, A., Bernard, F., Roulois, A., Xu, J., Jung, V., Pepinsky, B., 2009. Promotion of central nervous system remyelination by induced differentiation of oligodendrocyte precursor cells. Ann. Neurol. 65, 304–315.

Mia, S., Warnecke, A., Zhang, X.-M., Malmström, V., Harris, R.A., 2014. An optimized Protocol for Human M2 Macrophages using M-CSF and IL-4/IL-10/TGF-β Yields a Dominant Immunosuppressive Phenotype. Scand. J. Immunol. 79, 305–314.

Middleton, J., Patterson, A.M., Gardner, L., Schmutz, C., Ashton, B.A., 2002. Leukocyte extravasation: chemokine transport and presentation by the endothelium. Blood 100, 3853–3860.

Miller, A., Shapiro, S., Gershtein, R., Kinarty, A., Rawashdeh, H., Honigman, S., Lahat, N., 1998. Treatment of multiple sclerosis with Copolymer-1 (Copaxone®): implicating mechanisms of Th1 to Th2/Th3 immune-deviation. J. Neuroimmunol. 92, 113–121.

Miller, A.E., Wolinsky, J.S., Kappos, L., Comi, G., Freedman, M.S., Olsson, T.P., Bauer, D., Benamor, M., Truffinet, P., O'Connor, P.W., TOPIC Study Group, 2014. Oral teriflunomide for patients with a first clinical episode suggestive of multiple sclerosis (TOPIC): a randomised, double-blind, placebo-controlled, phase 3 trial. Lancet Neurol. 13, 977–986.

Miller, D., Weinshenker, B., Filippi, M., Banwell, B., Cohen, J., Freedman, M., Galetta, S., Hutchinson, M., Johnson, R., Kappos, L., Kira, J., Lublin, F., McFarland, H., Montalban, X., Panitch, H., Richert, J., Reingold, S., Polman, C., 2008. Differential diagnosis of suspected multiple sclerosis: a consensus approach. Mult. Scler. J. 14, 1157–1174.

Miller, S.D., Karpus, W.J., Davidson, T.S., 2007. Experimental autoimmune encephalomyelitis in the mouse. Curr. Protoc. Immunol. Chapter 15, Unit 15.1.

Miron, V.E., Boyd, A., Zhao, J.-W., Yuen, T.J., Ruckh, J.M., Shadrach, J.L., van Wijngaarden, P., Wagers, A.J., Williams, A., Franklin, R.J.M., Ffrench-Constant, C., 2013. M2 microglia and macrophages drive oligodendrocyte differentiation during CNS remyelination. Nat. Neurosci. 16, 1211–8.

Miyagishi, R., Kikuchi, S., Takayama, C., Inoue, Y., Tashiro, K., 1997. Identification of cell types producing RANTES, MIP-1 alpha and MIP-1 beta in rat experimental autoimmune encephalomyelitis by in situ hybridization. J. Neuroimmunol. 77, 17–26.

Miyamoto, K., Tanaka, N., Moriguchi, K., Ueno, R., Kadomatsu, K., Kitagawa, H., Kusunoki, S., 2014. Chondroitin 6-O-sulfate ameliorates experimental autoimmune encephalomyelitis. Glycobiology 24, 469–475.

Mokry, L.E., Ross, S., Ahmad, O.S., Forgetta, V., Smith, G.D., Leong, A., Greenwood, C.M.T., Thanassoulis, G., Richards, J.B., Ramagopalan, S., Sadovnick, A., Simpson, S., Blizzard, L., Otahal, P., Mei, I. Van der, Taylor, B., Hernán, M., Olek, M., Ascherio, A., Ebers, G., Munger, K., Zhang, S., O'Reilly, E., Hernan, M., Olek, M., Willett, W., Mowry, E., Krupp, L., Milazzo, M., Chabas, D., Strober, J., Belman, A., Mowry, E., Waubant, E., McCulloch, C., Okuda, D., Evangelista, A., Lincoln, R., Rosen, C., Adams, J., Bikle, D., Black, D., Demay, M., Manson, J., James, E., Dobson, R., Kuhle, J., Baker, D., Giovannoni, G., Ramagopalan, S., Burton, J., Kimball, S., Vieth, R., Bar-Or, A., Dosch, H.-M., Cheung, R., Kimball, S., Ursell, M., O'Connor, P., Vieth, R., Wright, S., Yadav, V., Bever, C., Bowen, J., Bowling, A., Weinstock-Guttman, B., Looker, A., Pfeiffer, C., Lacher, D., Schleicher, R., Picciano, M., Yetley, E., Yetley, E., Lawlor, D., Harbord, R., Sterne, J., Timpson, N., Davey, S.G., Voight, B., Peloso, G., Orho-Melander, M., Frikke-Schmidt, R., Barbalic, M., Jensen, M., Zacho, J., Tybjaerg-Hansen, A., Jensen, J., Grande, P., Sillesen, H., Nordestgaard, B., Cohen, J., Boerwinkle, E., Mosley, T., Hobbs, H., Wang, T., Zhang, F., Richards, J., Kestenbaum, B., Meurs, J. Van, Berry, D., Faye, L., Sun, L., Dimitromanolakis, A., Bull, S., Beecham, A., Patsopoulos, N., Xifara, D., Davis, M., Kemppinen, A., Polman, C., Reingold, S., Edan, G., Filippi, M., Hartung, H.-P., Kappos, L., McDonald, W., Compston, A., Edan, G., Goodkin, D., Hartung, H., Lublin, F., Poser, C., Paty, D., Scheinberg, L., McDonald, W., Davis, F., Ebers, G., Sawcer, S., Hellenthal, G., Pirinen, M., Spencer, C., Abecasis, G., Auton, A., Brooks, L., DePristo, M., Durbin, R., Handsaker, R., Davey, S.G., Hemani, G., Berry, D., Vimaleswaran, K., Whittaker, J., Hingorani, A., Hyppönen, E., Burgess, S., Butterworth, A., Thompson, S., Ehret, G., Munroe, P., Rice, K., Bochud, M., Johnson, A., Chasman, D., Dastani, Z., Hivert, M.-F., Timpson, N., Perry, J., Yuan, X., Scott, R., Patsopoulos, N., Evangelou, E., Ioannidis, J., Higgins, J., Thompson, S., Deeks, J., Altman, D., Higgins, J., Thompson, S., Dastani, Z., Li, R., Richards, B., Safadi, F., Thornton, P., Magiera, H., Hollis, B., Gentile, M., Haddad, J., Bikle, D., Siiteri, P., Ryzen, E., Haddad, J., Verboven, C., Rabijns, A., Maeyer, M. De, Baelen, H. Van, Bouillon, R., Ranter, C. De, Shinkyo, R., Sakaki, T., Kamakura, M., Ohta, M., Inouye, K., Kongsbak, M., Essen, M. von, Levring, T., Schjerling, P., Woetmann, A., Odum, N., Moon, M., Song, H., Hong, H., Nam, D., Cha, M.-Y., Oh, M., Rinaldi, A., Sanseverino, I., Purificato, C., Cortese, A., Mechelli, R., Francisci, S., Yang, M., Qin, Z., Zhu, Y., Li, Y., Qin, Y., Jing, Y., Browne, R., Weinstock-Guttman, B., Zivadinov, R., Horakova, D., Bodziak, M., Tamaño-Blanco, M., Willer, C., Schmidt, E., Sengupta, S., Peloso, G., Gustafsson, S., Kanoni, S., Luijn, M. Van, Kreft, K., Jongsma, M., Mes, S., Wierenga-Wolf, A., Meurs, M. van, Ramagopalan, S., Maugeri, N., Handunnetthi, L., Lincoln, M.,

Orton, S.-M., Dyment, D., O'Connell, K., Kelly, S., Kinsella, K., Jordan, S., Kenny, O., Murphy, D., Mokry, L., Ahmad, O., Forgetta, V., Thanassoulis, G., Richards, J., Smith, G., Ebrahim, S., Leong, A., Rehman, W., Dastani, Z., Greenwood, C., Timpson, N., Langsetmo, L., Ye, Z., Sharp, S., Burgess, S., Scott, R., Imamura, F., Consortium, I., Cooper, J., Smyth, D., Walker, N., Stevens, H., Burren, O., Wallace, C., Vimaleswaran, K., Cavadino, A., Berry, D., Jorde, R., Dieffenbach, A., Vimaleswaran, K., Berry, D., Lu, C., Tikkanen, E., Pilz, S., Hiraki, L., 2015. Vitamin D and Risk of Multiple Sclerosis: A Mendelian Randomization Study. PLOS Med. 12, e1001866.

Moransard, M., Dann, A., Staszewski, O., Fontana, A., Prinz, M., Suter, T., 2011. NG2 expressed by macrophages and oligodendrocyte precursor cells is dispensable in experimental autoimmune encephalomyelitis. Brain 134, 1315–1330.

Morimoto-Tomita, M., Uchimura, K., Werb, Z., Hemmerich, S., Rosen, S.D., 2002. Cloning and Characterization of Two Extracellular Heparin-degrading Endosulfatases in Mice and Humans. J. Biol. Chem. 277, 49175–49185.

Mosmann, T., 1983. Rapid colorimetric assay for cellular growth and survival: application to proliferation and cytotoxicity assays. J. Immunol. Methods 65, 55–63.

Multiple Sclerosis International Federation, 2013. Atlas of MS 2013: Mapping Multiple Sclerosis Around The World [WWW Document]. URL https://www.msif.org/wp-content/uploads/2014/09/Atlas-of-MS.pdf (accessed 1.17.17).

Munger, K.L., Levin, L.I., Hollis, B.W., Howard, N.S., Ascherio, A., 2006. Serum 25-hydroxyvitamin D levels and risk of multiple sclerosis. JAMA 296, 2832–8.

Munger, K.L., Zhang, S.M., O'Reilly, E., Hernán, M.A., Olek, M.J., Willett, W.C., Ascherio, A., 2004. Vitamin D intake and incidence of multiple sclerosis. Neurology 62, 60–5.

Neumann, H., Medana, I.M., Bauer, J., Lassmann, H., 2002. Cytotoxic T lymphocytes in autoimmune and degenerative CNS diseases. Trends Neurosci. 25, 313–9.

Nie, J., Li, Y.Y., Zheng, S.G., Tsun, A., Li, B., 2015. FOXP3(+) Treg Cells and Gender Bias in Autoimmune Diseases. Front. Immunol. 6, 493.

Niino, M., Bodner, C., Simard, M., Alatab, S., Gano, D., Kim, H.J., Trigueiro, M., Racicot, D., Guérette, C., Antel, J.P., Fournier, A., Grand'Maison, F., Bar-Or, A., 2006. Natalizumab effects on immune cell responses in multiple sclerosis. Ann. Neurol. 59, 748–54.

Noronha, A., Toscas, A., Jensen, M.A., 1993. Interferon β decreases T cell activation and interferon γ production in multiple sclerosis. J. Neuroimmunol. 46, 145–153.

Noseworthy, J.H., Lucchinetti, C., Rodriguez, M., Weinshenker, B.G., 2000. Multiple sclerosis. N. Engl. J. Med. 343, 938–52.

O'Callaghan, P., Li, J.-P., Lannfelt, L., Lindahl, U., Zhang, X., 2015. Microglial Heparan Sulfate Proteoglycans Facilitate the Cluster-of-Differentiation 14 (CD14)/Toll-like Receptor 4 (TLR4)-Dependent Inflammatory Response. J. Biol. Chem. 290, 14904–14.

O'Connor, R.A., Malpass, K.H., Anderton, S.M., 2007. The inflamed central nervous system drives the activation and rapid proliferation of Foxp3+ regulatory T cells. J. Immunol. 179, 958–66.

O'Connor, R.A., Prendergast, C.T., Sabatos, C.A., Lau, C.W.Z., Leech, M.D., Wraith, D.C., Anderton, S.M., 2008. Cutting edge: Th1 cells facilitate the entry of Th17 cells to the central nervous system during experimental autoimmune encephalomyelitis. J. Immunol. 181, 3750–4.

Oravecz, T., Pall, M., Wang, J., Roderiquez, G., Ditto, M., Norcross, M.A., 1997. Regulation of anti-HIV-1 activity of RANTES by heparan sulfate proteoglycans. J. Immunol. 159, 4587–92.

Otto, M., Lewczuk, P., Wiltfang, J., 2008. Neurochemical approaches of cerebrospinal fluid diagnostics in neurodegenerative diseases. Methods 44, 289–98.

Ousman, S.S., David, S., 2001. MIP-1alpha, MCP-1, GM-CSF, and TNF-alpha control the immune cell response that mediates rapid phagocytosis of myelin from the adult mouse spinal cord. J. Neurosci. 21, 4649–56.

Patel, J.R., Klein, R.S., 2011. Mediators of oligodendrocyte differentiation during remyelination. FEBS Lett. 585, 3730–7.

Patrikios, P., Stadelmann, C., Kutzelnigg, A., Rauschka, H., Schmidbauer, M., Laursen, H., Sorensen, P.S., Brück, W., Lucchinetti, C., Lassmann, H., 2006. Remyelination is extensive in a subset of multiple sclerosis patients. Brain 129, 3165–72.

Pender, M.P., Burrows, S.R., 2014. Epstein–Barr virus and multiple sclerosis: potential opportunities for immunotherapy. Clin. Transl. Immunol. 3, e27.

Poiesi, C., De Francesco, M.A., Baronio, M., Manca, N., 2008. HIV-1 p17 binds heparan sulfate proteoglycans to activated CD4(+) T cells. Virus Res. 132, 25–32.

Polman, C.H., O'Connor, P.W., Havrdova, E., Hutchinson, M., Kappos, L., Miller, D.H., Phillips, J.T., Lublin, F.D., Giovannoni, G., Wajgt, A., Toal, M., Lynn, F., Panzara, M.A., Sandrock, A.W., 2006. A randomized, placebo-controlled trial of natalizumab for relapsing multiple sclerosis. N. Engl. J. Med. 354, 899–910.

Polman, C.H., Reingold, S.C., Banwell, B., Clanet, M., Cohen, J.A., Filippi, M., Fujihara, K., Havrdova, E., Hutchinson, M., Kappos, L., Lublin, F.D., Montalban, X., O'Connor, P., Sandberg-Wollheim, M., Thompson, A.J., Waubant, E., Weinshenker, B., Wolinsky, J.S., 2011. Diagnostic criteria for multiple sclerosis: 2010 revisions to the McDonald criteria. Ann. Neurol. 69, 292–302.

Ponath, G., Ramanan, S., Mubarak, M., Housley, W., Lee, S., Sahinkaya, F.R., Vortmeyer, A., Raine, C.S., Pitt, D., 2017. Myelin phagocytosis by astrocytes after myelin damage promotes lesion pathology. Brain 140, 399–413.

Prayoonwiwat, N., Rodriguez, M., 1993. The potential for oligodendrocyte proliferation during demyelinating disease. J. Neuropathol. Exp. Neurol. 52, 55–63.

Properzi, F., Lin, R., Kwok, J., Naidu, M., van Kuppevelt, T.H., Ten Dam, G.B., Camargo, L.M., Raha-Chowdhury, R., Furukawa, Y., Mikami, T., Sugahara, K., Fawcett, J.W., 2008. Heparan sulphate proteoglycans in glia and in the normal and injured CNS: expression of sulphotransferases and changes in sulphation. Eur. J. Neurosci. 27, 593–604.

Proudfoot, A.E.I., 2006. The biological relevance of chemokine-proteoglycan interactions. Biochem. Soc. Trans. 34, 422–6.

Ramanujam, R., Hedström, A.-K., Manouchehrinia, A., Alfredsson, L., Olsson, T., Bottai, M., Hillert, J., 2015. Effect of Smoking Cessation on Multiple Sclerosis Prognosis. JAMA Neurol. 72, 1117.

Ransohoff, R.M., Hafler, D.A., Lucchinetti, C.F., 2015. Multiple sclerosis—a quiet revolution. Nat. Rev. Neurol. 11, 134–142.

Rawji, K.S., Mishra, M.K., Yong, V.W., 2016. Regenerative Capacity of Macrophages for Remyelination. Front. Cell Dev. Biol. 4, 47-60.

Reichardt, L.F., Tomaselli, K.J., 1991. Extracellular Matrix Molecules and their Receptors: Functions in Neural Development. Annu. Rev. Neurosci. 14, 531–570.

Rempe, R.G., Hartz, A.M., Bauer, B., 2016. Matrix metalloproteinases in the brain and blood–brain barrier: Versatile breakers and makers. J. Cereb. Blood Flow Metab. 36, 1481–1507.

Roan, N.R., Sowinski, S., Münch, J., Kirchhoff, F., Greene, W.C., 2010. Aminoquinoline surfen inhibits the action of SEVI (semen-derived enhancer of viral infection). J. Biol. Chem. 285, 1861–9.

Rottlaender, A., Villwock, H., Addicks, K., Kuerten, S., 2011. Neuroprotective role of fibroblast growth factor-2 in experimental autoimmune encephalomyelitis. Immunology 133, 370–8.

Rovaris, M., Riccitelli, G., Judica, E., Possa, F., Caputo, D., Ghezzi, A., Bertolotto, A., Capra, R., Falautano, M., Mattioli, F., Martinelli, V., Comi, G., Filippi, M., 2008. Cognitive impairment and structural brain damage in benign multiple sclerosis. Neurology 71, 1521–6.

Rovira, À., Wattjes, M.P., Tintoré, M., Tur, C., Yousry, T.A., Sormani, M.P., De Stefano, N., Filippi, M., Auger, C., Rocca, M.A., Barkhof, F., Fazekas, F., Kappos, L., Polman, C., Miller, D., Montalban, X., group, on behalf of the M. study, 2015. Evidence-based guidelines: MAGNIMS consensus guidelines on the use of MRI in multiple sclerosis—clinical implementation in the diagnostic process. Nat. Rev. Neurol. 11, 471–482.

Sajad, M., Zargan, J., Chawla, R., Umar, S., Khan, H.A., 2011. Upregulation of CSPG3 Accompanies Neuronal Progenitor Proliferation and Migration in EAE. J. Mol. Neurosci. 43, 531–540.

Sarrazin, S., Lamanna, W.C., Esko, J.D., 2011. Heparan sulfate proteoglycans. Cold Spring Harb. Perspect. Biol. 3, 1–33.

Sasaki, M., Lankford, K.L., Brown, R.J., Ruddle, N.H., Kocsis, J.D., 2010. Focal experimental autoimmune encephalomyelitis in the Lewis rat induced by immunization with myelin oligodendrocyte glycoprotein and intraspinal injection of vascular endothelial growth factor. Glia 58, 1523–31.

Scalfari, A., Neuhaus, A., Daumer, M., Muraro, P.A., Ebers, G.C., 2014. Onset of secondary progressive phase and long-term evolution of multiple sclerosis. J. Neurol. Neurosurg. Psychiatry 85, 67–75.

Schneemann, M., Schoeden, G., 2007. Macrophage biology and immunology: man is not a mouse. J. Leukoc. Biol. 81, 579-80.

Schoenfeld, R., Wong, A., Silva, J., Li, M., Itoh, A., Horiuchi, M., Itoh, T., Pleasure, D., Cortopassi, G., 2010. Oligodendroglial differentiation induces mitochondrial genes and inhibition of mitochondrial function represses oligodendroglial differentiation. Mitochondrion 10, 143–50.

Schönrock, L.M., Gawlowski, G., Brück, W., 2000. Interleukin-6 expression in human multiple sclerosis lesions. Neurosci. Lett. 294, 45–8.

Schuksz, M., Fuster, M.M., Brown, J.R., Crawford, B.E., Ditto, D.P., Lawrence, R., Glass, C.A., Wang, L., Tor, Y., Esko, J.D., 2008. Surfen, a small molecule antagonist of heparan sulfate. PNAS 105, 13075–80.

Segal, B.M., Constantinescu, C.S., Raychaudhuri, A., Kim, L., Fidelus-Gort, R., Kasper, L.H., Ustekinumab MS Investigators, 2008. Repeated subcutaneous injections of IL12/23 p40 neutralising antibody, ustekinumab, in patients with relapsing-remitting multiple sclerosis: a phase II, double-blind, placebo-controlled, randomised, dose-ranging study. Lancet Neurol. 7, 796–804.

Selvaraj, R.K., Geiger, T.L., 2008. Mitigation of experimental allergic encephalomyelitis by TGF-beta induced Foxp3+ regulatory T lymphocytes through the induction of anergy and infectious tolerance. J. Immunol. 180, 2830–8.

Serafini, B., Rosicarelli, B., Magliozzi, R., Stigliano, E., Aloisi, F., 2004. Detection of Ectopic B-cell Follicles with Germinal Centers in the Meninges of Patients with Secondary Progressive Multiple Sclerosis. Brain Pathol. 14, 164–174.

Shao, C., Shi, X., White, M., Huang, Y., Hartshorn, K., Zaia, J., 2013. Comparative glycomics of leukocyte glycosaminoglycans. FEBS J. 280, 2447–61.

Shen, Y., 2014. Traffic lights for axon growth: proteoglycans and their neuronal receptors. Neural Regen. Res. 9, 356–61.

Siebert, J.R., Osterhout, D.J., 2011. The inhibitory effects of chondroitin sulfate proteoglycans on oligodendrocytes. J. Neurochem. 119, 176–188.

Simon Davis, D.A., Parish, C.R., 2013. Heparan sulfate: a ubiquitous glycosaminoglycan with multiple roles in immunity. Front. Immunol. 4, 470.

Simpson, J.., Newcombe, J., Cuzner, M.., Woodroofe, M.., 1998. Expression of monocyte chemoattractant protein-1 and other β-chemokines by resident glia and inflammatory cells in multiple sclerosis lesions. J. Neuroimmunol. 84, 238–249.

Simpson, J.E., Newcombe, J., Cuzner, M.L., Woodroofe, M.N., 1998. Expression of monocyte chemoattractant protein-1 and other beta-chemokines by resident glia and inflammatory cells in multiple sclerosis lesions. J. Neuroimmunol. 84, 238–49.

Simpson, S., Blizzard, L., Otahal, P., Van der Mei, I., Taylor, B., 2011. Latitude is significantly associated with the prevalence of multiple sclerosis: a meta-analysis. J. Neurol. Neurosurg. Psychiatry 82, 1132–1141.

Smolders, J., Peelen, E., Thewissen, M., Cohen Tervaert, J.W., Menheere, P., Hupperts, R., Damoiseaux, J., 2010. Safety and T Cell Modulating Effects of High Dose Vitamin D3 Supplementation in Multiple Sclerosis. PLoS One 5, e15235.

Sobel, R.A., Ahmed, A.S., 2001. White matter extracellular matrix chondroitin sulfate/dermatan sulfate proteoglycans in multiple sclerosis. J. Neuropathol. Exp. Neurol. 60, 1198–207.

Song, J., Wu, C., Korpos, E., Zhang, X., Agrawal, S.M., Wang, Y., Faber, C., Schäfers, M., Körner, H., Opdenakker, G., Hallmann, R., Sorokin, L., 2015. Focal MMP-2 and MMP-9 Activity at the Blood-Brain Barrier Promotes Chemokine-Induced Leukocyte Migration. Cell Rep. 10, 1040–1054.

Sotirchos, E.S., Bhargava, P., Eckstein, C., Van Haren, K., Baynes, M., Ntranos, A., Gocke, A., Steinman, L., Mowry, E.M., Calabresi, P.A., 2016. Safety and immunologic effects of high- vs low-dose cholecalciferol in multiple sclerosis. Neurology 86, 382–90.

Spaeny-Dekking, E.H., Kamp, A.M., Froelich, C.J., Hack, C.E., 2000. Extracellular granzyme A, complexed to proteoglycans, is protected against inactivation by protease inhibitors. Blood 95, 1465–72.

Steward, W.P., Christmas, S.E., Lyon, M., Gallagher, J.T., 1990. The synthesis of proteoglycans by human T lymphocytes. Biochim. Biophys. Acta 1052, 416–25.

Tanaka, A., Jinno-Oue, A., Shimizu, N., Hoque, A., Mori, T., Islam, S., Nakatani, Y., Shinagawa, M., Hoshino, H., 2012. Entry of human T-cell leukemia virus type 1 is augmented by heparin sulfate proteoglycans bearing short heparin-like structures. J. Virol. 86, 2959–69.

Tanuma, N., Sakuma, H., Sasaki, A., Matsumoto, Y., 2006. Chemokine expression by astrocytes plays a role in microglia/macrophage activation and subsequent neurodegeneration in secondary progressive multiple sclerosis. Acta Neuropathol. 112, 195–204.

Taylor, S., Wakem, M., Dijkman, G., Alsarraj, M., Nguyen, M., 2010. A practical approach to RT-qPCR-Publishing data that conform to the MIQE guidelines. Methods 50, S1-5.

Tedeholm, H., Skoog, B., Lisovskaja, V., Runmarker, B., Nerman, O., Andersen, O., 2015. The outcome spectrum of multiple sclerosis: disability, mortality, and a cluster of predictors from onset. J. Neurol. 262, 1148–1163.

Teixé, T., Nieto-Blanco, P., Vilella, R., Engel, P., Reina, M., Espel, E., 2008. Syndecan-2 and -4 expressed on activated primary human CD4+ lymphocytes can regulate T cell activation. Mol. Immunol. 45, 2905–19.

Tettey, P., Siejka, D., Simpson Jr, S., Taylor, B., Blizzard, L., Ponsonby, A.-L., Dwyer, T., van der Mei, I., 2016. Frequency of Comorbidities and Their Association with Clinical Disability and Relapse in Multiple Sclerosis. Neuroepidemiology 46, 106–113.

The Canadian Burden of Illness Study Group, 1998. Burden of illness of multiple sclerosis: Part I: Cost of illness. The Canadian Burden of Illness Study Group. Can. J. Neurol. Sci. 25, 23–30.

Torrent, M., Nogués, M.V., Andreu, D., Boix, E., 2012. The “CPC Clip Motif”: A Conserved Structural Signature for Heparin-Binding Proteins. PLoS One 7, e42692.

Trapp, B.D., Peterson, J., Ransohoff, R.M., Rudick, R., Mörk, S., Bö, L., 1998. Axonal transection in the lesions of multiple sclerosis. N. Engl. J. Med. 338, 278–85.

Trojano, M., Paolicelli, D., Bellacosa, A., Cataldo, S., 2003. The transition from relapsing-remitting MS to irreversible disability: clinical evaluation. Neurol. Sci. 24, s268–s270.

Uhlin-Hansen, L., Wik, T., Kjellén, L., Berg, E., Forsdahl, F., Kolset, S.O., 1993. Proteoglycan metabolism in normal and inflammatory human macrophages. Blood 82, 2880–9.

Uhm, J.H., Dooley, N.P., Oh, L.Y., Yong, V.W., 1998. Oligodendrocytes utilize a matrix metalloproteinase, MMP-9, to extend processes along an astrocyte extracellular matrix. Glia 22, 53–63.

Umber, F., Störring, F.K., Föllmer, W., 1938. Erfolge mit Einem Neuartigen Depotinsulin Ohne Protaminzusatz (Surfen-Insulin). Klin. Wochenschr. 17, 443–446.

Vainchtein, I.D., Vinet, J., Brouwer, N., Brendecke, S., Biagini, G., Biber, K., Boddeke, H.W.G.M., Eggen, B.J.L., 2014. In acute experimental autoimmune encephalomyelitis, infiltrating macrophages are immune activated, whereas microglia remain immune suppressed. Glia 62(10), 1724-35..

Valentin-Torres, A., Savarin, C., Hinton, D.R., Phares, T.W., Bergmann, C.C., Stohlman, S.A., 2016. Sustained TNF production by central nervous system infiltrating macrophages promotes progressive autoimmune encephalomyelitis. J. Neuroinflammation 13, 46-52.

van Horssen, J., Bö, L., Dijkstra, C.D., de Vries, H.E., 2006. Extensive extracellular matrix depositions in active multiple sclerosis lesions. Neurobiol. Dis. 24, 484–91.

Vanpouille, C., Deligny, A., Delehedde, M., Denys, A., Melchior, A., Liénard, X., Lyon, M., Mazurier, J., Fernig, D.G., Allain, F., 2007. The heparin/heparan sulfate sequence that interacts with cyclophilin B contains a 3-O-sulfated N-unsubstituted glucosamine residue. J. Biol. Chem. 282, 24416–29.

Veugelers, K., Motyka, B., Goping, I.S., Shostak, I., Sawchuk, T., Bleackley, R.C., 2006. Granule-mediated killing by granzyme B and perforin requires a mannose 6-phosphate receptor and is augmented by cell surface heparan sulfate. Mol. Biol. Cell 17, 623–33.

Viglietta, V., Baecher-Allan, C., Weiner, H.L., Hafler, D.A., 2004. Loss of Functional Suppression by CD4+CD25+ Regulatory T Cells in Patients with Multiple Sclerosis. J. Exp. Med. 199.

Vogel, D.Y., Vereyken, E.J., Glim, J.E., Heijnen, P.D., Moeton, M., van der Valk, P., Amor, S., Teunissen, C.E., van Horssen, J., Dijkstra, C.D., 2013. Macrophages in inflammatory multiple sclerosis lesions have an intermediate activation status. J. Neuroinflammation 10, 35-47.

Wandinger, K., Jabs, W., Siekhaus, A., Bubel, S., Trillenberg, P., Wagner, H., Wessel, K., Kirchner, H., Hennig, H., 2000. Association between clinical disease activity and Epstein-Barr virus reactivation in MS. Neurology 55, 178–84.

Wang, L., Fuster, M., Sriramarao, P., Esko, J.D., 2005. Endothelial heparan sulfate deficiency impairs L-selectin- and chemokine-mediated neutrophil trafficking during inflammatory responses. Nat. Immunol. 6, 902–910.

Wanidworanun, C., Strober, W., 1993. Predominant role of tumor necrosis factor-alpha in human monocyte IL-10 synthesis. J. Immunol. 151, 6853–61.

Warren, H.S., Fitting, C., Hoff, E., Adib-Conquy, M., Beasley-Topliffe, L., Tesini, B., Liang, X., Valentine, C., Hellman, J., Hayden, D., Cavaillon, J., 2010. Resilience to Bacterial Infection: Difference between Species Could Be Due to Proteins in Serum. J. Infect. Dis. 201, 223–232.

Watson, K., Gooderham, N.J., Davies, D.S., Edwards, R.J., 1999. Nucleosomes bind to cell surface proteoglycans. J. Biol. Chem. 274, 21707–13.

Weaver, A., Goncalves da Silva, A., Nuttall, R.K., Edwards, D.R., Shapiro, S.D., Rivest, S., Yong, V.W., 2005. An elevated matrix metalloproteinase (MMP) in an animal model of multiple sclerosis is protective by affecting Th1/Th2 polarization. FASEB J. 19, 1668–70.

Wegrowski, Y., Milard, A.-L., Kotlarz, G., Toulmonde, E., Maquart, F.-X., Bernard, J., 2006. Cell surface proteoglycan expression during maturation of human monocytes-derived dendritic cells and macrophages. Clin. Exp. Immunol. 144, 485–93.

Willer, C.J., Dyment, D.A., Risch, N.J., Sadovnick, A.D., Ebers, G.C., Canadian Collaborative Study Group, T.C.C.S., 2003. Twin concordance and sibling recurrence rates in multiple sclerosis. PNAS 100, 12877–82.

Williamson, J., Rollo, I.M., 1959. Drug resistance in trapanososmes: cross-resitance analyses. Br. J. Pharmacol. Chemother. 14, 423–30.

Wingerchuk, D.M., Carter, J.L., 2014. Multiple sclerosis: current and emerging disease-modifying therapies and treatment strategies. Mayo Clin. Proc. 89, 225–40.

Winkler, S., Stahl, R.C., Carey, D.J., Bansal, R., 2002. Syndecan-3 and perlecan are differentially expressed by progenitors and mature oligodendrocytes and accumulate in the extracellular matrix. J. Neurosci. Res. 69, 477–487.

Wolinsky, J.S., Narayana, P.A., O'Connor, P., Coyle, P.K., Ford, C., Johnson, K., Miller, A., Pardo, L., Kadosh, S., Ladkani, D., 2007. Glatiramer acetate in primary progressive multiple sclerosis: results of a multinational, multicenter, double-blind, placebo-controlled trial. Ann. Neurol. 61, 14–24.

Woodruff, R.H., Franklin, R.J., 1999. Demyelination and remyelination of the caudal cerebellar peduncle of adult rats following stereotaxic injections of lysolecithin, ethidium bromide, and complement/anti-galactocerebroside: a comparative study. Glia 25, 216–28.

Woulfe, J.M., Gray, M.T., Gray, D.A., Munoz, D.G., Middeldorp, J.M., 2014. Hypothesis: a role for EBV-induced molecular mimicry in Parkinson's disease. Park. Relat. Disord. 20, 685–94.

Wrenshall, L.E., Stevens, R.B., Cerra, F.B., Platt, J.L., 1999. Modulation of macrophage and B cell function by glycosaminoglycans. J. Leukoc. Biol. 66, 391–400.

Xu, D., Esko, J.D., 2014. Demystifying Heparan Sulfate–Protein Interactions. Annu. Rev. Biochem. 83, 129–157.

Xu, D., Fuster, M.M., Lawrence, R., Esko, J.D., 2011. Heparan Sulfate Regulates VEGF165- and VEGF121-mediated Vascular Hyperpermeability. J. Biol. Chem. 286, 737–745.

Yamasaki, R., Lu, H., Butovsky, O., Ohno, N., Rietsch, A.M., Cialic, R., Wu, P.M., Doykan, C.E., Lin, J., Cotleur, A.C., Kidd, G., Zorlu, M.M., Sun, N., Hu, W., Liu, L., Lee, J.-C., Taylor, S.E., Uehlein, L., Dixon, D., Gu, J., Floruta, C.M., Zhu, M., Charo, I.F., Weiner, H.L., Ransohoff, R.M., 2014. Differential roles of microglia and monocytes in the inflamed central nervous system. J. Exp. Med. 211, 1533–49.

Yao, Y., Li, W., Kaplan, M.H., Chang, C.-H., 2005. Interleukin (IL)-4 inhibits IL-10 to promote IL-12 production by dendritic cells. J. Exp. Med. 201, 1899–903.

Yong, V.W., Power, C., Forsyth, P., Edwards, D.R., 2001. Metalloproteinases in biology and pathology of the nervous system. Nat. Rev. Neurosci. 2, 502–511.

Yong, V.W., Zabad, R.K., Agrawal, S., Goncalves DaSilva, A., Metz, L.M., 2007. Elevation of matrix metalloproteinases (MMPs) in multiple sclerosis and impact of immunomodulators. J. Neurol. Sci. 259, 79–84.

Yoshinaga, S.K., Whoriskey, J.S., Khare, S.D., Sarmiento, U., Guo, J., Horan, T., Shih, G., Zhang, M., Coccia, M.A., Kohno, T., Tafuri-Bladt, A., Brankow, D., Campbell, P., Chang, D., Chiu, L., Dai, T., Duncan, G., Elliott, G.S., Hui, A., McCabe, S.M., Scully, S., Shahinian, A., Shaklee, C.L., Van, G., Mak, T.W., Senaldi, G., 1999. T-cell co-stimulation through B7RP-1 and ICOS. Nature 402, 827–832.

Zhang, X., Koldzic, D.N., Izikson, L., Reddy, J., Nazareno, R.F., Sakaguchi, S., Kuchroo, V.K., Weiner, H.L., 2004. IL-10 is involved in the suppression of experimental autoimmune encephalomyelitis by CD25+CD4+ regulatory T cells. Int. Immunol. 16, 249–56.

Zhang, X., Reddy, J., Ochi, H., Frenkel, D., Kuchroo, V.K., Weiner, H.L., 2006. Recovery from experimental allergic encephalomyelitis is TGF- dependent and associated with increases in CD4+LAP+ and CD4+CD25+ T cells. Int. Immunol. 18, 495–503.

Zhang, X., Wang, B., O'Callaghan, P., Hjertström, E., Jia, J., Gong, F., Zcharia, E., Nilsson, L.N.G., Lannfelt, L., Vlodavsky, I., Lindahl, U., Li, J.-P., 2012. Heparanase overexpression impairs inflammatory response and macrophage-mediated clearance of amyloid-β in murine brain. Acta Neuropathol. 124, 465–78.

Zhang, X., Wu, C., Song, J., Götte, M., Sorokin, L., 2013. Syndecan-1, a cell surface proteoglycan, negatively regulates initial leukocyte recruitment to the brain across the choroid plexus in murine experimental autoimmune encephalomyelitis. J. Immunol. 191, 4551–61.

Zhou, J., Nagarkatti, P., Zhong, Y., Nagarkatti, M., 2010. Immune modulation by chondroitin sulfate and its degraded disaccharide product in the development of an experimental model of multiple sclerosis. J. Neuroimmunol. 223, 55–64.

Ziabreva, I., Campbell, G., Rist, J., Zambonin, J., Rorbach, J., Wydro, M.M., Lassmann, H., Franklin, R.J.M., Mahad, D., 2010. Injury and differentiation following inhibition of mitochondrial respiratory chain complex IV in rat oligodendrocytes. Glia 58, 1827–37.

Zivadinov, R., Cookfair, D.L., Krupp, L., Miller, A.E., Lava, N., Coyle, P.K., Goodman, A.D., Jubelt, B., Lenihan, M., Herbert, J., Gottesman, M., Snyder, D.H., Apatoff, B.R., Teter, B.E., Perel, A.B., Munschauer, F., Weinstock-Guttman, B., 2016. Factors associated with benign multiple sclerosis in the New York State MS Consortium (NYSMSC). BMC Neurol. 16, 102-12.

APPENDIX 1: SUPPLEMENTARY FIGURES

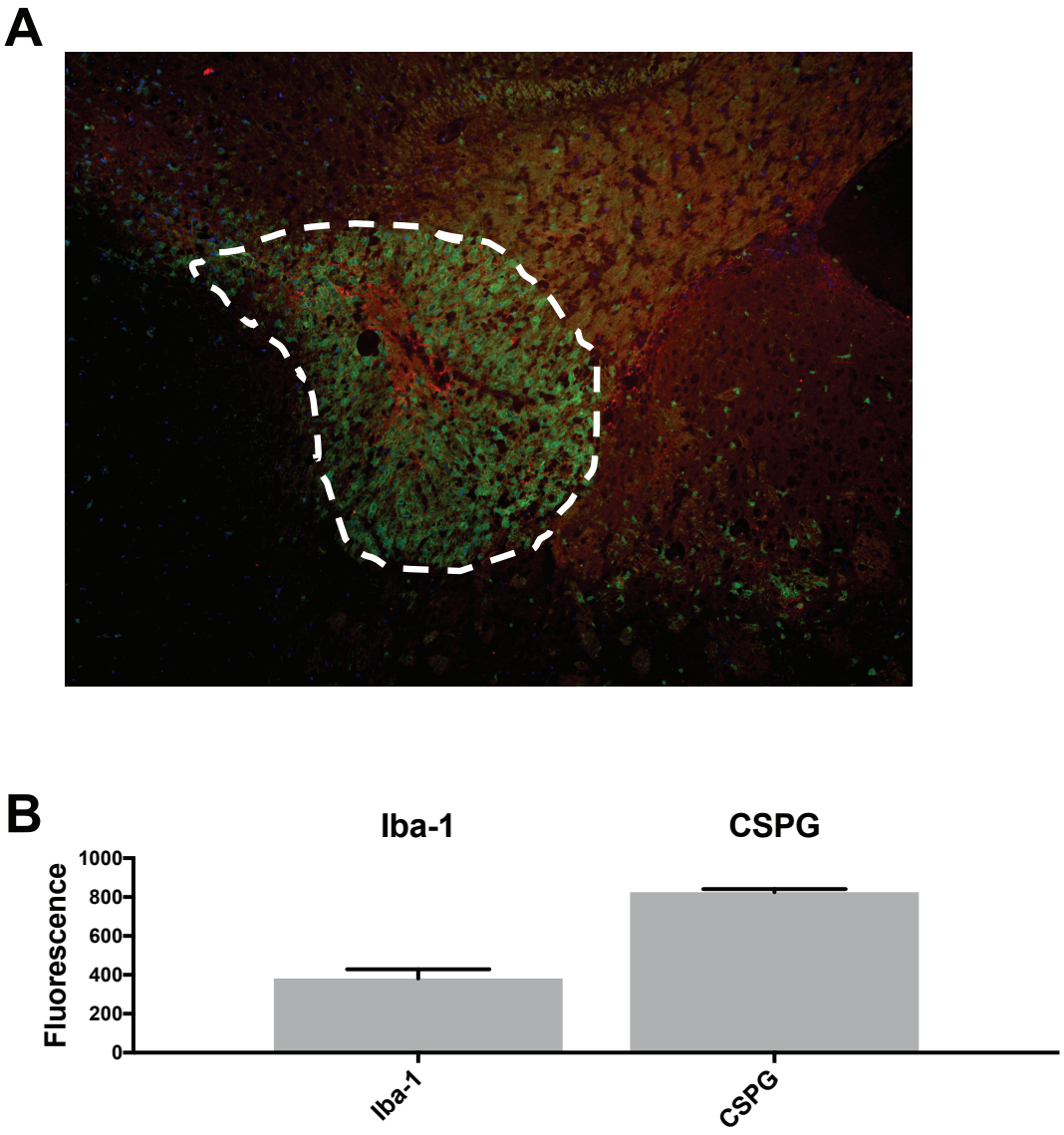

Appendix Figure 1: Iba-1 and CSPG expression at day 7 following mechanical damage into the corpus callosum two days following LPC injection. On day 0, female C57BL/6 mice received a 1 μL bilateral injection of 1% lysolecithin (lysophosphatidylcholine) into each side of the corpus callosum. A sham procedure involving the insertion of the neddle without injection of treatment was performed 48 h later as a control. Mice were sacrificed on day 7 and tissues processed for immunohistochemistry. **(A)** Representative photomicropgrah from a sham control animal. LPC lesion is outlined in white. **(B)** Fluorescent intensity was quantified per lesion area for both Iba-1 and CSPG.

APPENDIX 2: COPYRIGHT PERMISSION

ELSEVIER LICENSE
TERMS AND CONDITIONS

Feb 23, 2017

This Agreement between Jordan R Warford ("You") and Elsevier ("Elsevier") consists of your license details and the terms and conditions provided by Elsevier and Copyright Clearance Center.

License Number	4054841341490
License date	Feb 23, 2017
Licensed Content Publisher	Elsevier
Licensed Content Publication	Biochemical and Biophysical Research Communications
Licensed Content Title	Murine T cell activation is regulated by surfen (bis-2-methyl-4-amino-quinolyl-6-carbamide)
Licensed Content Author	Jordan Warford,Carolyn D. Doucette,David W. Hoskin,Alexander S. Easton
Licensed Content Date	10 January 2014
Licensed Content Volume	443
Licensed Content Issue	2
Licensed Content Pages	7
Start Page	524
End Page	530
Type of Use	reuse in a thesis/dissertation
Portion	full article
Format	both print and electronic
Are you the author of this Elsevier article?	Yes
Will you be translating?	No
Order reference number	
Title of your thesis/dissertation	The effects of the proteoglycan antagonist surfen on animal models of demyelination with comparison to in vitro T cell and macrophage responses
Expected completion date	Mar 2017
Estimated size (number of pages)	200
Elsevier VAT number	GB 494 6272 12
Requestor Location	Jordan R Warford 5552 Duffus St. Halifax, NS B3K2M4 Canada Attn: Jordan R Warford
Total	0.00 USD
Terms and Conditions	

INTRODUCTION

1. The publisher for this copyrighted material is Elsevier. By clicking "accept" in connection with completing this licensing transaction, you agree that the following terms and conditions apply to this transaction (along with the Billing and Payment terms and conditions established by Copyright Clearance Center, Inc. ("CCC"), at the time that you opened your Rightslink account and that are available at any time at http://myaccount.copyright.com).

GENERAL TERMS

2. Elsevier hereby grants you permission to reproduce the aforementioned material subject to the terms and conditions indicated.

3. Acknowledgement: If any part of the material to be used (for example, figures) has appeared in our publication with credit or acknowledgement to another source, permission must also be sought from that source. If such permission is not obtained then that material may not be included in your publication/copies. Suitable acknowledgement to the source must be made, either as a footnote or in a reference list at the end of your publication, as follows:

"Reprinted from Publication title, Vol /edition number, Author(s), Title of article / title of chapter, Pages No., Copyright (Year), with permission from Elsevier [OR APPLICABLE SOCIETY COPYRIGHT OWNER]." Also Lancet special credit - "Reprinted from The Lancet, Vol. number, Author(s), Title of article, Pages No., Copyright (Year), with permission from Elsevier."

4. Reproduction of this material is confined to the purpose and/or media for which permission is hereby given.

5. Altering/Modifying Material: Not Permitted. However figures and illustrations may be altered/adapted minimally to serve your work. Any other abbreviations, additions, deletions and/or any other alterations shall be made only with prior written authorization of Elsevier Ltd. (Please contact Elsevier at permissions@elsevier.com). No modifications can be made to any Lancet figures/tables and they must be reproduced in full.

6. If the permission fee for the requested use of our material is waived in this instance, please be advised that your future requests for Elsevier materials may attract a fee.

7. Reservation of Rights: Publisher reserves all rights not specifically granted in the combination of (i) the license details provided by you and accepted in the course of this licensing transaction, (ii) these terms and conditions and (iii) CCC's Billing and Payment terms and conditions.

8. License Contingent Upon Payment: While you may exercise the rights licensed immediately upon issuance of the license at the end of the licensing process for the transaction, provided that you have disclosed complete and accurate details of your proposed use, no license is finally effective unless and until full payment is received from you (either by publisher or by CCC) as provided in CCC's Billing and Payment terms and conditions. If full payment is not received on a timely basis, then any license preliminarily granted shall be deemed automatically revoked and shall be void as if never granted. Further, in the event that you breach any of these terms and conditions or any of CCC's Billing and Payment terms and conditions, the license is automatically revoked and shall be void as if never granted. Use of materials as described in a revoked license, as well as any use of the materials beyond the scope of an unrevoked license, may constitute copyright infringement and publisher reserves the right to take any and all action to protect its copyright in the materials.

9. Warranties: Publisher makes no representations or warranties with respect to the licensed material.

10. Indemnity: You hereby indemnify and agree to hold harmless publisher and CCC, and their respective officers, directors, employees and agents, from and against any and all claims arising out of your use of the licensed material other than as specifically authorized pursuant to this license.

11. No Transfer of License: This license is personal to you and may not be sublicensed, assigned, or transferred by you to any other person without publisher's written permission.

12. No Amendment Except in Writing: This license may not be amended except in a writing signed by both parties (or, in the case of publisher, by CCC on publisher's behalf).
13. Objection to Contrary Terms: Publisher hereby objects to any terms contained in any purchase order, acknowledgment, check endorsement or other writing prepared by you, which terms are inconsistent with these terms and conditions or CCC's Billing and Payment terms and conditions. These terms and conditions, together with CCC's Billing and Payment terms and conditions (which are incorporated herein), comprise the entire agreement between you and publisher (and CCC) concerning this licensing transaction. In the event of any conflict between your obligations established by these terms and conditions and those established by CCC's Billing and Payment terms and conditions, these terms and conditions shall control.
14. Revocation: Elsevier or Copyright Clearance Center may deny the permissions described in this License at their sole discretion, for any reason or no reason, with a full refund payable to you. Notice of such denial will be made using the contact information provided by you. Failure to receive such notice will not alter or invalidate the denial. In no event will Elsevier or Copyright Clearance Center be responsible or liable for any costs, expenses or damage incurred by you as a result of a denial of your permission request, other than a refund of the amount(s) paid by you to Elsevier and/or Copyright Clearance Center for denied permissions.

LIMITED LICENSE

The following terms and conditions apply only to specific license types:
15. **Translation**: This permission is granted for non-exclusive world **English** rights only unless your license was granted for translation rights. If you licensed translation rights you may only translate this content into the languages you requested. A professional translator must perform all translations and reproduce the content word for word preserving the integrity of the article.
16. **Posting licensed content on any Website**: The following terms and conditions apply as follows: Licensing material from an Elsevier journal: All content posted to the web site must maintain the copyright information line on the bottom of each image; A hyper-text must be included to the Homepage of the journal from which you are licensing at http://www.sciencedirect.com/science/journal/xxxxx or the Elsevier homepage for books at http://www.elsevier.com; Central Storage: This license does not include permission for a scanned version of the material to be stored in a central repository such as that provided by Heron/XanEdu.
Licensing material from an Elsevier book: A hyper-text link must be included to the Elsevier homepage at http://www.elsevier.com . All content posted to the web site must maintain the copyright information line on the bottom of each image.

Posting licensed content on Electronic reserve: In addition to the above the following clauses are applicable: The web site must be password-protected and made available only to bona fide students registered on a relevant course. This permission is granted for 1 year only. You may obtain a new license for future website posting.
17. **For journal authors:** the following clauses are applicable in addition to the above:
Preprints:
A preprint is an author's own write-up of research results and analysis, it has not been peer-reviewed, nor has it had any other value added to it by a publisher (such as formatting, copyright, technical enhancement etc.).
Authors can share their preprints anywhere at any time. Preprints should not be added to or enhanced in any way in order to appear more like, or to substitute for, the final versions of articles however authors can update their preprints on arXiv or RePEc with their Accepted Author Manuscript (see below).
If accepted for publication, we encourage authors to link from the preprint to their formal publication via its DOI. Millions of researchers have access to the formal publications on ScienceDirect, and so links will help users to find, access, cite and use the best available

version. Please note that Cell Press, The Lancet and some society-owned have different preprint policies. Information on these policies is available on the journal homepage.
Accepted Author Manuscripts: An accepted author manuscript is the manuscript of an article that has been accepted for publication and which typically includes author-incorporated changes suggested during submission, peer review and editor-author communications.
Authors can share their accepted author manuscript:

- immediately
  - via their non-commercial person homepage or blog
  - by updating a preprint in arXiv or RePEc with the accepted manuscript
  - via their research institute or institutional repository for internal institutional uses or as part of an invitation-only research collaboration work-group
  - directly by providing copies to their students or to research collaborators for their personal use
  - for private scholarly sharing as part of an invitation-only work group on commercial sites with which Elsevier has an agreement
- after the embargo period
  - via non-commercial hosting platforms such as their institutional repository
  - via commercial sites with which Elsevier has an agreement

In all cases accepted manuscripts should:

- link to the formal publication via its DOI
- bear a CC-BY-NC-ND license - this is easy to do
- if aggregated with other manuscripts, for example in a repository or other site, be shared in alignment with our hosting policy not be added to or enhanced in any way to appear more like, or to substitute for, the published journal article.

Published journal article (JPA): A published journal article (PJA) is the definitive final record of published research that appears or will appear in the journal and embodies all value-adding publishing activities including peer review co-ordination, copy-editing, formatting, (if relevant) pagination and online enrichment.
Policies for sharing publishing journal articles differ for subscription and gold open access articles:
Subscription Articles: If you are an author, please share a link to your article rather than the full-text. Millions of researchers have access to the formal publications on ScienceDirect, and so links will help your users to find, access, cite, and use the best available version.
Theses and dissertations which contain embedded PJAs as part of the formal submission can be posted publicly by the awarding institution with DOI links back to the formal publications on ScienceDirect.
If you are affiliated with a library that subscribes to ScienceDirect you have additional private sharing rights for others' research accessed under that agreement. This includes use for classroom teaching and internal training at the institution (including use in course packs and courseware programs), and inclusion of the article for grant funding purposes.
Gold Open Access Articles: May be shared according to the author-selected end-user license and should contain a CrossMark logo, the end user license, and a DOI link to the formal publication on ScienceDirect.
Please refer to Elsevier's posting policy for further information.
18. **For book authors** the following clauses are applicable in addition to the above:
Authors are permitted to place a brief summary of their work online only. You are not allowed to download and post the published electronic version of your chapter, nor may you scan the printed edition to create an electronic version. **Posting to a repository:** Authors are permitted to post a summary of their chapter only in their institution's repository.

19. **Thesis/Dissertation**: If your license is for use in a thesis/dissertation your thesis may be submitted to your institution in either print or electronic form. Should your thesis be published commercially, please reapply for permission. These requirements include permission for the Library and Archives of Canada to supply single copies, on demand, of the complete thesis and include permission for Proquest/UMI to supply single copies, on demand, of the complete thesis. Should your thesis be published commercially, please reapply for permission. Theses and dissertations which contain embedded PJAs as part of the formal submission can be posted publicly by the awarding institution with DOI links back to the formal publications on ScienceDirect.

Elsevier Open Access Terms and Conditions

You can publish open access with Elsevier in hundreds of open access journals or in nearly 2000 established subscription journals that support open access publishing. Permitted third party re-use of these open access articles is defined by the author's choice of Creative Commons user license. See our open access license policy for more information.

Terms & Conditions applicable to all Open Access articles published with Elsevier:

Any reuse of the article must not represent the author as endorsing the adaptation of the article nor should the article be modified in such a way as to damage the author's honour or reputation. If any changes have been made, such changes must be clearly indicated.

The author(s) must be appropriately credited and we ask that you include the end user license and a DOI link to the formal publication on ScienceDirect.

If any part of the material to be used (for example, figures) has appeared in our publication with credit or acknowledgement to another source it is the responsibility of the user to ensure their reuse complies with the terms and conditions determined by the rights holder.

Additional Terms & Conditions applicable to each Creative Commons user license:

CC BY: The CC-BY license allows users to copy, to create extracts, abstracts and new works from the Article, to alter and revise the Article and to make commercial use of the Article (including reuse and/or resale of the Article by commercial entities), provided the user gives appropriate credit (with a link to the formal publication through the relevant DOI), provides a link to the license, indicates if changes were made and the licensor is not represented as endorsing the use made of the work. The full details of the license are available at http://creativecommons.org/licenses/by/4.0.

CC BY NC SA: The CC BY-NC-SA license allows users to copy, to create extracts, abstracts and new works from the Article, to alter and revise the Article, provided this is not done for commercial purposes, and that the user gives appropriate credit (with a link to the formal publication through the relevant DOI), provides a link to the license, indicates if changes were made and the licensor is not represented as endorsing the use made of the work. Further, any new works must be made available on the same conditions. The full details of the license are available at http://creativecommons.org/licenses/by-nc-sa/4.0.

CC BY NC ND: The CC BY-NC-ND license allows users to copy and distribute the Article, provided this is not done for commercial purposes and further does not permit distribution of the Article if it is changed or edited in any way, and provided the user gives appropriate credit (with a link to the formal publication through the relevant DOI), provides a link to the license, and that the licensor is not represented as endorsing the use made of the work. The full details of the license are available at http://creativecommons.org/licenses/by-nc-nd/4.0.

Any commercial reuse of Open Access articles published with a CC BY NC SA or CC BY NC ND license requires permission from Elsevier and will be subject to a fee.

Commercial reuse includes:

- Associating advertising with the full text of the Article
- Charging fees for document delivery or access
- Article aggregation
- Systematic distribution via e-mail lists or share buttons

Posting or linking by commercial companies for use by customers of those companies.

20. **Other Conditions**:

v1.9

Questions? customercare@copyright.com or +1-855-239-3415 (toll free in the US) or +1-978-646-2777.